Development of New Tags for Solid-phase Peptide Synthesis

Inauguraldissertation

zur Erlangung der Würde eines Doktors der Philosophie
vorgelegt der
Philosophisch-Naturwissenschaftlichen Fakultät
der Universität Basel

von

**Steven Knecht
aus Eschlikon, Schweiz**

Basel, 2008

Genehmigt von der Philosophisch-Naturwissenschaftlichen Fakultät auf Antrag von:

Prof. Dr. Beat Ernst, Institut für Molekulare Pharmazie, Universität Basel
Prof. Dr. Alex N. Eberle, Departement Forschung, Universitätsspital Basel

Basel, den 24. Juni 2008

Prof. Dr. Hans-Peter Hauri
Dekan

In den Wissenschaften ist viel Gewisses, sobald man sich von den Ausnahmen nicht irre machen lässt und die Probleme zu ehren weiss.

(Johann Wolfgang von Goethe, 1749–1832)

CONTENTS OF THE THESIS

1.   SUMMARY

Solid-phase peptide synthesis (SPPS) was first developed by Bruce Merrifield for the synthesis of polypeptides. In 1984, he was awarded with the Nobel Prize "for his development of methodology for chemical synthesis on a solid matrix". Compared to solution-phase methods, solid-phase chemistry offers many advantages in terms of efficiency as well as purification procedures. Particularly for longer peptide sequences, in solution-phase chemistry the isolation of all peptide intermediates is required, whereas in a solid-phase approach simple wash and filter procedures enable the entire automation.

In organic chemistry, there is the goal to produce pure compounds with the highest possible efficiency. But the frequent nonexistence of suitable separation and purification methods often makes it impossible to fulfill these requirements. Thus, also in SPPS purification frequently limits the success of the synthesis. While a number of small proteins have been successfully assembled, practical limitations regarding the ability to purify and characterize the mixtures that inevitable result from less than complete reactions as well as side reactions limit most efforts to synthesize peptides with more than 100 amino acid residues.

Our approach to overcome these limitations is based on affinity purification strategies frequently applied to the purification of recombinant proteins. Immobilized metal ion affinity chromatography (IMAC) has become the most common method for the purification of proteins carrying either a C- or N-terminal histidine (His)-tag. This short amino acid sequence is able to bind to Ni^{2+} immobilized on a nitrilotriacetic acid (NTA) column. Despite its broad application in protein purification, only little is known about the binding properties of the His-tag, and therefore almost no thermodynamic and kinetic data are available. In a first phase, the binding mechanism of the His-tag to Ni^{2+}-NTA was investigated. Different series of histidine-containing peptide tags were synthesized using automated solid-phase peptide synthesis (SPPS). Binding to Ni^{2+}-NTA was analyzed both qualitatively and quantitatively with surface plasmon resonance (SPR) using commercially available NTA sensor chips. The hexahistidine-tag showed an apparent equilibrium dissociation constant (K_D) of 14 nM. This was the best affinity found for all synthesized peptides. Furthermore, it

could be demonstrated that two histidines separated by either one or four residues are the preferred binding motifs for Ni^{2+}-NTA. Elongation of such a binding motif led to a decrease in binding affinity, probably due to increased entropy costs upon binding.

To reduce the entropy costs, short three amino acid tags were designed with decreased rotational freedom to fix the two histidine residues in the binding conformation, as it was the case with His-Aib-His. Compared to the His-Gly-His (K_D = 54 μM) the binding affinity could be decreased by a factor of 1.5 with the aminoisobutyric acid (Aib) at position 2 to a K_D of 36 μM.

1,10-Phenanthroline and derivatives thereof show a high potential as a tag binding to Ni^{2+}-NTA and were analyzed in the Biacore assay. The high binding affinity of 1,10-phenanthroline (K_D = 650 nM) is mainly based on a slow dissociation rate constant (k_{off}) with a half-life time of about 5 min. Different parameters, such as the charge transfer between the binding nitrogen and nickel, rigidity, and additional interactions between the binding partners were found to influence the binding affinity. Among these factors, solubility played the most crucial role. Ligands establishing on the side directed towards the solvent a well-organized solvation shell, showed improved binding properties for the Ni^{2+}-surface. Therefore, 5-amino-1,10-phenanthroline (K_D = 407 nm) binds with a 1.6-fold higher affinity to Ni^{2+}-NTA than 1,10-phenanthroline (K_D = 650 nM). On the side involved in binding however, a weaker solvation is desired, because the removal of strongly bound solvent molecules prior to the binding lowers the gain of enthalpy in the process of the complex formation. In parallel to the Biacore assay, a computational approach to predict binding affinities of various ligands to Ni^{2+}-NTA was developed by Dr. Martin Smiesko, a member of the Institute of Molecular Pharmacy.

To study the phenanthroline-tag and demonstrate its suitability for SPPS, the following simple strategy was chosen: Phenanthroline was coupled via an acrylate spacer to the N-terminal of a test peptide. Interestingly, the affinity purification of the test peptide proved to be superior to the standard HPLC purification method and afforded a pure product with a yield of 43% compared to 34% for the HPLC purification. The potential of the new tag could also be demonstrated in a Biacore assay with the phenanthroline-tagged peptide, where a stable immobilization could be

achieved despite the negative influence of the peptide on the binding affinity, which led to a 20-fold increase in K_D.

After Ni^{2+}-NTA purification of a tagged protein, the tag has to be cleaved. For this purpose, a photolabile linker was introduced between the phenanthroline and the peptide. Due to the poor solubility, the synthesis of the tag-photolinker construct did work with only 11% yield. Because only small amounts of the phenanthroline-photolinker-construct could be purified, the photolinker approach was abandoned.

Finally, a screen to identify new tags using the Biacore and the computational model resulted in a promising scaffold, the picolinic acid. The 6-amino-picolinic acid turned out to be the best representative with a K_D of 10.9 μM. The aromatic nitrogen and one oxygen of the carboxylic acid occupy the two available coordination sites of Ni^{2+}-NTA. Compared to picolinic acid, the binding affinity was 1.4-fold increased due to the interaction of the anilinic nitrogen with the carboxylic acid of the NTA chelate.

With this work a new purification strategy using phenanthroline-tags could be presented. Furthermore, the knowledge about the binding properties of Ni^{2+}-NTA binding tags was increased. This may add to the development of new tags as presented for the picolinic acid.

2. ABBREVIATIONS

Aib	Aminoisobutyric acid
Arg	L-Arginine
Asp	L-Aspartic acid
Bipy	2,2'-Bipyridyl
BOP	Benzotriazole-1-yl-oxy-tris-(dimethylamino)-phosphonium hexafluorophosphate
CSD	Cambridge Structural Database
DMA	N,N-Dimethylacetamide
DMF	N,N-Dimethylformamide
DABS-Cl	4-(4-Dimethylaminophenylazo)benzenesulfonyl chloride
dba	1,5-Diphenyl-1,4-pentadien-3-one
DCC	N,N'-Dicyclohexylcarbodiimide
DCU	N,N'-Dicyclohexylurea
DIPCDI	N,N'-Diisopropylcarbodiimide
DIPEA	N,N-Diisopropylethylamine
Dtt	Dithiothreitol
EDC•HCl	1-ethyl-3-(3-dimethylaminopropyl)carbodiimide hydrochloride
Gly	Glycine
HATU	2-(1H-7-Azabenzotriazol-1-yl)-1,1,3,3-tetramethyl uronium hexafluorophosphate
HBTU	2-(1H-Benzotriazole-1-yl)-1,1,3,3-tetramethyluronium hexafluorophosphate
HCTU	5-Chloro-1-[bis(dimethylamino)methylene]-1H-benzotriazolium 3-oxide hexafluorophosphate
HEPES	4-(2-hydroxyethyl)-1-piperazineethanesulfonic acid
His	L-histidine
His-tag	Hexahistidine-tag
HMBA	4-Hydroxymethylbenzoic acid
HOBt	1-Hydroxybenzotriazole
HPLC	High-performance liquid chromatography

HR-MS	High resolution mass spectrometry
IDA	Iminodiacetic acid
IFC	Integrated fluidic cartridge
IMAC	Immobilized metal (ion) affinity chromatography
IMAP	Immobilized metal (ion) affinity partitioning
IMAGE	Immobilized metal (ion) affinity gel electrophoresis
IMACE	Immobilized metal (ion) affinity capillary electrophoresis
K_A	Equilibrium association constant
K_D	Equilibrium dissociation constant
k_{on}	Association rate constant
k_{off}	Dissociation rate constant
Lys	L-Lysine
MBHA	4-Methylbenzhydrylamine
MS	Mass spectrometry
NAPamide	[Nle$_4$, Asp$_5$, D-Phe$_7$, Lys$_{11}$]-MSH$_{4-11}$
Ni-NTA	[Ni(II)(nta)]$^-$ complex
Nle	L-Norleucine
NTA	Nitrilotriacetic acid
o/n	over night
PAM	4-hydroxymethyl-phenylacetamidomethyl
PEG	Polyethylene glycol
Phe	L-Phenylalanine
Phen	1,10-Phenanthroline
PL	Photolinker, photolabile linker
PPOA	4-Propionylphenoxy-acetic acid
RAM	Rink amide
rt	Room temperature
Sar	Sarcosine
SD	Standard deviation
S-Phos	2-Dicyclohexylphosphino-2',6'-dimethoxybiphenyl
SPR	Surface plasmon resonance
TBAF	Tetrabutylammounium fluoride

Abbreviations

TBTU	2-(1H-Benzotriazole-1-yl)-1,1,3,3-tetramethyluronium tetrafluoroborate
TCTU	1-[Bis(dimethylamino)methylene]-5-chloro-1H-benzotriazolium-3-oxide tetrafluoroborate
TFA	Trifluoroacetic acid
THF	Tetrahydrofuran
t_R	Retention time
Trp	L-Tryptophan
$T_{1/2}$	Half-life time
μW	Microwave
X-Phos	2-Dicyclohexylphosphino-2',4',6'-triisopropylbiphenyl

3. INTRODUCTION

Proteins form together with carbohydrates, lipids, and nucleic acids the "molecules of life". They are present in various forms in every living cell and structure the body of multicellular organisms in the form of skin, hair, callus, cartilage, muscles, tendons, and ligaments. As enzymes, hormones, antibodies, and globulins, they are involved in the control of chemical processes and transport of biomolecules, *e.g.* in the form of hemoglobin and myoglobin as carrier proteins for oxygen. The vide variety of their physiological function is also shown in their physical properties: Silk as a flexible fiber, horn as a tough rigid solid, and the enzyme pepsin, which forms water soluble crystals.

Nowadays, large biotechnology-based initiatives, like the Human Genome Project [*1*], as well as the improved understanding of fundamental biological processes, provides a huge number of new protein sequences. This leads to a rapid increase in the number of novel or important targets for drugs and agricultural applications. Therefore, there is a high demand of these new targets in at least micro- to multimilligram quantities. Obviously, access to these proteins should be provided within the shortest possible time frame. Mainly three different approaches are used to fulfill this requirement: (a) Isolation of native proteins, (b) recombinant expression of proteins in genetically engineered microorganisms or animals, and (c) chemical synthesis. Each approach has its own advantages and disadvantages. The selection of the feasible approach is driven by protein size, desired mutants or derivatives (such as post-translational modifications and isotopic labeling), time constraints, and economics.

Although most of the proteins have been obtained by recombinant methods, these approaches often suffer from the time used to generate milligram quantities. Formation of inclusion bodies, misfolding, and low expression levels further decreases the efficiency of this method [*2*]. Additionally, expressed heterogeneity and biological contamination (*e.g.* DNA impurities or endotoxins), may affect their use or activity.

A good solution to circumvent the above mentioned drawbacks is provided by their chemical synthesis. Besides avoiding biological contaminations, such a purely synthetic approach offers the possibility to incorporate unnatural amino acids or other

chemical modifications that may improve protein efficacy. Finally, introduction of biochemical or biophysical probes is facilitated in a fully synthetic approach [*3*].

Nowadays, the synthetic approach allows only the routine synthesis of small proteins with up to 50 amino acids. There are few examples of longer chains, such as ribonuclease A (124 residues) [*4*] and human immunodeficiency virus (HIV)-1 TaT (86 residues) [*5, 6*], or the green fluorescent protein, a 238-residue peptide chain [*6*]. Therefore, synthetic methods are mainly restricted to peptides rather than to proteins.

The name "peptide" was introduced from Emil Fischer [*5*] and is built from "**pept**on" (cleavage products of digestion of Pepsin; from greek *peptos* = digested) and polysacchar**ide**, which are also built from monomeric building blocks. Therefore, peptides are just smaller versions of proteins. A clear dividing line between peptides and proteins is not defined, as the numbers of residues vary between 50 and several hundreds. In the following section an overview about the current methods used in peptide synthesis is given.

3.1. Peptide Synthesis

In 1907, Emil Fischer initiated peptide chemistry by the synthesis of the dipeptide glycylglycine, obtained by hydrolysis of the diketopiperazine of glycine. However, already twenty years ago, Theodor Curtius synthesized the first N-protected dipeptide, benzoylglycylglycine, by treating the silver salt of glycine with benzoyl chloride [7]. Furthermore in 1904, he developed the first practical method for peptide synthesis, the azide coupling procedure, which enabled the synthesis of benzoylglycine peptides of various length [8]. In addition, only one year later, Emil Fischer presented a new method for the synthesis of peptides via acylchlorides, prepared from the corresponding free amino acid using PCl_5 in acetyl chloride as solvent [9].

3.1.1. Solid-phase Peptide Synthesis

Nowadays, peptides are mainly synthesized applying to the solid-phase strategy developed by Merrifield [10]. The genious idea of this strategy is to couple the first amino acid via its carboxylic acid to an insoluble and filtratable polymer and then to build up the peptide chain from its C-terminal end (Scheme 1).

The great advantage of this approach compared to solution-phase methods is the simplification of the synthetic procedure. In solution-phase methods, the product has to be isolated and purified after each reaction, prior to the next coupling step. In solid-phase peptide synthesis, byproducts are simply removed by washing the product immobilized on an insoluble support. Furthermore, the repetitive steps of the synthesis, *i.e.* deprotection, washing, coupling, washing, and again deprotection allows the use of a single reaction vessel and the automation of the peptide synthesis. For this fundamental contribution to peptide synthesis, Bruce Merrifield was awarded with the Nobel Prize in chemistry in 1984. The process of the Merrifield synthesis is now performed on automated synthesizers that can assemble sequences of up to 50 amino acids in a few days.

repetitive cycle

LINKER—⬤

↓ **Anchoring**

$Y-\overset{H}{N}-(Xaa_1)\overset{X}{\underset{O}{\|}}-O-LINKER-⬤$

↓ **Deprotection**

$H_2N-(Xaa_1)\overset{X}{\underset{O}{\|}}-O-LINKER-⬤$

↓ **Addition of amino acid**

$Y-\overset{H}{N}-(Xaa_2)\overset{X}{\underset{O}{\|}}-OH \ + \ H_2N-(Xaa_1)\overset{X}{\underset{O}{\|}}-O-LINKER-⬤$

↓ **Coupling**

$Y-\overset{H}{N}-(Xaa_2)\overset{X}{\underset{O}{\|}}-\overset{H}{N}-(Xaa_1)\overset{X}{\underset{O}{\|}}-O-LINKER-⬤$

↓ (1) **Deprotection**
(2) **Cleavage from resin**
(3) **Side chain deprotection**

$H_2N-(Xaa_n)\overset{X}{\underset{O}{\|}}-\left[\overset{H}{N}-(Xaa_x)\overset{X}{\underset{O}{\|}}\right]_{n-3}-\overset{H}{N}-(Xaa_2)\overset{X}{\underset{O}{\|}}-\overset{H}{N}-(Xaa_1)\overset{X}{\underset{O}{\|}}-OH$
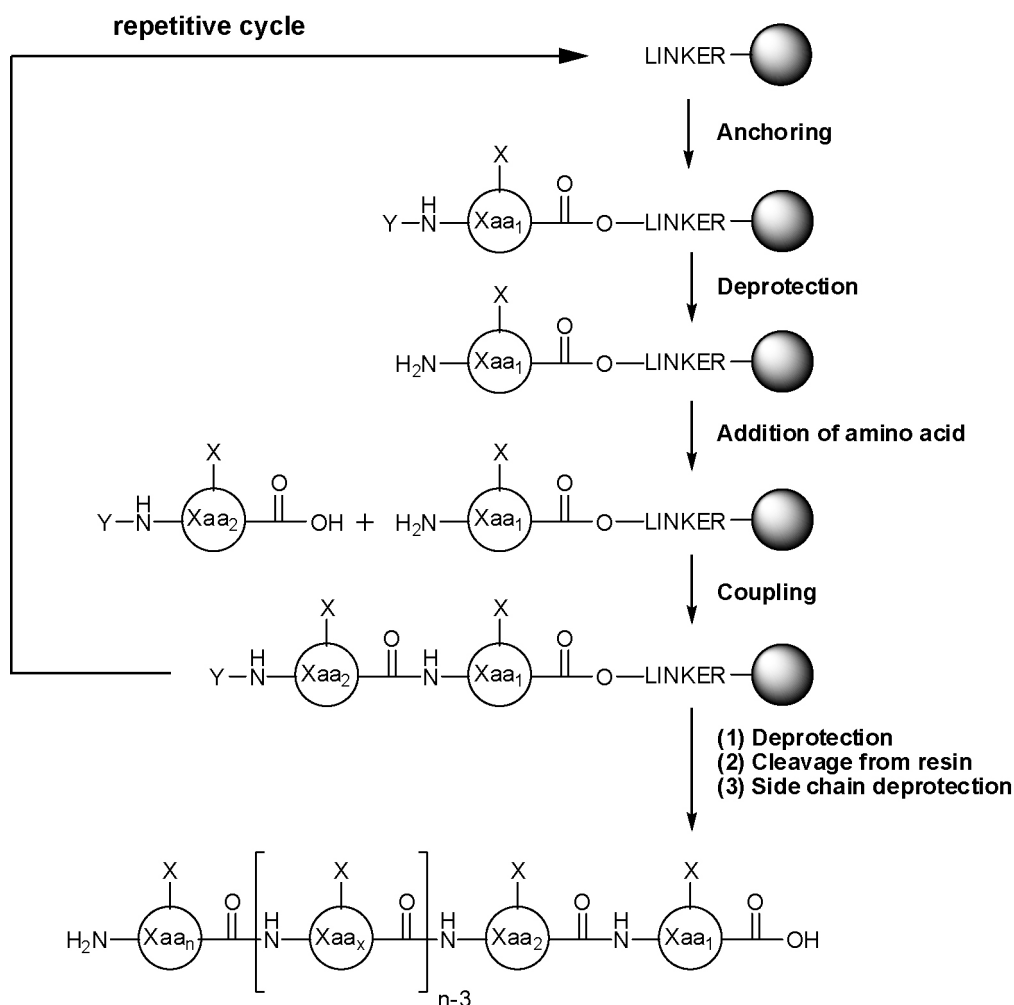
Scheme 1: Schematic principle of solid-phase peptide synthesis. X: protecting groups of amino acid side chains; Y: N^{α}-protecting group.

Generally, peptide synthesis is based on the appropriate combination of protecting groups and an efficient method for the activation of the carboxyl group prior to reaction with the amino terminal. Protecting groups have to prevent on one hand bond formation between two incoming amino acids (N-terminal protecting group), and on the other hand formations between the incoming amino acids and side chain functionalities (side chain protecting groups). In the Merrifield synthesis, the C-terminal is protected by the polymeric carrier.

For the Merrifield synthesis mainly, two protection schemes have been developed. The first one is the *tert*-butoxycarbonyl (Boc)/benzyl (Bzl) strategy, which depends on the different acid lability of the N-terminal protecting group (Boc) and the side-chain protecting group (Bzl) as described in the original publication of Merrifield [*10*]. The main drawback of this strategy is the use of hydrogen fluoride (HF) for the final cleavage and deprotection of the peptide. This procedure leads to various side

reactions, such as Friedel-Crafts reactions between aromatic groups of the resin and the side chains of the peptide, and/or promotion of an N→O acyl shift involving the side-chain groups of serine and threonine. For this purpose, Tam *et al.* developed a two-stage deprotection protocol. In a first step, low HF concentrations were used, followed by a second with higher concentrations, which minimized the occurrence of these side-reactions [*11*].

The second protection strategy was developed by L. A. Carpino and G. Y. Han [*12*] and is based on the use of the base labile 9-fluorenylmethyloxycarbonyl (Fmoc) group for the protection of α–amino groups. This allows the orthogonal protection of side-chain functions with acid labile protecting groups (Figure 1).
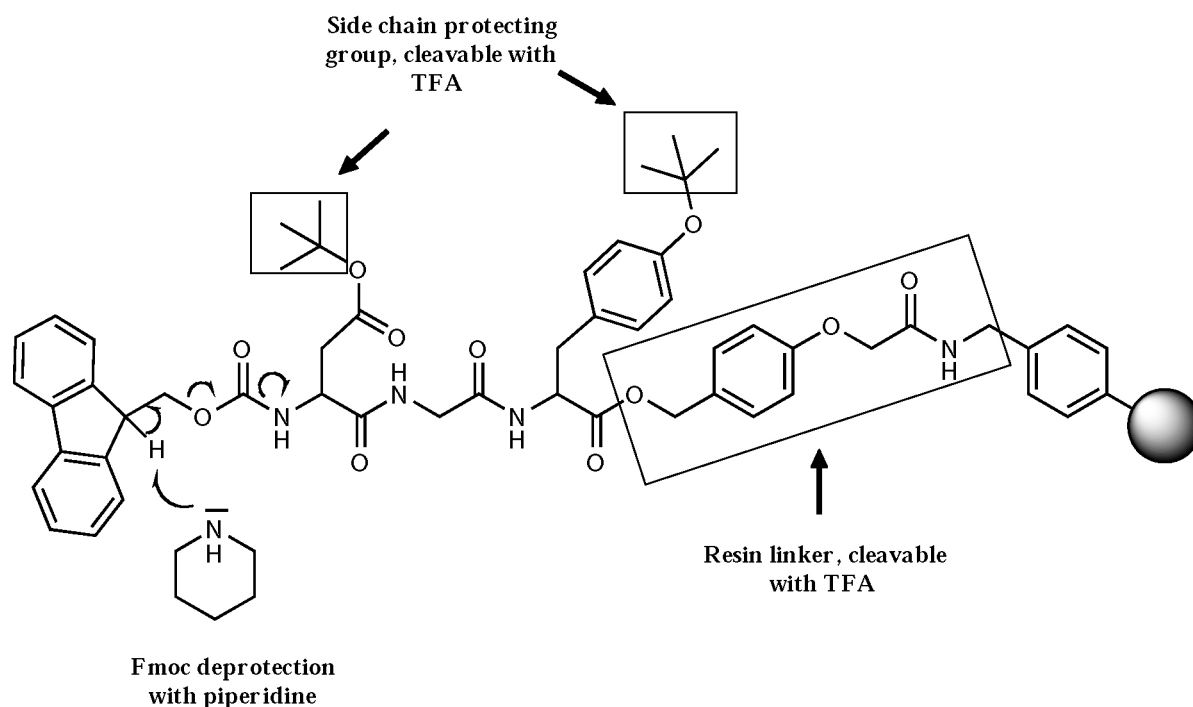
Figure 1: Fmoc strategy in solid-phase peptide synthesis. The Fmoc-group is cleaved under basic conditions with piperidine, while the side chain protecting groups and the linker are cleaved under acidic conditions using TFA.

The first solid support used in solid-phase peptide synthesis was a styrene-divinylbenzene co-polymer, functionalized by chlorination of benzyl groups. The benzyl chloride was then be used to anchor the C-terminal amino acid via an ester linkage to the solid support. Thus, when the product of the SPPS was cleaved from the solid support a carboxylic acid was obtained at the C-terminal. Later on, a broad variety of resins were developed leading to different functionalities at the C-terminal such as acids (Wang resin, 2-chlorotrityl resin, Merrifield, (4-hydroxymethyl)-

phenylacetamidomethyl (PAM), oxime resin), amides (Rink amide (RAM), 4-methylbenzhydrylamine (MBHA) resin), thioesters (4-sulfamylbutyryl resin), or alcohols (4-hydroxymethylbenzoic acid (HMBA) resin). Furthermore, oxime resins and 4-hydrazinobenzoyl resins are useful to generate esters, whereas the latter is also used for C-terminal thioesters and amides depending on the reagents used for the cleavage reaction. Finally, brominated PPOA ([4-(2-bromopropionyl)phenoxy]-acetic acid) resins are used for the generation of C-terminal peptide hydrazides.

The following properties of solid supports proposed by Miranda *et al*. use to be crucial for the success [*13*]: (a) particles should be of consistent shape and size to elicit a certain robustness; (b) they should be inert to all reagents and reaction conditions applied in the reaction cycles; (c) they should allow a fast solvent and reagent diffusion and access to all reactive sites; and finally (d) the particles should contain functionality to enable efficient anchoring of the linker or the first amino acid.

The most widely used resins are made of polystyrene or polyethylene glycol. As already mentioned, Merrifield used a polystyrene resin with 1% divinylbenzene (PS-DVB) for his synthesis. However, different batch-to-batch results of peptide syntheses clearly demonstrated that. slight variations in the swelling properties or the degree of functionalization may substantionally influence the synthetic outcome [*14*].

To increase the diffusion rates, a problem that inevitably arises in heterogeneous reactions, polyethylene glycol (PEG) spacers are anchored to the polystyrene beads, as demonstrated with TentaGel S RAM resin [*15*]. These resins however, are slightly unstable when treated with TFA [*16*], a problem that can be avoided with polyethylene glycolamine linkers (PEGA) [*17*]. These linkers show improved diffusion rates, but do not cause problems upon TFA treatment.

Thermodynamically, peptide bond formation is not favored, because of the highly stable ammonium carboxylate formed by the two starting materials (Scheme 2) [*18*].

$$RCOOH + R'NH_2 \rightleftharpoons R'NH_3^+ + RCOO^- \rightleftharpoons RCONHR' + H_2O$$
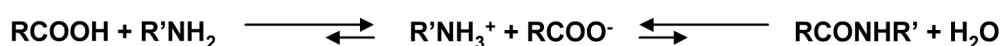
Scheme 2: The carboxylic acid forms a thermodynamically stable salt with the primary amine, which inhibits the formation of the amide.

A condensation of the salt requires elevated temperatures of 160 – 180°C [*19*] leading to degradation of the growing peptide. Therefore, the acid has to be activated by the attachment of a leaving group to support the nucleophilic attack by the amino group. Carboxylic acids are generally activated either by carbodiimides, formation of symmetrical anhydrides (anhydride formed from equivalent of the same amino acid), or formation of active esters. Since low yields, racemization, or degradation often accompany amide formation, coupling procedures are optimized not. only to provide high yields, but also to prevent racemization.

In solution-phase peptide synthesis, racemization is encountered upon activation of the acid (**i** – **iii**), which might lead to the formation of an oxazolone (**iv**). Under mild basic conditions, the oxazolone is deprotonated into a conjugated anionic intermediate (**v**). Since reprotonation occurs not enantioselectively, racemates of oxazolones are obtained (**vi** and **viii**). Because both react with the amino terminal of the growing peptide chains, chirality gets lost leading to an DL- (**vii**) and a LL-peptide (**ix**) (Scheme 3).
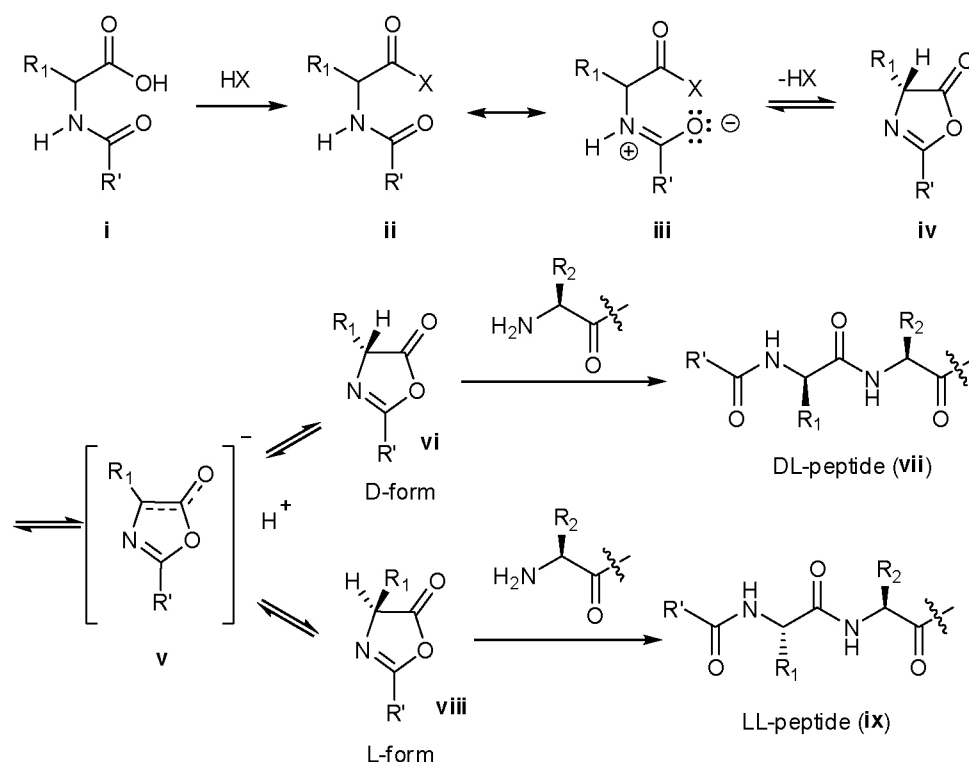
Scheme 3: Racemization via oxazolone mechanism. R_1, R_2: side chain residues.

In SPPS, this mechanism is prevented due to the fact that peptides are grown at the N-terminus and N^{α}-protected amino acids are used. Nevertheless, racemization might also occur due to a reversible proton exchange on the C_{α}-atom forming the carbanion as observed with activated cysteine or histidine residues [20, 21]. Similar to the oxazolone mechanism, reattachment of the proton is able to occur from both sides leading again to a racemic mixture.

Activation of the carboxylic acid allows to overcome the thermodynamic restrictions of the peptide bond formation as already mentioned above. Carbodiimides are highly popular as *in situ* activating reagents. In 1950, dicyclohexylcarbodiimide (DCC) was reported as an excellent coupling reagent for the apolar environment of polystyrene resins [22]. The mechanism of the reaction is depicted in Scheme 4 [23].
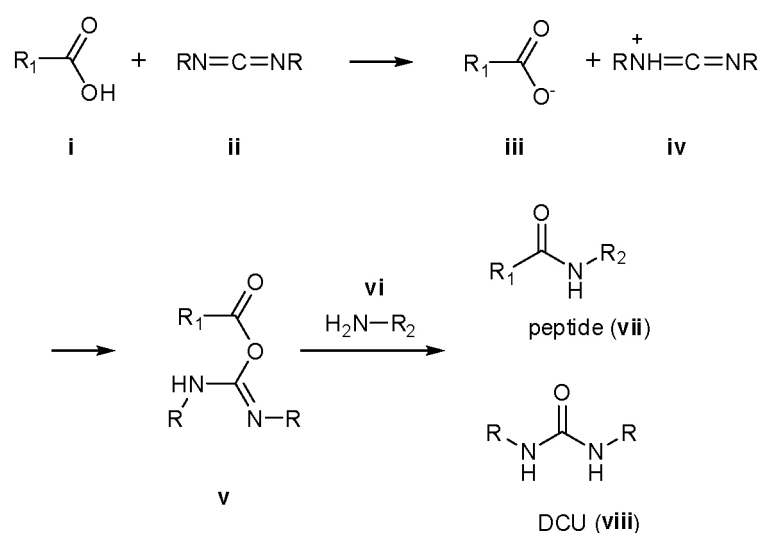
Scheme 4: Peptide coupling via carbodiimide. R: cyclohexyl residue; R_1: carboxy moiety; R_2: amino moiety.

The anion of the carboxylate (**iii**) is added to the protonated carbodiimide (**iv**) forming the highly reactive carbamimidic anhydride (**v**), which further reacts with amine **vi** to form amide **vii** dicyclohexylurea (DCU, **viii**) as a byproduct. The major drawback of DCC is the poor solubility of DCU in dichloromethane, the most common solvent used for the coupling reaction. A solution to this problem are modified carbodiimides as diisopropylcarbodiimide (DIPCDI) [24], *tert*-butylmethylcarbodiimide [25], or 1-ethyl-3-[3-dimethylaminopropyl]carbodiimide hydrochloride (EDC•HCl), which form more soluble products.

Symmetrical anhydrides are mainly used in combination with the Boc strategy [*26, 27*]. They are formed *in situ* using two equivalents of the protected amino acid and one equivalent of the DCC. Therefore, this approach wastes one equivalent of the amino acid reagent. As the formation of anhydrides is much faster in DCM than in DMF, Boc-protected amino acids are used for solubility reasons. Fmoc-protected amino acids, *e.g*. Gly, Ala, Nle, Cys(Acm), Gln(Mbh) are not soluble in DCM. Therefore, the addition of DMF is required for the formation of anhydrides [*28*].

The successful active ester method has been extensively studied [*29*] and is nowadays the most widely used method in solid-phase peptide synthesis. The peptide bond is formed via the $B_{Ac}2$-mechanism. The amino group of R_1NH_2 (**i**) nucleophilicly attacks the carboxyl carbon of **ii** leading to the tetrahedral intermediate **iii** (Scheme 5).
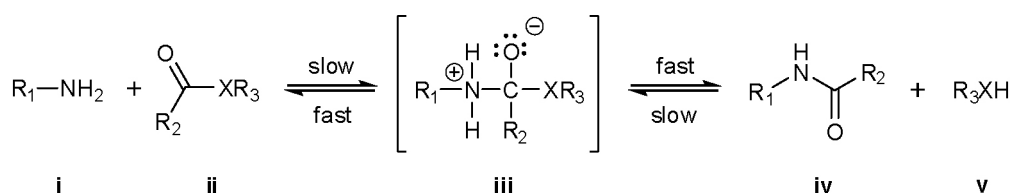
Scheme 5: Formation of peptide bond via $B_{Ac}2$ mechanism. R_1: amino moiety; R_2: carboxy moiety; R_3: leaving group.

Formation of **iii** is the rate determining step in this reaction. It can be positively influenced by activating the carboxy component with electron withdrawing groups. The second step, the peptide bond formation, is fast, if the C-X bond in **iii** is highly polarized.

The 1-hydroxybenzotriazolyl- (OBt) esters, which are formed *in situ* for example from DIPCDI and HOBt, are the most frequently used active esters following the mechanism described above. *In situ* activating agents are widely accepted in solid-phase peptide synthesis, as they lead to fast reactions even between sterically hindered amino acids. In addition, their use is generally free from side reactions. Most are based on phosphonium or aminium (formerly known as uronium) salts. The most commonly employed compounds are listed in Figure 2.
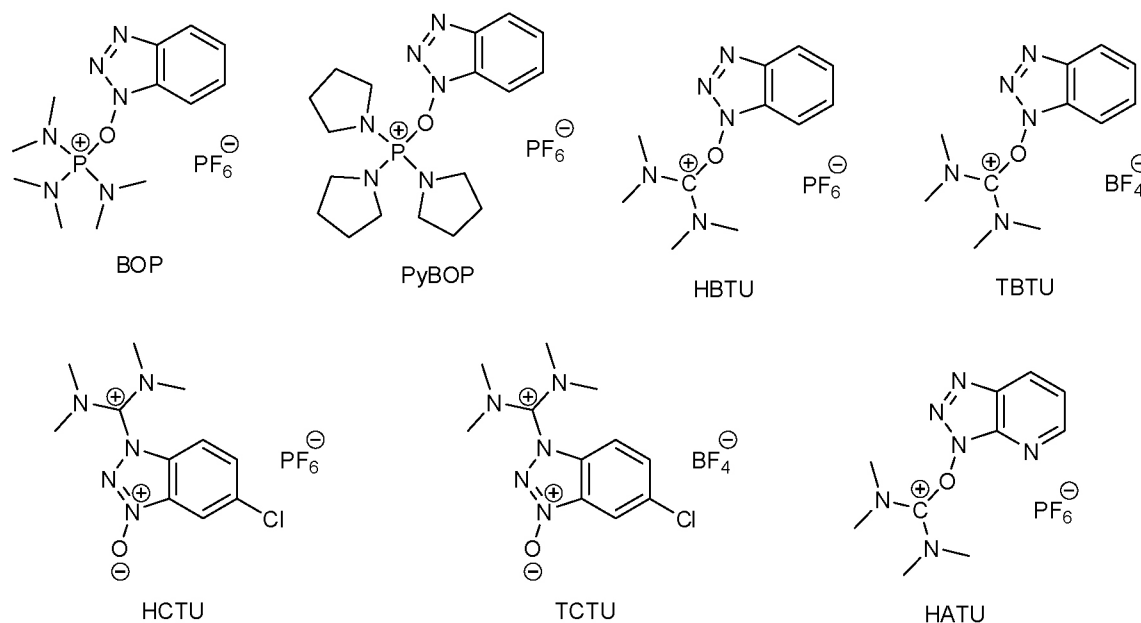
Figure 2: Structures of the most common coupling reagents to form active esters for peptide coupling.

Castro *et al.* developed the highly efficient phosphonium reagent benzotriazole-1-yl-oxy-tris-(dimethylamino)-phosphonium hexafluorophosphate (BOP) [*30*]. However, BOP has a strong tendency to racemization [*31*] and during the reaction the toxic byproduct hexamethylphosphoramide is formed. As an alternative, benzotriazole-1-yl-oxy-tris-pyrrolidino-phosphonium hexafluorophosphate (PyBOP) was developed [*32*]. The cytotoxic aminium salt HBTU is often replaced by the tetrafluoro borate TBTU [*33*].

Besides OBt esters, 1*H*-hydroxy-7-azabenzotriazole (OAt) esters show an increased reactivity due to the formation of a transition state stabilized by an additional H-bond as suggested by Carpino *et al.* [*34*]. This increases the aminolytic reactivity and additionally inhibits racemization with a high efficiency. In the transition state the amino component is fixed in a certain orientation facilitating the nucleophilic attack, whereas the oxazolone formation is significantly reduced due to the low activation of the ester group (Scheme 6).
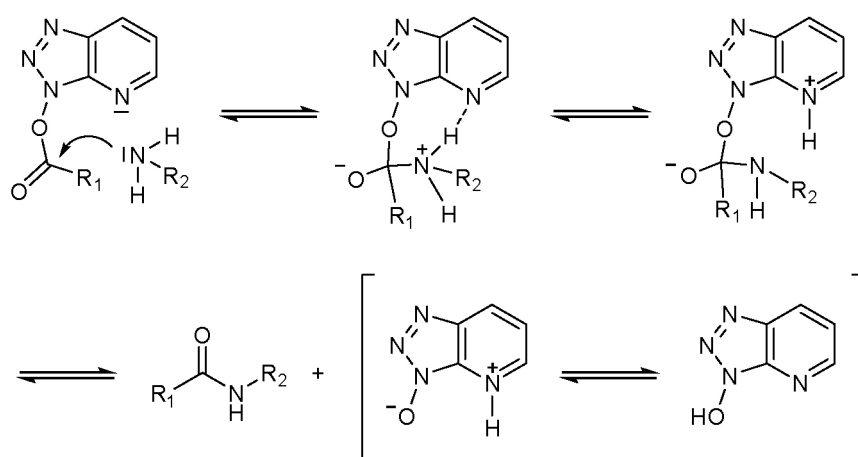
Scheme 6: Intramolecular base catalysis of HATU during aminolysis of OAt esters. R_1: carboxy moiety; R_2: amino moiety.

6-chlorobenzotriazole (OCt) esters have demonstrated a reactivity comparable to OAt esters. They can be formed with 5-chloro-1-[bis(dimethylamino)methylene]-1*H*-benzotriazolium 3-oxide hexafluoro-phosphate (HCTU) or its tetrafluoroborate variant TCTU. They were found to be nontoxic, stable in DMF, and available at much lower costs [*35*].

Less important as activated species are pentafluorophenyl (OPfp) esters [*36*]. Although they react significantly slower than *e.g.* symmetrical anhydrides, they showed only little side reactions during the amide bond formation. However, with some amino acids, the generation of the OPfp esters is cumbersome as they do not crystallize and are difficult to purify.

N-hydroxysuccinimide esters [*37*] are highly popular as they are easy to crystallize and show a high aminolysis activity. Additionally, due to their hydrolytic stability, they allow peptide synthesis in mixtures of H_2O with organic solvents (EtOH/water, dioxane/water, THF/water).

Finally, the deprotection and cleavage of the crude peptide from the solid-phase is accomplished with HF when Boc-strategy is applied and TFA in case of the Fmoc-strategy. In the latter case, concomitant removal of the side-chain protecting groups is possible when highly concentrated TFA solutions are used. When the production of protected peptides is addressed, deprotection with less than 10% TFA (*e.g.* trityl linkers) or employment of orthogonal protection groups (*e.g.* photolabile protection) is required. Under acidic conditions, the side-chain protecting groups form stabilized

carbocations, which are able to react with the electron-rich side chains of amino acids, *e.g.* present in Cys, Met, Tyr, Thr, Ser, and Trp. This leads to undesired side-products, which can be minimized by using scavengers to trap the cations formed by deprotection. Commonly used scavengers are thiol-based cocktails as ethane-1,2-dithiol, or thioanisole [*38, 39*], or the nonodorous and less toxic silane-based compounds as *e.g.* triisopropyl silane [*40*].

3.1.2. Limitations of Solid-phase Peptide Synthesis

Although the chemistry for SPPS is highly developed and allows high coupling efficiencies, the success of the synthesis is still depending on the sequence of the synthesized peptide.

Within so-called "difficult sequences" sequences, inaccessibility of the N-terminal amino group due to intermolecular aggregation (β-sheet formation) of the growing peptide chains in some cases makes an acylation impossible. These sequences are often found 5-15 residues away from the resin [*3*] Different strategies are known to avoid the development of these secondary structures: (a) development of highly efficient coupling methods, *i.e. in situ* neutralization (addition of base during coupling step improves swelling properties of the resin) [*41*], (b) the use of new supports that increase interchain separation and peptide chain solvation [*17*], (c) addition of chaotropic salts during or preceding the coupling step [*42*], (d) attachment of spacer units to increase the distance from the resin before synthesis of the target peptide [*43*], and finally (e) modifying the deprotection procedure or the coupling solvents [*44*].

The most powerful strategy to combat these difficult sequences is the introduction of secondary amino acid (imino acid) surrogates as analogs of proline or *N*-alkylamino acids, which disrupt the secondary structure. Pseudoprolines [*45*] and Dmb/Hmb (2,4-dimethoxybenzyl/2-hydroxy-4-methoxybenzyl) [*46*] amino acids are the most frequently used surrogates, which are cleaved into a physiological amino acid upon TFA treatment (Figure 3).
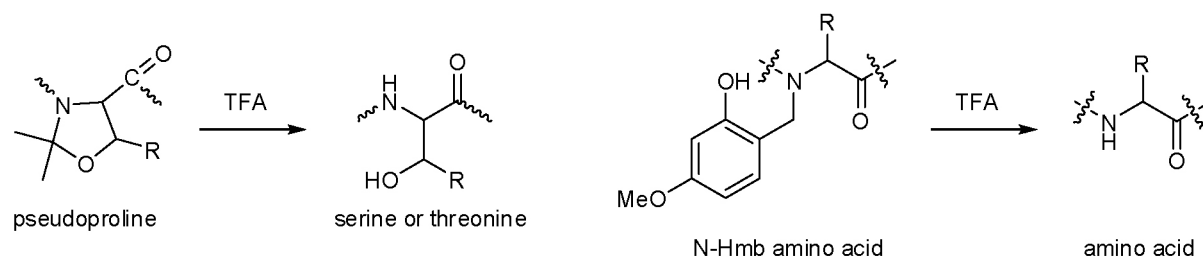
Figure 3: Secondary amino acid surrogates to disrupt formation of secondary structure during peptide synthesis.

The probability to encounter intermolecular aggregation in a peptide increases with peptide length. Therefore, the synthesis of larger peptides (more than 50 residues) or even proteins via SPPS is limited.

Different ligation strategies have evolved during the last decades for the synthesis of small proteins of more than 100 amino acid residues from smaller fragments synthesized by SPPS. The most popular method is the chemoselective ligation suitable for the preparation of C-terminal thioester and thioacid functionalities [47]. An elegant method is the so-called native chemical ligation (NCL) [48] (Scheme 7).
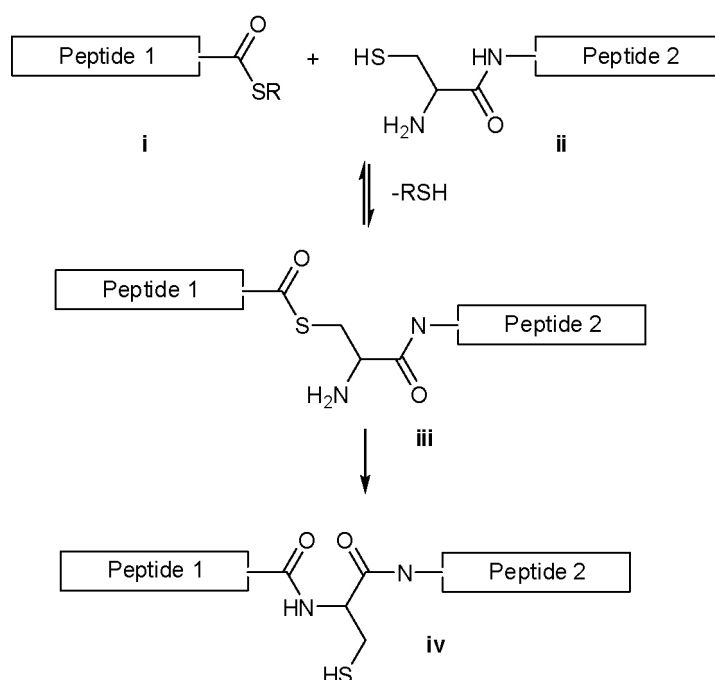
Scheme 7: Native chemical ligation (NCL) of the peptide fragments **i** and **ii**.

A C-terminal α-thioester (**i**) is reacted with a second unprotected peptide containing an N-terminal cysteine residue (**ii**). The reaction occurs via a reversible

transsthioesterification in aqueous solvents at *pH* 7 to from the thioester intermediate **iii**. After a spontaneous S→N acyl shift the native peptide bond at the ligation site is formed (**iv**).

The initial ligations in a solution-phase approach were followed by solid-phase ligation strategies from Canne *et al*. in 1999 [*49*] (Scheme 8).
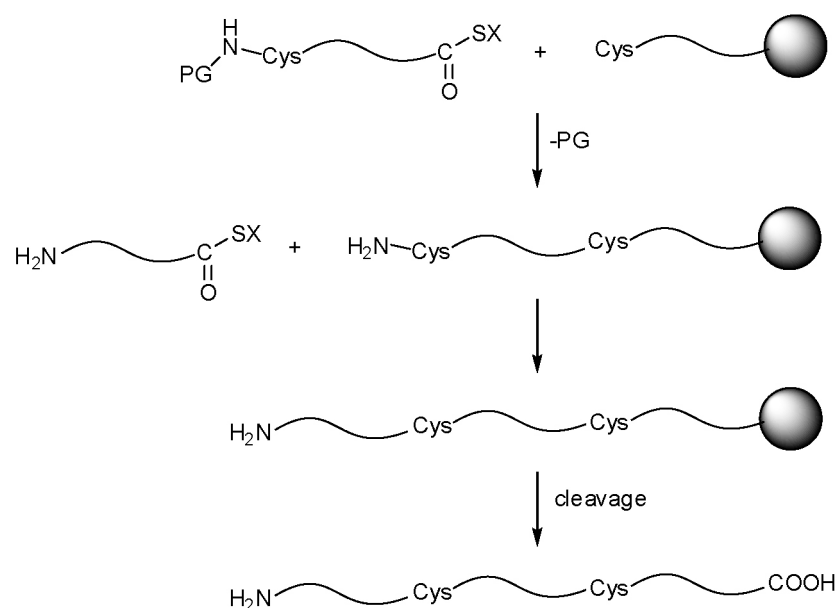
Scheme 8: General concept of solid-phase chemical ligation. N-terminal cysteines are used for the formation of the native peptide bond between the segments.

The advantages of such a solid-phase approach are reduced losses by avoiding a series of intermediate purification steps following each ligation. In addition, as common for all solid-phase approaches, the use of excess quantities of each segment drives the reaction nearly to completion.

With the increase in efficiency of the synthesis of longer peptides the challenges for the purification increases as well. The crude product obtained by deprotection/cleavage of a peptide synthesized on solid support contains a variety of byproducts. Generally, these impurities consist of shortened peptides with a single internal amino acid missing (deletion peptides, formed during chain assembly), and peptides with chemical modifications due to side reactions in the final deprotection. The key to a successful synthesis is the formation of product as uniform as possible. This task becomes more and more difficult for peptides of 50 or more residues. Nowadays, most cleavage protocols involve precipitation of the crude product using

cold diethylether or *tert*-butylmethylether prior to the purification by reversed-phase high performance liquid chromatography (RP-HPLC). Depending on the peptide sequence, an additional treatment with oxidizing agents to form disulfide bonds before HPLC purification is necessary. In principle, purification should be carried out by the consecutive application of mechanistically different purification methods to lead to a high purity of the final product. However, such a multistep purification procedure is time consuming and rather expensive. Furthermore, by the increase of the number of manipulations the yield can drop significantly. Most of the smaller peptides (2 – 50 amino acids) can be purified by a single step preparative HPLC. Reversed-phase HPLC may not be satisfactory for the purification of products containing a lot of late-eluting impurities, because the more hydrophobic components can displace the target peptide [*3*]. At a peptide length of about 50 amino acids, a single HPLC approach is no longer efficient, due to an onset of relatively stable and slowly exchanging folded structures of the peptide chain [*50*]. As a consequence, a single peptide leads a variety of chromatographically separable conformers. If a proper folding of the peptide chain prior to the HPLC purification is not possible, conformationally independent methods have to be applied, such as isoelectric focusing in immobilized *pH* gradients, ion exchange chromatography, or high-resolution gel filtration.

Finally, solubilizing a peptide can be quite a challenge. Improper solubilization results in the loss of the peptide and/or failure of the purification. Whereas small peptides with five or less residues generally are soluble in aqueous media, the situation looks different for larger peptides [*51*]. Peptides containing less than 25% hydrophobic and more than 25% charged residues are considered as non-problematic to dissolve and to be purified by reversed-phase HPLC purifications. Peptides containing 50 to 75% hydrophobic residues are only poorly soluble in aqueous solvents, and peptides with more than 75% hydrophobic residues will generally not dissolve in water.

The purification of synthetic products is still one of the biggest challenges in chemical peptide synthesis. As peptides and proteins are a heterogeneous class of compounds in respect to their physiochemical properties, it is difficult to find a "general purification procedure" suitable for all peptides and proteins. Therefore, the use of affinity tags for the purification would enable a certain standardization of the cumbersome purification protocols.

3.2. Affinity Chromatography

In the post-genomic area, the procedures for the purifications of biomolecules became more and more important. Because the focus shifted from high-throughput analysis of genome sequences to functional and structural studies of the proteins, encoded by these genes. For peptides and proteins synthesized by solid-phase methods, the chemical and structural diversity is not different to recombinant proteins. Therefore, for the purification of peptides, the same techniques are applied as for recombinant protein (Table 1).

Table 1: Common techniques used for the purification of recombinant proteins.

Purification according to:	Technique
Charge	Ion exchange chromatography
Size	Size exclusion chromatography
Polarity	Normal-phase chromatography
Hydrophobicity	Reversed-phase chromatography
Biorecognition (ligand specific)	Affinity chromatography

Affinity chromatography is unique in purification technology since it enables the purification of biomolecules according to their biological function or individual chemical structure. The pioneering work of Porath and colleagues [52] and cyanogen bromide activation initiated the development of ligand immobilization chemistries, which allow the specific binding of affinity labels to chromatographic supports. The specifically adsorbed biomolecules can then be eluted leading to a product of high purity. The first affinity chromatography separation was performed by Anfinsen *et al*. [53], who demonstrated a successful purification of *Staphylococial* nuclease using porous gel technology.

Affinity chromatography is based on the highly specific and reversible interaction of a protein or peptide with a ligand, which is immobilized on a solid support. It is performed as a single-step purification and therefore offers immense time savings over less selective multistep purification procedures. Due to the concentration effect, large volumes of complex crude mixtures can be processed. Some of the specific interactions used for affinity purifications are listed in Table 2.

Table 2: Common techniques used for the purification of recombinant proteins.

Immobilized ligand	Purification target
Enzyme	substrate analog, inhibitor, cofactor
Antibody	antigen, virus, cell
Lectin	polysaccharide, glycoprotein, cell surface receptor, cell
Nucleic acid	complementary base sequence, histones, nucleic acid polymerase, nucleic acid binding protein
Hormone, Vitamin	receptor, carrier protein
Metal ions	Poly (His) fusion proteins, native proteins with histidine, cysteine and/or tryptophan residues on their surfaces

In recent years, affinity purification of recombinant proteins has been greatly facilitated by the employment of affinity tags, obtained by recombinant expression. The protein to purify is expressed together with the tag and is loaded as a crude cell lysate onto the affinity column for the purification. Such an affinity tag should share the following features [54]: It should (a) allow purification in one single step; (b) have a minimal effect on tertiary structure and biological activity of the protein; (c) allow an easy and specific removal to produce the native protein; (d) allow a simple and accurate detection of the recombinant protein during purification; and finally (e) be applicable to a number of different proteins.

3.2.1. Purification Tags

During the past years, a plethora of different tag systems evolved, which have been applied to the production of recombinant proteins on a large scale. The most commonly used small peptide tags are the poly-Arg- [55], FLAG- [56], c-myc- [57], S- [53, 54], Strep II- [58], and the His-tag [59]. Small tags are thought to interfere less with the fused protein and are therefore preferred over bigger tags. When a small tag has no effect on the tertiary structure, it may even not be removed from the fusion protein. Bucher *et al*. could demonstrate that the effect of small tags on the tertiary structure and therefore on the bioactivity of the recombinant proteins is depending on the location and on the amino acid composition [60]. Larger tags, often used to increase the solubility of the target protein, may have an impact on the folding properties of the protein. Examples of larger tags are HAT (natural histidine affinity

tag) [*60*], the calmodulin-binding peptide [*61*], the cellulose-binding domain [*59, 60*], the streptavidin-binding protein [*62*], the chitin-binding domain [*63*], the glutathione S-transferase [*64*], and the maltose-binding protein [*65*]. In the following, a selection of different tag systems will be briefly discussed. Information about the His-tag will be given in section 3.2.4 in more detail. Table 3 presents all tags including their purification matrix and elution conditions.

Table 3: Overview about the most frequently used affinity tags for the purification of recombinant proteins (from [*54*]).

Affinity tag	Matrix	Elution condition
Poly-Arg	Cation-exchange resin	NaCl, linear gradient at *pH* >8.0
His-tag	Ni^{2+}-NTA, Co^{2+}-CMA (Talon)	Imidazole or low *pH*
FLAG	Anti-FLAG monoclonal antibody	*pH* 3.0 or 2 - 5 mM EDTA
Strep-tag II	Strep-Tactin	Desthiobiotin
c-myc	Monoclonal antibody	Low *pH*
S	S-fragment of RNase A	Guanidine thiocyanate, citrate, $MgCl_2$
HAT	Co^{2+}-CMA (Talon)	Imidazole or low pH
3x FLAG	Anti-FLAG monoclonal antibody	*pH* 3.0 or 2 - 5 mM EDTA
Calmodulin-binding peptide	Calmodulin	EGTA (additional NaCl)
Cellulose-binding domain	Cellulose	Family I: guanidine HCl or urea Family II/III: ethylene glycol
Streptavidin-binding protein	Streptavidin	Biotin
Chitin-binding domain	Chitin	Fused with intein: dithiothreitol, β-mercaptoethanol or cysteine
Glutathione S-transferase	Glutathione	Reduced glutathione
Maltose-binding protein	Cross-linked amylase	Maltose

For each affinity tag specific buffer conditions are applied, which could affect the protein of interest. Therefore, the proper choice of a purification system is crucial for the success of the purification. The sequences and sizes of the different tags are shown in Table 4.

The **poly-Arg-tag** consists of five to six arginine residues, which can be used for purification by cation exchange chromatography. Generally, the tag is attached to the C-terminal of recombinant proteins expressed in bacterial systems. It leads to proteins with a purity of more than 95% and yields of 44% [*55*]. Elution is performed under basic conditions and addition of sodium chloride to compete with the positively charged arginine residues. In some cases, the purification is hampered due to a hindered accessibility of the tag. In this regard, Sassenfeld *et al.* reported interactions

of the poly-Arg-tag with hydrophobic C-terminal regions of target proteins [55]. The poly-Arg-tag is further used for the immobilization of various targets on flat surfaces as routinely used in scanning probe microscopy [66].

Table 4: Sequence and size of affinity tags (from [54]).

Affinity tag	No. of residues	Sequence	Size [kDa]
Poly-Arg	5 – 6	RRRRR	0.80
His-tag	5 – 6	HHHHHH	0.84
FLAG	8	DYKDDDDK	1.01
Strep-tag II	8	WSHPQFEK	1.06
c-myc	11	EQKLISEEDL	1.20
S	15	KETAAAKFERQHMDS	1.75
HAT	19	KDHLIHNVHKEFHAHAHNK	2.31
3x FLAG	22	DQKDHDGDYKDHDIDYKDDDDK	2.73
Calmodulin-binding peptide	26	KRRWKKNFIAVSAANRFKKISSSGAL	2.96
Cellulose-binding domain	27 – 189	Domains	3.00-20.00
Streptavidin-binding protein	38	MDEKTTGWRGGHVVEGLAGELEQLRARLEHHPQGQREP	4.03
Chitin-binding domain	51	TNPGVSAWQVNTATYTAGQLVTYNGKTYKCLQPHTSLA GWEPSNVPALWQLQ	5.59
Glutathione S-transferase	211	Glutathione	26.00
Maltose-binding protein	396	Cross-linked amylase	40.00

The **FLAG-tag** is a short, hydrophilic peptide consisting of eight residues. It still remains controversial, whether its binding to the monoclonal M1 antibody is calcium-dependent [67] or not. Since non-denaturing conditions can be used for the purification, the isolation of active proteins is possible. Elution can easily be done by addition of EDTA or by a transient reduction of the *pH*. Schuster *et al.* reported a successful purification of FLAG-tagged proteins expressed in yeast cells with a purity of 90% [68]. The development of the 3x FLAG system was purely motivated by the improvement of the detection limit via antibodies down to 10 fmol of expressed protein.

The **Strep-tag II** was developed for the purification on Strep-Tactin columns. The octapeptide shows an affinity of about 1 µM to Strep-Tactin [69]. The purification conditions are highly variable, allowing their specific adoption to the target protein.

Additions like chelating agents, mild detergents, reducing detergents, or salt up to 1 M do not destroy the specific binding. For the elution, 2.5 mM desthiobiotin is applied. The method is suitable for the purifications of native proteins with the tag attached either to the N- or the C-terminal [70] and for metal-containing enzymes [71]. The application range of the Strep-tag has permanently increased during the past years, since the tag is also used in NMR experiments and crystallization [72].

N- or C-terminally **c-myc-tag**-bearing proteins can be purified by covalently coupling the monoclonal antibody 9E10 to divinyl sulphone-activated agarose [73]. Washing can be achieved under physiological conditions followed by elution at low *pH*, which proved harmful for the target protein. The application of the c-myc-tag is predominantly focused to detection than to purification.

The **S-tag** is a 15 amino acid-tag derived from RNase A [53, 54]. It interacts with a strong K_D of 100 nM to the 103 amino acid S-protein, which is also derived from RNase A. This strong interaction depends on *pH*, temperature, and ionic strength [74]. Due to four cationic, three anionic, and three polar residues the S-tag is highly soluble in aqueous solvents. Due to its high binding affinity, elution has to be performed under very harsh conditions such as *pH* 2. Due to the discovery of a hypersensitive fluorogenic substrate for RNase A, the system has gained special interest for detection in combination with high-throughput screenings [75].

The **calmodulin-binding peptide** is a widely used tag due to its high specificity to calmodulin. This tag is often used for the purification of recombinant proteins derived from *E. coli*, because no endogenous proteins of this organism are known to interact with calmodulin. This leads to high recoveries of fusion proteins of 80-90%. The tag consists of a 26 amino acids, which binds calmodulin in the nanomolar range in presence of 0.2 mM $CaCl_2$ [76]. The tight binding allows stringent wash conditions, which lead to only few contaminants after elution with EGTA. The system is not suitable for purifications in eukaryotic cells, as many endogenous proteins interact with calmodulin in a calcium-dependent manner [77].

The main driving forces for the binding of the **cellulose-binding domain** (CBD) to cellulose are hydrogen bond formation and van der Waals interactions [78]. Over 120 different CBD sequences have been identified and classified into at least 11 families [79]. Domains belonging to family I, II and III are predominantly used as

affinity tags. Tags belonging to family I are inert, available in many different forms, and have been approved for many pharmaceutical and human uses. In addition, it can be used in a wide *pH* range from 3.5 up to 9.5. The only disadvantage is the tight binding, which requires elution buffers containing urea or guanidine hydrochloride. Therefore, the target protein has to be refolded after purification. For this reason, McCormick *et al.* [*80*] developed a milder purification system using CBDs from family II and III, which can be eluted using ethylene glycol.

The **streptavidin-binding peptide** (SBP-tag) has a length of 38 amino acids and developed from the Strep-tag II. It binds with a high affinity (K_D = 2.5 nM) to immobilized streptavidin [*62*], and can therefore be used for stable immobilization of proteins on streptavidin coated chips [*81*].

The **chitin-binding domain** is a 51 amino acid-tag, which is derived from *Bacillus circulans*. The tag suffers from rather high non-specific binding, which can be lowered by the use of non-ionic detergents and high salt concentrations. Elution has to be done using 1% SDS in 6 M guanidine•HCl leading to unfolded proteins. Therefore, it is mostly used together with so-called self-splicing inteins, which will be discussed later in this section.

One of the most frequently used tags is the **glutathione S-transferase** (GST)-tag. The first application with this 26-kDa tag was performed by Taylor *et al.* [*82*] with a fusion protein expressed in *E. coli*. In most cases, after elution with 10 mM reduced glutathione, the fusion proteins are stable, however they sometimes form dimers. However, in some cases, the fusion protein is partially or even totally insoluble, a property associated with the presence of hydrophobic regions in the GST sequence. Interestingly, insolubility was more pronounced for fusion proteins larger than 100 kDa.

Proteins fused to the 40-kDa **maltose-binding protein** (MBP) can be purified by one-step affinity chromatography on cross-linked amylase. Elution is activated with 10 mM maltose in physiological buffer. The MBP-tag is often used to increase solubility in combination with smaller affinity tags for poorly soluble fusion proteins [*83*].

Besides their purification task, affinity tags may elicit a number of positive effects on the expression of recombinant protein such as enhancement of solubility, efficient initiation of translation, or an increased stability against degradation. Thus, some tags

are employed for the sole reason to enhance solubility and do not show any affinity to the purification matrix (*e.g.* NusA [*84*], thioredoxin [*85*], or SET [*86*]).

3.2.2. Removal of Tags and Combinatorial Approaches

Especially large tags have a tendency to interfere with the proper protein folding. Therefore, they might have an impact on the biological activity, might impede the crystallization, or influence the behavior of the fusion protein. Hence, it is usually desirable to remove the tag, to obtain the pure and native protein. Nowadays, highly specific endoproteases are available, such as those encoded by the tobacco etch virus AcTEV from Invitrogen [*87*] or the human rhinovirus PreScission from Amersham Biotech [*88*]. Nevertheless, the processing efficiency highly varies for each fusion protein leading to time-consuming optimizations of the digestions.

Factor X_a with the recognition sequence IEGR and enterokinase with DDDDK are well suited for the cleavage of N-terminal tags (Table 5). Since they cleave at the C-terminal end of the recognition sequence, native N-termini of the target protein can be generated. Unfortunately both proteases often cleave fusion proteins at locations other than the desired site due to low sequence specificity [*83, 84*]. More stringent proteases like TEV and PreScission have recognition sites, leading to one or two amino acid truncs on the native protein stemming from the tag.

Table 5: Cleavage site of different proteases.

Protease	Recognition sequence
Factor X_a	Tag-IEGR-↓Protein Tag-DDDDK↓-Protein
TEV	Tag-ENLYFQ↓S-Protein
PreScission	Tag-LEVLFQ↓GP-Protein

↓ cleavage site of the protease

Proteolytic methods for the C-terminal cleavage of tags are much more difficult to find, as all of them usually leave at least 4-6 extra non-native residues on the C-terminus of the native protein. Therefore, they have been used only to a limited extent to remove short C-terminal tags [*89, 90*].

An elegant method is the so-called intein method, reported by Chong *et al.* [*91*]. The idea is to integrate a self-cleaving element, called an intein, between the target protein and the tag (Figure 4).
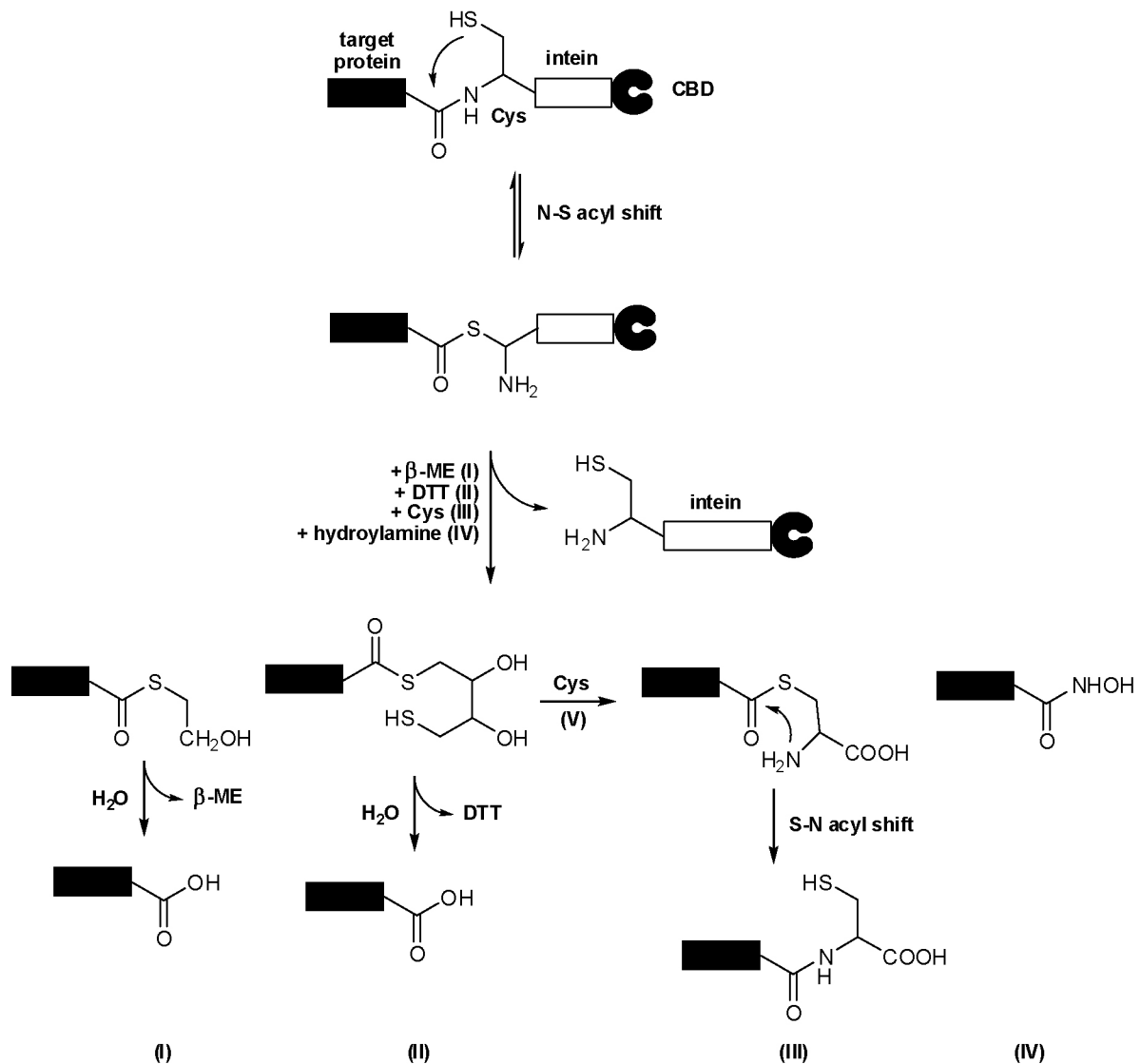
Figure 4: Autolytical splicing of intein from host protein. Fusion protein consists of target protein and a C-terminal chitin-binding domain (CDB). The tag is linked via the intein to the C-terminal end of the target protein. The intermediate thioester is cleaved upon addition of I, II, III, or IV. Final workup depends on the desired C-terminal end; from [*91*].

Per definition an intein is a segment of a protein, which is able to excise itself and connect the remaining parts, the exteins, by a peptide bond. Most of these inteins contain an endonculease domain to cleave the peptide bonds. Therefore, a mutant (Asn454Ala) of the VMA intein from *Saccharomyces cerevisiae* was produced to inactivate its splicing and C-terminal cleavage activity. Now, the mutated intein is able to catalyze an N-S acyl shift at its N-terminal cysteine residue, which results in a

thioester bond. Addition of β-mercaptoethanol, dithiothreitol (dtt), cysteine, or hydroxylamine leads finally to the cleavage of the thioester bond.

Despite the innovative approach, the intein method suffers from the large size of the catalytic machinery, which forces the cells to produce this huge construct. As for most cleavage methods, the efficiency is highly dependent on the sequence at the cleavage site. In addition, the autoprocessing occurs at a very slow rate, a further drawback of this strategy.

As no single tag is ideal for all proteins, a combinatorial approach was developed by Tropea *et al.* [*92*] using a dual tag system consisting of a His_6-MBP affinity tag (Figure 5).
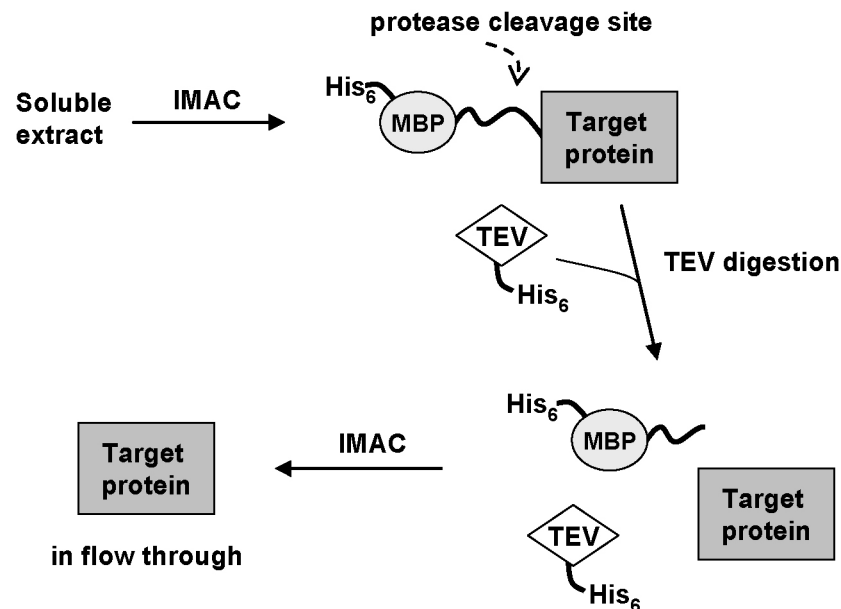
Figure 5: Schematic illustration of combinatorial tag approach using His_6-MBP tag. IMAC: immobilized metal ion affinity chromatography; MBP: maltose-binding protein; TEV: tobacco etch virus protease.

The MBP part is only attached to improve the yield and enhance the solubility and is not used for purification purposes. After a first purification of the fusion protein via a Ni-NTA column directed towards the hexahis-tag, the tag is cleaved by the TEV protease. This protease is His-tagged as well and can therefore by removed together with the His_6-MBP tag in a second IMAC. The uncleaved fusion proteins, His_6-MBP tags, and the His_6-TEV will be retained, whereas the pure protein is eluted in the flow-through.

3.2.3. Immobilized Metal Ion Affinity Chromatography (IMAC)

A special affinity purification method is the so-called immobilized metal ion affinity chromatography (IMAC). This technique was first proposed by Porath *et al.* in 1975 [*93*]. Actually, the principle of IMAC was developed much earlier [*94*], but Porath *et al.* were the first to apply this purification principle to the separation and isolation of proteins. The method is based on different affinities of proteins for metal ions, which are tightly bound to a metal chelator, which is immobilized on the solid support. Electron-donating groups present on the protein surface coordinate to the metal ion. The principle of IMAC is demonstrated in Figure 6.
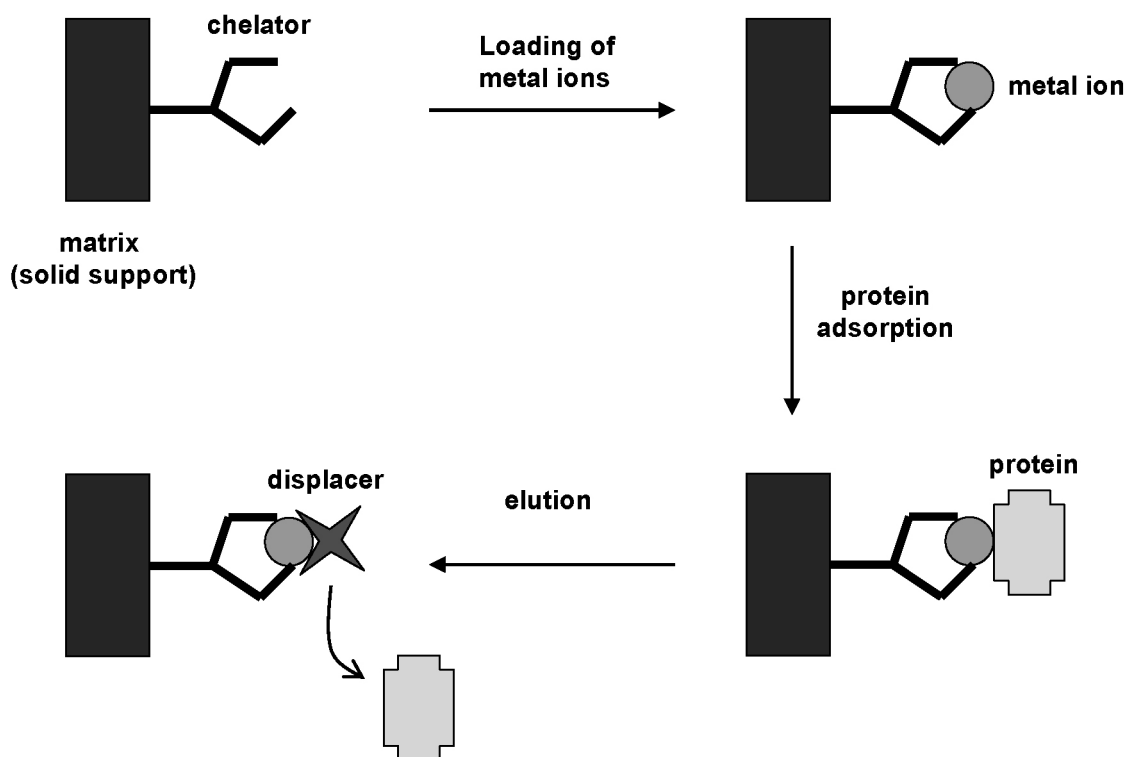
Figure 6: The principle of immobilized metal ion affinity chromatography (IMAC). After loading of the solid support with the metal ions, the protein is able to adsorb to the solid support. Elution is performed by addition of a displacing molecule.

In a first step, the metal ions are loaded onto the column by coordination with the immobilized metal ions. The oligodentate chelator is able to bind the ion tightly to the solid support. With its free coordination sites, the metal ion can coordinate with the protein. For the final elution of the protein a displacer (*e.g.* imidazole) is added. The

strength of the interaction between protein and metal ions is protein dependent, which allows the separation and isolation of a specific target.

The differences in affinity of the proteins to the metal ion can be explained by the hard-soft-acids-base (HSAB) theory [95]. For each interaction formed, one of the binding partner acts as a Lewis acid and the other as a Lewis base. The strength of the interaction is depending on the atoms rating as "hard" or "soft". The theory states that bonds between atoms with similar ratings, *e.g.* soft acid combined with soft base, are stronger than the one between odd partners. Metal ions such as K^+, Ca^{2+}, Mg^{2+}, and Fe^{3+} belong into the group of hard Lewis acids, whereas electron-rich ions like Ag^+ and Cu^+ are classified as soft Lewis acids. In between hard and soft Lewis acids, there are the so-called borderline acids, such as the transition metal ions Co^{2+}, Zn^{2+}, Cu^{2+}, and Ni^{2+}. According to the HSAB theory, three major types of ligands can be predicted for the various metal ions. Ligands containing oxygen (*e.g.* carboxylate), aliphatic nitrogen (*e.g.* asparagine and glutamine), and phosphor (*e.g.* phosphorylated amino acids) form the group of the hard Lewis bases. Ligands with sulfur (*e.g.* cysteine) are classified as soft Lewis bases, and those with aromatic nitrogens (*e.g.* histidine, tryptophan) belong to the group of borderline bases. Therefore, the transition metals mentioned above prefer to coordinate with aromatic nitrogens and to a lesser extent with sulfur atoms [96].

As already stated by Porath *et al.* [93], His, Trp, and Cys undergo the strongest interactions to borderline metal ions and are therefore the key players in IMAC technology. In addition, they all provide electrochemical and redox stability under chromatographic conditions as well as redox stability [97]. However, a high retention on the sold support does not enforcedly correlate with good separation, since a high retention capability could also lead to an increased adsorption of impurities [98]. In many cases, the retention behavior is largely controlled by histidines exposed on the protein surface [99, 100], because His can interact via imidazole with the immobilized metal ion. In addition, cysteines also display metal ion affinity, although to a lesser extent [98, 101], by an interacting with their sulfhydryl group. Several other functionalities present on protein surfaces can influence the retention on metal ion matrices: α-amino groups via a direct interaction to the metal ion [102]; Trp, Phe, and Tyr acting directly via their aromatic side chains [98]; and Arg, Lys, Asp, and Glu

acting indirectly on the accessibility of His residues [98]. Finally, special amino acid sequences, folding, and overall surface properties further complicate the prediction of the retention behavior of a specific protein. Nevertheless, Kagedal *et al.* [103] proposed a rule for the choice of the correct metal ion based on accessible His und Trp residues on the protein surface (Table 6) leading to satisfying results in separation of the target protein from the impurities.

Table 6: Protein metal ion affinity prediction based on accessible His and Trp residues.

Occurrence of accessible His and Trp on the protein surface	Metal ions providing retention
No His/Trp	-
1 His	Cu(II)
> 1 His	Cu(II), Ni(II)
His clusters	Cu(II), Ni(II), Zn(II), Co(II)
Several Trp, no His	Cu(II)

In IMAC, oligodentate chelators are used to immobilize metal ions. The chelators are covalently linked to the support by linkers of various length and composition. To allow interaction with the protein, the chelators must leave free coordination sites on the metal ion. Iminodiacetic acid (IDA) [93] and nitrilotriacetic acid (NTA) [59] are the most frequently used chelators in IMAC (Figure 7).

Ni(II)-IDA   **Ni(II)-NTA**
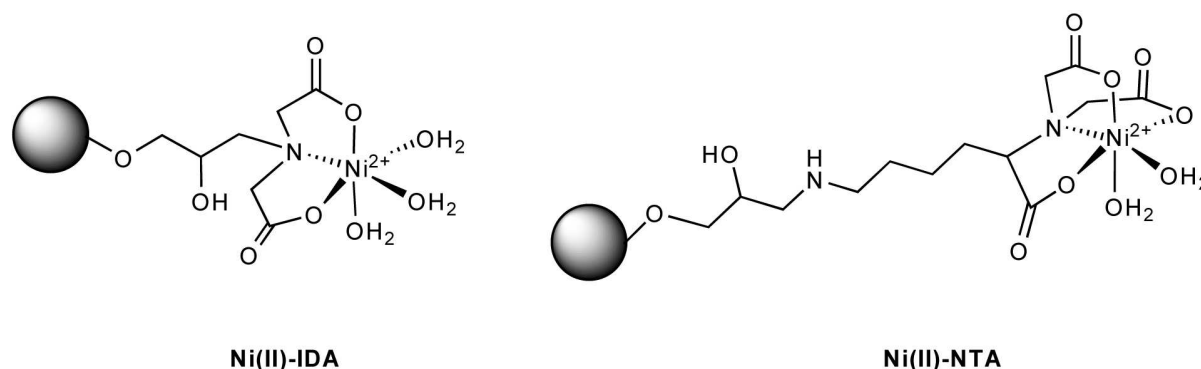
Figure 7: Structures of the two commonly used chelators in IMAC. Chelators are covalently attached to a solid support and can be loaded with metal ions (*e.g.* Ni^{2+}, Co^{2+}, Fe^{2+}, Zn^{2+}).

IDA binds a metal ion via two carboxylate oxygens and the central nitrogen. Thus, with Ni^{2+} having an octahedral coordination site, three additional interactions with the protein are possible. In NTA, an additional carboxylate leads to a stronger chelation of

the metal ion. However, protein retention may be decreased as only two coordination sites are left in case of Ni^{2+} [103]. Due to a stronger metal binding in case of NTA, the risk of metal leaching is lowered leading to a more stable surface and less contamination of the protein with metal ion. [104].

Many other chelators have been designed over the last few decades, all having advantages as well as limitations. Some of them are, similar to IDA and NTA, based on carboxymethylated amines such as tetraethylene pentamine (TEPA) or carboxymethylated aspartic acid (CM-ASP) [101]. Other commonly used chelators with different chemical structures are reactive dye light-resistant yellow 2KT [105], dipicolylamine (DPA) [106], *O*-phosophoserine (OPS) [107], and 8-hydroxyquinoline (8-HQ) [107]. For the structures of the different chelating ligands see in Figure 8.
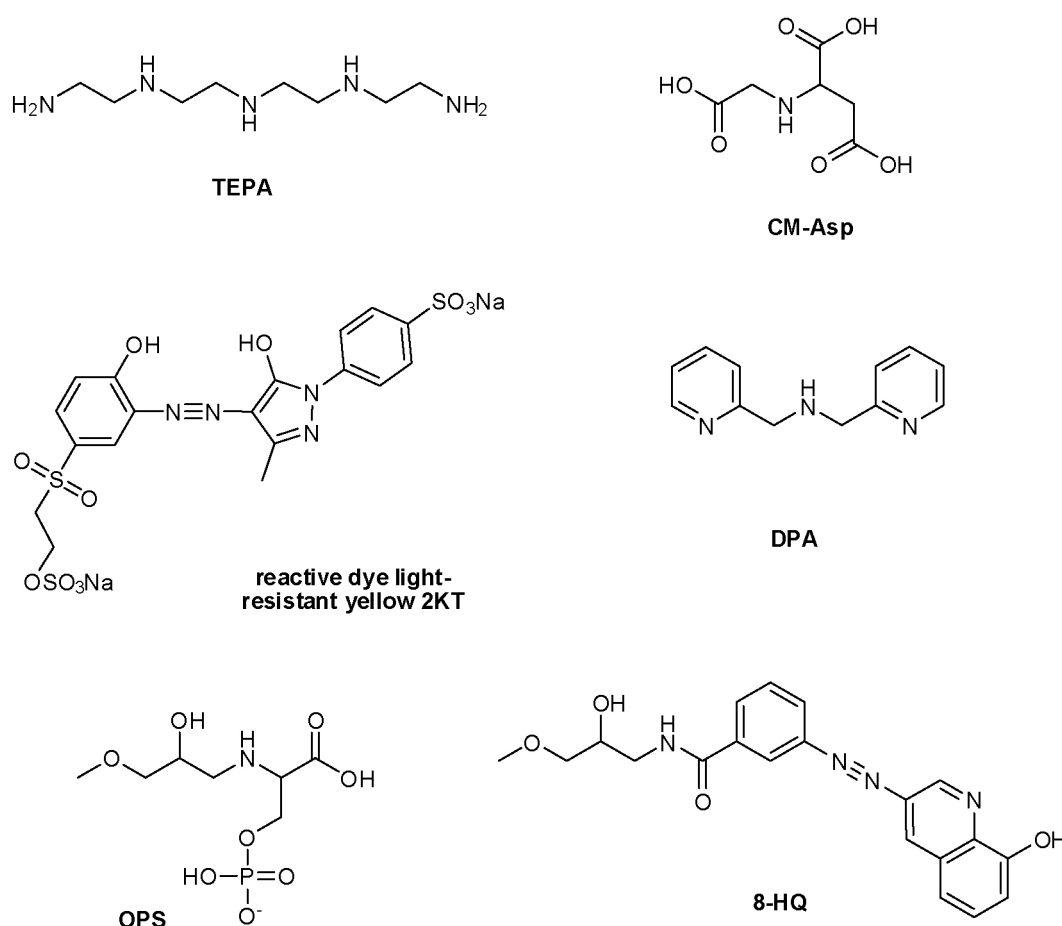
Figure 8: Structures of different metal ion chelators used in IMAC technology binding either in a tri- or tetradentate manner.

The proper combination of chelator and metal ion is crucial in regard to protein retention. Chelators were found to influence protein retention, such as complex coordination geometry, charge, steric bulk, and chirality [98]. Finally, Lehr *et al.* stated that also the resins can alter protein retention as a result of interactions between the protein-metal complex and the chelating resin [108].

The transfer of metal ions from the chelators to the protein in solution is called "metal ion transfer". When a protein or solute is able to disrupt the chelator-metal binding and therefore to strip off the metal ion from the solid support, the protein will be found in the flow through, contaminated with metal ions [109].

Originally, the column material, to which the chelator is covalently attached, was mainly agarose. Nowadays, different supports are used such as cellulose, cross-linked agarose, different polymers, silica, or polystyrene [103]. According to Ueda *et al.* [97], the ideal support should meet the following physicochemical characteristics: It should (a) be easy to derivatize, (b) not exhibit non-specific adsorption, (c) display good physical, mechanical, and chemical stability, (d) possess high porosity to provide easy ligand accessibility, (e) allow use of high flow-rates, (f) be stable to eluents including denaturing reagents, (g) permit regeneration of columns without degeneration of the matrix, and (h) provide a stable gel bed with no shrinking or swelling during the chromatographic run.

The influence of the chelate structure and the metal ions on protein retention were already discussed. Other factors altering protein selectivity in IMAC are ionic strength of the buffer or *pH* [103]. When sodium chloride (0.1 – 1.0 M) is used, ionic interactions between sample and matrix are suppressed, whereas *pH* changes alter the protonation state of the binding amino acids. Generally, when a *pH* range between 6 and 8 is used, the coordination of His and Cys residues is favored. At higher *pH*s, deprotonation of Lys and Arg leading to additional coordination ligands decreases the selectivity of the purification process [101].

Addition of detergents is widely accepted as selectivity enhancer in IMAC, because of their capability to diminish undesirable interactions [103]. A similar effect is achieved when the proteins are eluted with displacers showing a higher affinity for the adsorption sites than the protein. The monomeric ligand imidazole by can be

improved by the formation of imidazole polymers, which show an improved elution strength and therefore a better selectivity [*110*].

As all purification methods, IMAC has also its pros and cons. To understand the success of IMAC in protein purification, a comparison to other types of affinity chromatography, especially immunoaffinity chromatography should be made. Although, both techniques are based on the specific interaction between protein and ligand, but nevertheless, IMAC elicits a number of advantages as presented in Table 7 [*97*].

Table 7: Comparison between IMAC and standard affinity chromatography.

Feature	Metal affinity	"Bio-affinity"
Ligand stability	High	Low
Protein loading	High	Low
Elution conditions	Mild	Often extreme
Ligand recovery after column regeneration	Complete	Generally incomplete
Selectivity	Low-medium	High
Costs	Low	High

Since most proteins lack metal affinity and cannot be purified via this technique, purification tags are attached to overcome this limitation. Insertion of a N- or C-terminal oligohistidine-tag, which is exposed on the protein surface, allows a selective purification of the target protein [*90*]. Now, the lack of metal affinity of most proteins is beneficial, as they will not undergo unspecific interactions. Nevertheless, some proteins do show metal affinity, *e.g.* superoxide dismutase expressed from *E. coli*, and will therefore disturb the purification process [*100*].

Since there is no need for extreme *pH* conditions during loading, washing and elution, IMAC is regarded as a mild purification method. The high selectivity in case of an attached affinity tag allows in most cases a single step purification with high protein loading capacities of $0.1 - 10$ µM per mL of gel [*96*]. IMAC can also be applied to industrial applications, as the costs are low and upscaling fairly easy and reproducible [*96*]. In addition, the same resin can be regenerated several hundred times with a high recovery [*96*]. Upon addition of strong chelators as EDTA or EGTA, metal ions can be removed, and the same resin can be loaded with different metal ions providing a certain degree of flexibility. This is also ensured because various buffers

can be used, as IMAC is known to be compatible with high ionic force and chaotropic components [*96*]. The use of IMAC is not only restricted to the purification of recombinant proteins, but can also be used for transient sterilization (removal of metal ions essential for bacterial growth) [*96*], or for the concentration of dilute protein solutions [*96*].

Recently, new variants of IMAC have been developed as alternatives to the existing technique. One new application is immobilized metal ion affinity partitioning (IMAP) in aqueous two-phase systems, where polyethylene glycol (PEG), covalently linked to metal chelates and loaded with metal ions, is introduced to increase the partitioning of metal binding proteins in the PEG phase [*111*]. IMAP is also used to study surface features among structurally related proteins. Finally, a further development of IMAC is immobilized metal ion affinity gel electrophoresis (IMAGE) [*112, 113*] and capillary electrophoresis (IMACE) [*114*].

3.2.4. The Hexahistidine-Tag (His-tag)

For the purification of recombinant proteins, IMAC is often used in combination with oligohistidine-tags as demonstrated in the pioneering work of Hochuli *et al*. [*90, 115*]. Typically, tags consisting of five to six consecutive histidine residues are used. Since it is rather rare that such oligohistidine segments are expressed in naturally occurring proteins, 5His- or 6His-tags guarantee high selectivity. Binding of the His-tag occurs via its imidazole nitrogens, which are able to occupy two coordination sites in the Ni-NTA complex. The column material consists of Sepharose covalently linked to NTA (Figure 9).

Besides the successful Ni-NTA resin, BD TALON™ resins are an alternative to purify recombinant His-tagged proteins [*116*]. TALON resins are loaded with Co^{2+} instead of Ni^{2+}, and the tetradentate chelator has a slightly modified structure compared to Ni-NTA (Figure 9). Both chelators were mainly introduced due to the higher metal ion binding affinity between chelator and metal ion compared to IDA. As a consequence, metal ion leaching could be reduced.
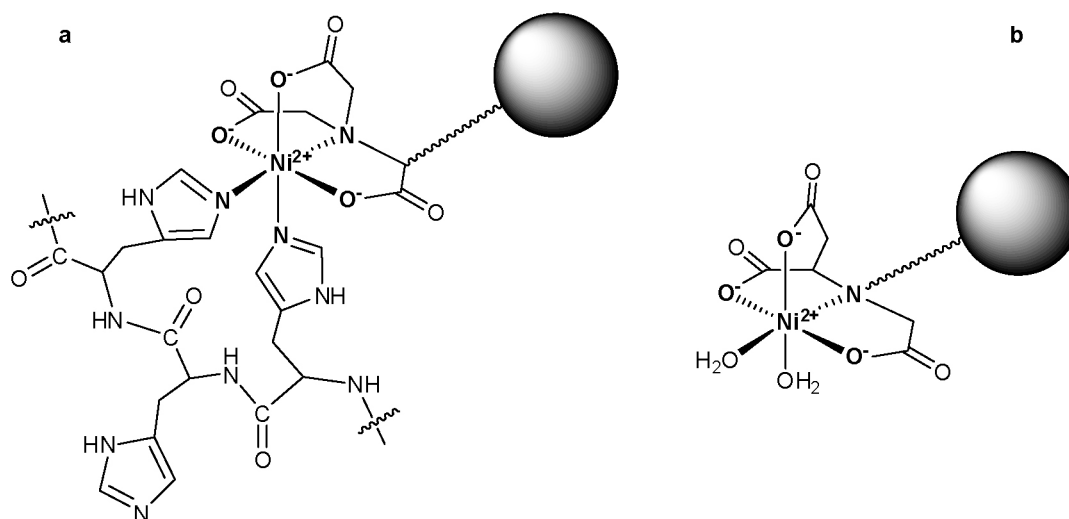
Figure 9: a: His-tag bound to Ni-NTA via imidazole nitrogens. Ni^{2+} is complexed by three carboxylic acids and the central nitrogen of NTA, which is covalently attached to a solid support. b: TALON resin from Clontech Laboratories.

The histidine sequence is introduced on the DNA level to the N- or C-terminal end of the target protein. After cell lysis, the crude mixture containing the overexpressed protein and all other cell fragments is loaded onto a Ni(II)- or Co(II)-NTA column, which retains the His-tagged protein, whereas the rest of the cell content can be eluted. In the next step, the bound target protein is eluted by increasing the concentration of imidazole. Numerous successful purifications using N- or C-terminally bound His-tags were reported, *e.g.* the purification of glutathione S-transferase P1-1 [*117*], murine interleukin 12 [*108*], cytochrome b5 [*118*], green fluorescent protein [*119*], chicken lactate dehydrogenase [*120*], mitochondrial ADP/ATP carrier protein [*121*], HTLV-I surface envelope glycoprotein fragment [*122*], just to mention the most prominent examples.

Although the His-tag is mainly used for the separation of recombinant proteins, its utilization is much more diverse. A common drawback of protein expression in bacteria is the formation of inclusion bodies containing the target protein in a misfolded and non-functional state. Even in the presence of aid devices, which should support help for proper folding (*e.g.* co-expression of chaperones, optimization of growth conditions), a refolding step is usually unavoidable to achieve acceptable yields of functional protein from inclusion bodies [*123*]. Addition of a His-tag may help in a "matrix-assisted refolding". In this procedure, the renaturation step is carried out by applying a linear change from denaturing to renaturing conditions or by

iterative refolding, a technique based on repeated cycles of renaturation and denaturation. During the matrix-assisted refolding, the target protein is bound via the His-tag to the Ni-NTA support. After renaturation, the fully functional protein can be eluted in its native and soluble form [*105, 124*]. Another application is the immobilization of His-tagged proteins to a matrix in a defined spatial orientation. Immobilization of target proteins is generally used to study interactions between biomolecules, such as protein-protein, protein-lipids, protein-drugs, and protein-DNA interactions. A site-specific immobilization is advantageous compared to random immobilization as it allows improved accessibility of the binding sites and increased stability [*125*]. Especially in the field of the evolving biosensors methods, site-specific immobilizations are highly demanded. For the Biacore system, using surface plasmon resonance detection to determine thermodynamic and kinetic binding parameters, a Ni(II)-chelating NTA-chip is commercially available (GE Healthcare) allowing the preparation of stable immobilized protein chips, which can be applied for repetitive injections [*126*]. Zhu *et al*. [*127*] reported another application, the successful stable immobilization of His-tagged proteins on a nickel-coated glass slide. Proteins immobilized via Histidine-tags clearly were superior to proteins immobilization via aldehyde-treated glass slides. Finally, the NTA/His-tag system was also used to anchor proteins to an atomic force microscopy tip applied for the investigation of binding forces of receptor-ligand systems at a single molecule level [*128*].

3.2.5. The Need for New Purification Tags

Although the His-tag technology has become a standard procedure for the purification as well as the immobilization of recombinant proteins [*126, 129*], the chelating properties of His-tags at a molecular level are still not fully understood. Only some recent studies contributed a few basic mechanistic information: Investigations with single-molecule experiments using scanning force microscopy revealed that His-tags are forming various types of complexes, which significantly differ in stability and energy profile along their dissociation pathway [*128, 130*]. It was demonstrated that a 2His-tag forms less stable complexes with Ni-NTA, compared to a 6His-tag. In addition, the binding mechanism of metal ions to various His-tag motifs was

investigated by computational approaches [*131*], which showed that a 6His-tag has mainly two preferred binding motifs, 1-3 (**His**-His-**His**) and 1-6 (**His**-His-His-His-His-**His**). This was at least partly confirmed by an investigation of Bernaudat *et al.* [*132*], who studied different His-tags coupled to lactate dehydrogenase to gain more information about the influence of the target protein on the binding properties. The **His**-Xaa-**His** motif elicited the best retention on Ni-IDA columns as also the most stable immobilization on Ni-NTA chips in Biacore experiments. Furthermore, a study on the stability of His-tagged proteins/Ni^{2+}-NTA complexes and their applicability to protein immobilization in surface plasmon resonance experiments was published by Plückthun and collaborators [*126*]. Very recently, Kozlov *et al.* [*133*] reported results of a huge peptide series investigating their behavior on Ni-NTA columns. They found that the retention of the histidine-containing peptides depends on the arrangement of histidines within the sequence, but also on the amino acid composition of neighboring sequences. Trp and Arg, and to a lesser extent Lys and Phe, seem to increase the affinity, whereas Glu and Asp decrease the affinity of His-tagged peptides on Ni-NTA columns. A more structurally related investigation reported on differences of His-tagged versus non-tagged proteins present as crystal structures [*134*]. From the presented structures, no structural impacts of the His-tag on the protein was observed although the *B* factors of the tagged structures were slightly increased because the N-terminal or C-terminal His-tags were generally disordered.

In spite of all advantages of the IMAC technology, the method has also its limits. The immobilization step, and consequently the whole purification procedure for recombinant proteins, is often greatly hampered by the inaccessibility of the His-tag caused steric hindrance [*135*]. When extended tags, *e.g.* 10His-tag [*136, 137*], or a combination of two His-tags at both termini of the protein [*126*] are introduced for improved accessibility, undesired changes in protein properties may often result, such as decreased solubility [*138*], misfolding [*139*], dimerization [*140*], inhibition of complex assembly [*141*], or even degradation [*142*]. A further drawback, especially for industrial use, is the problem of metal ion leakage or metal ion transfer [*96, 101*]. This leads to a contamination of the final product, which is absolutely not tolerable for pharmaceutical application. With the use of an additional chelating gel column this problem could be circumvented. However, this extra step would cause additional costs

and problems for the disposal of the contaminated metal residues. Furthermore, since the native structure is required for pharmaceutical-grade proteins, the His-tag has to be removed by chemical or enzymatic means after it has fulfilled its purpose in the purification step. Therefore, there is a need for tags with chelating properties that can be adapted according to the type of application. Independent of their use, ranging from purification to site-directed and stable immobilization on analytical surfaces, these tags should not interfere with the conformation and function of the native protein [143].

The need of new tags did not just evolve recently. During the last decades several newly developed metal ion-binding tags were reported. Smith *et al.* investigated the properties of various metal chelating peptides such as His-Gly-His, His-Tyr-NH$_2$, and His-Trp coupled to luteinizing hormone-releasing hormone (LHRH) for purification on Ni-IDA columns [144, 145]. Similar investigations are reported for angiotensin I, a decapeptide with high affinity for various metal ions [146]. This peptide was coupled to TEM-β-lactamase for the purification on Ni-IDA columns [147]. Finally, Ljungquist *et al.* achieved a satisfying retention of protein A domains and β-galactosidase on Zn-IDA columns with tags containing 4-8 repetitive His-Gly-His sequences [148].

For the development of new tags, a better understanding of the interaction mechanism of the Ni-NTA system would be beneficial. The determination of thermodynamic (K_A and K_D) and kinetic data (k_{on} and k_{off}) of ligands binding to Ni-NTA might add to a more profound knowledge of such purification systems and could therefore lead to further improvements.

3.3. Surface Plasmon Resonance (SPR)-based Biosensor: Biacore

Biacore measurements are based on the physical principle called surface plasmon resonance (SPR), arising from an electron density wave caused by an interaction of a p-polarized incident light beam with a metallic thin films [149]. In the 80ies Pharmacia Biosensor AB launched the first SPR detection system. In 1996, the company became Biacore AB and finally merged in 2006 with GE healthcare.

3.3.1. The Theory of Surface Plasmon Resonance

The SPR-phenomenon is based on total internal reflection (TIR), an evanescence electric field, and surface plasmon waves. When a beam of light propagating through a first medium of higher refractive index n_1 (*e.g.* a glass or quartz prism), meets the interface with a second medium of lower refractive index n_2 (*e.g.* an aqueous solution), total internal reflexion for all incident angles greater than a critical angle θ will occur (Figure 10, A). Despite the total reflexion, the incident beam establishes an electromagnetic field E_1 that penetrates a small distance into the second medium. Propagation in the second medium is always parallel to the plane of the interface. The amplitude of the evanescent wave E_1 decreases exponentially with distance from the surface, and the effective penetration depth is usually less than a wavelength of the incident light and therefore only a few hundred nanometers [150]. When a thin metal film is inserted at the interface between the glass/liquid interface, the phenomenon of surface plasmon resonance [151] can occur (Figure 10, B). Surface plasmons are waves of an oscillating surface charge density (conducting electrons) E_2, which propagate along the metal surface between the metal and the aqueous phase. Similar to the situation without metal film, the field amplitude of the surface plasmons decays with increasing distance perpendicular to the metal surface. Usually, the penetration of the evanescent wave reaches 100 – 200 nm into the dielectric medium. Surface plasmons are excited when an evanescence field, produced by the internal reflexion of a p-polarized incident beam, penetrates this layer and thereby enhances the evanescent wave. Surface plasmons are waves and are equivalent to photons in the case of light. A non-magnetic metal like gold is normally used for these metal layers [152-154].

To fully describe photons or surface plasmons, quantum physics is needed due to their electromagnetic nature. However, a simplification can be made by depicting each of the two wave momenta as a vector. The light photon momentum at the interface can be resolved into two vector components (parallel and perpendicular to the interface) as demonstrated in Figure 10, C. The magnitude of these incident light vectors directly depends on the light angle. Similarly, the surface plasmon wave is also described as a vector, which depends on a number of factors such as metal properties, layer thickness, surrounding media. In case that the energy and the momentum of the incident light vector exactly correspond to the one of the surface plasmon vector, resonance occurs, leading to the conversion of energy from photons into plasmons. The energy conversion can be detected by a drop in intensity of the totally reflected light beam. This drop is restricted to resonance conditions, otherwise no such conversion arises and the light is fully reflected (Figure 10, D).
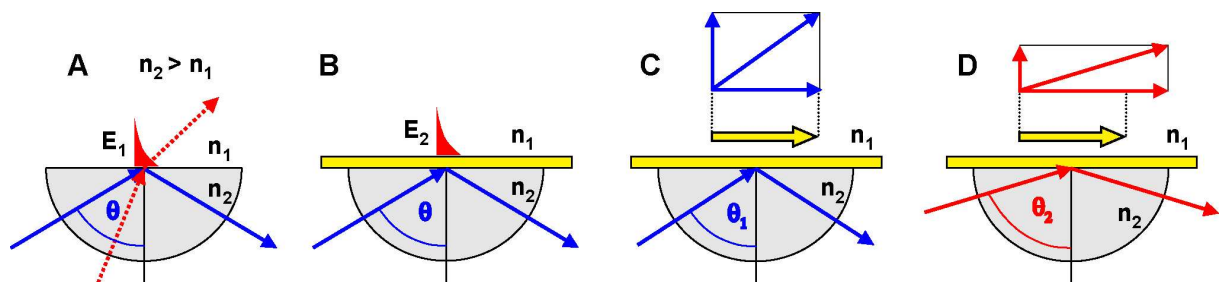
Figure 10: Principles of SPR. A: Total internal reflection (blue line) and refraction (red line) of a light beam in dependence of the incidence angle θ at the interface of two different media (n_1, n_2). B: Evanescence field wave leaking through a thin metal film (yellow). C, D: SPR in the gold surface. If the incident light vectors (component parallel to metal film) has not the same value than the surface plasmon vector, light is fully reflected (C). Only a specific angle leads to a matching of the two vectors and a resulting resonance (D).

In an experimental setup, metal nature and thickness as well as the properties of one medium are kept constant and resonance can be obtained only by variation of the angle of the incident light and the refractive index of the second medium. This allows monitoring refractive index changes in the second medium adjusting the incident light angle until a dip in light intensity (resonance) is detectable [*152-154*].

For Biacore experiments, sensor chips that carry a thin gold layer (50 nm) on a glass support are applied. The gold surface is in direct contact with a flow cell (sample) and a prism follows the glass side. A monochromatic, plane-polarized light beam at a wavelength of 760 nm is focused in a wedge on the gold surface and the total internal reflection is monitored on a diode array. The described evanescence field

wave penetrates into the flow cell and enables detection of refractive index properties to a distance of about 700 nm from the surface.

Biomolecular interaction measurements with SPR make use of the fact that binding of molecules to sensor surfaces alters the refractive index near this surface. In Biacore systems such a change is recorded by a change of the incidence light angle at which resonance occurs. This change can finally be converted into a response signal (Figure 11). The response signal is measured in resonance units (RU) corresponding to a shift in the resonance angle of approximately 10^{-4} degree [153]. The mass of the molecule and its influences on the refractive index is directly related, explaining why SPR biosensors are often referred to as mass detectors. The correlation between sensor signal and mass increase was found to be 1 pg/mm^2 for 1 RU [155]. This experimental value was determined for a protein that binds to the metal surface.
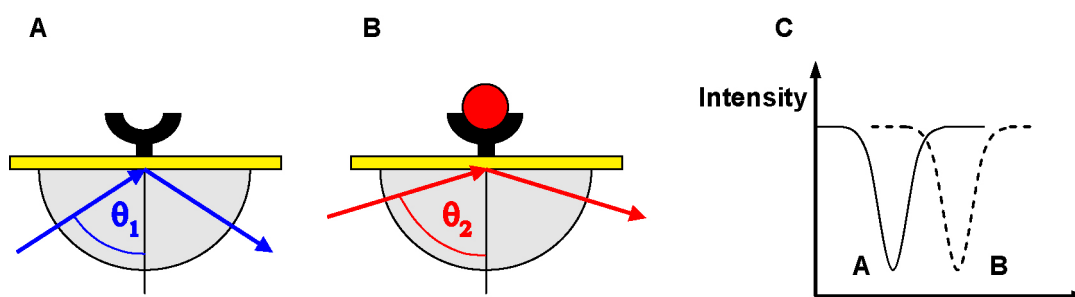
Figure 11: Detection of biomolecular interaction by SPR. A, B: Sensor surface before and after interaction of ligand. C: Shift of light intensity dip upon interaction.

This correlation is almost constant for molecules with high protein and low lipid and carbohydrate content [153]. The relationship can be extrapolated to other molecules such as nucleic acids, carbohydrates, lipids or conjugate molecules. Despite some variations depending on the type of ligand, nearly all molecules binding to the sensor chip can be detected [154]. Deviations in signal intensity are a consequence of the three dimensional distribution of the ligand within the matrix near the metal surface and due to the exponential decay of the evanescent wave with increasing distance to the surface. Additional effects around the interface, *e.g.* electrostatic attraction or conformational changes, will further influence signals as described by Mannen *et al.* [156].

Biacore experiments are generally used to study interactions between binding partners. For this purpose, one binding partner *e.g.* a receptor or an enzyme is

immobilized on the sensor chip and the other (*e.g.* agonist, antagonist, inhibitor, substrate) is injected. A direct surface attachment of *e.g.* proteins to a solid (gold) support often leads to loss in affinity and potentially unspecific binding events. Therefore, a special surface chemistry was developed involving a 'protecting polymer', which carries functional groups for easy immobilization. On standard Biacore biosensor chips, thiolated carboxymethyl dextran chains are directly attached to the gold surface via the sulfur atom. Carboxyl groups distributed over the whole dextran matrix (three dimensionally distributed) enable immobilization via well-defined chemistry. Due to the hydrophilic environment, the immobilized biomolecules are kept in a quasi-solvent environment [*157*], which increases the stability of *e.g.* labile proteins. As electrostatic artifacts could be caused by free carboxyl groups on the chip surface and sample contaminants a routine addition, salts *e.g.* 150 mM NaCl are routinely added to the running buffer [*153*]. Other reagents, such as EDTA or polysorbate are highly recommended to further limit non-specific signals. A schematic overview of the entire experimental setup is visualized in Figure 12.
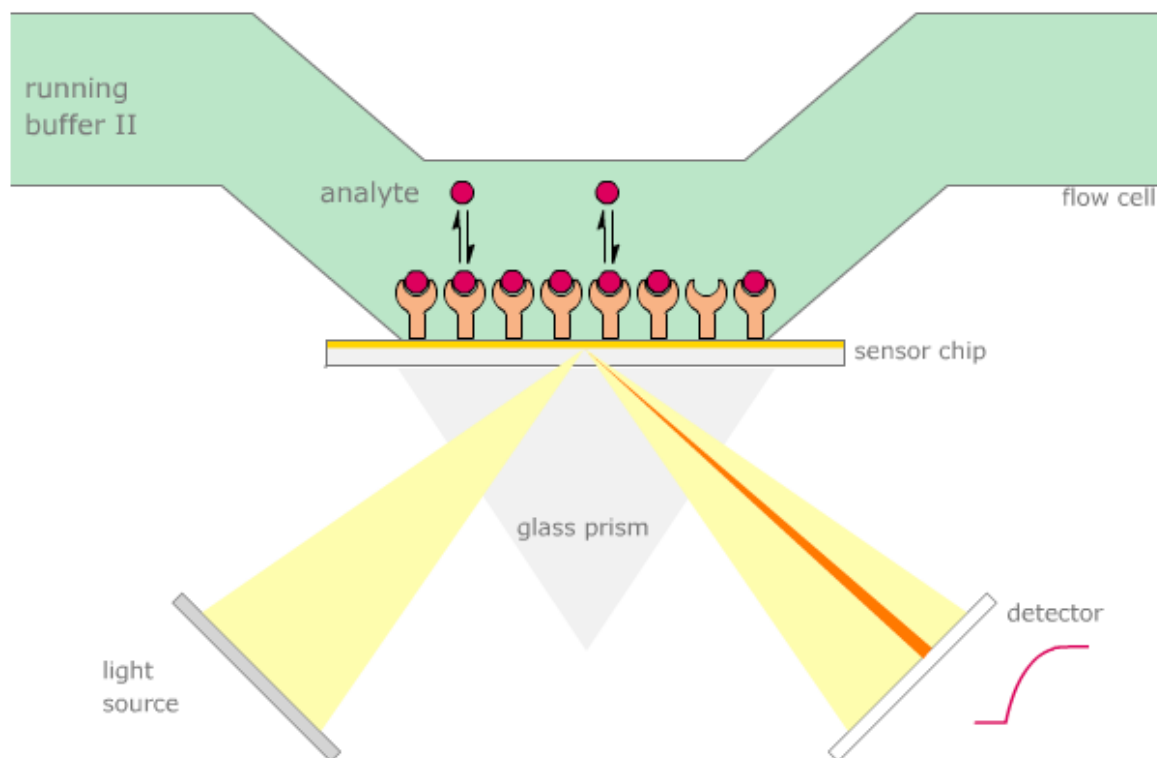
Figure 12 (by courtesy of A. Vögtli): Schematic overview of the experimental setup of the Biacore 3000. Precise sample delivery is conducted by the integrated fluidic cartridge (IFC). Binding of a ligand to an immobilized target is monitored in real-time by the SPR-based detection system.

Biacore experiments are performed under continuous flow conditions. This minimizes effects like mass transport of molecules to the surface, a phenomenon observed in stationary systems. In such a system, the required incubation times of several hours to ensure reliable results would not correlate with real-time systems as Biacore. The flow system consists of a micro-flow cell, which offers a continuous transport of sample to and from the surface, therefore minimizing the diffusion and convection effects. Developments in miniaturization led to an integrated fluidic cartridge (IFC), which further reduced sample consumption and sample plug dispersion after injection [*153*].

The shift in resonance angle is monitored in real-time and plotted in dependence of time. In such a signal versus time plot, called sensorgram, the different stages of a binding event are visualized (Figure 13). During a first phase, running buffer is injected over the surface leading to a stable baseline. Continuous injection of sample, which binds to the surface, is monitored by the increase of the binding curve during association phase (A). The shape of the curve during association is influenced by dissociation occurring already at this stage. Depending on the ligand, steady state is reached after a specific injection time, where associating and dissociating molecules are in equilibrium (B). With the stop of sample injection and change to continuous buffer flow, the dissociation phase starts and becomes visible by the decreasing signal in the sensorgram (C). In case of very slow dissociation, an additional regeneration step is required to reach the baseline again (D).
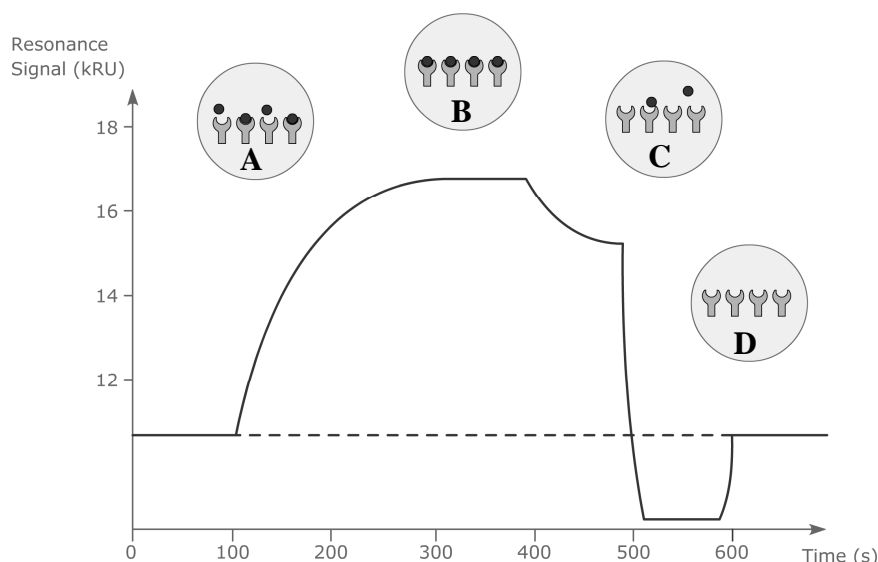
Figure 13 (by courtesy of A. Vögtli): A typical sensorgram obtained for a standard interaction measurement. Ligand from a sample starts to bind to the target (A) until a steady state is reached (B). After changing to pure buffer, dissociation of the ligand is visible (C). In case of remaining ligand a subsequent regeneration step is required (D).

Due to the real time set up of Biacore, kinetic parameters such as the association and dissociation rate constants (k_{on}, k_{off}) can be derived from the sensorgram. The equilibrium dissociation constant (K_D) can be directly calculated from the kinetic rate constants using Equation 1 or independently from the steady state signals at different concentrations. Steady state affinity is calculated based on Equation 2, where R_{eq} is the equilibrium response signal, K_D the equilibrium dissociation constant, c the sample concentration, and R_{max} the maximal response at saturation level.

$$K_A = \frac{k_{on}}{k_{off}} \quad ; \quad K_D = \frac{k_{off}}{k_{on}} \qquad \textbf{[Equation 1]}$$

$$R_{eq}(c) = \frac{c \times R_{max}}{K_D + c} \qquad \textbf{[Equation 2]}$$

To demonstrate the effect of different kinetics on sensorgrams an *in silico* experiment can be performed, where eight concentrations (100 μM – 0.25 μM) of four virtual compounds (A – D) are injected. The affinity (K_D) is for all compounds identical, but they differ in their association and dissociation rate constants (Table 8).

Table 8: Data of the virtual compounds A, B, C, D.

Compound	K_D [µM]	k_{on} [$M^{-1}s^{-1}$]	k_{off} [s^{-1}]
A	10	10000	0.1
B	10	1000	0.01
C	10	500	0.005
D	10	100	0.001

For compound C and D, a steady state affinity analysis is already complicated because steady state for the lower concentrations is not reached within injection time (Figure 14). In such a case, only kinetically determined K_Ds are available.
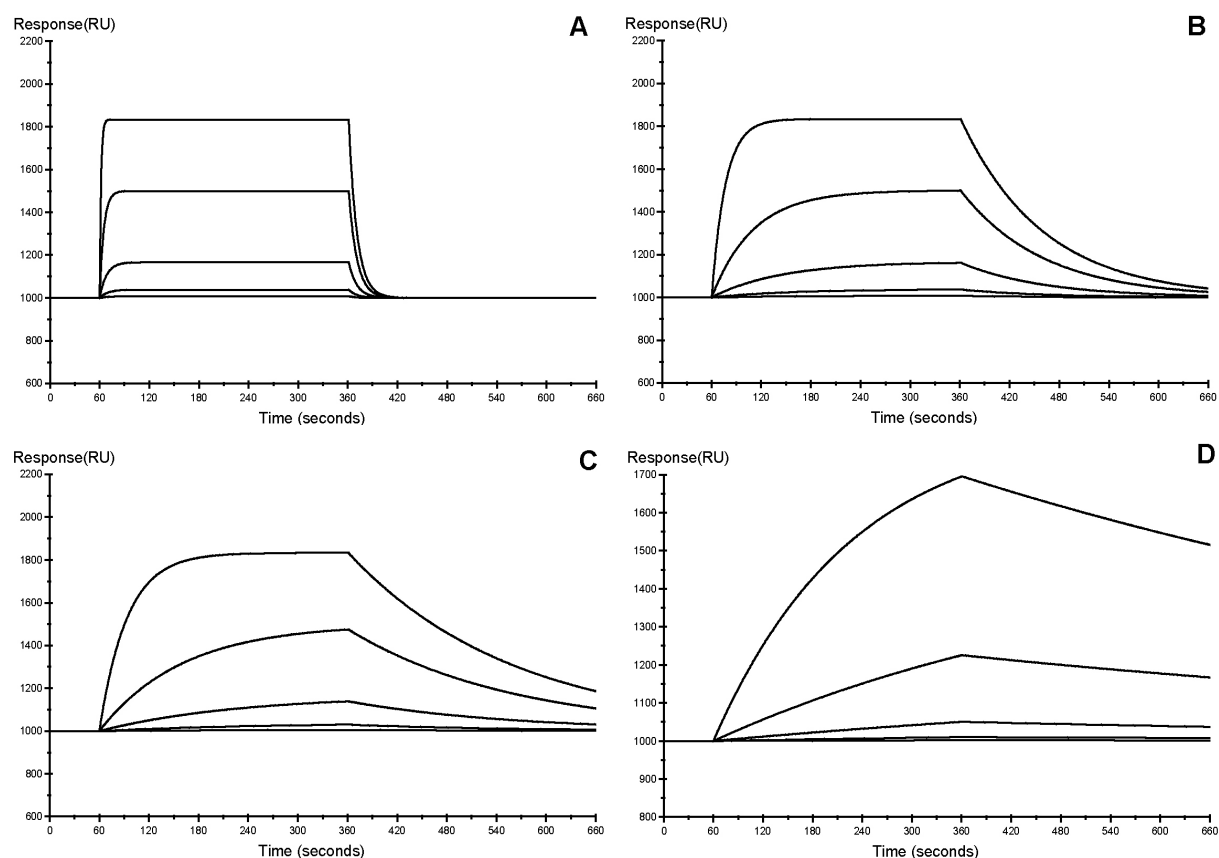
Figure 14: Importance of kinetics demonstrated by a simulation with four virtual compounds (A, B, C, and D) all displaying a K_D of 10 µM.

3.3.2. Immobilization Assay Using NTA-chips

To measure binding affinities and kinetics of Ni-NTA complexes with various ligands, one of the interacting molecules has to be immobilized on the chip surface.

Biacore produces a commercially available sensor chip with covalently attached NTA to the dextran matrix (Figure 15) [158].
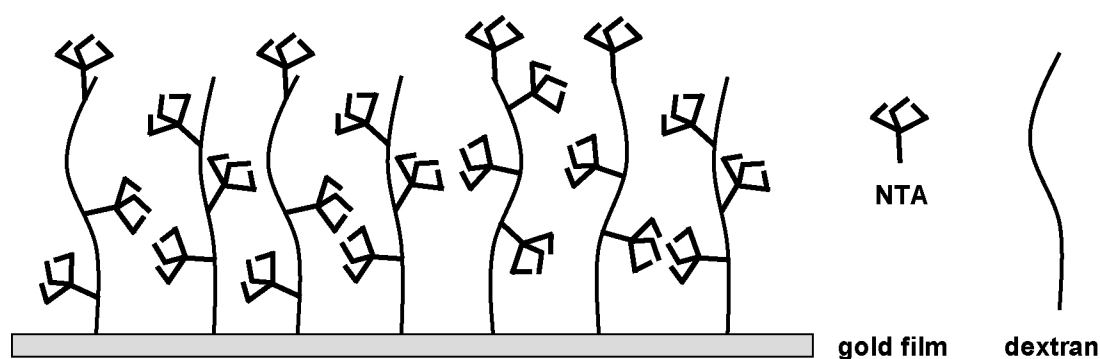
Figure 15: Commercially available NTA chip from Biacore (GE Healthcare, Freiburg, Germany). Dextran is coupled via sulfur groups to the gold surface.

After addition of aq. $NiCl_2$ solution, the chip forms Ni-NTA complexes are formed, allowing the immobilization of His-tagged proteins. The NTA-chip is also appropriate for the analysis of potential tags binding to Ni-NTA. With such an experimental setup, it is possible to simulate the purification process on a Ni-NTA column. A comparison of the standard Biacore assay used for the investigation of Ni-NTA complexes as proposed by Nieba *et al.* [126] and a Ni-NTA purification is given in Figure 16.

The basic principle of the two experiments is the same. In both cases, the ligand (tag, tagged protein) is injected after the initial Ni(II) loading step. After the binding process the surface or the column material is regenerated again for the next round of ligand injection. Whereas in the purification process the product is eluted with imidazole to get a pure product, this step is not necessary in the Biacore experiment. Addition of EDTA leads to a complete release of Ni(II) and sample together. This is not desired in the purification experiment as it would lead to a Ni^{2+}-contaminated products.
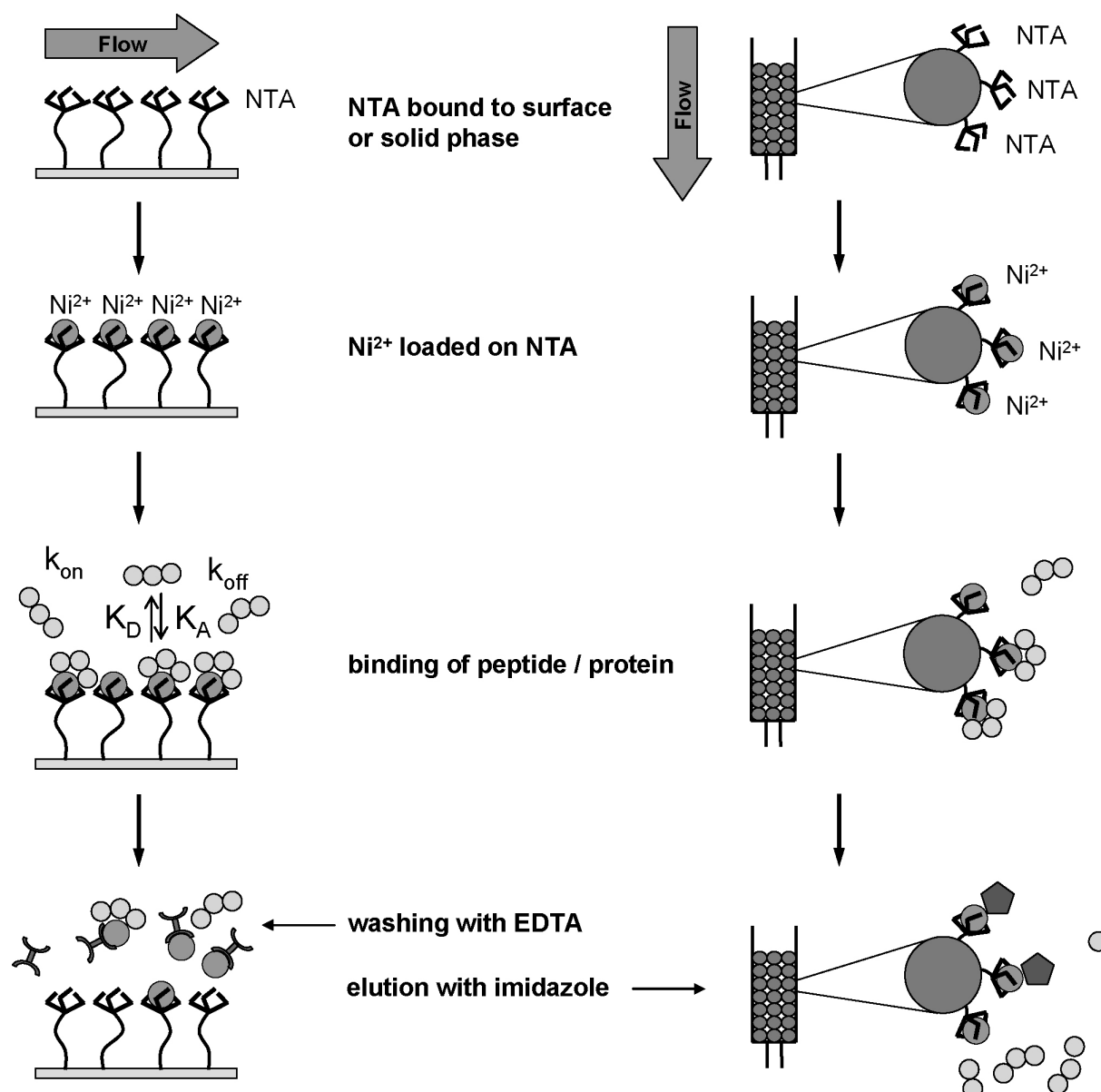
Figure 16: Comparison between Biacore assay using Ni-NTA chips and IMAC purification using Ni-NTA columns.

From the shape of association, steady state, and dissociation phase, the parameters K_D, k_{on}, and k_{off} can be calculated. The correct evaluation and interpretation of the obtained sensorgrams is critical. Many reported data in literature are either unreliable due to poor quality or to bad processing [159]. Deviations from an expected binding model are often caused by poor experimental design, low purity of ligands and/or target heterogeneity. Unfortunately, such data can often be fitted to a more complex binding model, simply because of the increased number of variables taken into consideration [160]. Hence, before reporting new binding mechanisms for a certain interaction all possible influences have to be eliminated.

To exclude unspecific binding, subtraction of a proper reference flow cell is needed. A reference flow cell should mimic the target flow cell as close as possible. For this purpose, one flow cell is generally used without injection of Ni^{2+} to eliminate unspecific binding either to the dextran matrix or the covalently attached NTA. In addition, injections of buffer blanks over the target flow cell cause small deviations from the reference and should be included as well. Both, subtraction of blanks and signal from the reference flow cell, also known as double referencing lead to higher data quality [161].

Generally, data should first be fitted to a simple 1:1-binding model according to Equation 3. Since some targets possess more than one binding site, the equation has to be extended to a two independent binding site model. In such a case two binding affinities (K_A^1 and K_A^2) as well as two k_{on} and k_{off} values can be determined (Equation 4). If mass transport effects are suspected or reported, a mass transport coefficient (k_m) might be introduced (Equation 5).

$$A + B \underset{k_{off}}{\overset{k_{on}}{\rightleftharpoons}} AB \qquad \textbf{[Equation 3]}$$

$$A \underset{k_{off}^1}{\overset{k_{on}^1}{\rightleftharpoons}} AB \underset{k_{off}^2}{\overset{k_{on}^2}{\rightleftharpoons}} AB_2 \qquad \textbf{[Equation 4]}$$

$$A_0 \underset{k_m}{\overset{k_m}{\rightleftharpoons}} A + B \underset{k_{off}}{\overset{k_{on}}{\rightleftharpoons}} AB \qquad \textbf{[Equation 5]}$$
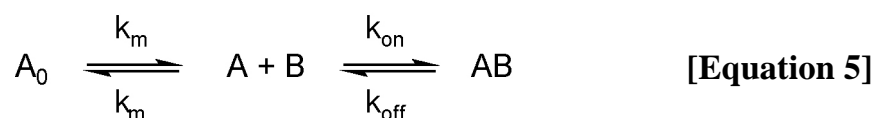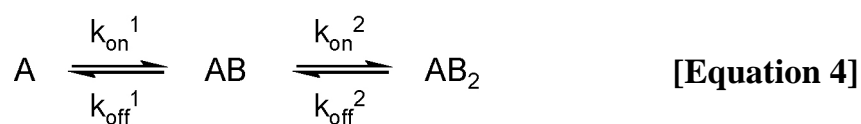
Mass transfer is very likely to appear for association rate constant (k_{on}) higher than $10^6 \, M^{-1}s^{-1}$. At these high on rates, the measured binding rate in some cases may reflect the transfer of analyte into the matrix rather than the reaction rate itself [162]. As mass transfer is dependent on the flow rate, it is easily detectable by measuring the same analyte concentrations at different flow rates. Deviations of the binding curve might indicate the existence of a mass transfer. Generally, higher flow rates are less prone to mass transfer, but increase significantly the analyte consumption.

A proper data processing is especially important for fitting kinetic data (k_{on} and k_{off}). Initially, different algorithms using curve transformation [163] or nonlinear least square analysis [162] were used for the evaluation of the binding kinetics. However, these methods only fitted single binding curves (or even portions thereof) and were found to be often insufficient to discriminate between different binding mechanisms [160]. In the global analysis approach, the association and dissociation phases of the entire data set are fitted to a model simultaneously, resulting in accurate and robust data [164].

Finally, to exclude experimental artifacts, triplicate injections are applied. Such a treatment also helps to foresee changes of the chip surface over time, which could lead to deviations in further experiments and therefore unreliable data. Repreparation and reinjection of sample solutions additionally helps to avoid systematic errors based on manipulations.

3.4. Affinity Tags in Solid-phase Peptide Synthesis

Nowadays, the principle of solid-phase peptide synthesis together with chemical ligation enables the production of large polypeptide or even protein chains [*165*]. However, due to limitations in the standard HPLC purification and the lack of suitable purification methods for SPPS, synthesis is quite often hampered (see section 3.1.2). Especially, in solid-phase based synthesis of large proteins using chemical ligation, the repetitive HPLC purifications of the fragments before each ligation is highly laborious and prone to significant losses. Furthermore, one pot reactions, which do not require intermediate HPLC purifications of fragments but only one single HPLC isolation of the product [*166*], are often limited as they need near-quantitative reaction yields for each fragment. However, in the field of production of recombinant proteins overexpressed in engineered cells, the attachment of tags to the N- or C-terminal end of the proteins is a common strategy to yield products in an acceptable amount and of good purity. The most successful and most frequently used method is IMAC purification in combination with His-tags (see section 3.2.4). Kent *et al.* presented a possible approach to make use of the successful hexahis-tag for SPPS [*167*]. For the chemical synthesis of a 17-kDa protein (tetratrico peptide repeat) via the natural chemical ligation strategy, they used a C-terminal hexahis-tag to facilitate the isolation and handling of intermediate products formed during the reaction and also to enable the final purification of the complete product (Figure 17).

The attachment of an affinity tag would not only support the chemical synthesis of larger proteins but also the synthesis of larger peptides, which do not require chemical ligation. Secondary structures (*e.g.* helix, beta sheet) and tertiary structures (*e.g.* leucine-zipper, disulfide bridging domains) are also present in peptides of 40 and more amino acids and have to be established after synthesis. Upon detachment of the product from the solid-phase, the peptides form often multimolecular aggregates, which do not show the desired biological activity. Therefore, attachment of a metal binding tag prior to the cleavage from the solid support, would allow to load the peptide onto a Ni-NTA column to perform a refolding step similarly done with proteins expressed as inclusion bodies [*123*].
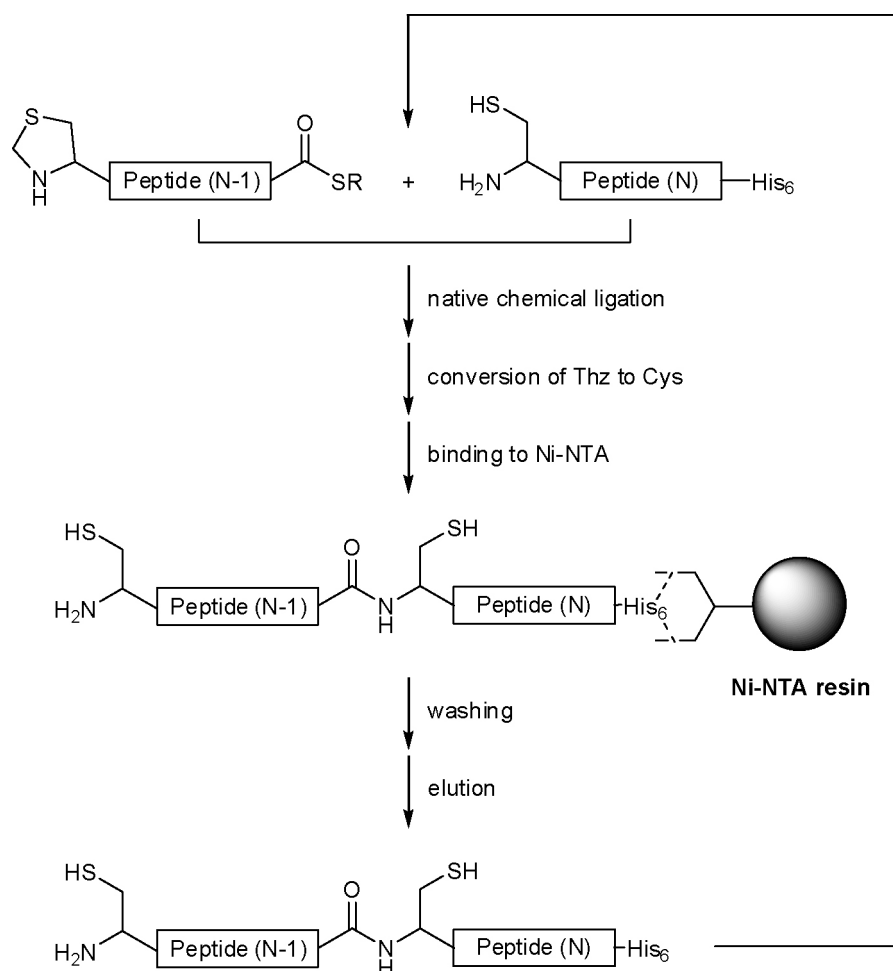
Figure 17: His-tag assisted solid-phase peptide synthesis of polypeptide chains using native chemical ligation (from [*167*]).

The first attempt to use metal affinity for SPPS was made from Comely *et al.* in 2001, although with a slightly different aim [*168*]. These authors complexed an amino acid via chromium to a solid-phase using aromatic π–donor systems (*e.g.* as present in Phe). After the final coupling step, the peptide was detached from the solid-phase by elution with a competitor. The purification was finally performed using flash chromatography and not by the means of the attached metal chelator, which significantly differs from the strategy of Kent *et al.* with the His-tag [*167*].

The approach of Kent *et al.* suffers from mainly two drawbacks: Attachment of a C-terminal hexahis-tag means six additional coupling steps to the growing peptide chain, which further lowers the overall yield of the synthesis. Furthermore, as already described in section 3.2.5, the His-tag has some major drawbacks, which could also have an impact on fully synthetical proteins.

The interaction mechanism between metal ions and His-tags with a variable number of His residues has not yet been experimentally investigated at a molecular level. In fact, Hochuli *et al.* [*90*] compared the binding of His-tags consisting of 2 – 6 residues, but only by means of retention and elution efficiency on Ni-NTA columns. Larger tags with up to ten histidine residues have also been described [*137*], however without any characterization of their binding properties. Hence, the hexahistidine tag (**5**) has been empirically determined as suitable for most of the applications and is therefore by far the most widely used affinity tag.

For the development of new purification strategies using tags with improved chelation properties a better understanding of the mechanism of hexahis binding to Ni-NTA is crucial. Very recently, an alternative to the approach of Kent *et al.* [*167*] was presented in a patent application of Frank *et al.* [*169*], who used a chemically cleavable phenanthroline-tag attached to the N-terminal of a synthetic peptide. Purification was performed with Ni-NTA due to the Ni(II)-chelating properties of phenanthroline. Unfortunately, no investigations on binding properties of such phenanthroline structures were performed within this patent.

3.5. Aim of the Thesis

The aim of this thesis was to gain a better understanding of the basic principles involved in the binding process of various ligands to Ni-NTA. Such an improved knowledge will then be used for the development of new metal-chelating tags with improved chelation properties and fewer drawbacks as encountered with the existing strategies.

With the Biacore system in house, a tool was available to screen libraries of different potential tags for Ni-NTA columns. In the first part of the thesis, the focus is mainly on amino acid tags suitable as affinity tags for solid-phase peptide synthesis. The binding assay using SPR should enable the determination of binding affinities (K_D) and kinetic data (k_{on}, k_{off}). In addition, a qualitative analysis of the sensorgram should allow to gain a deeper insight into the binding mechanisms.

Besides, a slightly modified purification strategy based on the method of Frank *et al.* [169] using a phenanthroline-tag was set up and studied intensively by Biacore. In addition, the phenanthroline-tag was also applied for the preparative purification of a peptide synthesized using standard SPPS.

Furthermore, the possible introduction of a photolabile linker was tested. This would offer an efficient cleavage method for the removal of the tag [170]. Different tag-linker constructs were synthesized and analyzed by Biacore to demonstrate the effect on the chelation properties of the tags.

In a last part, new potential tags as *e.g.* picolinic acid were identified, using the standard Biacore assay supported by a newly developed computational model [171].

4. MATERIALS AND METHODS

4.1. General Procedures

Chromatography

Column chromatography was performed using silica gel 60 (40-63 μm) from Fluka.

LC-MS:

LC-MS separations were carried out using Waters sunfire C_{18} columns (analytical: 2.1 x 50 mm, 3.5 μm; preparative: 19 x 150 mm, 5.0 μm) on a Waters 2525 LC system, equipped with Waters 2996 photodiode array and Waters micromass ZQ MS for m/z detection. If nothing else is mentioned, standard gradients of 15 min duration in analytic mode and 30 min in preparative mode were run.

Mass spectrometry

Mass spectra were obtained on a Waters micromass ZQ or a Finnigan LCQ Deca System. High resolution mass spectrometry (HR-MS) spectra were performed on an ESI Bruker Daltonics microTOF spectrometer equipped with a TOF hexapole detector.

Microwave reactions

Microwave reactions were carried out in a CEM Discover microwave apparatus.

Nuclear magnetic resonance

Nuclear magnetic resonance spectroscopy was performed on a Bruker Advance 500 Ultra Shield spectrometer at 500 MHz (^{1}H NMR) or 125 MHz (^{13}C NMR). Chemical shifts are given in ppm and were assigned in relation to the solvent signals on the δ-scale or to tetramethylsilane (0 ppm) as internal standard. ^{1}H: 7.26 ppm ($CDCl_3$), 5.32 ppm (CD_2Cl_2), 3.31 ppm (CD_3OD), 4.79 ppm (D_2O), 2.50 ppm ((CD_3)$_2$SO); ^{13}C: 77.00 ppm ($CDCl_3$), 53.50 ppm (CD_2Cl_2), 49.00 ppm CD_3OD, 39.43 ppm ((CD_3)$_2$SO). Coupling constants J are given in Hertz (Hz). The following

abbreviations are used for the multiplicities: s (singlet), d (doublet), dd (double doublet), t (triplet), dt (double triplet), q (quartet), dq (double quartet), m (multiplet). Assignment of ^{1}H and ^{13}C NMR spectra was achieved using 2D methods (COSY, HSQC, HMQC, HMBC). Abbreviations used for the assignment of peaks are the following: tBu, *tert*-butyl; MeO, methoxy; Me ester, methyl ester.

Solvents

All solvents were obtained from Fluka and dried prior to use if necessary: Diethylether, dioxane, toluene, and tetrahydrofuran (THF) by refluxing with sodium/benzophenone and subsequent distillation. Pyridine was freshly distilled from CaH$_2$, whereas dichloromethane (CH$_2$Cl$_2$) was dried by filtration over Al$_2$O$_3$ (Fluka, type 5016 A basic). DMF and DMSO were liberated from water by stirring over activated molecular sieves 4Å over night, followed by microfiltration. Methanol was dried by distillation from sodium methoxide.

Thin layer chromatography

TLC was performed using silica gel 60 coated glass plates containing fluorescence indicator from Merck KGaA (Darmstadt, Germany) using either UV light (254 nm) or Mostain solution [0.8 g Cer(SO$_4$)$_2$, 40 g (NH$_4$)$_6$(Mo$_7$O$_{24}$)•4 H$_2$O dissolved in 300 mL of 10% aq. H$_2$SO$_4$] followed by heating to 140°C for 5 minutes to visualize the substances.

4.2. Solid-phase Peptide Synthesis

Four peptide series were synthesized to be used in the Biacore experiments: The oligohistidine (**1** - **9**), the His$_2$Ala$_4$ (**10** - **14**), the His$_x$Ala$_y$ (**15** - **19**), and the HXH (**20** - **24**) series. In addition, the α-MSH derivative NAPamide (**25**) and His$_6$-amide (**26**) were produced for a closer investigation of the Ni-NTA purification process. An overview about the peptide sequences and the compound names is given in Table 9. As long as not stated explicitly, the L-form of the amino acids was utilized. All reactions were performed at room temperature (rt).

Table 9: Peptides synthesized by solid-phase peptide synthesis.

Compound	No.	Sequence
His2	(**1**)	H-His-His-OH
His3	(**2**)	H-His-His-His-OH
His4	(**3**)	H-His-His-His-His-OH
His5	(**4**)	H-His-His-His-His-His-OH
His6	(**5**)	H-His-His-His-His-His-His-OH
His7	(**6**)	H-His-His-His-His-His-His-His-OH
His8	(**7**)	H-His-His-His-His-His-His-His-His-OH
His9	(**8**)	H-His-His-His-His-His-His-His-His-His-OH
His10	(**9**)	H-His-His-His-His-His-His-His-His-His-His-OH
His$_2$Ala$_4$1	(**10**)	H-Ala-Ala-Ala-Ala-His-His-OH
His$_2$Ala$_4$2	(**11**)	H-Ala-Ala-Ala-His-Ala-His-OH
His$_2$Ala$_4$3	(**12**)	H-Ala-Ala-His-Ala-Ala-His-OH
His$_2$Ala$_4$4	(**13**)	H-Ala-His-Ala-Ala-Ala-His-OH
His$_2$Ala$_4$5	(**14**)	H-His-Ala-Ala-Ala-Ala-His-OH
His$_x$Ala$_y$1	(**15**)	H-His-Ala-His-Ala-Ala-His-OH
His$_x$Ala$_y$2	(**16**)	H-His-Ala-Ala-His-Ala-His-OH
His$_x$Ala$_y$3	(**17**)	H-Ala-Ala-Ala-His-His-OH
His$_x$Ala$_y$4	(**18**)	H-Ala-Ala-His-His-OH
His$_x$Ala$_y$5	(**19**)	H-Ala-His-His-OH
HGH	(**20**)	H-His-Gly-His-OH
HAH	(**21**)	H-His-Ala-His-OH
HSarH	(**22**)	H-His-Sar-His-OH
HAibH	(**23**)	H-His-Aib-His-OH
HPH	(**24**)	H-His-Pro-His-OH
NAPamide	(**25**)	H-Nle-Asp-His-D-Phe-Arg-Trp-Gly-Lys-NH$_2$
His$_6$-amide	(**26**)	H-His-His-His-His-His-His-NH$_2$

Reagents

9-Fluorenylmethoxycarbonyl-(Fmoc) protected His(Trt)-NovaSyn TGT resin Fmoc-Aib-OH, Fmoc-Ala-OH, Fmoc-Arg(Pbf)-OH, Fmoc-Asp(OtBu)-OH, Fmoc-Gly-OH, Fmoc-Phe-OH, Fmoc-Nle-OH, Fmoc-Pro-OH, Fmoc-Sar-OH, Fmoc-Trp(Boc)-OH, and 1-hydroxybenzotriazole (HOBt) were purchased from NovaBiochem (VWR International AG, Lucerne, Switzerland). The resins Rink Amide Novagel and Fmoc-PAL-PEG-PS were from AppliedBiosystems (Rotkreuz, Switzerland), dihistidine (**1**), Fmoc-protected His(Trt), as well as 2-(1H-benzotriazole-1-yl)-1,1,3,3-tetramethyluronium tetrafluoroborate (TBTU) from Bachem (Bachem AG, Bubendorf, Switzerland). 2-(1H-7-Azabenzotriazol-1-yl)-1,1,3,3-tetramethyl uronium hexafluorophosphate (HATU) was purchased from PerSeptive Biosystems. All solvents used for the automated peptide synthesis were purchased from PerSeptive Biosystems or Applied Biosystems. HPLC-grade water, *t*-butyl methyl ether, acetonitrile, and trifluoroacetic acid (TFA) used during peptide purification were purchased from Fluka (Fluka AG, Buchs, Switzerland).

Equipment

All the peptides except His2 (**1**) and HSarH (**22**) were synthesized on a fully automated Pioneer peptide synthesis system. The purification of the peptides was done on different HPLC and mass spectrometry systems: The oligohistidines (**2 – 9**), the His_xAla_y (**15 - 19**), HGH (**20**), HSarH (**22**), and HAibH (**23**) were purified on a Jasco HPLC systems consisting of a Jasco UV-1570 intelligent UV/VIS detector (Jasco GmbH, Gross-Umstadt, Germany). An Agilent 1100 purification system (Agilent AG, Basel, Switzerland) was used for His_2Ala_4 (**10 - 14**), HAH (**21**), HPH (**24**), NAPamide (**25**), and His_6-amide (**26**). This system consisted of a quaternary pump, a cooled well-plate autosampler, a column thermostat, a DAD detector, and a cooled analytical fraction collector.

The purification of the oligohistidines (**2 – 9**) except His3 (**2**) was performed using a preparative C18 column (SymmetryPrep, 19 × 150 mm, 7 μm; Waters AG, Rupperswil, Switzerland), whereas all other peptides were purified with different analytic C18 columns: His3 (**2**), His_xAla_y1 (**15**), His_xAla_y4 (**18**), and His_xAla_y5 (**19**), HPH (**24**), and His_6-amide (**26**) with a Vydac 218TP54 (4.6 × 250 mm, 5 μm; Vydac,

Basel, Switzerland). All peptides from the His_2Ala_4 series (**10 – 14**) were purified with a Phenomenex Jupiter C18 (4.6 × 250 mm, 5 μm; Brechbühler AG, Schlieren, Switzerland), while purification of His_xAla_y2 (**16**), His_xAla_y3 (**17**), HGH (**20**), HAH (**21**), HSarH (**22**), and HAibH (**23**) was performed on a Reprosil-Pur Basic C18 column (4.6 × 250 mm, 5 μm; Dr. Maisch GmbH, Ammerbuch, Germany). NAPamide (**25**) was purified using the Agilent 1100 HPLC system with a Phenomenex Gemini C18 column (4.6 × 250 mm, 5 μm; Brechbühler AG, Schlieren, Switzerland).

Mass spectrometry analysis of the peptides was performed on the Finnigan LCQ Deca System in case of the peptides His5 (**4**), His6 (**5**), His7 (**6**), His10 (**9**), and His_xAla_y3 (**17**), while all the other peptides were analyzed on the Waters micromass ZQ system.

Buffer *pH* values were controlled with a combined *pH* glass electrode from Metrohm (Metrohm AG, Herisau, Switzerland).

4.2.1. Synthesis and Purification of Oligohistidines (1 – 9)

All oligohistidines (**2 – 9**), except His2 (**1**), which was commercially available, were synthesized with a Pioneer Peptide Synthesizer using fully automated continuous-flow technology and Fmoc-strategy. A NovaSyn TGT resin preloaded with the C-terminal histidine (0.19 mmol/g) was used for the synthesis leading to a C-terminal acid after cleavage from the solid-phase. 0.5 g of resin was pre-swollen in 10 mL DMF for 30 min. Afterwards, the resin was loaded on the column, which was directly connected to the lines of the peptide synthesizer. Theoretical yields between 43 mg and 125 mg depending on the peptide sequence were expected. For each cycle an automated program was executed using 20% piperidine (v/v) in DMF for removal of the Fmoc-group, followed by several washing steps with DMF. Coupling steps were performed using 0.5 M DIPEA in DMF and TBTU/HOBt (both 0.5 M in DMF) as activator solutions, followed again by washing with DMF to start the next coupling cycle. Four equivalents of amino acids were added for the coupling. Detailed information about the coupling cycle is summarized in Table 10.

Table 10: Coupling cycle on Pioneer Peptide Synthesizer.

No.	Step	Duration [s]	Flow [mL/min]	Reagent
1	Deblocking	300	5	20% piperidine in DMF
2	Wash	50	30	DMF
3	Activation of AA [a]	12	8	0.5 M DIPEA in DMF 0.5 M TBTU and 0.5 M HOBt in DMF
4	Recycling through column [b]	3600	30	activated AA
5	Wash	40	30	DMF

[a] Amino acid is activated in separate vial prior to injection onto column

[b] The solution containing the activated amino acid is pumped several times through the column containing the resin

At the final stage of the peptide synthesis the N-terminal Fmoc group was removed by the peptide synthesizer, and the resin was transferred onto a frit for extensive washing with 2-propanol.

For cleavage and deprotection of the oligopeptides from the resin, a TFA solution containing 5% thioanisole, 4.5% water and 0.5% ethane-1,2-dithiol (all v/v) was employed. The resin was resuspended in 3 mL of the TFA solution and filtered for 45 min. For washing 3 mL of TFA solution were added dropwise over of 45 min. As the final steps, the filtrate containing the solubilized crude peptide was concentrated *in vacuo* and precipitated with iced *tert*-butyl methyl ether to afford the crude peptide as a white solid.

Analysis and purification of the oligohistidines were performed with HPLC and mass spectrometry. The crude peptides, except His3 (**2**), were dissolved in 0.1% aqueous formic acid (10 mg/mL) and purified with a linear gradient of acetonitrile in water (0-35%, containing 0.1% TFA). For His3 (**2**) the aqueous phase had to be changed to 10 mM ammonium acetate *pH* 8.8 to get longer retention and the purification was performed on a Vydac C18 column using the same gradient. For all oligohistidines (**2** – **9**) major peaks were collected and analyzed by mass spectrometry. The correct fractions were lyophilized leading to a white lyophilisate. The HPLC and mass spectrometry data are delivered in Table 11.

Table 11: Analytical Data of Oligohistidines (**2** – **9**).

Compound	No.	Retention time t_R [min]	Calculated monoisotopic mass	Found monoisotopic mass
His3	(**2**)	7.86 [a]	428.2	428.2
His4	(**3**)	4.47	566.3	566.2
His5	(**4**)	4.68	703.3	703.2
His6	(**5**)	6.11	840.4	840.3
His7	(**6**)	9.01	977.4	977.4
His8	(**7**)	12.52	1114.4	1114.4
His9	(**8**)	13.41	1250.5	1250.7
His10	(**9**)	14.15	1388.6	1388.5

[a] Purification was performed with a different buffer system compared to the other peptides, see above

Lyophilized products were stored at -20°C and their stability was regularly verified by HPLC.

4.2.2. Synthesis and Purification of His$_2$Ala$_4$ Series (10 – 14)

The synthesis of the His$_2$Ala$_4$ series (**10** – **14**) was performed as described for the oligohistidines (**2** – **9**). To achieve a theoretical yield of 55 mg, 0.5 g of Fmoc-His(Trt)-NovaSyn TGT resin (0.19 mmol/g) was employed. After cleavage, the TFA solution was evaporated and the crude product was resuspended in 10% acetic acid and lyophilized.

Purification of the His$_2$Ala$_4$ (**10** – **14**) was performed by a former member of the Institute of Molecular Pharmacy, Dr. Daniel Ricklin. Only small amounts of the crude, lyophilized peptides for further experiments with Biacore were purified by HPLC. Due to their small size and relatively high hydrophilicity, purification under acidic conditions was not possible. Therefore, separation was performed using 10 mM ammonium acetate buffer at *pH* 8.8, above the theoretical *pI* of 6.92 (calculated using the *PeptideMass* tool [*172*]), using a silica-based Phenomenex Jupiter C18 column. After sample injection, an isocratic phase of 2 min was run, followed by a linear gradient up to 5% acetonitrile. After collecting the relatively wide peaks, solvents and ammonium acetate were removed by lyophilization over night. Analytical data are shown in Table 12.

Table 12: Analytical Data of His_2Ala_4 (**10** – **14**).

Compound	No.	Retention time t_R [min]	Calculated monoisotopic mass	Found monoisotopic mass
$His_2Ala_4$1	(**10**)	11.78	576.3	576.1
$His_2Ala_4$2	(**11**)	10.49	576.3	576.1
$His_2Ala_4$3	(**12**)	11.75	576.3	576.1
$His_2Ala_4$4	(**13**)	12.03	576.3	576.1
$His_2Ala_4$5	(**14**)	14.42	576.3	576.1

The pure white lyophilisates of the peptides were stored at -20°C. The purity was checked by HPLC from time to time.

4.2.3. Synthesis of His_xAla_y Series (15 – 19)

The synthesis of the His_xAla_y peptides (**15** – **19**) was performed as described for the oligohistidine series (**2** – **9**). Again, 0.5 g of Fmoc-His(Trt)-NovaSyn TGT resin (0.19 mmol/g) was used to produce peptides with a theoretical yield between 36 and 64 mg.

Only peptides His_xAla_y1 (**15**), His_xAla_y2 (**16**), and His_xAla_y3 (**17**) were precipitated with iced *tert*-butyl methyl ether prior to HPLC purification. Analytical HPLC afforded about 5 mg of product the Biacore assay. The peptides were purified using 10 mM ammonium acetate buffer at *pH* 8.8. A linear gradient from 5 to 50% acetonitrile was run on a Vydac C18 column for the peptides His_xAla_y1 (**15**), His_xAla_y4 (**18**), and His_xAla_y5 (**19**). Peptides **16** and **17** were purified with the ReprosilPur Basic column from Dr. Maisch GmbH using the same gradient mentioned above. Retention times and monoisotopic masses of the peptides are given in Table 13.

Table 13: Analytical Data of His_xAla_y (**15 – 19**).

Compound	No.	Retention time t_R [min]	Calculated monoisotopic mass	Found monoisotopic mass
His_xAla_y1	(**15**)	12.45	642.3	642.4
His_xAla_y2	(**16**)	12.48[a]	642.3	642.4
His_xAla_y3	(**17**)	11.63[a]	505.2	505.3
His_xAla_y4	(**18**)	5.33	434.2	434.2
His_xAla_y5	(**19**)	4.51	363.2	363.2

[a] Purification was performed with a different column compared to the other peptides, see text.

Fractions containing the desired product were collected, pooled and lyophilized. The peptides were stored at -20°C, and their purity was verified by HPLC.

4.2.4. Synthesis of HXH Series (20 – 24)

Synthesis of HGH (**20**), HAH (**21**), HAibH (**23**), and HPH (**24**) was performed with the same protocol used for the oligohistidines (**2 – 9**). For the synthesis, 0.5 g of Fmoc-His(Trt)-NovaSyn TGT resin (0.19 mmol/g) was employed. The cleavage solution was changed to 5% triisopropylsilane and 5% water in TFA, as to improve the yield. 3 mL of the solution were added to the peptide still bound to the resin, and after 1 hour the resin was washed with additional 3 mL of the TFA solution. Finally, the cleaved peptide was concentrated and precipitated with diethyl ether to get the crude peptide as a white solid.

The synthesis of HSarH (**22**) was done manually. For this purpose, Fmoc-His(Trt)-NovaSyn TGT (0.14 g, 0.19 mmol/g, 1 eq) was deprotected in 20% piperidine in DMF (5 mL). After 20 min the resin was washed with DMF (5 × 5 mL), transferred to a new flask and resuspended in DMF (2 mL). Prior to the first coupling step, Fmoc-Sar-OH (34 mg, 0.106 mmol, 4 eq), HATU (50 mg, 0.128 mmol, 4.8 eq), and DIPEA (38 µL, 0.106 mmol, 4 eq) were pre-activated in DMF (3 mL) for 10 min, before the reaction mixture was added to the deprotected resin. The reaction vial was permanently agitated over night. Finally, the resin was washed with DMF (5 × 5 mL). The next coupling cycle was performed twice to ensure proper coupling of N-terminal His residue to the secondary amine of Sar. Using exactly the same procedure as for the

first step, Fmoc-His(Trt)-OH (68 mg, 0.106 mmol, 4 eq), HATU (50 mg, 0.128 mmol, 4.8 eq), and DIPEA (38 μL, 0.106 mmol, 4 eq) were used for the reaction. After washing the peptide resin 5 times with DMF, Fmoc-His(Trt)-OH, HATU, and DIPEA were added again in the same amounts as described above. The final washing steps were done with DMF (5 × 5 mL) and isopropanol (5 × 5 mL).

The purification was done with a ReprosilPur Basic column from Dr. Maisch GmbH using ammonium acetate *pH* 8.8 as the water phase and a gradient of pure acetonitrile from 0-50%. For HAH (**21**) and HPH (**24**) the HPLC system from Agilent was used, whereas for HGH (**20**), HSarH (**22**), and HAibH (**23**), the Jasco system was chosen. Data resulting from the purification are shown in Table 14.

Table 14: Analytical Data of HXH (**20** – **24**).

Compound	No.	Retention time t_R [min]	Calculated monoisotopic mass	Found monoisotopic mass
HGH	(**20**)	4.45	349.2	349.1
HAH	(**21**)	6.00 [a]	363.2	363.2
HSarH	(**22**)	11.73	363.2	363.2
HAibH	(**23**)	3.51	377.2	377.2
HPH	(**24**)	3.90 [a]	389.2	389.0

[a] Purification was performed with a different HPLC system compared to the other peptides, see text

Fractions containing the desired product were collected, pooled and lyophilized. After prolonged storage at -20°C, peptide purity was checked by HPLC.

4.2.5. Synthesis of NAPamide (25)

The first amino acid of NAPamide (**25**) was manually coupled to the resin. Fmoc-PAL-PEG-PS resin (0.8 g, 0.19 mmol/g, 1 eq) was pre-swollen in DMF for 30 min. Then, 20% piperidine in DMF was added to cleave the Fmoc-group. After 20 min the resin was washed with DMF (5 × 5 mL). Fmoc-Lys(Boc)-OH (202 mg, 0.456 mmol, 3 eq) was pre-activated with DIPCDI (68 μL, 0.456 mmol, 3 eq) and HOBt (76 mg, 0.456 mmol, 3 eq) in DMF for 10 min. Finally, the pre-activated solution was added to the pre-swollen resin, and the reaction mixture was constantly agitated for 6 h. After the resin was washed with DMF (5 × 5 mL), free amino groups were acetylated

(capping) by treating with 10 mL of a solution of 6% 2,6-lutidine and 5% acetic anhydride in DMF for 30 min. Finally, the resin was washed with DMF (5 × 5 mL) and then loaded onto the column of the peptide synthesizer.

The other steps of the synthesis of the NAPamide were done as described for the oligohistidines (**2 – 9**) on the peptide synthesizer, with the additional capping step after each coupling cycle during the automated synthesis. After step 5 (see Table 10) the resin was flushed with 15 mL/min of capping solution (6% 2,6-lutidine, 5% acetic anhydride in DMF) during 15 s. After a reaction time of 300 s, the resin was washed again (DMF, 30 mL/min, 40 s) to start the next cycle. After synthesis, the resin was weighed and divided into small aliquots of 35 mg (corresponding to 5.8 mg peptide).

One aliquot (0.00549 mmol) was used for cleavage and deprotection as described for the oligohistidines (**2 – 9**). After precipitation with *tert*-butyl methyl ether, the crude peptide was purified by LC-MS using a gradient of acetonitrile in water (both containing 0.1% HCOOH) from 5 to 95%. The result of this purification is shown in Table 15. Fractions containing the desired product were collected, pooled and lyophilized to afford pure NAPamide.

Table 15: Analytical Data of NAPamide (**25**).

Compound	No.	Retention time t_R [min]	Calculated monoisotopic mass	Found monoisotopic mass
NAPamide	(**25**)	5.78	1056.6	1056.4

The rest of the 35 mg aliquots were further used as described in section 4.6.1 for the attachment of the phenanthroline tag.

4.2.6. Synthesis of His$_6$-amide (26)

Rink Amide Novagel (238 mg, 0.63 mmol/g, 1 eq) was pre-swollen in DMF (5 mL) for 30 min. Fmoc-His(Trt)-OH (465 mg, 0.750 mmol, 5 eq), HOBt (101 mg, 0.750 mmol, 5 eq), and DIPCDI (116 µL, 0.750 mmol, 5 eq) pre-activated DMF (4 mL) for 10 min. Finally, the pre-activated amino acid was added to the resin and the mixture was constantly agitated for 6 h. Afterwards the resin was washed 5 times with DMF and loaded onto the column of the peptide synthesizer. The remaining 5

histidines were coupled as described for the oligohistidines (**2** – **9**). After the last coupling step, the last Fmoc-group was cleaved, and the resin washed with isopropanol (5×5 mL) and transferred into a new flask.

To verify the success of the synthesis, 0.0119 mmol of resin (theoretical yield of 10 mg pure **25**) were taken for cleavage and deprotection. 5 mL of a TFA solution containing 1 % triisopropyl silane and 4% water were added to the resin for 2 h. Afterwards, the resin was washed with another 5 mL of the TFA solution. After concentration *in vacuo* and precipitation with diethyl ether, the crude peptide was purified on the Agilent 1100 system using a Vydac C18 column. A gradient (5 – 80%) of acetonitrile in water, both containing 0.1% TFA, was run to afford 3.4 mg (34%) of the pure peptide (Table 16).

Table 16: Analytical Data of His$_6$-amide (**26**).

Compound	No.	Retention time t_R [min]	Calculated monoisotopic mass	Found monoisotopic mass
His$_6$-amide	(**26**)	3.10	839.4	839.6

The remaining resin was further used for the attachment of the photolinker as described in section 4.7.1.

4.3. Determination of the Salt Content of Peptides

Synthesis and purification of peptides finally leads to a pure product containing a certain amount of counter ions firmly bound to the product. For an exact determination of binding affinities of these peptides by means of surface plasmon resonance, the fraction of salt bound to the peptide samples has to be determined.

Reagents

4-(4-Dimethylaminophenylazo)benzenesulfonyl chloride (DABS-Cl) was obtained from Fluka (Fluka AG, Buchs, Switzerland) and recrystallized as previously described [*173*]. Hydrochloric acid (6 N) and the amino acid standard were both obtained from Sigma (Fluka AG, Buchs, Switzerland).

Equipment

For the gas-phase hydrolysis a Waters vessel (custom-made) was used. This vessel is a flat-bottom glass tube (2.7 cm i.d. × 9 cm), which could take up to 12 small hydrolysis tubes (4 mm i.d. × 50 mm). A heat-resistant plastic screw cap, equipped with a Teflon valve, is used to firmly close the vessel after vacuumization. HPLC was performed on an Agilent 1100 purification system (Agilent AG, Basel, Switzerland) containing a quaternary pump, a cooled well-plate autosampler, a column thermostat, a DAD detector, and a cooled analytical fraction collector. The column for the analysis was a Waters Symmetry® C18 (2.1 × 150 mm, 5 μm; Waters AG, Rupperswil, Switzerland).

4.3.1. General Procedures

Derivatization of the peptide to determine the salt concentration was performed as previously described [*174*]. Briefly, samples of approximately 2 μg of peptide, dissolved either in water or eluent buffer (10 mM HEPES, 150 mM NaCl, 50 μM EDTA, pH 7.4), were placed in hydrolysis tubes and dried in a vacuum centrifuge. Afterwards, 400 μL of 6 N HCl were added into each hydrolysis tube, and the tubes

were placed into the Waters hydrolysis vessel. The gas-phase hydrolysis was carried out at <0.1 mbar for 14 h at 110°C. An amino acid standard was processed under the same conditions in parallel with the samples. Standard and samples were measured in duplicates. After the hydrolysis, samples and standard were dissolved in 20 μL of 50 mM sodium bicarbonate *pH* 8.1. 40 μL of a freshly prepared DABS-Cl solution (4 nmol/μL in acetonitrile) was added to each sample to start the derivatization. Sealed with silicon-rubber caps, the tubes were heated at 70°C for 10 min. After dabsylation the samples were diluted with 50 mM sodium phosphate (*pH* 7.0 / ethanol, 1:1, v/v) to suitable volumes for HPLC analysis. The volume was chosen according to the expected amount of peptide: For about 0.5 μg of peptide (or 500 pmol of standard) a volume of 1 mL was added. 20 μL of this solution were injected into the HPLC system using a gradient of 25 mM sodium acetate *pH* 6.5, containing 4% DMF as solvent A and pure acetonitrile as solvent B (15% to 40% in 20 min, 40% to 70% from 20 to 32 min, kept at 70% from 32 to 34 min, and back to 15% from 34 to 36 min).

4.4. Protection of Hydroxyethyl Photolinker (PL)

The following reactions were performed to protect the free hydroxyl group on the photolinker (PL) by formation of a *tert*-butyldimethylsilyl ether.

Reagents

Hydroxyethyl photolinker was purchased from NovaBiochem (VWR International AG, Lucerne, Switzerland) and was always protected from prolonged light exposure. Thionyl chloride (SOCl$_2$) was purchased from Fluka (Fluka AG, Buchs, Switzerland), and *tert*-butyldimethylsilyl chloride was purchased from Aldrich (Fluka AG, Buchs, Switzerland).

Equipment

All vials containing the light-sensitive PL were wrapped in aluminum foil if possible.

4.4.1. Formation of PL-ester: Methyl 4-[4-(1-hydroxyethyl)-2-methoxy-5-nitrophenoxy]butanoate (27)
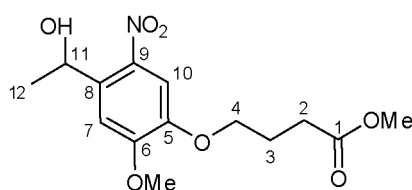
PL (500 mg, 1.67 mmol, 1 eq) was dissolved in dry methanol (5 mL) and dry DMF (1.8 mL). SOCl$_2$ (280 μL, 3.68 mmol, 2.2 eq) was added dropwise at 0°C to the dissolved PL. Then, the reaction mixture was stirred over night at rt. To stop the reaction, saturated NaHCO$_3$ was added to the mixture until *pH* 9 was reached. The mixture was transferred into a separation funnel and was extracted with ethyl acetate (3 × 15 mL). The combined organic layers were dried over Na$_2$SO$_4$, filtered and

concentrated *in vacuo*. After drying in high vacuum, the pure product **27** was achieved as a yellow solid (517 mg, quant.).

ESMS: m/z calcd for $C_{14}H_{19}NO_7$ 336.11 $[M + Na]^+$; found, 336.12 $[M + Na]^+$. ^{1}H NMR (CDCl$_3$, 500 MHz): 7.55 (s, 1H, H-10), 7.24 (s, 1H, H-7), 5.55 (q, 1H, J = 6.3 Hz, H-11), 4.09 (m, 2H, H-4), 3.95 (s, 3H, Me ether), 3.68 (s, 3H, Me ester), 2.55 (t, 2H, J = 7.2 Hz, H-2), 2.17 (tt, 2H, J = 6.9 Hz, H-3), 1.54 (d, 3H, J = 6.3 Hz, H-12). ^{13}C NMR (CDCl$_3$): 173.57 (C-1), 154.28 (C-6), 147.03 (C-5), 139.64 (C-9), 137.22 (C-8), 109.21 (C-7), 108.87 (C-10), 68.39 (C-2), 65.89 (C-11), 56.50 (Me ether), 51.91 (Me ester), 30.55 (C-4), 24.48, 24.43 (C-3, C-12).

4.4.2. Silylation of Photocleavable Linker: Methyl 4-[4-(1-(*tert*-butyldimethylsilyloxy)ethyl)-2-methoxy-5-nitrophenoxy]butanoate (28)
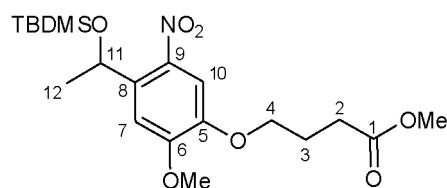

27 (517 mg, 1.65 mmol, 1 eq), *tert*-butyldimethylsilyl chloride (622 mg, 4.13, 2.5 eq) and imidazole (315 mg, 4.62 mmol, 2.8 eq) were dissolved in dry DMF (8 mL). The reaction was stirred at rt over night. To quench the reaction, the mixture was diluted with ethyl acetate (40 mL) and washed with saturated aqueous NaHCO$_3$, saturated aqueous NH$_4$Cl, and brine (each 3×40 mL). The organic layer was dried over Na$_2$SO$_4$, filtered and evaporated. The crude product was purified by column chromatography (petroleum ether/ethyl acetate, 8:1 to 6:1) to afford silyl ether **28** (692 mg, 98%) as a dark-red oil.

ESMS: m/z calcd for $C_{20}H_{33}NO_7Si$ 450.2 $[M + Na]^+$; found, 450.2 $[M + Na]^+$. ^{1}H NMR (CDCl$_3$, 500 MHz): 7.56 (s, 1H, H-10), 7.35 (s, 1H, H-7), 5.58 (q, 1H, J = 6.1, H-11), 4.08 (t, 2H, J = 6.2 Hz, H-4), 3.92 (s, 3H, MeO), 3.67 (s, 3H, Me ester), 2.54 (t, 2H, J = 7.2 Hz, H-2), 2.16 (m, 2H, H-3), 1.41 (d, 3H, J = 6.1 Hz, H-12), 0.85 (s, 9H,

SiC(CH_3)$_3$), 0.05 (s, 3H, Si(CH_3)), -0.07 (s, 3H, Si(CH_3)). ^{13}C NMR (CDCl$_3$): 173.57 (C-1), 154.17 (C-6), 146.71 (C-5), 139.00 (C-9), 138.61 (C-8), 109.32 (C-7), 108.87 (C-10), 68.30 (C-2), 66.80 (C-11), 56.36 (MeO), 51.93 (Me ester), 30.60 (C-4), 26.53 (C-12), 25.98 (SiC(CH_3)$_3$), 24.48 (C-3), 18.33 (SiC(CH_3)$_3$), -4.76 (Si(CH_3)), -4.81 (Si(CH_3)).

4.4.3. Hydrolysis of Ester: Sodium 4-[4-(1-(*tert*-butyldimethylsilyloxy)-ethyl)-2-methoxy-5-nitrophenoxy]butanoate (29)
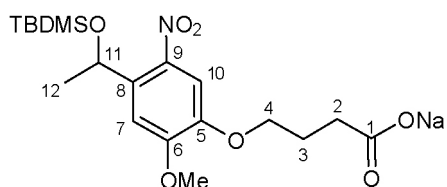
Ester **28** (175 mg, 0.409 mmol, 1 eq) was dissolved in methanol (2 mL) and 1 M NaOH solution was added (738 μL, 0.227 mmol, 1.8 eq). The reaction was stirred at rt over night, followed by evaporation of methanol and water. Product **29** (185 mg, quant.) contained a surplus of 0.8 eq sodium, which was taken into account for further experiments and calculations.

ESMS: m/z calcd for C$_{19}$H$_{30}$NNaO$_7$Si 436.2 [M + H]$^+$; found, 436.1 [M + H]$^+$. ^{1}H NMR (CD$_3$OD, 500 MHz): 7.57 (s, 1H, H-10), 7.36 (s, 1H, H-7), 5.56 (q, 1H, J = 6.1, H-11), 4.07 (t, 2H, J = 6.5, H-4), 3.91 (s, 3H, MeO), 2.54 (t, 2H, J = 7.5, H-2), 2.16 (m, 2H, H-3), 1.43 (d, 3H, J = 6.1 Hz, H-12), 0.89 (s, 9H, SiC(CH_3)$_3$), 0.05 (s, 3H, Si(CH_3)), -0.07 (s, 3H, Si(CH_3)). ^{13}C NMR (CD$_3$OD): 181.84 (C-1), 155.43 (C-6), 148.61 (C-5), 140.21 (C-9), 138.61 (C-8), 110.23 (C-7), 109.74 (C-10), 70.31 (C-2), 67.80 (C-11), 56.62 (MeO), 35.20 (C-4), 27.19 (C-12), 26.64 (C-3), 25.09 (SiC(CH_3)$_3$), 18.99 (SiC(CH_3)$_3$), -4.94 (Si(CH_3)$_2$).

4.5. Attachment of Spacers to Phenanthroline

To provide an anchor point for a linkage between phenanthroline and a peptide, or an introduction of a (photo)chemical or an enzymatic cleavage, two different derivatizations of the phenanthroline were performed, either an attachment of an amino group or an introduction of a carboxylic acid to the phenanthroline.

Reagents

5-Chloro-1,10-phenanthroline, Pd(OAc)$_2$, Pd$_2$(dba)$_3$, 2-dicyclohexylphosphino-2',6'-dimethoxy-biphenyl (S-Phos), 2-dicyclohexylphosphino-2',4',6'-triisopropyl-biphenyl (X-Phos), and 4-methoxycarbonylphenylboronic acid were purchased from Aldrich (Fluka AG, Buchs, Switzerland). 5-Nitro-1,10-phenanthroline was purchased from Sigma (Fluka AG, Buchs, Switzerland). Pd/C (E 101 N/W, 10%) was purchased from Degussa (Evonik Degussa GmbH, Hanau, Germany). Fmoc-Gly-OH was purchased from NovaBiochem (VWR International AG, Lucerne, Switzerland), and HATU was obtained from PerSeptive Biosystems.

4.5.1. Introduction of an Amino Group I: 5-Amino-1,10-phenanthroline (30)
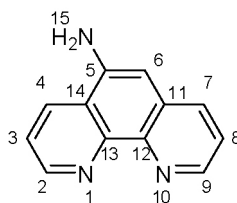
5-Nitro-1,10-phenanthroline (400 mg, 1.78 mmol) and Pd/C (E 101 N/W, 10%) were suspended in dry methanol (16 mL) under an argon atmosphere. After 24 h of hydrogenation under atmospheric pressure at rt, the mixture was filtered over celite and the celite washed with methanol (20 mL). Finally, the filtrate was concentrated *in vacuo* to afford **30** as a yellow solid (323 mg, 93%).

ESMS: m/z calcd for $C_{12}H_9N_3$ 196.1 $[M + H]^+$; found, 195.7 $[M + H]^+$. ^{1}H NMR (DMSO, 500 MHz): 9.05 (m, 1H, H-4), 8.68 (m, 2H, H-2, H-9), 8.04 (m, 1H, H-7), 7.74 (m, 1H, H-3), 7.51 (m, 1H, H-8), 6.86 (s, 1H, H-6), 6.16 (s, 2H, H-15). ^{13}C NMR (DMSO): 149.36 (C-4), 146.19 (C-11), 144.83 (C-9), 142.69 (C-13), 140.51 (C-14), 132.72 (C-7), 130.82 (C-1), 130.58 (C-5), 123.22 (C-8), 122.08 (C-3), 121.82 (C-12), 101.74 (C-6).

4.5.2. Introduction of an Amino Group II: (9*H*-Fluoren-9-yl)methyl 2-(1,10-phenanthrolin-5-ylamino)-2-oxoethylcarbamate (31)
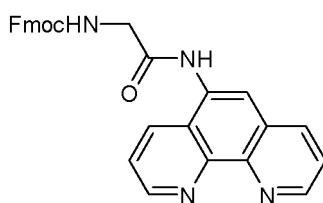
5-Amino-1,10-phenanthroline (**30**, 102 mg, 0.522 mmol, 1 eq), Fmoc-Gly-OH (777 mg, 2.61 mmol, 5 eq), and HATU (978 mg, 2.57 mmol, 4.9 eq) were dissolved in DMF (5 mL). After addition of DIPEA (890 μL, 5.22 mmol, 10 eq), the reaction was stirred at rt over night. Finally, the crude product was concentrated *in vacuo*, dissolved in water/acetonitrile (30:70), and purified by LC-MS using a gradient of acetonitrile in water (both containing 0.1% HCOOH) from 30 to 95% to afford product **31** (t_R = 6.07 min, 114 mg, 46%) as a yellow solid.

ESMS: m/z calcd for $C_{29}H_{22}N_4O_3$ 475.2 $[M + H]^+$; found, 475.1 $[M + H]^+$.

4.5.3. Introduction of an Amino Group III: 2-Amino-*N*-(1,10-phenanthrolin-5-yl)acetamide (32)
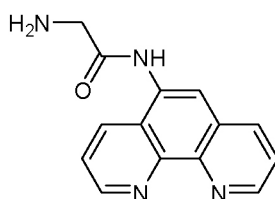
Compound **31** (20 mg, 0.421 mmol) was dissolved in 20% piperidine in DMF (5 mL) and stirred at rt for 2 h. After concentration and evaporation *in vacuo*, crude product **32** was analyzed by mass spectrometry. The product was directly used for fusion reactions with **29** without further purification (section 4.6.2).

ESMS: m/z calcd for $C_{14}H_{12}N_4O$ 253.1 $[M + H]^+$; found, 252.9 $[M + H]^+$.

4.5.4. Introduction of Carboxylic Acid I: (*E*)-*tert*-Butyl 3-(1,10-phenanthrolin-5-yl)acrylate (33)

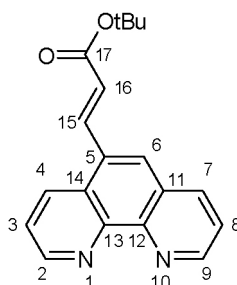Pd(OAc)$_2$ (3.1 mg, 0.0138 mmol, 0.15 eq) and 2-dicyclohexylphosphino-2',4',6'-triisopropylbiphenyl (X-Phos, 3.1 mg, 0.0279 mmol, 0.3 eq) were placed in a microwave tube, which was flushed with argon and evacuated several times. DMF (1.3 mL), which was flushed with argon for 10 min prior to the experiment, was added and the catalyst was stirred at rt under argon. After 30 min, CsCO$_3$ (75 mg, 0.230 mmol, 2.5 eq), 5-chloro-1,10-phenanthroline (20 mg, 0.0932 mmol, 1 eq), and *tert*-butyl acrylate (27 μL, 0.186 mmol, 2 eq) were added. The tube was flushed again with argon and firmly closed. The reaction was heated under microwave irradiation at 80°C for 3 h. Finally, the mixture was concentrated and purified by LC-MS using a gradient of acetonitrile in water (both containing 0.1% HCOOH) from 5 to 95%. For an increased purity an additional purification was performed on the Agilent 1100 system using the same reagents and a Phenomenex Gemini C18 column (4.6 × 250 mm, 5 μm; Brechbühler AG, Schlieren, Switzerland) to afford pure product **33** (19.7 mg, 69%) as a red solid.

HR-MS: m/z calcd for $C_{19}H_{18}N_2O_2$ 329.1260 [M + Na]$^+$; found, 329.1261 [M + Na]$^+$. ^{1}H NMR (CD$_3$OD, 500 MHz): 9.11 (m, 1H, H-2), 9.07 (m, 1H, H-9), 8.70 (m, 1H, H-4), 8.48 (m, 1H, H-7), 8.36 (d, 1H, J = 15.7, H-15), 8.24 (s, 1H, H-6), 7.83 (m, 1H, H-3), 7.77 (m, 1H, H-8), 6.68 (d, 1H, J = 15.7, H-16), 1.58 (s, 9H, tBu). ^{13}C NMR (CD$_3$OD): 167.48 (C-17), 151.80 (C-2), 151.20 (C-9), 147.07 (C-11), 146.72 (C-13), 140.23 (C-15), 138.53 (C-7), 134.01 (C-4), 132.60 (C-14), 129.70 (C-12), 128.58 (C-5), 126.84 (C-6). 126.15 (C-16), 125.27 (C-8), 125.00 (C-3), 82.46 (C(CH$_3$)$_3$), 28.59 (C(CH_3)$_3$).

4.5.5. Introduction of Carboxylic Acid II: (*E*)-3-(1,10-Phenanthrolin-5-yl)acrylic acid (34)
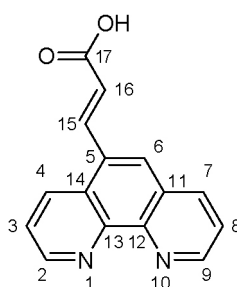
tert-Butyl ester **33** (46 mg, 0.151 mmol) was dissolved in 5 mL of TFA and stirred at rt over night. After concentration and evaporation *in vacuo*, the red oil was verified by mass spectrometry as product **34**. It was further used for the fusion reaction with NAPamide (section 4.6.1) after a purity check on the Agilent 1100 system using acetonitrile in water from 5 to 90% on a Phenomenex Gemini C18 (4.6 × 250 mm, 5 μm; Brechbühler AG, Schlieren, Switzerland).

HR-MS: m/z calcd for $C_{15}H_{10}N_2O_2$ 251.0815 [M + H]$^+$; found, 251.0818 [M + H]$^+$. ^{1}H NMR (CD$_3$OD, 500 MHz): 9.16 (m, 1H, H-2), 9.13 (m, 1H, H-9), 8.81 (m, 1H, H-4), 8.58 (m, 1H, H-7), 8.48 (d, 1H, J = 15.7, H-15), 8.34 (s, 1H, H-6), 7.90 (m, 1H, H-3), 7.85 (m, 1H, H-8), 6.77 (d, 1H, J = 15.7, H-16). ^{13}C NMR (CD$_3$OD): 169.64 (C-17), 151.44 (C-9), 150.96 (C-2), 146.16 (C-11), 145.86 (C-13), 141.00 (C-15), 139.28 (C-7), 134.74 (C-4), 132.89 (C-14), 129.91 (C-12), 128.79 (C-5), 126.94 (C-6), 125.54 (C-8), 125.30 (C-3), 125.22 (C-16).

4.5.6. Alternative for Carboxylic Acid: Methyl 4-(1,10-phenanthrolin-5-yl)benzoate (35)
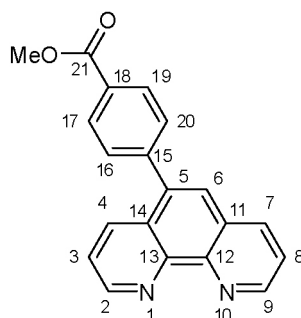
4-Methoxyphenylboronic acid (126 mg, 0.699 mmol, 1.5 eq), 5-chloro-1,10-phenanthroline (100 mg, 0.466 mmol, 1 eq), CsF (211.4 mg, 1.39 mmol, 3 eq), S-Phos (19.2 mg, 41.1 mmol, 88 eq), and Pd$_2$(dba)$_3$ (24.0 mg, 51.8 mmol, 111 eq) were resuspended under argon in dry dioxane (6 mL). The reaction was stirred at 80°C for 7 d. The mixture was diluted with ethyl acetate (20 mL) and washed with saturated aqueous NaHCO$_3$ (2 × 20 mL) and brine (2 × 10 mL). The organic phase was dried over Na$_2$SO$_4$ and concentrated *in vacuo*. Recrystallization in methanol afforded product **35** (61.3 mg, 42%) as a slightly yellow powder. For an increased purity 10 mg of the product were further purified by LC-MS, leading to 6.8 mg of pure product **35**.

ESMS: m/z calcd for C$_{20}$H$_{14}$N$_2$O$_2$ 315.1 [M + H]$^+$; found, 315.0 [M + H]$^+$. ^{1}H NMR (DMSO, 500 MHz): 9.18 (m, 2H, H-2, H-9), 8.64 (m, 1H, H-7), 8.30 (m, 1H, H-4), 8.18 (m, 2H, H-17, H-19), 8.09 (s, 1H, H-6), 7.89 (m, 1H, H-8), 7.82 (m, 1H, H-3), 7.77 (m, 2H, H-16, H-20).

4.6. Fusion Reactions of Phenanthroline with NAPamide (25)

To prove the concept of a peptide purification by attachment of a tag binding to Ni-NTA, phenanthroline was coupled to the test peptide NAPamide (**25**). A direct fusion to the N-terminus was performed with (*E*)-3-(1,10-phenanthrolin-5-yl)acrylic acid (**34**). In addition, another tag construct was synthesized with a covalently attached photolinker (PL). For this purpose, 2-amino-*N*-(1,10-phenanthrolin-5-yl)-acetamide (**32**) was used.

Reagents

1-Ethyl-3-(3-dimethylaminopropyl)carbodiimide hydrochloride (EDC•HCl) was purchased from Pierce (Pierce Biotechnology, Rockford IL, USA), and HATU was from PerSeptive Biosystems. Tetrabutyl ammonium fluoride (TBAF) was purchased from Fluka (Fluka AG, Buchs, Switzerland).

4.6.1. Direct Fusion of Phenanthroline with NAPamide: (*E*)-3-(1,10-Phenanthrolin-5-yl)acryoyl-NAPamide (36)

Carboxylic acid **34** (12 mg, 0.0464 mmol, 8.4 eq) was pre-activated with HATU (18 mg, 0.0464 mmol, 8.4 eq) and DIPEA (16 µL, 0.0947 mmol, 8.4 eq) in DMF (1 mL) at rt for 10 min. The pre-activated mixture was added to resin-bound NAPamide-PAL-PEG-PS (35 mg, 0.00549 mmol, 1 eq), which was equal to a theoretic yield of 5.8 mg peptide. The reaction mixture was agitated at rt over night and washed with DMF (5 × 5 mL) and isopropanol (3 × 5 mL) to give red-stained polystyrene beads. Cleavage from the resin and deprotection of the construct was performed in 5 mL TFA mixture (90% TFA, 5% EDT, 4.5% H_2O, 0.5% thioanisole) at rt for 45 min. Afterwards, the suspension was immediately filtered and the resin was washed with TFA (3 × 5 mL). The crude product **36** was concentrated *in vacuo* and analyzed by mass spectrometry to be further used for the Ni-NTA purification (section 4.8.2).

ESMS: m/z calcd for $C_{65}H_{80}N_{18}O_{11}$ 1289.6 $[M + H]^+$, found, 1289.7 $[M + H]^+$.

4.6.2. Fusion of Phenanthroline with Photolinker I: *N*-[2-(1,10-Phenanthrolin-5-ylamino)-2-oxoethyl]-4-[4-(1-(*tert*-butyldimethylsilyloxy)ethyl)-2-methoxy-5-nitrophenoxy]butanamide (37)
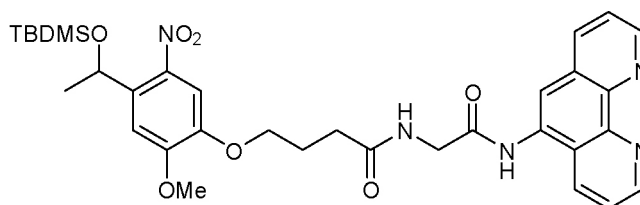
The crude sodium salt **29** (25 mg, 0.0548 mmol, 1.3 eq) was dissolved together with crude amine **32** (27 mg, 0.0421 mmol, 1 eq), EDC•HCl (17 mg, 0.110 mmol, 2.6 eq), HOBt (17 mg, 0.110 mmol, 2.6 eq), and DIPEA (30 µL, 0.169 mmol, 4 eq) in DMF (4 mL). The reaction was stirred at rt over night. Analytic LC-MS analysis was performed using a gradient of acetonitrile in water (including 0.1% HCOOH) from 5% to 95% to detect product **37** (t_R = 7.35). The crude product was directly used for desilylation.

ESMS: m/z calcd for $C_{33}H_{41}N_5O_7Si$ 648.3 [M + H]$^+$; found, 648.2 [M + H]$^+$.

4.6.3. Fusion of Phenanthroline with Photolinker II: *N*-[2-(1,10-phenanthrolin-5-ylamino)-2-oxoethyl]-4-[4-(1-hydroxyethyl)-2-methoxy-5-nitrophenoxy]butanamide (38)
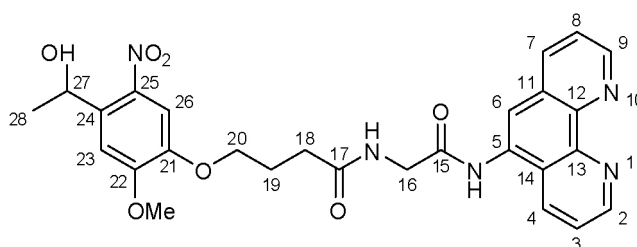
Crude product **37** (0.042 mmol) was dissolved in THF (1 mL), and TBAF (126 µL, 1 M in THF) was added to the solution. The reaction mixture was stirred at rt over night and then concentrated *in vacuo*. For purification, the residue had to be injected twice into the LC-MS system using a linear gradient of acetonitrile in water (17 – 20%, both solvents containing 0.2% HCOOH) to afford pure product **38** (2.4 mg, 11%).

ESMS: m/z calcd for $C_{27}H_{27}N_5O_7$ 534.2 $[M + H]^+$; found, 534.2 $[M + H]^+$. ^1H NMR (CD$_3$OD, 500 MHz): 9.11 (m, 1H, H-2), 9.07 (m, 1H, H-9), 8.62 (m, 1H, H-4), 8.42 (m, 1H, H-7), 8.11 (s, 1H, H-6), 7.81 (m, 1H, H-3), 7.77 (m, 1H, H-8), 7.58 (m, 1H, H-26), 7.33 (m, 1H, H-23), 5.40 (q, 1H, J = 6.2, H-27), 4.23 (s, 2H, H-16), 4.15 (t, 2H, J = 6.2, H-20), 3.94 (s, 3H, MeO), 2.61 (t, 2H, J = 7.1, H-18), 2.21 (m, 2H, H-19), 1.42 (d, 3H, J = 6.2, H-28).

4.7. Fusion of His$_6$-amide to Photolinker: 2-(2-(2-(4-(4-(1-(*Tert*-butyldimethylsilyloxy)ethyl)-2-methoxy-5-nitrophenoxy)-butanoylhexahistidineamide (PL-His$_6$-amide) (41)

To test the amide formation between the photolinker and a potential tag, His$_6$-amide (**26**) was coupled to the sodium salt of the protected photolinker (**29**). The reagents used for this reaction are mentioned in section 4.6.

4.7.1. General Procedure

His$_6$-amide-Rink amide Novagel resin (**26**, 133 mg, 0.0367 mmol, 1 eq), the sodium salt of the protected photolinker **29** (20 mg, 0.0441 mmol, 1.2 eq), EDC•HCl (15 mg, 0.0918 mmol, 2.5 eq), HOBt (14 mg, 0.0918 mmol, 2.5 eq), and DIPEA (26 µL, 0.147 mmol, 4 eq) were resuspended in DMF (5 mL). The reaction was run under constant agitation at rt for 60 h. Then, the resin was washed with DMF (3 x 5 mL) and isopropanol (5 × 5 mL), and dried *in vacuo* to yield the protected PL-His$_6$-amide resin (**39**). For the hydrolysis of the silyl ether, the resin was transferred into THF (5 mL) and TBAF (1 M solution in THF, 150 µL, 0.147 mmol, 4 eq) was added. After 2 h of agitation at rt, the resin was washed with isopropanol (5 × 5 mL) and dried *in vacuo* to yield the PL-His$_6$-amide resin (**40**). Finally, the construct was deprotected and cleaved from the resin using 10 mL of a TFA solution (95% TFA, 4% water, 1% triisopropyl silane) at rt for 2 h. The resin was filtered and washed with another 10 mL of TFA solution. The filtrate was concentrated and dried *in vacuo* to afford crude product **41**. For purification, LC-MS was performed using the Agilent purification system with a C18 Vydac 218TP54 reversed-phase column. A gradient of acetonitrile in water (both containing 0.1% TFA) from 5 to 50% was run to achieve the pure product **41** (t_R = 2.98 min, 8.8 mg, 65%).

ESMS: m/z calcd for $C_{49}H_{60}N_{20}O_{12}$ 1121.5 $[M + H]^+$; found, 1121.7 $[M + H]^+$.

4.8. Ni-NTA Purifications

The purification of the test peptide NAPamide using a tag and a commercially available Ni-NTA column was one of the main tasks in this work. In a first step, the purification was established with 1,10-phenanthroline alone, later on, the purification was performed with the NAPamide construct **36**.

Reagents

HBS-N (0.01 M HEPES *pH* 7.4, 0.15 M NaCl) was purchased from Biacore (Biacore AB, Uppsala, Sweden). Acetonitrile was purchased from Fluka (Fluka AG, Buchs, Switzerland). 1,10-Phenanthroline monohydrate was achieved from Riedel-deHaën (Fluka AG, Buchs, Switzerland).

Equipment

For the purification standard single use syringes were used from ONCE. The HisTrap HP (1 mL) column was purchased from GE Healthcare (GE Healthcare, Otelfingen, Switzerland). Injection, equilibration, and washing steps were performed manually by connecting the syringe directly to the HisTrap column. A Molecular Devices SpectraMax plus UV absorbance plate reader was used to analyze the elution and wash fractions photometrically. UV Star 96-well microtiter plates were ordered from Greiner Bio-One (Greiner Bio-One GmbH, Frickenhausen, Germany) to allow analysis in the UV range.

4.8.1. Evaluation with 1,10-Phenanthroline

Prior to the experiment, absorbance spectra (190 to 700 nm, 5 nm steps) of a 10-fold dilution series of 1,10-phenanthroline (2.8 mg/mL to 0.0028 mg/mL) in elution buffer (HBS-N/acetonitrile, 1:1, including 500 mM imidazole) were recorded, to be later compared with wash and elution fractions. Before loading the phenanthroline, the HisTrap column was equilibrated with 10 mL loading buffer (HBS-N/acetonitrile, 1:1). Phenanthroline (4 mg) was dissolved in loading buffer (400 μL) and loaded onto the column. The column was washed with loading buffer (10 mL), and wash fractions

were collected (each 1.5 mL, fractions "wash I"). A small portion of each wash fraction (200 µL) was photometrically analyzed in the plate reader measuring the absorbance between 190 and 400 nm (steps of 5 nm). Elution was performed using 10 mL of elution buffer and fractions were collected (each 1.5 mL, fractions "elution I"). Again, 200 µL samples of the collected elution fractions were analyzed in the plate reader. Wash fractions still containing 1,10-phenanthroline were reloaded onto the column after equilibration with loading buffer (10 mL) and collected as well (each 1.5 mL, fraction "intermediate"). After washing with loading buffer (wash II), elution was performed again with elution buffer until no absorbance of phenanthroline was detectable any more (elution II). All fractions were pooled according to their origin (wash I, elution I, intermediate, wash II, and elution II) and concentrated *in vacuo*. For quantification, a 1,10-phenanthroline standard was prepared (25 µg/mL to 0.781 µg/mL in loading buffer), and absorbance was measured at 260 nm. Samples were diluted with loading buffer (1:100) and measured in triplicates. Three samples (200 µl) of loading buffer were used as blanks. For long-term storage the HisTrap column was washed with methanol (10 mL) and stored in the same solvent at -20°C.

4.8.2. Purification of (*E*)-3-(1,10-phenanthrolin-5-yl)acryoyl-NAPamide (36)

Product **36** was purified as described for 1,10-phenanthroline (section 4.8.1) with minor variations: The whole amount of **36**, synthesized before (0.00549 mmol, theoretical yield of 5.8 mg pure peptide), was dissolved in 2 mL loading buffer. After equilibration of the column with loading buffer (5 mL), half of the freshly prepared solution (1 mL) was loaded onto the column with the syringe and stored at -20°C over night. The next morning, the procedure was continued as described above. The fractions from the first elution round (e1) were pooled and stored separately from the pooled elution fractions of the second elution (e2). Both fractions e1 and e2 were concentrated *in vacuo* and dissolved in 1 mL of water/acetonitrile (1:1, including 0.2% HCOOH) for HPLC analysis. HPLC analysis was performed for a qualitative investigation using the Agilent 1100 HPLC system with a Phenomenex Gemini C18 (4.6 × 250 mm, 5 µm; Brechbühler AG, Schlieren, Switzerland) column. For

quantification fractions e1 and e2 were separated from imidazole by HPLC purification using the same system mentioned above. Single peak at 9.64 min was collected and analyzed by hydrolysis and dabsylation as described in section 4.3.

4.9. SPR Experiments

Interaction analyses between Ni-NTA surfaces and various ligands were performed to determine the binding affinities and kinetics of different potential tags and tag constructs. These qualitative and quantitative experiments were carried out on a Biacore system using surface plasmon resonance (SPR).

Reagents

Degassed and ready-to-use running buffers HBS-N (0.01 M HEPES *pH* 7.4, 0.15 M NaCl) and HBS-EP (0.01 M HEPES pH 7.4, 0.15 M NaCl, 3 mM EDTA, 0.005% v/v surfactant P20) were purchased from Biacore (GE Healthcare, Freiburg, Germany). Sensor chips with covalently attached NTA, BIAdesorb 1 (0.5% SDS), BIAdesorb 2 (50 mM glycine *pH* 9.5), and BIAdisinfectant (sodium hypochlorite) solutions were ordered from Biacore, too. $NiCl_2 \cdot 6H_2O$, DMSO, EDTA, and 5-nitro-1,10-phenanthroline were purchased from Sigma (Fluka AG, Buchs, Switzerland). 2-Aminopyridine and picolinic acid were purchased from Fluka (Fluka AG, Buchs, Switzerland). Methyl picolinate, 3-aminopyrazine-2-carboxylic acid, neocuproine, and 4,7-dimethoxy-1,10-phenanthroline were ordered from Aldrich (Fluka AG, Buchs, Switzerland). 1,10-Phenanthroline was achieved from Riedel-deHaën (Fluka AG, Buchs, Switzerland), 4-aminopyridine-2-carboxylic acid was ordered from Apollo Scientific Ltd (Stockport, UK). 2-Amino-1,10-phenanthroline and 6-(acetylamino)pyridine-2-carboxylic acid were purchased from Specs (Specs, Delft, Netherlands), 6-amino-2-(2-pyridyl)pyrimidin-4-ol was ordered from Maybridge (Tintagel, UK).

Equipment

All SPR analyses were performed on a Biacore 3000 system (GE Healthcare, Freiburg, Germany). In addition, a Thermo Haake C10/K10 water bath system (Digitana AG, Horgen, Switzerland) was used for temperature control of the Biacore 3000 autosampler. All vials and caps were purchased from GE Healthcare.

For degassing of buffers, a Branson 2510 ultrasonic water bath (Merck Schweiz AG, Dietikon, Switzerland) was used.

Data processing and determination of binding affinities (K_A, K_D) and kinetics (k_{on}, k_{off}) was performed with the software Scrubber 1.0g or 2.0a (BioLogic Software Pty Ltd., Campbell, Australia).

4.9.1. General Procedures

To achieve reproducible data of high quality, different cleaning and maintenance procedures were performed. Desorb procedures using BIAdesorb solutions were carried out on a weekly basis, and sanitize routines were performed with BIAdisinfectant solution to inhibit bacterial growth at least every month. All running buffers were degassed every day in the ultrasonic bath under reduced pressure (<50 mbar) prior to use. Samples to be injected into the system were centrifuged to remove air bubbles trapped at the bottom of the vial. In addition, the flow cell system was always kept under constant flow even between experiments.

Two different buffers were used in parallel for each experiment: HBS-N with additional 50 μM of EDTA, to scavenge contaminating ions, was used as eluent buffer, HBS-EP was applied as dispensor buffer. The eluent buffer was connected to the left pump of the Biacore 3000, which is responsible to maintain a constant flow and to carry out sample injections. Dispensor buffer was connected to the right pump used for the sample preparation and wash steps. The standard flow rate for all experiments was 20 μl/min. The temperature within the Biacore system was maintained at 25°C.

NTA sensor chips were stored in eluent buffer at -20°C. Before reusing, the chip surface was extensively washed with water and finally dried under nitrogen flow before insertion into the Biacore 3000 system.

To compare the binding affinities or kinetics of different ligands the sensorgrams of the SPR experiments were processed with the software Scrubber 1.0g or 2.0a. Only the latter allowed determination of kinetics (k_{on}, k_{off}). A single value of k_{on} and k_{off} was calculated for each triplicate injection, to determine the mean value of k_{on} and k_{off} as well as the standard deviations from all triplicate injections. To eliminate bulk effects

or systemic artifacts double referencing was applied to all measurements [*175*], which was included in the software, too. For the calculations, all concentrations were corrected with the deviation determined by the dabsylation experiment (see section 4.3).

4.9.2. Oligohistidine Binding Assay

Tenfold dilution series of oligohistidines (**1** – **9**) were freshly prepared in eluent buffer before each experiment. Loading of Ni^{2+} on the NTA chip was performed with a $NiCl_2$ solution (500 μM in eluent buffer) and regeneration with imidazole (500 mM in water), followed by regeneration solution (10 mM HEPES, 150 mM NaCl, 0.005% polysorbate 20, 350 mM EDTA *pH* 7.4), and finally 0.5% SDS.

The experiment was started with a 1 min injection of $NiCl_2$ solution to load the NTA chip. Then, each oligohistidine sample was injected for 5 min followed by 5 min of undisturbed dissociation time. The regeneration procedure consisted of two subsequent 1-min injections of imidazole and regeneration solution. Finally, the surface was washed with 0.5% SDS in water for 1 min at a flow rate of 100 μl/min. Regeneration and washing was performed twice for each cycle. Oligohistidine solutions were injected in five different concentrations at different concentration ranges depending on the binding affinity (Table 17).

Table 17: Concentration Range of Oligohis (**1** – **9**).

Compound	No.	Concentration range
His2	(**1**)	5 mM – 500 nM
His3	(**2**)	500 μM – 50 nM
His4	(**3**)	50 μM – 5 nM
His5	(**4**)	5 μM – 500 pM
His6	(**5**)	5 μM – 500 pM
His7	(**6**)	5 μM – 500 pM
His8	(**7**)	5 μM – 500 pM
His9	(**8**)	5 μM – 500 pM
His10	(**9**)	5 μM – 500 pM
PL-His$_6$-amide	(**41**)	200 μM – 3 nM
L-histidine [a]	-	20 mM – 610 nM

[a] L-histidine was included for comparison reasons with the other peptides in this series

Each concentration was measured in triplicates in a randomized order. The temperature of the autosampler rack was kept at 17°C. A NTA flow cell without Ni^{2+} was used as reference cell. Three buffer blanks before, one between the sample series, and one at the end of the experiment were used for double referencing during data processing.

The binding assay of L-histidine was slightly modified: 20 µl of His as 2-fold dilution series was injected during the association phase. Undisturbed dissociation was performed during 60 s to reach baseline level again. A single injection of 20 µl regeneration solution was sufficient to regenerate the surface.

4.9.3. His_2Ala_4 Binding Assay

The binding assay for the His_2Ala_4 series was developed by Dr. Daniel Ricklin (Institute of Molecular Pharmacy, University of Basel). The same experimental setup was used as described for the oligohistidines (section 4.9.2). Stock solutions (25 mM in eluent buffer) of peptides **10** – **14** were freshly prepared before the experiment. Peptide samples of fivefold linear dilutions ranging from 0.32 – 5000 µM were injected. The autosampler rack was kept at 17°C. After preparation of the surface with Ni_2Cl solution, the samples were injected with a 1 min pulse followed by a dissociation time of 20 s. Regeneration of the surface was performed with a single 1 min pulse of regeneration solution. Again, 3 blanks were included at the beginning, one in between the triplicates, and one at the end of the experiment. All blanks were included into the double referencing (see section 4.9.1).

4.9.4. His_xAla_y Binding Assay

Analysis of the His_xAla_y series (**15** – **19**) was performed as mentioned for the oligohistidines (section 4.9.2). Before each experiment the chip surface was washed with 20 µl NaOH solution (100 mM) at a flow rate of 20 µl/min for an increased stability of the binding curves. Stock solutions of the peptides (5 mM in eluent buffer) and 5-fold dilutions were freshly prepared before the experiment. In case of His2 (**1**),

the dilution factor was 10. The concentration ranges of the different peptides are shown in Table 18.

Table 18: Concentration Range of His_xAla_y (**15** – **19**).

Compound	No.	Concentration range
His_2Ala_41 [a]	(**10**)	5 mM – 320 nM
His_xAla_y1	(**15**)	200 µM – 12.8 nM
His_xAla_y2	(**16**)	200 µM – 12.8 nM
His_xAla_y3	(**17**)	5 mM – 320 nM
His_xAla_y4	(**18**)	5 mM – 320 nM
His_xAla_y5	(**19**)	5 mM – 320 nM
His2 [a]	(**1**)	5 mM – 500 nM

[a] His_2Ala_41 and His2 were included in this series to ensure same conditions (chip, solvents) for all peptides to be compared within this series

The temperature of the autosampler rack was maintained at 19°C. After a 1 min injection of $NiCl_2$, 20 µl of the peptide sample was injected and followed by a dissociation phase of 30 s. To finish the cycle, the surface was washed with 20 µl of regeneration solution followed by two pre-programmed wash routines "wash needle" and "wash IFC". Double referencing was again used including blanks as described in section 4.9.2.

4.9.5. HXH Binding Assay

The same experimental setup was used as described for the oligohistidines (section 4.9.2). Stock solutions were freshly prepared prior to the experiment (1 mM for **20**, **21**, and **22**; 5 mM for **23** and **24**; all in eluent buffer). After injection of $NiCl_2$ solution, 20 µl of sample (5-fold dilutions in eluent buffer) was injected, followed by a dissociation phase of 30 s. Concentration ranges are shown in Table 19.

Table 19: Concentration Range of HXH (20 – 24).

Compound	No.	Concentration range
HGH	(20)	1 mM – 64 nM
HAH	(21)	1 mM – 64 nM
HSarH	(22)	1 mM – 64 nM
HAibH	(23)	5 mM – 320 nM
HPH	(24)	5 mM – 320 nM

To wash the surface 20 µl of regeneration solution was injected and additionally the two routines "wash needle" and "wash IFC" were performed for a better signal quality. The temperature of the autosampler rack was kept at 19°C.

4.9.6. Phenanthroline Binding Assay

The phenanthroline binding assay was performed as described for the oligohistidines in section 4.9.2 using the same washing procedures with imidazole, regeneration solution and SDS. The number of blank injections at the beginning of the experiment was increased to five injections. The temperature was kept constant at 19°C. After Ni^{2+} loading, 60 µl of sample was injected followed by a dissociation phase of 180 s. The different phenanthrolines and phenanthroline derivatives, which were measured in the phenanthroline assay, are shown in Table 20.

Table 20: Concentration Range of Phenanthroline-like Structures.

Compound	No.	Concentration range	Dilutions
2,2'-Bipyridyl	(30)	1 mM – 64 nM	10-fold
1,10-Phenanthroline	(42)	10 µM – 100 pM	10-fold
Neocuproine	(43)	250 µM – 16 nM	5-fold
4,7-Dimethoxy-1,10-phenanthroline	(44)	2.5 µM – 20 nM	2-fold
2-Amino-1,10-phenanthroline	(46)	10 µM – 39 nM	2-fold
5-Amino-1,10-phenanthroline	(47)	2 µM – 7.8 nM	2-fold
5-Nitro-1,10-phenanthroline	(48)	250 µM – 16 nM	5-fold
3-(1,10-phenanthrolin-5-yl)prop-2-enoic acid	(34)	10 µM – 4 nM	5-fold
N-[2-(1,10-phenanthrolin-5-ylamino)-2-oxoethyl]-4-[4-(1-hydroxyethyl)-2-methoxy-5-nitrophenoxy]butanamide	(38)	200 µM – 13 nM	5-fold

All samples had to be prepared in DMSO for better solubility. For this purpose, stock solutions 20-fold above the highest concentration to be injected (Table 20) were prepared in 100% DMSO. Finally, to achieve a DMSO concentration of 5% eluent buffer was added, which resulted in the correct sample concentration. The remaining dilutions were prepared using eluent buffer containing 5% DMSO.

Because of the influence of DMSO on the binding signal, a calibration was necessary [176]. Different mixtures of two solutions (A = 1 mL running buffer + 50 μl eluent buffer, B = 1 mL running buffer + 1 μl DMSO; running buffer = 5% DMSO in eluent buffer) according to Table 21 had to be prepared and were injected between 5 blank injections at the very beginning of the experiment and the first sample.

Table 21: DMSO Calibration Solutions.

Calibration	A [μl]	B [μl]
1	400	0
2	300	100
3	200	200
4	100	300
5	0	400

Signal corrections based on the calibration solutions were directly performed during binding evaluation in the software Scrubber 2.0a.

4.9.7. Picolinic acid Binding Assay

The picolinic acid binding assay was performed as described for the oligohistidines in section 4.9.2. Stock solutions of all samples were prepared freshly before the experiment in eluent buffer. Association of the samples to the Ni^{2+}-surface was performed by 60 μl injections using different concentration ranges and dilution factors (Table 22), followed by a dissociation phase of 180 s.

Table 22: Concentration Range of Picolinic acid Structures.

Compound	No.	Concentration range	Dilutions
2-Aminopyridine	(**51**)	80 mM – 625 µM	2-fold
Picolinic acid	(**52**)	500 µM – 6.4 nM	5-fold
3-Aminopyrazine-2-carboxylic acid	(**53**)	1 mM – 64 nM	5-fold
Methyl picolinate	(**54**)	20 mM – 39 µM	2-fold
4-Aminopyridine-2-carboxylic acid	(**55**)	5 mM – 1.6 µM	5-fold
6-(Acetylamino)pyridine-2-carboxylic acid	(**56**)	2 mM – 26 nM	5-fold
6-Amino-2-(2-pyridyl)pyrimdin-4-ol	(**57**)	100 µM – 195 nM	2-fold
5-Methoxypyrimidine-2-carbohydrazide	(**58**)	100 µM – 195 nM	5-fold

The autosampler temperature was kept at 19°C during the experiment. Surface regeneration was performed by a 20 µl injection of imidazole solution (500 mM in water) and 20 µl of regeneration solution. 5 blanks at the beginning and one between the triplicate measurements were included for the evaluation in Scrubber 2.0a.

5.   RESULTS AND DISCUSSION

5.1. Qualitative and Quantitative Analysis of the His-Tag

IMAC has become the most common method for the purification of proteins carrying either a C- or N-terminal histidine (His)-tag. However, only little is known on the binding properties of the His-tag to Ni-NTA. Qualitative and quantitative investigations, such as the determination of equilibrium association constants (K_A), equilibrium dissociation constants (K_D), association rate constants (k_{on}), and dissociation rate constants (k_{off}) would add to a better understanding of this interaction. Surface plasmon resonance (SPR)-based biosensors, *e.g.* Biacore, are suitable systems for the determination of these constants. Biacore (GE Healthcare, Freiburg, Germany) provides commercially available sensor chips with covalently attached NTA chelates, which can be used as a model setup for a Ni-NTA purification system. It was planned to design and synthesize different peptide tags and analyze them with the SPR system. As tags attached to "model" proteins could suffer from the drawbacks as mentioned in section 3.2.5, only uncoupled tags were included into the first part of the study.

5.1.1. The Oligohistidine Series

In general, five or six consecutive histidine residues are attached to a protein as earlier described by Hochuli *et al*. for the purification on a Ni-NTA column [*59*]. The length of six residues turned out to be the optimal length for the purification as demonstrated by Hochuli *et al*. The oligohistidine series (**1** – **9**) should therefore deliver explanations, whether this is also true for the binding affinity.

Synthesis and Purification

The synthesis on the solid-phase using a trityl-based linker was performed without any particular problems, with good yields of at least 40% for all peptides synthesized in this series. This means a coupling efficiency of more than 90% for each step. Histidine is one of the most critical amino acids in peptide synthesis, as it is prone to enantiomerization during the coupling step due to the reactivity of the imidazole

nucleus. The most effective way to suppress enantiomerization is blocking either the π-nitrogen or the τ–nitrogen [*177, 178*].

The purification of the peptides was much more difficult, especially for the short peptide His3 (**2**). As expected, the retention times (t_R) of the HPLC correlates with the length of the tag (Figure 18). Because His3 (**2**) was purified under different conditions, it does not fit into this correlation.
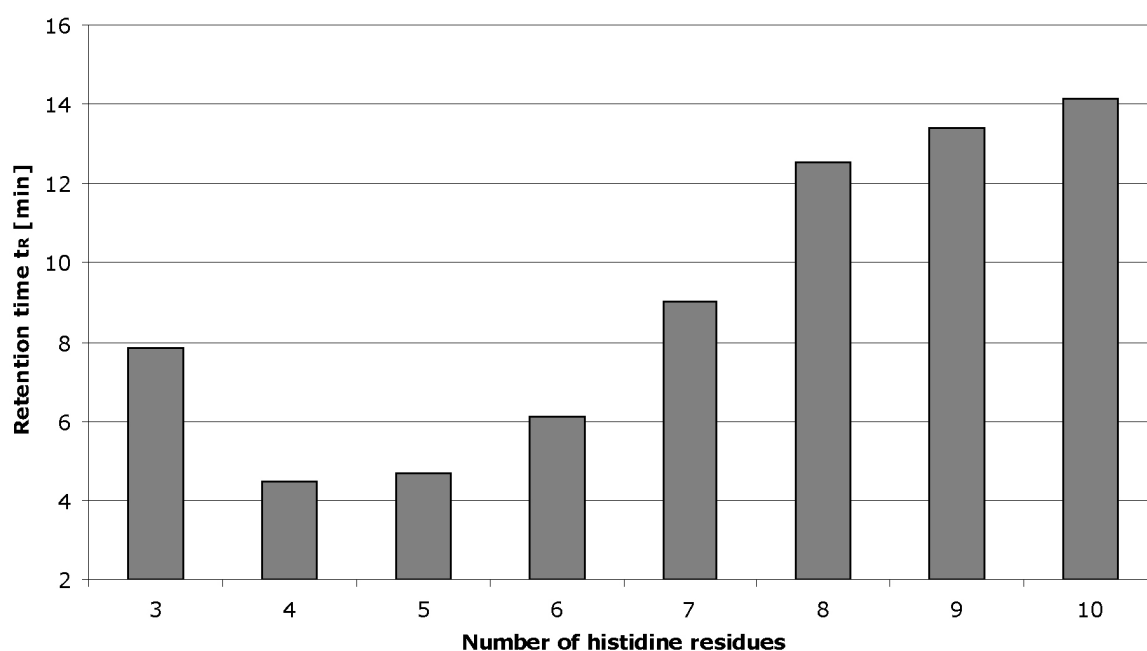

Figure 18: Retention time t_R of HPLC analysis in correlation to peptide length of the different oligohistidines). His3 (**2**) was purified on a different column using a different buffer system, which explains the high t_R.

The difference between two peptides with n and n+1 histidine residues was rather small for n = 4 and 5, as well as for n = 8, 9, and 10. During the synthesis of His5 (**4**), His4 (**3**) will appear as a byproduct, which has to be separated from the desired product. The difference of 0.2 min between product (**4**) and byproduct (**3**) was at the lower limit for a baseline separation. The differences in t_R between peptides with n = 5, 6, 7, and 8 histidines were larger and therefore purification did not reveal any problems.

Purification of His3 (**2**) was problematic due to the low retention on the reversed-phase C18 columns. Both running buffers contained 0.1% TFA lowering the *pH* below the *pI* of histidine (7.6). Therefore, His3 (**2**) is at least partially protonated. This led to highly hydrophilic peptides with poor retention on reversed-phase columns. Therefore,

the buffer system for the purification of His3 (**2**) was changed from 0.1% TFA to ammonium acetate buffer at *pH* 8.8 to decrease the average charge on the molecule. This prolonged the retention of His3 (**2**) from initially 2.5 min (injection peak) with the water/acetonitrile/TFA system up to 7.9 min with the ammonium acetate/acetonitrile system.

After HPLC the lyophilized peptides contain a certain amount of salt. Therefore, the peptides were hydrolyzed and than derivatized with 4-(4-dimethylaminophenylazo)benzenesulfonyl chloride (DABS-Cl). Comparison with an amino acid standard treated with the same procedure allowed the determination of the amino acid amount in the samples. The results from the dabsylation experiments demonstrated the necessity of such salt content determinations to gain reliable data in the SPR experiments of synthetic peptides, where the knowledge of the exact concentration of the samples is crucial (Table 23).

Table 23: Salt Content of Oligohis (**1** – **9**).

Compound	No.	Salt Content [%, w/w]
His2	(**1**)	49 [a]
His3	(**2**)	23
His4	(**3**)	62
His5	(**4**)	64
His6	(**5**)	60
His7	(**6**)	59
His8	(**7**)	55
His9	(**8**)	54
His10	(**9**)	58

[a]   A salt content of 50% was given by the manufacturer

The salt content was in most cases more than 50%. Therefore, a K_D determined by simply weighing the peptide on the scales would underestimate the binding affinity by a factor of 2. His2 (**1**) could be used for the validation of the derivatization method. The value specified by the manufacturer was 50% and therefore similar to the value obtained by dabsylation (49%). The high amount of salt after purification with HPLC is a result of the buffer conditions. For example, in hexahistidine dissolved in a 0.1% TFA, probably all imidazole residues and the N-terminal amine are protonated. Therefore, up to 7 TFA counter ions are bound to the peptide after lyophilization,

leading to a calculated salt content of 48% (w/w). The only molecule containing a significant lower amount of salt was His3 (**2**), which was purified under basic conditions at *pH* 8.8. At this *pH,* the histidine residues are mostly uncharged.

Binding Assay

The method used for the binding assay was already published in a study of Nieba *et al*. [*126*] and was available as a recommendation note of Biacore [*158*]. Nevertheless, the eluent buffer was slightly modified and prepared without addition of polysorbate 20. When the samples were kept in eluent buffer containing polysorbate, no binding of His6 (**5**) could be detected even at high concentrations. When polysorbate was omitted in the eluent buffer, the binding signal rose with increasing peptide concentration as expected. A clear explanation for this effect was not found. Complexation effects could be a possible reason for the inhibition of the binding of His6 (**5**) to the Ni-NTA surface. To avoid carry over effects, especially after injections of highly concentrated samples, wash steps with 500 mM imidazole and 0.1% SDS had to be introduced in addition to the regeneration with 350 mM EDTA. To guarantee high signal intensities and reproducibility of the triplicate measurements, the complete regeneration of the surface was crucial. Thus, the surface could be freshly loaded with nickel before each sample injection, and the signal derived from the nickel loading step could be used as a monitor of the chip quality. Generally, the amount of nickel loaded onto the surface varied slightly from flow cell to flow cell. After several weeks of chip usage, a slight decrease of the nickel signal was observed and the chip had to be exchanged. An overview of the binding signals for the oligohistidine series is shown in Figure 19.
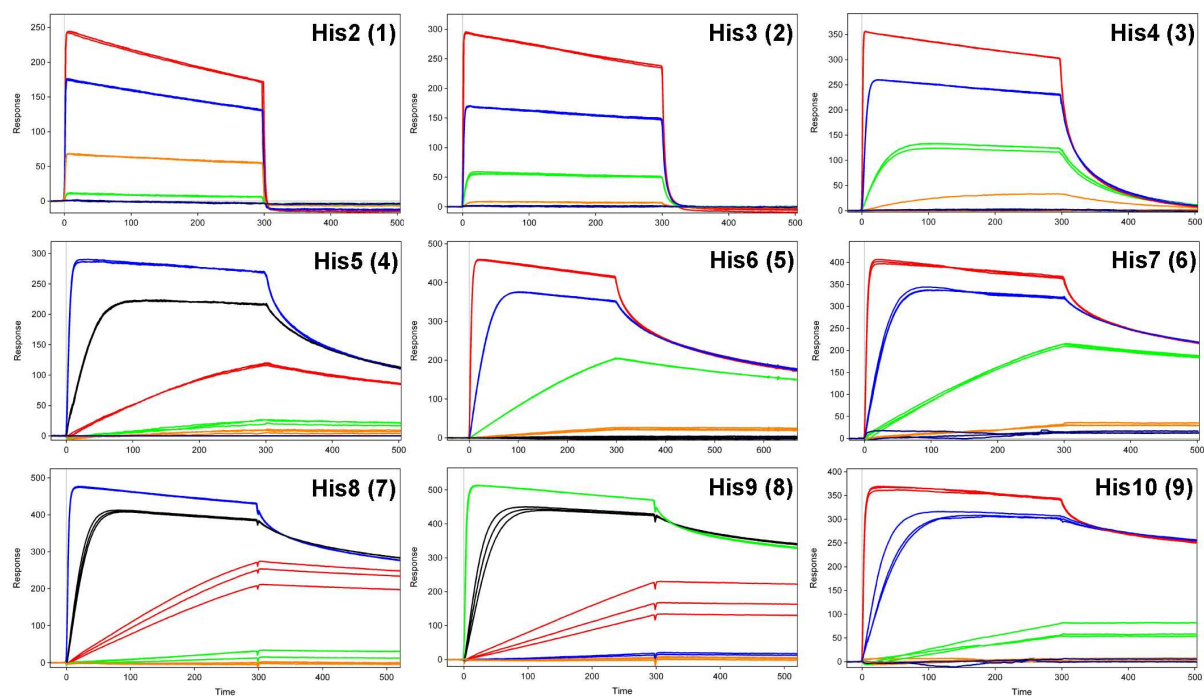
Figure 19: Sensorgrams of the oligohistidine series (**1** – **9**). The samples were measured in triplicate injections. The concentration ranges and dilution factors are given in 4.9.2, Table 17.

The sensorgrams showed highly reproducible triplicates up to His7 (**6**). With increasing peptide length (more than seven amino acids) the triplicates deviated, especially at concentrations around saturation level. Reasons like carry over effects or reduced binding activity could be excluded, because no changes were detected in case of altered injection orders or wash procedures. Furthermore, the signals were checked for mass transfer by running the experiment at different flow rates from 10 to 100 μl/min. And finally, impurities or degradation of peptides were excluded by HPLC analysis before and after SPR experiments. As the effects are only visible for long peptides, time-dependent conformational changes might be considered as a possible reason for this phenomenon.

Looking at the steady state phases, another abnormality becomes visible. All peptides showed a linear decrease in binding signal during steady state phase. This decrease is most likely due to the removal of Ni^{2+} from the NTA surface ('nickel leaching') and its full coordination by the peptide in solution. As a consequence, the binding level dropped below the initial baseline after dissociation of the analyte (see sensorgrams of the His2 (**1**) and His3 (**2**) in Figure 19). The same loss was also visible for other peptide series and will be discussed in more detail in section 5.1.3.

According to the sensorgrams, the dissociation rates for tags consisting of four or more histidines altered with different concentrations of analyte, indicating multiple binding events [*126*]. Therefore, the dissociation did not follow a normal exponential decay, and the baseline was not reached within dissociation time. At peptide concentrations below saturation of the nickel surface, the dissociation rate was found to be remarkably slow, probably caused by fast rebinding to vacant metal ions. At concentrations near saturation level, an initial dissociation was observed up to a certain level, where a stable binding signal was reached. At this stage, a temporary equilibrium is reached, at which the amount of free metal ions is high enough to enable rebinding. Finally, the rebinding and therefore the stability of the binding between the tag and the metal depends on the peptide length. When comparing the dissociation phases of oligohistidines **3** – **9** normalized by their molecular weights at same concentrations, the His10 (**9**) elicited the most pronounced rebinding (Figure 20).
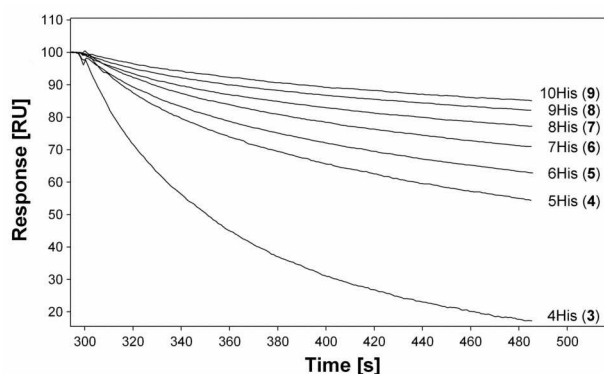

Figure 20: Normalized overlay plots showing the dissociation phase of a selection of oligohistidines [His4 (**3**) to His10 (**9**)] at the same concentration.

The response at the beginning of dissociation was set to 100 and a value of 0 signifies complete dissociation. 90% of His10 (**9**) was still bound to the chip surface after 180 s of dissociation, whereas His4 (**3**) has almost completely dissociated within the same time span. The higher the binding capacity of a molecule, the more rebinding occurs.

The strong rebinding effect as well as the drift during steady state made a kinetic evaluation of the binding curves impossible. The latter effect and the drop below baseline after dissociation also aggravated a determination of the binding affinity of the oligohistidines to Ni-NTA. Nevertheless, fitting of the data to a simple 1:1 binding

model (Equation 2) with the response during steady state R_{eq} allowed at least the determination of apparent K_Ds.

Despite these problems, a comparison of the K_Ds of the oligohistidines was still possible, because all peptides showed a similar behavior. For the calculation of the K_Ds, R_{eq} on the drifting steady state curve were determined as an average value of a 2 s time period ten seconds before the end of the injection. Concentration plots thus obtained fitted well with a 1:1 binding model (Figure 21). Values at higher concentrations (500 nM and 5 μM) deviated more from the fitted data, which might be influenced by the more pronounced decrease of binding signal during steady state at these concentrations.
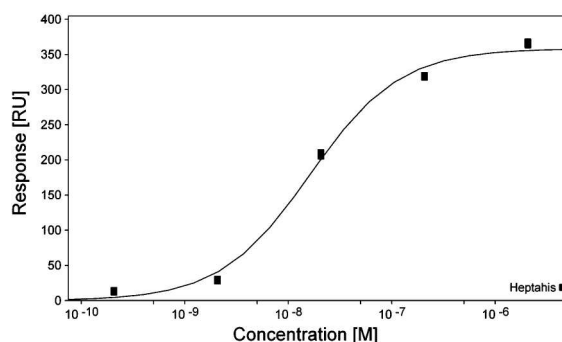

Figure 21: Fit of Langmuir isotherm (single-site-interaction model of His7 (**6**) (5 μM, 500 nM, 50 nM, 5 nM, 500 pM).

The above mentioned method was used to determine the equilibrium dissociation constant and binding affinities of the oligohistidines (**1 – 9**) (Table 24).

Table 24: Apparent K_Ds and K_As of Oligohistidines (**1 – 9**).

Compound	No.	App. K_D [μM]	App. K_A [10^5 M^{-1}]
His2	(**1**)	62.7 ± 3.4	2
His3	(**2**)	2.23 ± 0.15	45
His4	(**3**)	0.313 ± 0.031	319
His5	(**4**)	0.024 ± 0.002	4202
His6	(**5**)	0.014 ± 0.001	7246
His7	(**6**)	0.016 ± 0.001	6173
His8	(**7**)	0.020 ± 0.002	4902
His9	(**8**)	0.047 ± 0.002	2119
His10	(**9**)	0.070 ± 0.007	1437

His2 (**1**) showed the highest K_D (62.7 μM) of all oligohistidines. Addition of another histidine increased the affinity by a factor 28. Another 7-fold gain in activity was achieved with His4 (**3**). This tendency continued up to six histidines, which showed the maximal affinity of the series (K_D = 14 nM). Every further addition of histidines did not improve the binding affinity, demonstrated by the 7-fold lower affinity of His10 (**9**) compared to His6 (**5**). Therefore, six histidines are the optimal length for such an oligohistidine tag. The initial improvement in binding affinity from His2 (**1**) to His6 (**5**) might be explained by an increase in binding enthalpy (ΔH) due to the higher number of possible interactions (Figure 22). There are several reports describing such a cooperative mechanism for the binding of proteins to IMAC adsorbents due to multipoint interactions between residues on the protein and the immobilized metal ions [*179-181*].
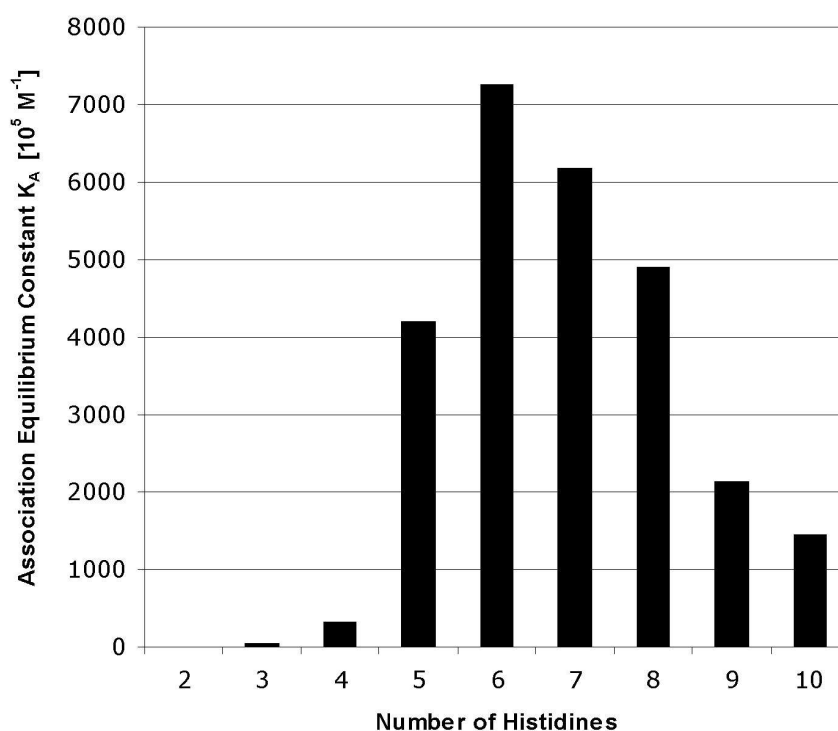

Figure 22: Binding affinity K_A (1/K_D) of different oligohistidines to Ni-NTA chips in surface plasmon resonance experiment. Due to a better illustration the K_As instead of the K_Ds are presented within this chart.

Furthermore, the increase in rotatable bonds for short peptides might as well lead to a more flexible peptide increasing the possibility of such multiple binding events.

However, the free Gibbs energy (ΔG) also depends on the entropy term ($T\Delta S$), which explains the lower affinity of His10 (**9**) compared to His6 (**5**) (Equation 6).

$$\Delta G = \Delta H - T\Delta S \qquad\qquad \textbf{[Equation 6]}$$

When the peptide length exceedes to more than six residues, the entropy term outbalances the enthalpic contribution. The loss of entropy by forcing the ligand into the binding conformation rises with each additional residue. Above a certain chain length, this leads to a weaker binding. A peptide length of six histidine residues represents therefore an optimal balance between enthalpic and entropic components.

To complete the oligohistidine series, L-histidine was included in the series, too. The difference between the oligohistidine series and L-histidine lies in the valency of the ligand. While all oligohistidine binding curves were fitted to a simple 1:1-binding model, L-histidine had to be fitted to a two-binding-site model, because two ligand molecules are able to bind simultaneously to Ni-NTA. The sensorgram and binding curve of L-histidine are shown in Figure 23.
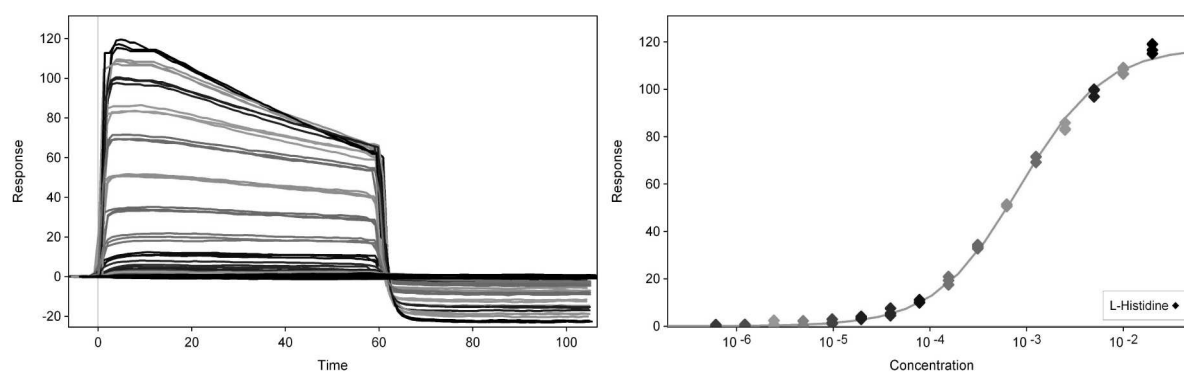

Figure 23: Sensorgram and Langmuir isotherm (single-site interaction model) of L-histidine (20 mM – 610 nM).

The sensorgrams of L-histidine looked similar to those of His2 (**1**). A pronounced drop during steady state made the determination of a binding affinity again difficult. In addition, the fit did not show a clear two-binding-site behavior with clearly separated binding steps. This might indicate that both K_Ds for each step are similar, leading to a simultaneous binding of two histidine molecules. Another reason could be that binding of a second ligand occurs with a much lower affinity (K_D higher than 20 mM) *e.g.* due to increased steric hindrance or unfavorable electrostatic interactions. Unfortunately,

Biacore is not design to measure K_Ds in the medium or even high millimolar range. Due to the lack of a clear two-binding-site behavior, determination of an apparent K_D was performed by fitting the data set to a simple 1:1 binding model. The resulting K_D of 430 μM was about 7-fold higher than the K_D of His2 (**1**). The best bidentate ligand consisting of two histidine residues would therefore be a ligand with a K_D of 180 nM (430 μM × 430 μM), which is 3-fold lower than the value for His2 (**1**). This indicates most probably an unfavorable arrangement of two vicinal histidines for the binding to Ni-NTA (*e.g.* non-optimal distance).

5.1.2. The Preferred Binding Motif: His$_2$Ala$_4$ series

Nickel is coordinated by NTA in a tetradentate manner (3 COO$^-$, 1 N). To complete the requested octahedral coordination, two additional interactions are required. Therefore, only two histidines can bind simultaneously via their imidazole nitrogens to the metal ion. Therefore, the His$_2$Ala$_4$ series (**10 – 14**) was synthesized to evaluate the optimal distances between two coordinating histidines. The C-terminal histidine residue was kept constant and the other His residue was shifted through the peptide. Ala was chosen as the second amino acid building block because it is inert, non-problematic in solid-phase peptide synthesis, and widely used in similar experiments (*e.g.* Ala screen). All peptides of the His$_2$Ala$_4$ series (**10 – 14**) were analyzed with SPR.

Synthesis and Purification

The synthesis of this peptide series did not reveal any relevant problem except for precipitation, which was impossible either with diethylether or with *tert*-butylmethylether. Therefore, the crude peptide was directly concentrated after cleavage and lyophilized from a 10% acetic acid solution. Since only lower concentrated peptide solutions could be injected into the HPLC system, extended purification times resulted. Furthermore, when water/acetonitrile/TFA was used, all peptides eluted within the injection peak together with other impurities (*e.g.* reagents, byproducts). Similar to His3 (**2**), the purification system had to be changed to ammonium acetate/acetonitrile resulting in longer retention times and purer products.

Finally, the purification yielded peptides with an average salt content of up to 75%, which is significantly higher than for the oligohistidines (**1** – **9**).

Binding Assay

The binding assay for His_2Ala_4 (**10** – **14)** peptides was based on the experience from the oligohistidine assay (section 4.9.2). The overall shape of the sensorgrams was similar for all peptides (Figure 24). However, differences regarding signal intensity and steady state drift were observed.
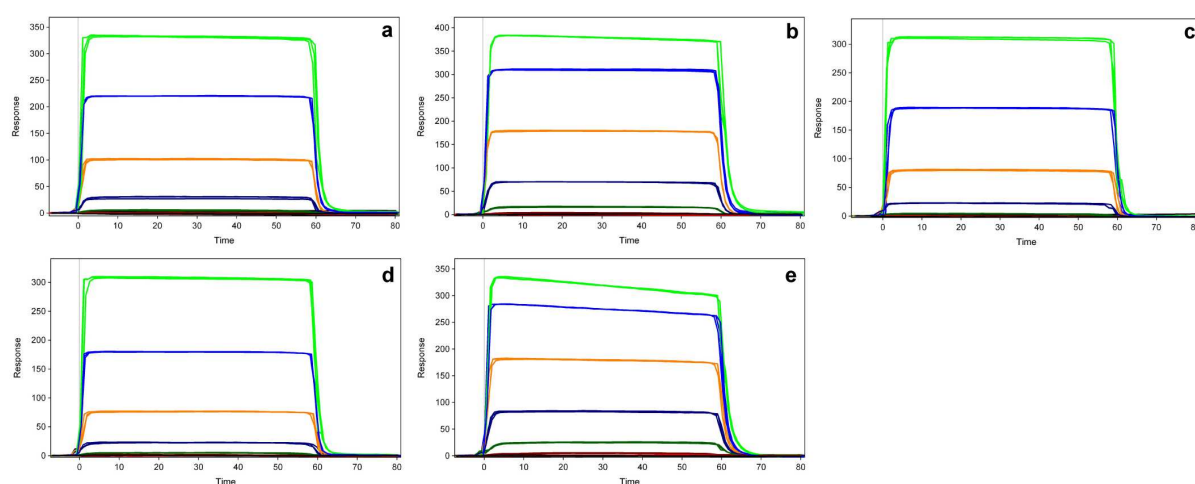

Figure 24: Sensorgrams of His_2Ala_4 series (**10** – **14**). Triplicate injections were measured over a concentration range of 0.32 - 5000 μM (fivefold dilutions). a: AAAAHH (**10**); b: AAAHAH (**11**); c: AAHAAH (**12**); d: AHAAAH (**13**); e: HAAAAH (**14**).

Compared to the oligohistidine series (Figure 19), the kinetic rate constants were much faster than for most of the oligohistidines. The binding curves rapidly reached baseline level after the start of the dissociation phase. This simplified the washing procedure to a great extent. After complete dissociation of the analyte, a single injection of a 350 mM EDTA solution was sufficient for regenerating the chip surface and for achieving highly reproducible data as demonstrated with the triplicate injections. A steady state drift of the binding curve was observed for peptides AAAHAH (**11**) and HAAAAH (**14**). The effect was less pronounced compared to His2 (**1**). Nevertheless, the signals allowed the determination of an apparent K_D by fitting steady state binding signals. The dissociation followed a normal exponential decay and did not show extensive rebinding effects as observed for the

oligohistidines ($1 - 9$). Therefore, the His_2Ala_4 series was fitted kinetically (Figure 25) to determine k_{on}, k_{off}, and K_D.
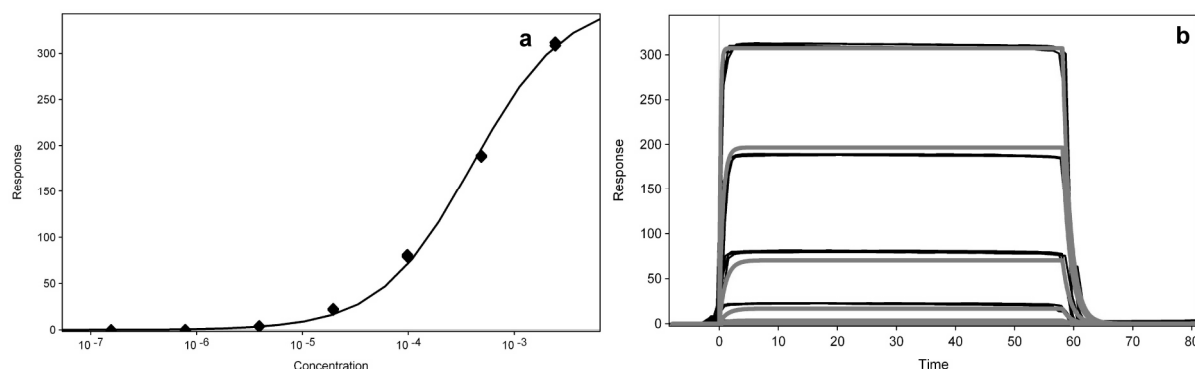

Figure 25: a: Steady state fit of AAHAAH (**12**) to a simple 1:1 binding model. b: Kinetic fit of AAHAAH (**12**) to a simple 1:1 binding model. Light gray lines represent binding curves of calculated single-site binding model. Black curves represent experimental values.

The steady state fit showed a good correlation with the experimental values. The same was true for the kinetic fit, which showed an excellent overlap with the experimental data. Minor deviations are most likely due to small rebinding effects, binding of both or only one histidine residue to Ni-NTA, or the slight decrease during injection of the analyte. The residual standard deviation (res SD) of the fit was 6.05. The fits were of similar quality for all His_2Ala_4 peptides (**10** – **14**) allowing a comparison of kinetic and affinity data within this series. These data are shown in Table 25.

The binding affinities obtained by steady state affinity or kinetically were in good agreement. Standard deviations (SD) lay below 3%. The kinetic data showed a much higher SD of up to 42% for the k_{off} of AHAAAH (**13**). This might be due to the fact that the kinetic rate constants are extremely fast ($T_{1/2} < 2.2$ min) and therefore difficult to determine. With fast kinetics, a small deviation of the fitting curve can lead to huge differences in the calculated values.

Table 25: Evaluation of kinetics and binding affinity of His_2Ala_4 series (**10 – 14**).

Compound	No.	K_D (ss [a]) [µM]	k_{on} [$M^{-1}s^{-1}$]	k_{off} [s^{-1}]	$T_{1/2}$ [s]	K_D (kin [b]) [µM]
AAAAHH	(**10**)	288 ± 3	1164 ± 180	0.334 ± 0.053	2.1	288 ± 1
AAAHAH	(**11**)	112 ± 1	5970 ± 274	0.685 ± 0.021	1.0	111 ± 1
AAHAAH	(**12**)	402 ± 4	2181 ± 592	0.877 ± 0.258	0.8	401 ± 9
AHAAAH	(**13**)	440 ± 6	2011 ± 849	0.889 ± 0.372	0.8	442 ± 4
HAAAAH	(**14**)	70 ± 1	10194 ± 1320	0.709 ± 0.094	1.0	70 ± 1

[a] steady state fit

[b] kinetic fit, $K_D = k_{off}/k_{on}$

AAAHAH (**11**) (K_D = 112 µM) and HAAAAH (**14**) (K_D = 70 µM) showed the lowest K_Ds of the series. This indicates a favorable arrangement for two histidine residues separated either by one (binding motif 1-3) or by 4 amino acids (binding motif 1-6) when binding to Ni-NTA. This confirmed the observations of molecular simulations from Liu *et al.* with oligohistidines and free nickel ions in solution, who found the 1-3 and the 1-6 as the preferred binding motifs, too [*131*]. The higher flexibility of HAAAAH (**14**) compared to AAAHAH (**11**) might simplify an optimal arrangement of the binding imidazole nitrogens explaining the slightly higher affinity of **14**. AAAAHH (**10**) was a factor 2.6 weaker than AAAHAH (**11**). The two peptides with the lowest affinity were AAHAAH (**12**) and AHAAAH (**13**) with K_Ds of 402 µM and 440 µM, respectively. The 4-fold lower affinity of AAAAHH (**10**) compared to His2 (**1**, 5.1.1, Table 24) was explained by entropic and steric effects.

The differences in binding affinity within the His_2Ala_4 (**10 – 14**) series were mainly based on differences in the association rates. Peptides **11** and **14** showed significantly higher k_{on}s compared to **12** and **13.** The dissociation rates of **11** and **14** were only slightly slower and did not contribute that much to the higher affinity. AAAAHH (**10**) elicited a different behavior. The k_{on} was even lower than for peptides **12** and **13,** but the dissociation rate was the slowest among this series. The proximity of the two histidines in **10** explains the low k_{off}. When one histidine residue is dissociating from the Ni-NTA complex, its rotational freedom and its flexibility in respect to the other histidine residue, which is still bound to Ni-NTA, is rather small. Therefore, the probability of rebinding to the same complex is much higher compared to a His with an increased flexibility. Thus, the complex might be more stable leading

to an increased half-life time. This trend continues throughout the series, except for HAAAAH (**14**). This means the larger the distance between the two histidines, the faster is the dissociation rate constant. With **14**, the k_{off} decreased again, because as a result of the high flexibility, contacts to neighboring Ni-NTA complexes are becoming possible leading to increased rebinding.

As already observed for the oligohis series, the His_2Ala_4 (**10 – 14**) also showed a steady loss in binding signal during steady state phase. This constant loss in steady state level and the subsequent drop of the baseline signal under the initial level before injection of the analyte was further analyzed. Complexation of Ni^{2+} from the surface by free analyte molecules could explain this decrease in binding signal as already mentioned in section 5.1.1. "Metal ion transfer" was first observed by Belew *et al.* although for a slightly different metal complex [*109*]. They reported some tri- and tetrapeptides consisting of histidine residues, which did not bind to a Superose-Cu(II) column because of their high affinity to the Cu(II) ions. This high affinity enables to strip off the Cu(II) ions from the solid support. The same phenomenon was observed by Andersson *et al.* when human serum albumin was run on a Ni^{2+}-IDA column [*182*].

A possibility to quantify this effect in the Biacore experiment was provided by the peptides His2 (**1**), His3 (**2**), and HAAAAH (**14**). For these peptides the fast kinetics led to a complete dissociation of the analyte, which enabled to quantify the drop below baseline level. If this drop is due to a loss of Ni^{2+} from the chip surface, it could be correlated with the decreasing signal during steady state using Equation 7. This equation is generally used to predict the binding signal at saturation level for a certain analyte-target system:

$$R_{max} \text{ calc.} = \frac{MW_{analyte}}{MW_{target}} \times R_{target} \times \text{valency} \qquad \textbf{[Equation 7]}$$

R_{max} calc. was compared with the experimental signal decrease during steady state (R_{max} exp). R_{target} is the experimental drop in baseline level, MW_{target} the molecular weight of Ni (58.7 g/mol), and $MW_{analyte}$ the molecular weight of the peptide, which was analyzed. For better illustration Figure 26 shows the experimental R values for His2 (**1**).
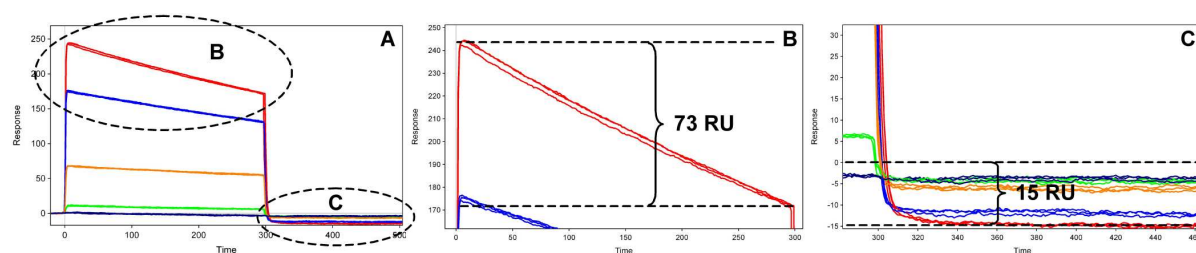
Figure 26: Decrease in steady state signal during sample injection of His2 (**1**). A: Full size of sensorgram of His2 (**1**). B: Magnification of drifting signal at 5 mM concentration (red binding curve). C: Drop below initial baseline level after dissociation of 5 mM (red) binding curve.

The calculations were performed with the three peptides mentioned above (**1**, **2**, and **14**), which showed the most pronounced signal decrease during steady state phase. This allowed a precise determination of the experimental values shown in Figure 26. The results of the calculations are presented in Table 26. With most of the peptides from the oligohistidine series (**1** – **9**) this calculation could not be performed due to the rebinding effect. For the His_2Ala_4 peptides **10**, **11**, **12**, and **13,** the baseline drop was too small for detection. This problem could be circumvented by an increased injection time, although analyte consumption would be significantly higher.

Table 26: Quantitative Analysis of 'Metal Ion Drift'.

Compound	No.	R_{max} exp. [RU]	R_{target} [RU]	R_{max} calc. [RU]
His2	(**1**)	73	15	76
His3	(**2**)	59	8	59
HAAAAH	(**14**)	38	4	40

For all three peptides, the calculations fitted well with the experimental value. Due to the loss of Ni^{2+} during steady state phase, the binding capacity of the surface is decreased. Therefore, less analyte molecules are able to bind to the surface leading to the significant decrease in binding signal. Finally, after dissociation, the binding curve drops below the baseline level because of the decreased number of Ni^{2+} bound to the chip surface.

Further explanations, which might support the Ni^{2+} complexation theory, can be found in solution-based stability constants [*183*]. The affinity of Ni-NTA in solution ($logK_D = -11.26$) is about 350 times higher than the affinity of the Ni^{2+}-His interaction ($logK_D = -8.69$). This value could be decreased if other histidine residues are present

in the proximity of the Ni-NTA, leading to a strong competition between the peptide and the nickel ion.

5.1.3. Entropic Effect and Combination of Preferred Binding Motifs: The His_xAla_y Series

As a consequence of the comparison between the oligohistidine series (**1** – **9**) and His_2Ala_4 series (**10** – **14**), the impact of entropy on the binding affinity was closer investigated. The increase in peptide length of the oligohistidine series led to a decrease in binding affinity due to the increased entropy penalty upon binding. The same is true when comparing His2 (**1**) and AAAAHH (**10**), which contain both a 1-2 binding motif. The His_xAla_y series (**15** – **19**) was synthesized to analyze this effect in more detail by SPR experiments. For this purpose, peptides AAAHH (**17**), AAHH (**18**), and AHH (**19**) all containing vicinal histidine residues but containing a variable number of alanine residues at the N-terminus were synthesized. Together with the peptides HH (**1**) and AAAAHH (**10**) they complete the series His_2Ala_{0-4}. Furthermore, the peptides HAHAAH (**15**) and HAAHAH (**16**) were added to this series, which both include the two preferred binding motifs 1-3 and 1-6 in one molecule (see section 5.1.2).

Synthesis and Purification

The synthesis and purification of the His_xAla_y series (**15** – **19**) revealed similar problems as the His_2Ala_4 series (section 5.1.3). Especially for shorter peptides such as AAHH (**18**) and AHH (**19**), precipitation prior to HPLC purification was not possible. As a consequence, the products are characterized by a high salt content (Table 27).

Table 27: Salt Content of His_xAla_y (**15** – **19**).

Compound	No.	Salt Content [%, w/w]
HH	(**1**)	49
AAAAHH	(**10**)	75
HAHAAH	(**15**)	36
HAAHAH	(**16**)	35
AAAHH	(**17**)	42
AAHH	(**18**)	75
AHH	(**19**)	73

The different salt content – peptides **15**, **16**, and **17** contained up to a factor 2.1 less salt after HPLC purification compared to **18** and **19** – cannot be rationalized. As both peptides, **18** and **19,** showed a good retention (t_R = 5.3 min for **18** and t_R = 4.5 min for **19**) on the reversed-phase column, co-elution with byproducts could vastly be excluded. Therefore, no anomalous binding signal due to an impure sample was observed in the SPR analysis.

Binding Assay

The binding assay for the His_xAla_y series (**15** – **19**) was performed with the same wash routine as already described for the His_2Ala_4 (section 5.1.2). In the experimental part, no relevant problems occured, apart from a continuous increase in baseline signal visible during long-term experiments (>8 hours). With several 1-min injections of 100 mM NaOH at a flow rate of 20 µl/min, the chip surface could be regenerated to achieve the initial baseline level again. Therefore, this procedure was performed before each experiment. Furthermore, reproducibility and life-time of the NTA sensor chip could be increased, when adding wash procedures as "wash needle" and "wash IFC" after each injection cycle. This procedure provided a proper removal of precipitates or aggregates sticking to the needle or the IFC unit.

The binding assay for the His_xAla_y series (**15** – **19**) was completed with peptides from previous experiments such as His2 (**1**, section 5.1.1) and AAAAHH (**10**, section 5.1.2). An overview about the sensorgram is shown in Figure 27.
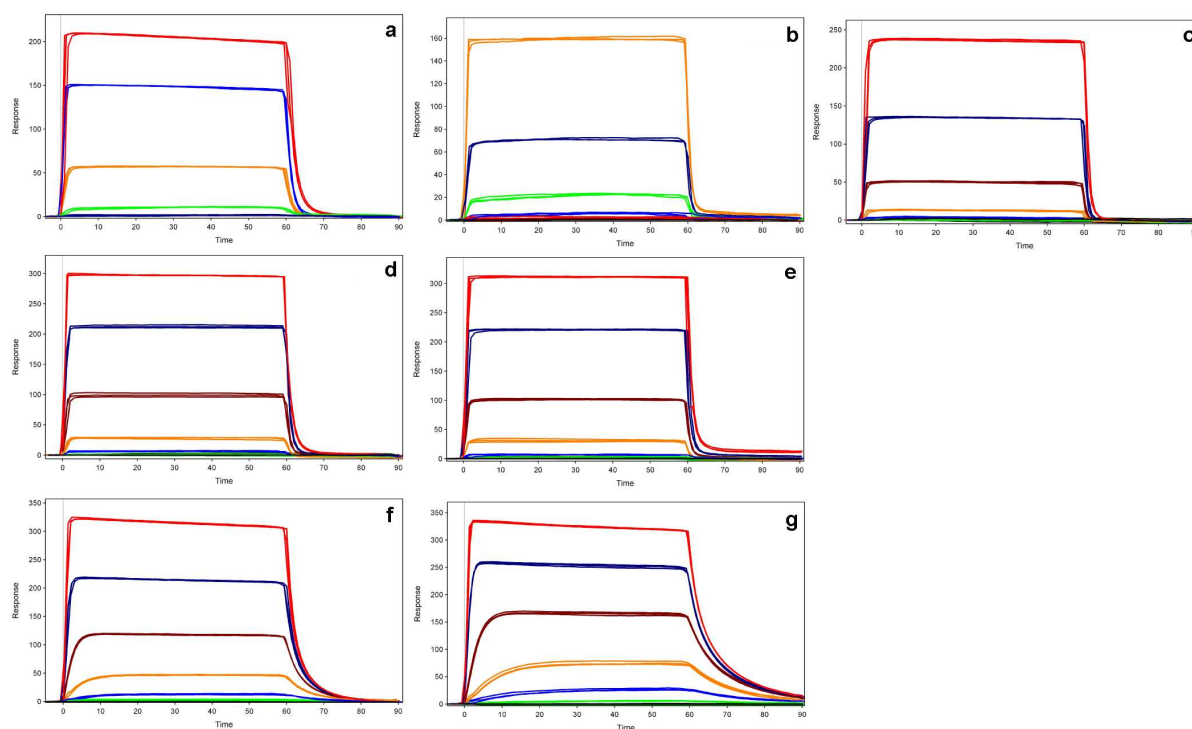
Figure 27: Sensorgrams of the His$_x$Ala$_y$ series (**1**, **10**, and **15** – **19**): a: HH (**1**); b: AHH (**19**); c: AAHH (**18**); d: AAAHH (**17**); e: AAAAHH (**10**); a: HAHAAH (**15**); a: HAAHAH (**16**). The samples were measured in triplicate injections. The concentration ranges and dilution factors are given in 4.9.4, Table 18.

The sensorgrams for HH (**1**), AHH (**19**), AAHH (**18**), AAAHH (**17**), and AAAAHH (**10**) were similar in shape to those of the His$_2$Ala$_4$ series (Figure 24). Rapid association and fast dissociation phases led to a complete return to the baseline level of the binding signal within seconds. The shape of the binding curves for HAHAAH (**15**) and HAAHAH (**16**) looked different compared with the other sensorgrams of this peptide series. At low concentrations of 8 µM (brown curve), 1.6 µM (orange curve), and 320 nM (blue curve), the time span to reach steady state level was significantly increased. In addition, the dissociation phase is slightly delayed, a clear sign for rebinding. The effect is less pronounced than in the case of *e.g.* His9 (**8**) or His10 (**9**) (section 5.1.1, Figure 19). With a closer look at the dissociation phases of the two peptides **15** and **16** (Figure 28), the rebinding phase was closer analyzed.

The first 2 s of the dissociation phase at the three highest sample concentrations of each peptide were fitted manually with a normal exponential decay of a 1:1 interaction model. The rebinding effect becomes visible due to the delayed dissociation of the experimental dissociation curve compared to the simulated curve around 65 s. Such a dissociation profile cannot be fitted with a regular exponential dissociation model.
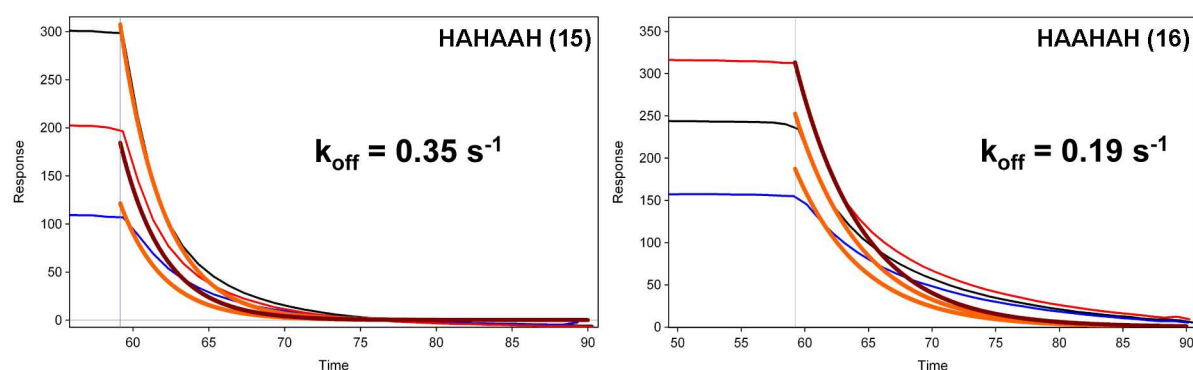
Figure 28: Close-up of dissociation phases of HAHAAH (**15**) and HAAHAH (**16**). 200 µM (upper curve), 40 µM (middle curve), and 8 µM (lower curve) sample concentrations were compared with a normal exponential decay (thick orange lines) with the k_{off} indicated for each peptide.

Due to the observed decrease of the steady state signal and the rebinding, a kinetic investigation of the His_xAla_y series was not possible. Therefore, an apparent K_D was determined using steady state signals as already described for the oligohistidine series (section 5.1.1). The results are shown in Table 28.

Table 28: Evaluation of K_Ds of His_xAla_y series (**1**, **10**, and **15 – 19**).

Compound	No.	K_D (ss [a]) [µM]
HH	(**1**)	62.7 ± 3.4
AHH	(**19**)	175 ± 4
AAHH	(**18**)	266 ± 4
AAAHH	(**17**)	279 ± 4
AAAAHH	(**10**)	288 ± 3
HAHAAH	(**15**)	10.7 ± 0.4
HAAHAH	(**16**)	6.10 ± 0.16

[a] steady state fit

As expected, the binding affinity is decreased (K_D increased) for each additional alanine residue, most probably due to increased entropy costs upon binding. Furthermore, binding is sterically more hindered due to the additional alanine residues. The difference in binding affinity between HH (**1**) and AHH (**19**) was of a factor 2.4, This difference became less pronounced for longer peptides as demonstrated for AAAHH (**17**) and AAAAHH (**10**), which differed only by a factor 1.03 in affinity.

Peptides **15** and **16** with two possible binding motifs exhibited a stronger binding affinity to Ni-NTA compared to the peptides AAAHAH (**11**, 112 µM) and HAAAAH (**14**, 70 µM), respectively.

5.1.4. Impact of Rotational Freedom: The HXH Series

Shorter tags have many advantages compared to the existing hexahistidine tag as already described in section 3.2.5. Therefore, tags with two histidine residues linked via different spacer sequences were developed. Two histidine residues separated by one amino acid are able to adopt a favorable conformation for binding to Ni-NTA as demonstrated with AAAHAH (**11**, $K_D = 112$ µM). However, the affinity of **11** is still a factor 8000 below the one His6 (**5**). Shortening of the peptide to the sequence HAH increased the binding affinity due to the smaller entropy costs upon binding. With rotational restrictions between the two histidines leading to a pre-organisation of the binding conformation should further increase the affinity. This hypothesis was tested with the HXH series (**20** – **24**) (Figure 29).

Five tripeptides containing either a glycine, an alanine, a sarcosine (Sar), an aminoisobutyric acid (Aib), or a proline at position 2 were synthesized. The peptide HGH (**20**) with its non-substituted C_α-atom should have a higher degree of rotational freedom than *e.g.* **24** containing a cyclic proline residue. As sixth peptide of this series His3 (**2**) was included (see also section 5.1.1).
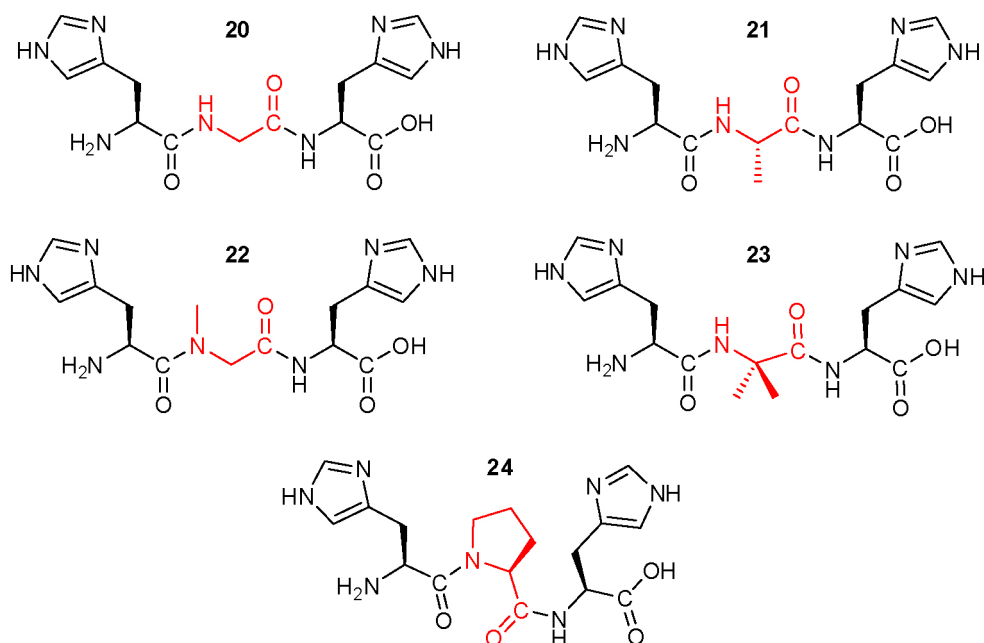
Figure 29: The HXH (**20** – **24**) series with different amino acids at position 2 (marked in red): glycine (**20**), alanine (**21**), sarcosine (**22**), aminoisobutyric acid (**23**), and proline (**24**).

Synthesis and Purification

Syntheses of HGH (**20**), HAH (**21**), HAibH (**22**), and HPH (**23**) were performed on the Pioneer Peptide Synthesizer.

The purification was performed with the ammonium acetate/acetonitrile system, which provided longer retention and therefore better separation from reagents and byproducts present in the crude peptide. This was important, because precipitation of these short peptides was not possible.

Synthesis of HSarH (**22**) was more difficult to perform. With the standard procedure on the peptide synthesizer, the chromatograms after HPLC purification showed a heterogeneous profile instead of one major peak as usually obtained for short sequences. The problem might be caused by an incomplete coupling of the His to the secondary amine of Sar. Therefore, HATU instead of HOBt/TBTU was used for the coupling procedure [*34, 184*]. Furthermore, the mode was changed from automated continuous-flow to manual batch synthesis. Finally, using two over night couplings HSarH (**22**) was obtained in sufficient amounts for the Biacore assays.

For all tripeptides, derivatization with DABS-Cl showed a huge salt contents of approximately 70% and for HAH (**21**) even 89%.

Binding Assay

The binding assays for the HXH series (**20** – **24**) were performed using the same washing procedures as for the oligohistidines (**1** – **9**) including the wash routines "wash needle" and "wash IFC". Due to the rather fast kinetics, short association and dissociation times of 1 min and 30 s, respectively could be used lowering the analyte consumption significantly (Figure 30).
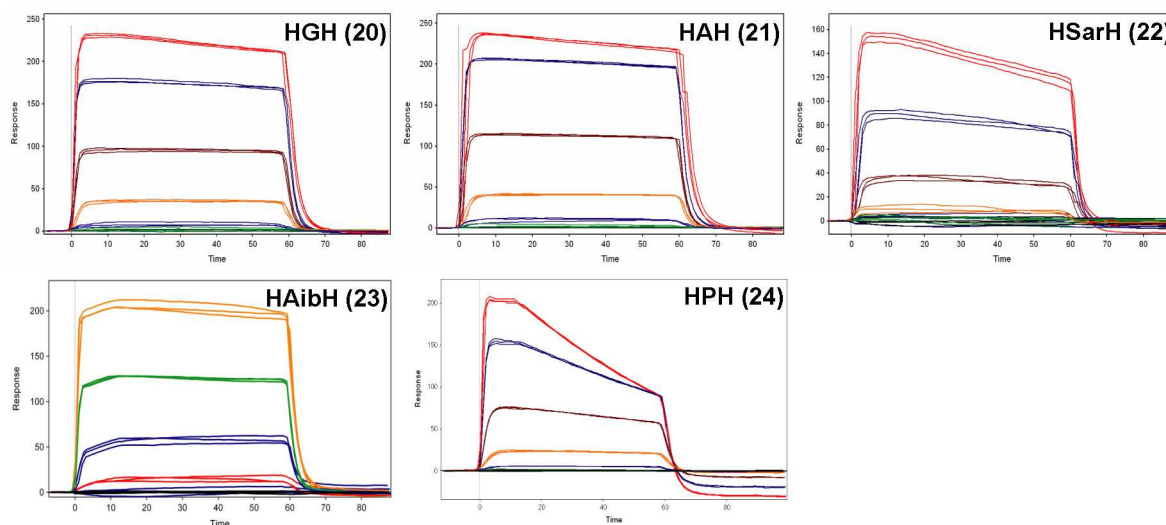

Figure 30: Sensorgrams of the HXH series (**20** – **24**). The samples were measured in triplicate injections. The concentration ranges and dilution factors are given in 4.9.5, Table 19.

All peptides showed a linear decrease in binding signal during the steady state phase. HSarH (**22**) and HPH (**24**) elicited the highest loss in binding signal. Looking closer to the sensorgram of HPH, the steady state phase can be divided into two parts [see concentrations of 1 mM (red curve) and 200 μM (blue curve)]. After reaching the steady state level, the binding signal remains constant for 10 s (intermediate steady state level) before starting a pronounced linear decrease until the dissociation phase starts. After dissociation the signal drops again below the initial baseline level, which was true for all peptides of this series. The decrease was analyzed quantitatively as already done in section 5.1.2 using Equation 7. The values of these calculations are given in Table 29.

Table 29: Quantitative Analysis of 'Metal Ion Drift'.

Compound	No.	R_{max} exp. [RU]	R_{target} [RU]	R_{max} calc. [RU]
HGH	(**20**)	10	2	12
HAH	(**21**)	20	3	19
HSarH	(**22**)	41	9	55
HAibH	(**23**)	27	3	26
HPH	(**24**)	120	4	185

The analysis was done with the highest concentrations of each peptide. HSarH (**22**) and HPH (**24**) showed the highest deviation between the calculated and the experimental value. For the three peptides **20**, **21**, and **23,** deviations from the experimental values lay within 20%. The calculated value for HPH (**24**) was more than 50% higher than the experimental value. This means that the decrease of the binding signal during steady state is less pronounced than expected. The same overestimation was found for HSarH (**22**). The two molecules might be regarded as outliners due to their strange behavior in the binding assay (biphasic dissociation).

Despite some deviations from a standard sensorgram, the binding curves were analyzed to determine binding affinities and kinetic parameters. For HPH (**24**), a kinetic fit was not possible, because the decrease in binding level during steady state was too high. Therefore, only a fit of the steady state level to a simple 1:1 Langmuir isotherme was made using steady state levels immediately after reaching steady state. Calculated data from the steady state and kinetic fits are shown in Table 30.

Table 30: Evaluation of kinetics and binding affinity of HXH series (**20** – **24**).

Compound	No.	K_D (ss [a]) [µM]	k_{on} [$M^{-1}s^{-1}$]	k_{off} [s^{-1}]	$T_{1/2}$ [s]	K_D (kin [b]) [µM]
HGH	(**20**)	54 ± 1	10123 ± 725	0.478 ± 0.022	1.5	47 ± 2
HAH	(**21**)	41 ± 1	11697 ± 822	0.535 ± 0.035	1.3	41 ± 1
HSarH	(**22**)	154 ± 17	3262 ± 187	0.389 ± 0.036	1.9	123 ± 17
HAibH	(**23**)	36 ± 3	13916 ± 632	0.406 ± 0.052	1.7	36 ± 3
HPH	(**24**)	77 ± 2	-	-	-	-
His3	(**2**)	2.23 ± 0.15	-	-	-	-

[a] steady state fit

[b] kinetic fit, $K_D = k_{off}/k_{on}$

The quality of the kinetic fits was satisfying with res SDs below 6.0. Only the fit of HSarH (**22**) had a res SD of 9.6. The lower quality of the fit for **22** was also obvious from the difference between the two K_D values from the kinetic and the steady state fit. Furthermore, the SD for both values was significantly higher compared to the other peptides of this series. Despite the difference of the two K_D values, the ranking of this series did not change. Consecutive substitution of the C_α-atom with one (HAH) or two (HAibH) methyl groups decreased the K_D. HGH (**20**) with a high degree of rotational freedom due to its unsubstituted C_α-atom had a slightly lower (1.3-fold for the steady state fit or 1.1-fold for the kinetic fit) binding affinity than HAH (**21**). HAibH (**23**) with two methyl groups at the C_α is even more restricted in its rotational freedom, therefore the entropy costs upon binding is smaller than *e.g.* for HGH.

However, rotational restriction does only guarantee a high affinity, when the molecule can adapt a conformation close or similar to the binding conformation. The increased k_{on} of HAibH (**23**) compared to HGH (**20**) and HAH (**21**) indicates that this is the case for **23**. The other contribution to the slightly higher binding affinity of **23** is a consequence of the lowered off-rate (k_{off} = 0.406 s^{-1}). HSarH (**22**) contains a methylated nitrogen in its peptide backbone. Although the rotational freedom should be restricted in comparison with **20, 22** showed a significantly higher K_D (2.9-fold compared to **20**). The low affinity was due to the much slower on-rate (3.1-fold compared to **20**), most probably because the methyl group on the nitrogen leads to a pre-organization in an undesired conformation, aggravating the association of the complex. The affinity of HPH (**24**) lays between HSarH (**22**) and HGH (**20**). In this case the decreased flexibility did not elicit a positive effect on the binding affinity. Again, the binding conformation and the equilibrium conformation in solution might be different. In addition, X-Pro bonds are known to populate both the cis and trans isomers. However, for binding, one isomer is preferred. The necessary cis-trans-isomerization lowers the affinity.

The difference in binding affinity between HAibH (**23**) and His3 (**2**) is huge. His3 (**2**) shows a 16-fold higher affinity to Ni-NTA than HAibH (**23**), the best ligand from the HXH series (**20** – **24**). Due to the additional histidine residue in His3 (**2**), binding either in a 1-3 or a 1-2 binding mode to Ni-NTA is possible. Therefore, the

probability for binding to Ni-NTA is increased. This could not be compensated with the pre-organization of the two ligands in HAibH (**23**).

5.1.5. General Considerations about the His-tag

A better understanding of the binding mechanism of the widely used hexahistidine-tag (**5**) has been one goal of our investigations described in section 5.1. For this purpose, tag fragments of different peptide length and composition were compared in respect to thermodynamic and kinetic behavior. Even though these peptide tags are usually attached to a much larger protein, the idea was to investigate only the isolated peptide tag in order to avoid any binding interference with the protein. Such an approach allows the characterization and selective improvement of the existing tag independently of the attached protein.

Depending on the desired application, affinity tags have to fulfill specific requirements. When they are used for target immobilization in ligand binding assays, a stable interaction is indispensable. Conversely, when the tag is used for affinity purification, only moderate dissociation constants [*104, 105*] are required in order to allow a mild elution from the affinity column.

In case of Ni-NTA affinity chromatography [*56, 78, 104*], the stability constants of four complexes have to be taken into consideration; (i) Ni^{2+}/6His-tagged protein ($K_D \approx \cdot 10^{-6}$ M, [*126*]), (ii) Ni^{2+}/imidazole ($K_D = 9.8 \cdot 10^{-4}$ M,), (iii) Ni^{2+}/NTA ($K_D = 1.8 \cdot 10^{-11}$ M, [*183*]), and (iv) Ni^{2+}/EDTA complex ($K_D = 3.6 \cdot 10^{-18}$, [*183*]). The differences between these dissociation constants guarantee that the captured His-tagged protein can be eluted with imidazole under mild, non-destructive conditions, while the nickel ions remain tightly bound. Finally, the affinity chromatography support can be regenerated by complete removal of the Ni^{2+} ions with EDTA followed by reloading the NTA chelators with Ni^{2+} ions (Figure 31).
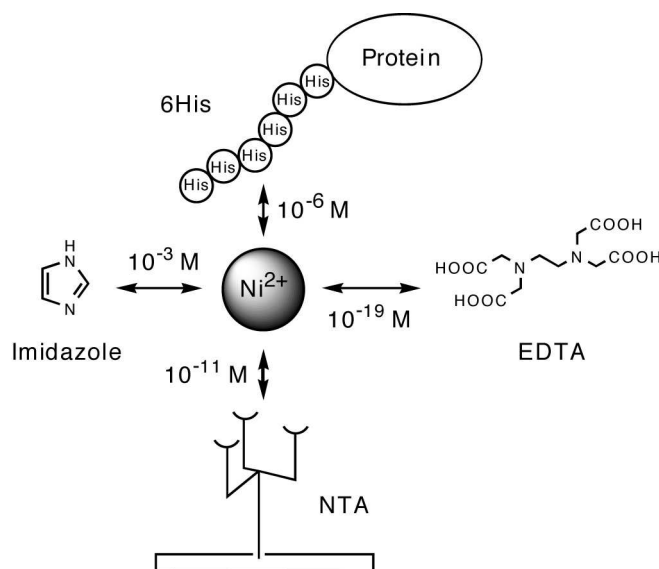
Figure 31: Illustration of all interactions involved during the purification with Ni-NTA affinity column.

In this tailored network of dissociation constants, the K_D for Ni^{2+}/NTA, Ni^{2+}/imidazole, and Ni^{2+}/EDTA complexes form the given constraints, whereas the binding properties of the His-tag can be adapted according to the needs of a specific application by varying the numbers of histidines or by modifying the amino acid sequence. For example, two consecutive 6His-tags are recommended for a stable immobilization of proteins on SPR surfaces for the purpose of ligand binding assays [126]. For purification reasons, the affinity has generally to be lower, otherwise the much higher imidazole concentrations needed for elution might lead to protein denaturation [185].

The apparent K_D value for the best ligand in all of the presented peptide series, the free His6 (**5**) peptide, is more than 20 times lower than that reported for fusion proteins with a single hexahis-tag (~700 nM) by Nieba *et al.* [126]. Limited accessibility of the tag, caused by steric hindrance by the attached protein, or electrostatic interactions are possible explanations for the decrease in binding affinity of the tagged protein compared to the free tag. The same authors also investigated the interaction of the free His6 (**5**) with a nickel surface, but did not report any K_D values [126].

The widespread usage of the hexahistidine tag might somehow astonish because of the moderate binding constant when coupled to a protein. Compared to strong interactions as measured with complexes of avidin and biotin ($K_D = 10^{-14}$ M), the

affinity of the hexahistidine peptide to Ni-NTA is more than a factor 10^5 lower. Nevertheless, the secret of the success of the hexahistidine-tag lies in its low "pseudo" off-rate. Speaking of a real dissociation rate constant is not correct due to the rebinding observed with the oligohistidine series (**1** – **9**). For peptides with eight (**7**) to ten histidine (**9**) residues, stable binding with little dissociation is achieved at analyte concentration in the range of the K_D. Alternating dissociation and reassociation phases lead to a "sliding" of the peptide over the chip surface (Figure 32) instead of a complete dissociation. This leads to a stable binding to the Ni-NTA surface. At higher concentrations, however, when free coordination sites are in short supply, dissociation becomes visible.
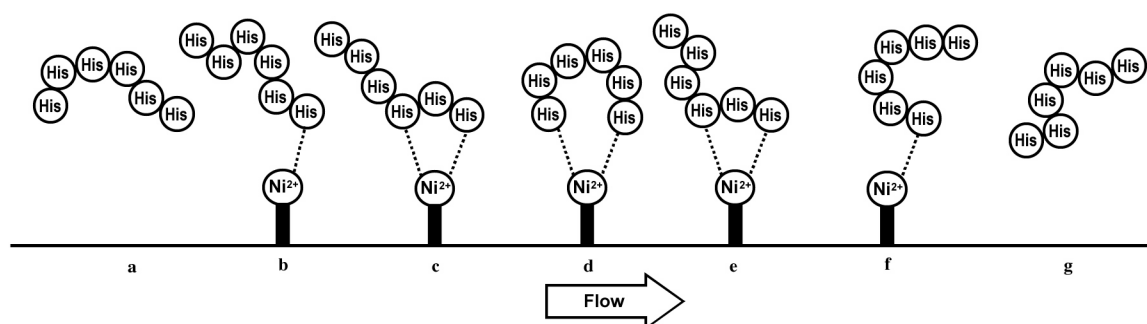
Figure 32: Overall binding process of hexahistidine to Ni-NTA at moderate concentrations. Ni^{2+} is immobilized to the surface of the sensor chip via NTA. One imidazole group of the hexahis-tag (a) makes first contact with Ni^{2+} (b). After the monovalent interaction is established, the high local concentration of his ligand facilitates the interaction with a second imidazole forming a divalent complex with histidines from the i and i+2 position (c). By consecutive dissociation and reassociation (d, e) the molecule 'slides' over the chip surface, which explains the observed rebinding effect in the SPR measurements. Finally, the hexahis dissociates from the Ni^{2+} (f, g).

This demonstrates that high binding affinities are not mandatory for affinity purification. Moderate binding affinities can be compensated by rebinding prolonging the interaction of the tag with the solid support.

Finally, in the His6 (**5**) an optimal ratio of entropy costs vs. binding events leads to the best apparent K_D. Overall, fifteen different binding motifs are available within one hexahistidine molecule: 5 times the 1-2 motif, 4 times the 1-3 motif, 3 times the 1-4 motif, 2 times the 1-5 motif, and once the 1-6 motif.

5.2. 1,10-Phenanthroline, an Alternative to the His-tag

In section 5.1, the limitations of an affinity tag exclusively consisting of amino acids has been demonstrated. Therefore, non-amino acid tags were also studied. The idea to couple 1,10-phenanthroline (phen) to a protein or a peptide, and purify the construct on a Ni-NTA column was published by Frank *et al.* from Lonza AG (Basel, Switzerland) [*169*]. In their patent application, they attached phen to a peptide, synthesized via SPPS and purified the construct via a solid-phase bearing various metal ions M^{n+} (n =1 to 3). The phenanthroline, acting as the purification tag, was coupled via a chemically cleavable tag to a test peptide enabling the synthesis of native peptides.

Complexes between Ni(II) and 1,10-phenanthroline have been known for more than a century [*186*], but no reliable kinetic or equilibrium constants were reported until 1956 when Margerum *et al.* [*187*] published equilibrium constants of the mono-, di-, and tri-(1,10-phenanthroline)-nickel(II) complex in solution (Figure 33).
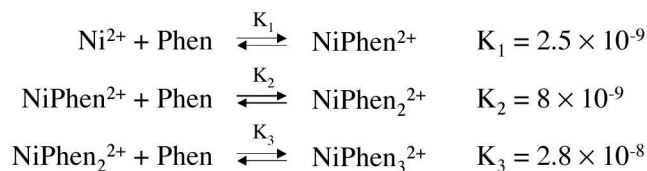
$$Ni^{2+} + Phen \xrightarrow{K_1} NiPhen^{2+} \qquad K_1 = 2.5 \times 10^{-9}$$

$$NiPhen^{2+} + Phen \xrightarrow{K_2} NiPhen_2^{2+} \qquad K_2 = 8 \times 10^{-9}$$

$$NiPhen_2^{2+} + Phen \xrightarrow{K_3} NiPhen_3^{2+} \qquad K_3 = 2.8 \times 10^{-8}$$

Figure 33: Equilibrium constants of the mono-, di-, and tri-(1,10-phenanthroline)-nickel(II) complex. K is equal to K_D of the described complexation reaction.

1,10-phenanthroline is a bidentate ligand coordinating with Ni(II) via its two aromatic nitrogens. Therefore, three molecules are able to bind to Ni^{2+} in solution. The existence off all three complexes has been demonstrated by Vosburgh and Cooper [*188*]. The K_D for the binding of the first phenanthroline is about a factor 10 lower than the value for the third ligand. This is due to steric hindrance and unfavorable electrostatic interactions between phenanthroline ring systems. For the Ni-NTA system, conditions are similar. Ni^{2+} bound to NTA has only two coordination sites and thus binds one phenanthroline molecule. Therefore, the K_D for the complexation of the third phenanthroline gives at least an idea about the potential of a phenanthroline-tag binding to Ni-NTA. The K_D (K_3 in Figure 33) of 30 nM is in the

range of the value for His6 obtained in SPR experiments (Table 24, 14 nM). A comparison of these two values is rather delicate due to the different ligands involved in binding. Up to now, no affinity measurements and kinetic evaluations of phenanthroline and derivatives thereof binding to Ni-NTA were reported. To fill this gap, the phenanthroline series (**42** – **49**) was analyzed with using SPR to obtain more information about the binding properties of phen to Ni-NTA (Figure 34).
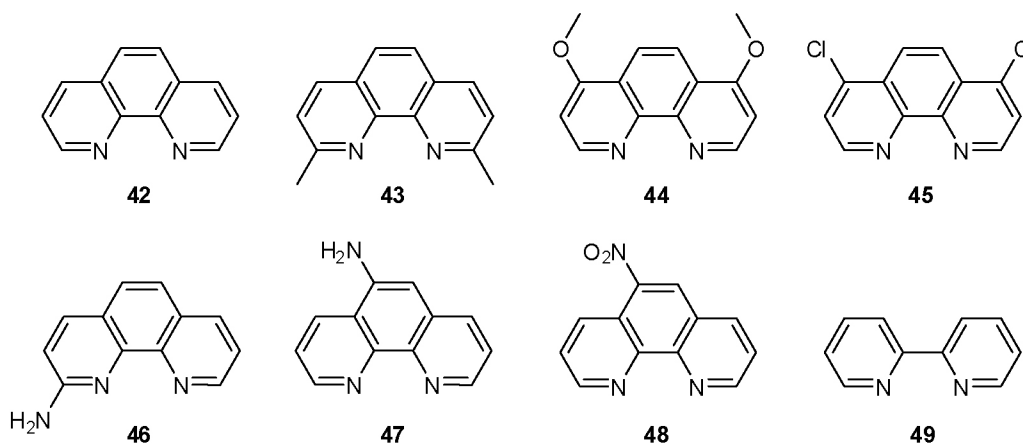

Figure 34: Compounds of the phenanthroline series: 1,10-Phenanthroline (**42**), neocuproine (2,9-dimethyl-1,10-phenanthroline) (**43**), 4,7-dimethoxy-1,10-phenanthroline (**44**), 4,7-dichloro-1,10-phenanthroline (**45**), 2-amino-1,10-phenanthroline (**46**), 5-amino-1,10-phenanthroline (**47**), 5-nitro-1,10-phenanthroline (**48**), 2,2'-bipyridyl (**49**).

The set of the different phenanthrolines was completed with 2,2'-bipyridyl (bipy, **49**). Bipy has the same scaffold as phen, but a freely rotatable σ-bond.

5.2.1. Computational Model for the Prediction of Binding Affinities to Ni-NTA

In parallel to the Biacore approach, Dr. Martin Smiesko, Institute of Molecular Pharmacy, established a computational method that for the prediction of binding affinities of various ligands to Ni-NTA [*171*]. The software used for all calculations was Gaussian 03. All the operations necessary for the development of such a model are briefly summarized below:

1. Geometry optimization of the complexes was performed using *ab initio* density functional theory methods at B3LYP level in combination with the triple-zeta

basis set with polarization and diffuse functions 6-311++G(d,p) in the solvent phase (water) using the conductor-like polarizable continuum method.

2. At optimized geometries, the gas-phase part of the interaction energy was calculated in a single point calculation using the same level of the theory as in step 1, but without solvent.

3. Similarly to point 2, the solvation effects were evaluated in a single point calculation at the optimized geometry using the Hartree-Fock level of theory in combination with the double zeta basis set with polarization functions for heavy atoms 6-31G(d) employing the conductor-like polarizable continuum method.

4. The final interaction energy was calculated from the partial results of step 2 and 3.

One of the major problems during the development of the computational model was the lack of a crystal structure of 1,10-phenanthroline binding to Ni-NTA. For the geometry optimization such a crystal structure is needed to calibrate the *ab initio* calculations. Only two complexes of NTA binding in a tetradentate manner to Ni^{2+} were found, $[Ni^{II}(NTA)(H_2O)_2]^-$ and $[Ni^{II}(NTA)(adeninium)(H_2O)]^-$ [*189*]. Therefore, the complex $[Ni(NTA)(phen)]^-$ was synthesized to obtain the X-ray crystal structure depicted in Figure 35.
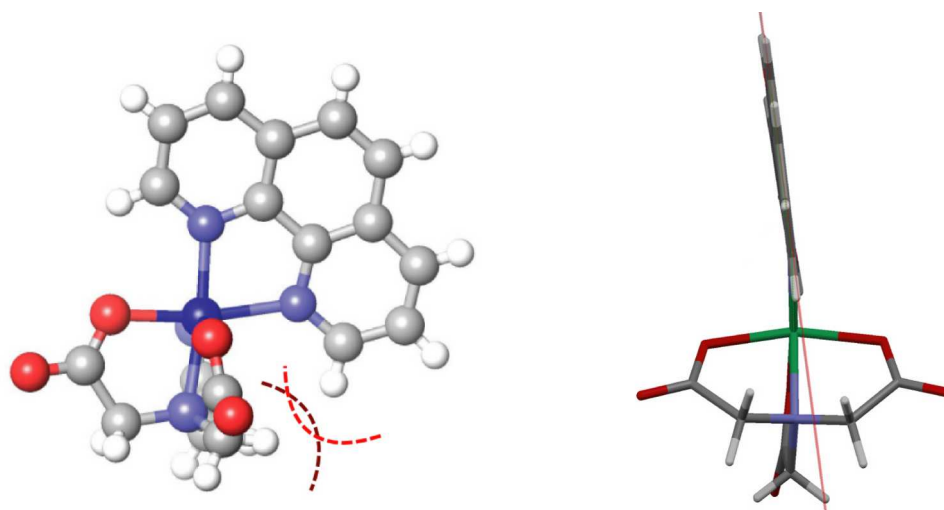

Figure 35 (by courtesy of Dr. Martin Smiesko): Crystal structure of the complex as stick and ball (left) and with a highlighted phenanthroline plane (right).

An unexpected property was found. The whole complex does not show the expected symmetry with the phen lying in the same plane as the one formed by the

nitrogen, the axial carboxylic acid arm, and the metal (Figure 35). Therefore, two enantiomeric complexes are possible, which are both found in the crystal structure. The missing symmetry leads to differences in the length of the coordination bonds between nickel and each of the coordinating nitrogens. The equatorial coordination bond is significantly elongated to a value of 2.143 Å, whereas the axial one measures only 2.053 Å. The asymmetric complex leading to different lengths of the two Ni-N bonds, indicate some unfavorable interactions within the complex. A steric clash of phen with the two CH_2 groups of the NTA (Figure 35, left) might be the most probable explanation.

The computational model established by Dr. Martin Smiesko was finally able to estimate binding affinities of various phenanthroline derivatives as demonstrated by the good correlation (R^2 = 0.87) between the experimental and calculated data (Figure 36).
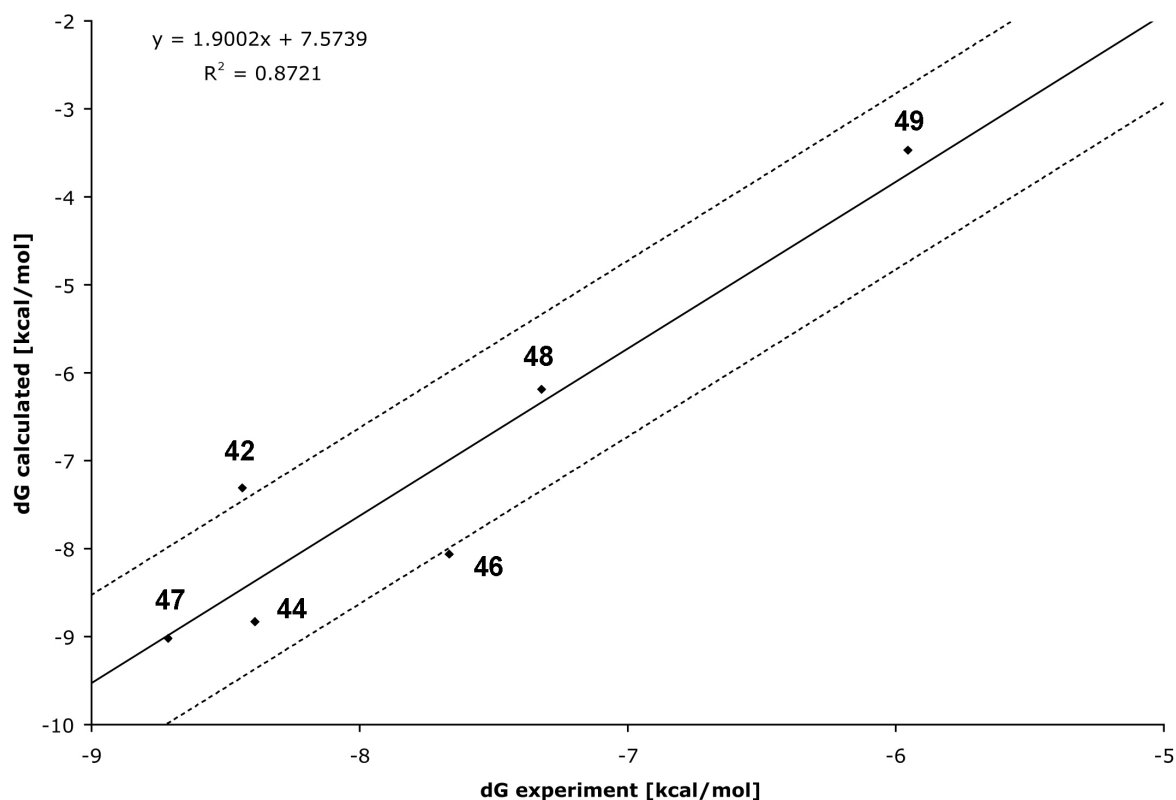

Figure 36: Correlation between experimental and calculated ΔG for binding to the Ni-NTA system. Substances: **42**: 1,10-phenanthroline; **44**: 4,7-dimethoxy-1,10-phenanthroline; **46**: 2-amino-1,10-phenanthroline; **47**: 5-amino-1,10-phenanthroline; **48**: 5-nitro-1,10-phenanthroline; **49**: 2,2'-bipyridyl.

Only two values are not within 1 kcal/mol of the prediction. 1,10-Phenanthroline (**42**) was underestimated by the model and 2-amino-1,10-phenanthroline (**46**) was overestimated. At least for **46** the explanation was quite clear: The model does not consider a protonation of the adjacent ring nitrogen. This issue, together with the results of the Biacore experiment and the information derived from the calculations will be discussed later in section 5.2.3.

5.2.2. Biacore experiments with 1,10-Phenanthroline and 2,2'-Bipyridyl

The Biacore assay with 1,10-phenanthroline (**42**) was rather difficult to establish. Signals were unstable and the quality was highly dependent on the injected concentrations: The higher the applied concentrations, the more unstable the signal was. On the other hand, the concentrations should approach saturation level for the exact determination of binding affinities and kinetics. However, this was not possible for the whole phenanthroline series due to the low signal quality at high concentrations. The unstable curves at high concentrations might be associated with the low solubility in water. However, Sengupta *et al.* published a solubility of 3 mg/mL was reported [*190*], which is actually much higher than the concentrations used in the Biacore experiment (100 µM, 0.0180 mg/mL). Nevertheless, aggregation within the IFC could significantly decrease the solubility leading to the strange signals observed. Finally, several wash steps using 0.5% SDS after each injection of phenanthroline helped to improve the signal quality. In addition, omitting of high concentrations allowed a further stabilization of the signal. This enabled kinetic fitting of the data to a simple 1:1 binding model as demonstrated in Figure 37.
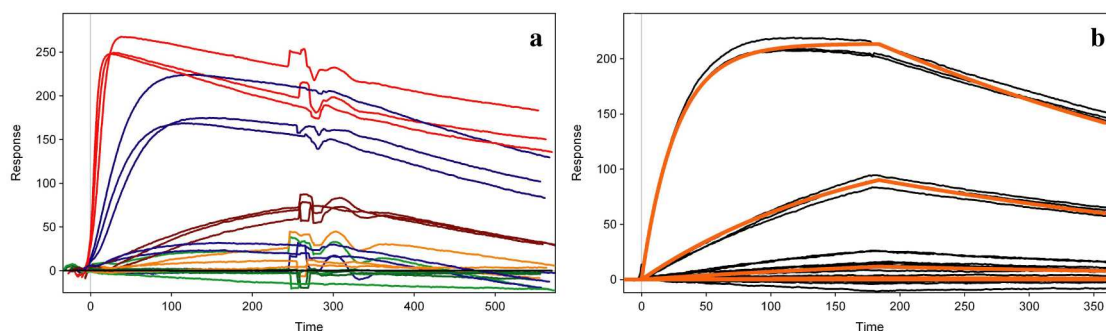
Figure 37: a: Sensorgram of 1,10-phenanthroline (**42**) over a concentration range of 100 μM - 1 nM; b: Sensorgram of 1,10-phenanthroline (**42**) over a concentration range of 10 μM - 100 pM including kinetic fit (orange curve) to simple 1:1 binding model.

With the additional SDS wash, stable triplicates could be achieved over the whole duration of the experiment. However, the life-time of the NTA-chips was significantly shorter compared to the measurements with the peptide tags. After 4 to 5 triplicate measurements, the binding curves became more and more unstable, which could only be solved by a change of the flow cells or an exchange of the chip. The res SD of the kinetic fit lay at 8.0, which was higher than for the His_2Ala_4 (section 5.1.2) and HXH (section 5.1.4) series (around 6.0 for both), indicating a slightly lower quality of the fits.

For 2,2'-bipyridyl (**49**) the situation was even worse: The signals were highly unstable with significantly deviating triplicates. The preferred conformation of bipy in solution was found to be with the two nitrogens facing into opposite directions, as could be demonstrated *in silico* using a conformational search. Hence, before binding, a conformational change is needed for a proper alignment of the two pyridine rings. A kinetic fit was impossible, but a steady state fit to a simple 1:1 binding model gave at least an estimate of the apparent K_D in comparison to 1,10-phenanthroline. The values obtained from the analysis of 2,2'-bipyridyl and 1,10-phenanthroline are presented in Table 31.

Table 31: Evaluation of kinetics and binding affinity of 2,2'-bipyridyl and 1,10-phenanthroline.

Compound	No.	k_{on} [M^{-1}s^{-1}]	k_{off} [s^{-1}]	$T_{1/2}$ [min]	K_D [μM]
1,10-Phen	(**42**)	3546 ± 181	0.00229 ± 0.00021	5.0	0.650 ± 0.093 [a]
2,2'-Bipyridyl	(**49**)	-	-	-	≈ 43 [b,c]

[a] kinetic fit, $K_D = k_{off}/k_{on}$

[b] steady state fit

[c] mean value of several measurements

The difference in binding affinity between bipy and phen is about a factor 60. The weaker binding of bipy to Ni-NTA is most likely due to the additional rotatable bond in the molecule, leading to the entropic costs upon binding of compound **49**. The penalty for a single, freely rotatable bond has been estimated from model compounds to be in the range of $16 - 20 \, \text{Jmol}^{-1}\text{K}^{-1}$ [*191*]. A change of $20 \, \text{Jmol}^{-1}\text{K}^{-1}$ would be equal to a change of $5960 \, \text{Jmol}^{-1}$ in ΔG at 25°C. ΔG is linked with the K_D via the formula $\Delta G = RT\ln K_D$. According to this equation, the K_D of bipy should be 11-fold higher than for phen. This value is significantly lower compared to the 60-fold difference of the experimental values, indicating further unfavorable properties of bipy. Indeed, bipy was shown to prefer an *anti* conformation (two nitrogens pointing into opposite directions) in solution as demonstrated *in silico* with a conformational search. Therefore, additional energy is needed for the rotation into the more unstable *syn* conformation.

The k_{off} of 1,10-phenanthroline leading to a $T_{1/2}$ of 5 min was very low compared to the peptide tags. Higher half-life times were only found with peptides showing rebinding. The high affinity of the complex is based on the slow k_{off}, whereas the association rate is only moderate compared *e.g.* with the almost 4-fold faster k_{on} of HAibH (**25**, Table 30).

1,10-Phenanthroline proves a high potential due to the high half-life time and due to the nanomolar affinity for Ni-NTA. The moderate binding affinity fits excellently into the Ni-NTA purification setup as already described in section 5.1.5 (Figure 31).

5.2.3. Analysis of Phenanthroline Derivatives

Further investigations on phenanthroline were performed due to the promising results obtained by the Biacore assay. For this purpose, different commercially available phenanthroline derivatives were measured by SPR.

Sample preparation was critical for the phenanthroline assay. For all compounds, pure DMSO was used to avoid precipitation during the experiment. However, 5% DMSO is the maximal concentration tolerated for Biacore experiments. Therefore, dilutions had to be prepared with water-based eluent buffer to reach the final DMSO

concentration. 4,7-Dichloro-1,10-phenanthroline (**46**) did not dissolve at all and could therefore not be analyzed by SPR. The sensorgrams of the remaining compounds are presented in Figure 38. For comparison reasons 1,10-phenanthroline (**42**) is included as well.
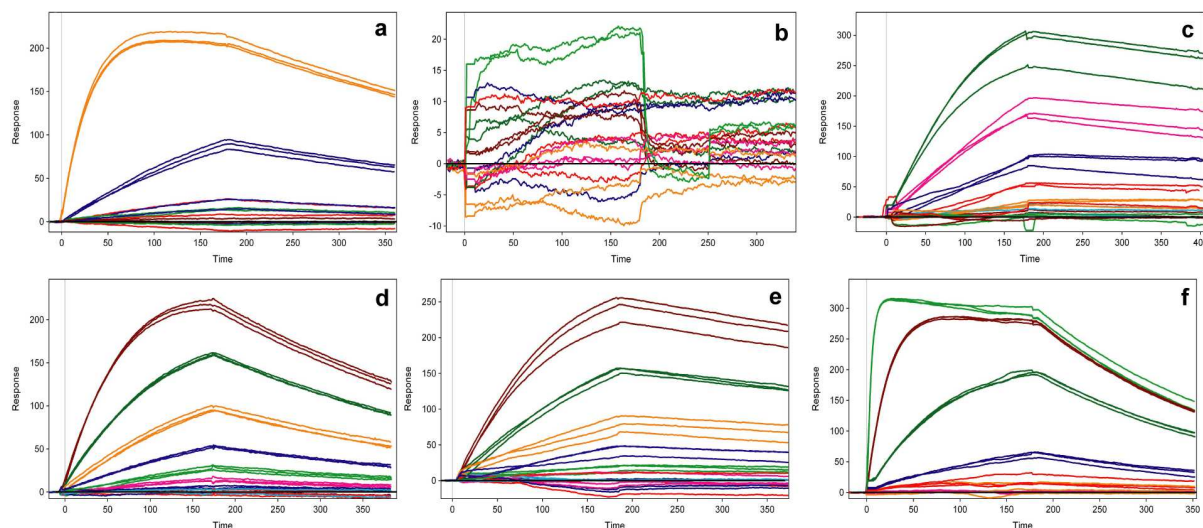

Figure 38: Biacore assay with phenanthroline derivatives: a: 1,10-phenanthroline (**42**); b: neocuproine (4,7-dimethyl-1,10-phenanthroline) (**43**); c: 4,7-dimethoxy-1,10-phenanthroline (**44**); d: 2-amino-1,10-phenanthroline (**46**); e: 5-amino-1,10-phenanthroline (**47**); f: 5-nitro-1,10-phenanthroline (**48**). The concentration ranges and dilution factors are given in 4.9.6, Table 20.

Compounds 1,10-phenanthroline (**42**), 2-amino-1,10-phenanthroline (**46**), and 5-nitro-1,10-phenanthroline (**48**) gave good triplicates, whereas neocuproine (**43**), 4,7-dimethoxy-1,10-phenanthroline (**44**), and 5-amino-1,10-phenanthroline (**47**) did not show a good reproducibility. Only low binding signals were detected for **43** at a concentration of 250 μM due to the weak affinity for Ni-NTA. In this case, the K_D will most probably lie in the millimolar range and therefore beyond the limit required for Biacore measurements. The signals of compounds **44**, **46**, **47**, and **48** showed slow dissociation phases similar to phen (**42**). The binding affinity had to be determined by kinetic fits, because steady state was only reached for high concentrations.

Kinetic fitting of the binding curves to a simple 1:1 binding model was delicate, because of the low reproducibility, especially for 4,7-dimethoxy-1,10-phenanthroline (**44**). The kinetic fit of this compound showed a high res SD of 10 due to the deviating triplicates. As a consequence, K_D, k_{on}, and k_{off} for **44** showed high SDs of more than 80% (Table 32). The quality of the fits for compounds **42**, **46**, **47**, and **48** was significantly higher. Interpretation of the data obtained by the kinetic fit was

supported by the computational model. Several parameters (*e.g.* partial charges on binding nitrogens, solvation energies, or gas-phase binding affinity) obtained by calculation were used to interpret the data qualitatively.

Table 32: Evaluation of kinetics and binding affinity of phenanthroline series.

Compound	No.	k_{on} [M^{-1}s^{-1}]	k_{off} [s^{-1}]	$T_{1/2}$ [min]	K_D (kin [a]) [μM]
1,10-Phen	(**42**)	3546 ± 181	0.00229 ± 0.00021	5.0	0.650 ± 0.093
Neocuproine	(**43**)	-	-	-	> 1000
4,7-Dimethoxy-1,10-phen	(**44**)	1864 ± 1222	0.000512 ± 0.000360	22.6	0.704 ± 0.604
2-Amino-1,10-phen	(**46**)	1138 ± 74	0.00282 ± 0.00010	4.1	2.39 ± 0.23
5-Amino-1,10-phen	(**47**)	2662 ± 429	0.00107 ± 0.00005	10.8	0.407 ± 0.050
5-Nitro-1,10-phen	(**48**)	922 ± 11	0.00394 ± 0.00019	2.9	4.28 ± 0.25

[a] kinetic fit, $K_D = k_{off}/k_{on}$

5-amino-1,10-phenanthroline (**47**) showed the highest affinity of the series (K_D = 407 nM). The 1.6-fold higher affinity compared to 1,10-phenanthroline (**42**) was obtained due to the slower k_{off} resulting in a prolonged half-life time of 10.8 min. The difference between phen (**42**) and **47** is the amino group, directed to the solvent when bound to the Ni-NTA complex. Therefore, the difference was thought to be due to a better solvation of the outer face of **47**. An impact of the amino group on the charge transfer could be excluded. The calculated partial charges on the two binding nitrogens did not show any difference between **47** and **42**. This was different for the dimethoxy compound (**44**), where each of the two methoxy groups in para position to the binding nitrogen influence the charge via the +M-effect. This might explain the low k_{off} resulting in a high half-life time of 22.6 min for this compound. However, the lower on-rate of **44** compared to phen leads to a similar K_D. Due to the higher charge, solvation of the nitrogens will be increased. Therefore, impeded desolvation prior to binding leads to a smaller enthalpic contribution for binding [*192*].

The low binding affinity of neocuproine (**43**) could be explained by the steric clash already observed in the crystal structure with phen (Figure 35). Sterically demanding methyl groups in ortho position to the coordinating nitrogens lead to unfavorable interactions with the CH_2-groups of NTA aggravating binding to Ni-NTA.

An amino group at position 2 as present in 2-amino-1,10-phenanthroline (**46**) was thought to increase the binding affinity due to an additional interaction (H-bond) of the

ligand to the carboxyl group of NTA. Furthermore, the electron donating group increases the negative charge on the adjacent nitrogen from –0.412 to –0.488 obtained by the computational model. The k_{off} was in the same range as for phen, but k_{on} was more than a factor 3 lower than for **42**, leading to a much lower binding affinity (3.7-fold). Reasons are manifold, *e.g.* the loss of symmetry in the molecule upon addition of an amino group (only one instead of two orientations are possible in the binding mode), the increased solvation around the coordinating nitrogens and the additional amino group, or the significantly increased pK_a of the nitrogen at position 1 from 4.94 in **42** [*193*] to 6.9 in **46** [*194*]. Due to the latter, the fraction of protonated nitrogens at pH 7.4 (pH of eluent buffer) will be much higher than for **42**. In its protonated state, the lone pair of the nitrogen is occupied and is not able to interact with the d-orbital of the metal.

The final compound **48** with a nitro functionality at position 5 is an example of low solubility on the outer face of phenanthroline leading to a low affinity of 4.28 μM. As already observed for **47**, the charges on the aromatic nitrogens were not influenced by the substituent.

Unfortunately, the dichloro compound **45** could not be measured by Biacore due to solubility problems. However, the binding affinity can be predicted using the computational model. The electron donating substituents at position 4 and 7 laed to a higher binding affinity at least in the gas-phase. However, due to the poorer solvation of the outer face of the ligand, the overall binding constant dropped to a low binding affinity in the millimolar range.

Figure 39 summarizes all effects that may improve the binding affinity of phenanthroline for Ni-NTA. The influence of a neutral or positive charge on binding was not addressed by SPR and is therefore purely speculative. The phen-Ni-NTA complex is negatively charged and therefore counter ions must be present equalizing this charge. The counter ion in the crystal structure is formed by $[Ni^{II}(phen)_2(H_2O)_2]^{2+}$. In the Biacore or the purification column, the negative charge will most probably be equalized by free sodium ions present in high amounts in the running buffer. Therefore, a positive charge of the ligand could help in establishing a strong binding to Ni-NTA. However, the positive charge of Ni^{2+} could lead to a repulsion of a positively

charged ligand despite the negative overall charge. A positive charge that can be distributed over the molecule *e.g.* by mesomery could be the optimal solution.

Finally, electron donating substituents in ortho- or para-position increase the binding affinity, as could be demonstrated with the dimethoxy (**44**) and the 2-amino compound (**46**). However, salvation has to be considered as well.
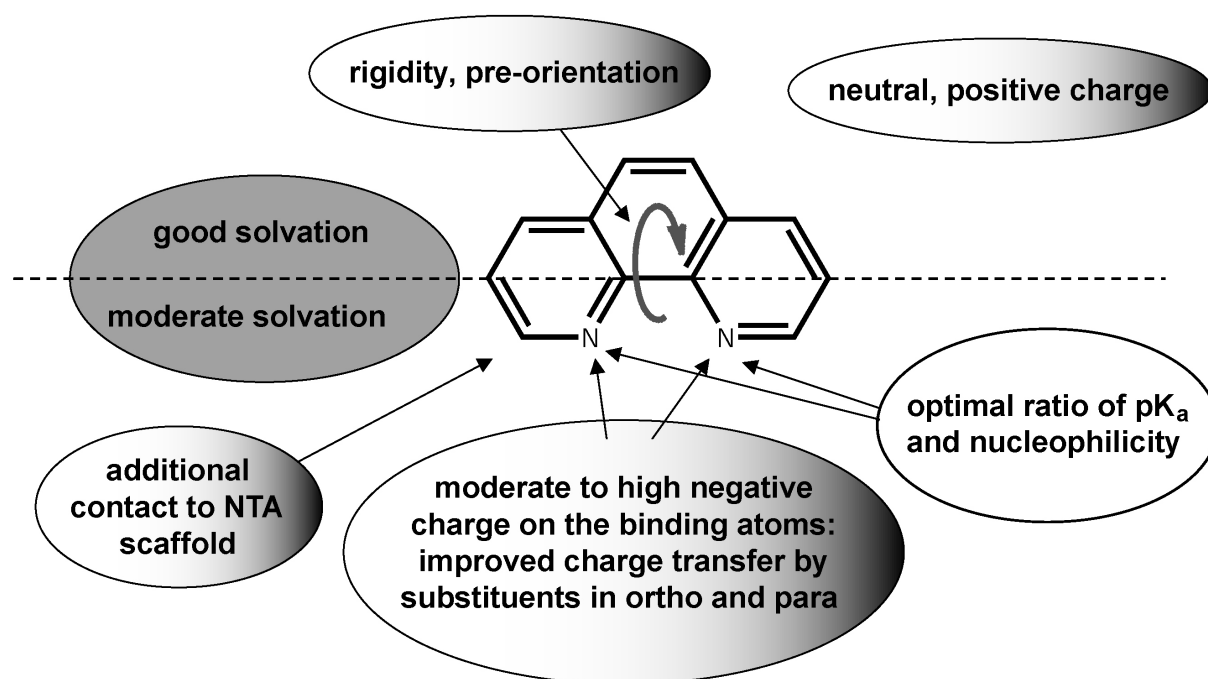

Figure 39: Summary of positive effects on binding affinity of phenanthroline scaffold to Ni-NTA.

5.3. Purification Strategy with 1,10-Phenanthroline

IMAC purification with NTA-bound Sepharose is a well established technique. The potential of 1,10-phenanthroline as a tag had been demonstrated in section 5.2. To use 1,10-phenanthroline as a tag, a spacer has to be attached to the molecule in order to enable coupling to a peptide or a protein. This spacer should contain a functional group allowing its application in solid-phase peptide synthesis. Coupling of the tag to the peptide, which is still bound to the solid-phase. This would allow a simple removal of excessive tag molecules prior to the loading step onto the column. Otherwise, the final product would be contaminated with non-coupled tags, because both tag and tagged peptides would be retained on the purification column.

First of all, a suitable technique with the test peptide NAPamide containing a directly coupled phenanthroline tag was developed. Its suitability for a purification process on Ni-NTA columns and the application on Biacore systems was investigated. The whole strategy is shown in Figure 40.
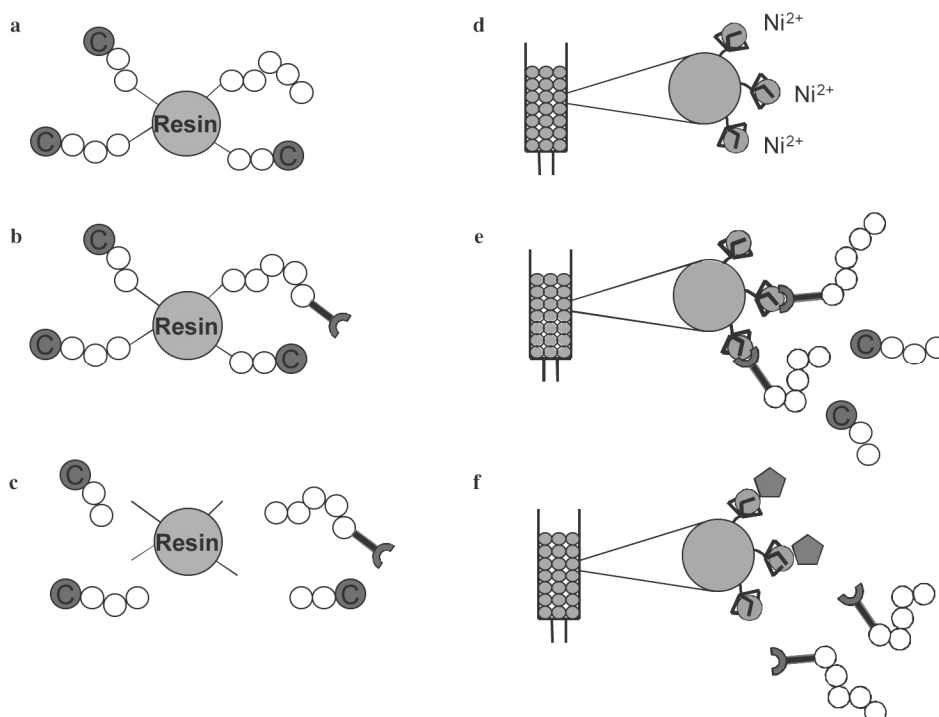

Figure 40: Synthesis and purification of a synthetic peptide (white). A: Peptide is synthesized on solid-phase, free amino groups are capped (C). b: Attachment of tag via spacer to complete peptides (black-red). C: Cleavage and deprotection. D: Purification on Ni-NTA column. E: Tag binds to Ni-NTA. F: Elution with excess of imidazole (pentagon).

A further sensitive point to be mentioned is the capping. It is absolutely necessary that only complete peptides with the correct sequence are substituted with the tag. For this reason, after each coupling step free amino groups are capped by acetylation in order to exclude them from the further coupling steps. The quality of the final product (purity) is strongly dependent on this step.

5.3.1. Attachment of Spacers to 1,10-Phenanthroline

In a first step, a 1,10-phenanthroline derivative applicable in solid-phase peptide synthesis was prepared. Derivatization of phen at position 5 is a straightforward approach, as many derivatives of phenanthroline functionalized at this position are commercially available. Introduction of a carboxylic acid would be beneficial for the direct attachment to the peptide. Activation of the carboxylic acid would then allow the amide formation with the free amino group of the N-terminal amino acid in analogy to the common solid-phase peptide synthesis protocols.

The Suzuki Coupling (Nadine Hafner, Master student)

From the numerous reactions available for the introduction of the spacer, a Suzuki coupling was investigated as shown in Scheme 9. Addition of the phenylboronic acid and subsequent cleavage of the methyl ester should furnish a phenanthroline derivative suitable for coupling to the N-terminal of a peptide.

Compared to preliminary experiments, performed with 4-methoxyphenylboronic acid, the Suzuki coupling with 4-methoxycarbonylphenyl boronic acid proceeded extremely slow. This might be due to the fact that electron-rich organoboranes are much more reactive [195], which is the case for a methoxy group, that increases the electron density of the benzene ring. Various parameters were tested to optimize the reaction yield, *e.g.* solvent, catalyst, base, and ligand. Finally, an acceptable yield of 42% using S-Phos as the ligand and dioxane as the solvent was obtained. A direct purification of the product by LC-MS was not possible as product and starting material coeluted on the C18 reversed-phase column. Recrystallization prior to chromatography improved the purity of the final product, although small traces of the boronic acid were

still visible. π-π stacking between the boronic acid and product **35** might be the reason, as will be discussed later.
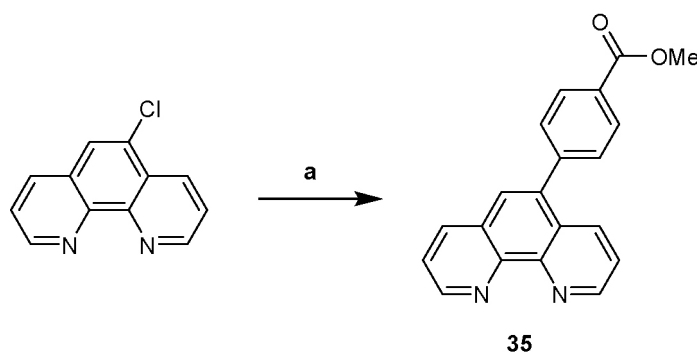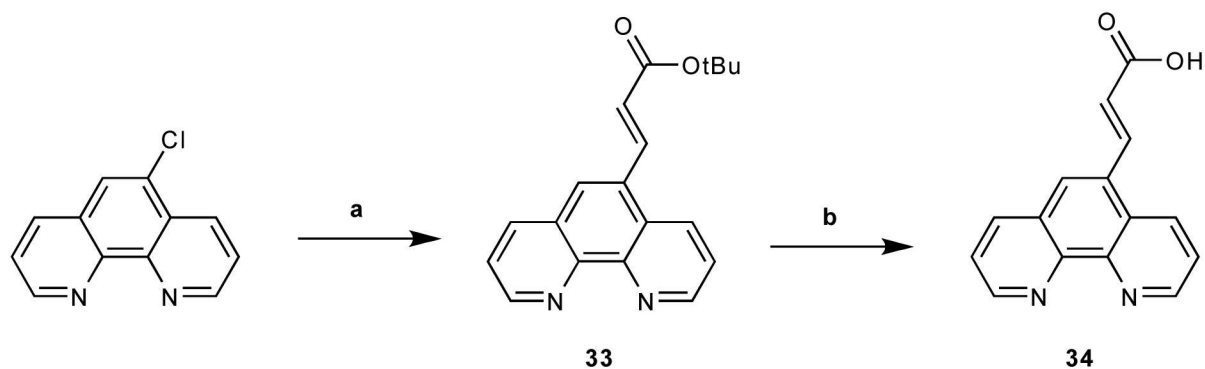

Scheme 9: Synthesis of 4-(1,10-phenanthrolin-5-yl)benzoic acid. a) 4-methoxycarbonylphenylboronic acid, Pd$_2$(dba)$_3$, S-Phos, dioxane, 80°C, 96h (42%).

Solubility of product **35** in aqueous solvents was very poor, aggravating the HPLC purification significantly. Even solvent mixtures containing an increased amount of methanol or acetonitrile did not solve the problem. Analysis on the Biacore system was not possible, as only solutions containing at least 50% DMSO enabled a proper dissolving of the Suzuki product **35** at concentrations needed for the experiments. According to the recommendations of the manufacturer, the upper limit of DMSO is 8%. Furthermore, insolubility in water would also complicate the application in IMAC chromatography, where mainly water based buffers are used. Therefore, no further efforts were put into this approach and final hydrolysis of the ester was skipped.

The Heck Coupling

Due to the poor solubility of the Suzuki product, an alternative spacer was tested. Attachment of an acrylic acid residue instead of a methoxycarbonylphenyl group would yield a more hydrophilic product. Furthermore, the improved solubility on the outer face of the molecule would improve the binding affinity, as already demonstrated in the phenanthroline series (section 5.2.3). The reaction was done with a palladium-catalyzed Heck coupling (Scheme 10).

Scheme 10: Synthesis of 3-(1,10-phenanthrolin-5-yl)prop-2-enoic acid (**34**). a) *tert*. butyl acrylate, PdOAc, CsCO₃, X-Phos, DMF, µW 80°C, 4h (69%); b) TFA, rt, o/n.

The first Heck coupling was tried with $Pd_2(dba)_3$, NaOAc, and $P(tBu)_3$ as ligand, which proved to be highly effective for couplings of non-activated aryl chlorides [196]. Incubation for totally 9 h in the microwave at 80°C did not show any product peak after LC-MS analysis. The temperature was increased to 100°C which led to a small product peak. However, a further increase to 120°C led to the complete degradation of the aryl chloride into 1,10-phenanthroline. In addition, an exchange of the catalyst to $Pd(OAc)_2$ and the ligand to S-Phos did not improve the result. However, an improvement was observed with the highly active X-Phos ligand, which was reported for amination reactions of aryl bromides and chlorides [197]. This bulky ligand forms a stable metal complex. The quantification of the UV signal after HPLC analysis gave a starting material-to-product-ratio of 1 : 0.35. A further effect was found using $CsCO_3$ instead of NaOAc, which improved the starting material-to-product-ratio by a factor of 10, leading to a yield of 69% after HPLC purification. With S-Phos ligand and $CsCO_3$ the yield was more than 2-fold lower after HPLC purification (34%). Trials with *N,N*-dimethylacetamide (DMA) instead of DMF did not furnish any product.

For all attempts, both the cis and trans product **33** were detectable, although the cis-product could only be detected by MS. The trans isomer was clearly identified by ¹H-NMR due to the *J*-coupling constant of 15.7 Hz between H-15 and H-16.

Upscaling of the Heck coupling was problematic because of the increase in the concentration of the reagents. As soon as the amount of the starting material was increased to 100 or even 400 mg (both in 5 mL DMF), the efficiency of the coupling nearly dropped to zero. For comparison, the same reaction was successful using 20 mg

starting material in 1.3 mL DMF. A possible reason could be the formation of aggregates due to π-π stacking of starting material with starting material or starting material with product. Increased π-π stacking was demonstrated between unsubstituted benzenes and benzenes with electron withdrawing substituents by Sinnokrot *et al.* [*198*]. Addition of the acrylate to the phenanthroline might therefore even further increase π-π stacking, especially at high concentrations. Therefore, the Heck coupling was performed only with small batches of 20 mg (in 1.3 mL DMF) and the products from each synthesis were pooled.

The final deprotection of the carboxylic acid by with performed quantitatively. The purity of free acid was finally checked by HPLC, before it was further used for coupling to the test peptide.

The initial idea for the attachment of the carboxylic acid spacer to 1,10-phenanthroline was to hydrogenate the double bond of the acrylic acid. But as none of the numerous attempts to reduce the double bond with Pd on charcoal at atmospheric pressure was successful, the last step was omitted. A selective hydrogenation of the acrylate double bond was not possible. A small fraction of the desired product was detected by MS after 36 h of reduction at atmospheric pressure. After 62 h complex **34** was completely reduced yielding 3-(tetradecahydro-1,10-phenanthrolin-5-yl)propanoic acid. Hydrogenation before the hydrolysis of the *tert*-butyl ester did also not alter the result.

5.3.2. Synthesis of the Test Peptide NAPamide

As a test peptide an α–MSH analog was chosen, which was well known from a synthetic point of view. It was developed for tumor-targeting, where it demonstrated great potential for diagnostics and treatment of melanoma cells . The sequence of this octapeptide is shown in section 4.2 (Table 9, entry **25**) containing two non-proteinogenic amino acids in the sequence at position 1 (norleucine) and 3 (D-phenylalanine). The crucial capping was performed with acetic anhydride as a highly reactive reagent to block free amino groups by acetylation. As base 2,6-lutidine was used as suggested by the manufacturer manual of the Pioneer peptide synthesizer. After the synthesis, the resin was divided into small portions of 35 mg. With one batch

(theoretical yield of 5.8 mg pure peptide) the conventional process with cleavage, precipitation and subsequent purification by HPLC was performed (standard method). The HPLC purification was also used for the qualitative analysis of the NAPamide synthesis. Figure 41 shows the chromatogram of the HPLC analysis of the crude NAPamide treated via the standard method.
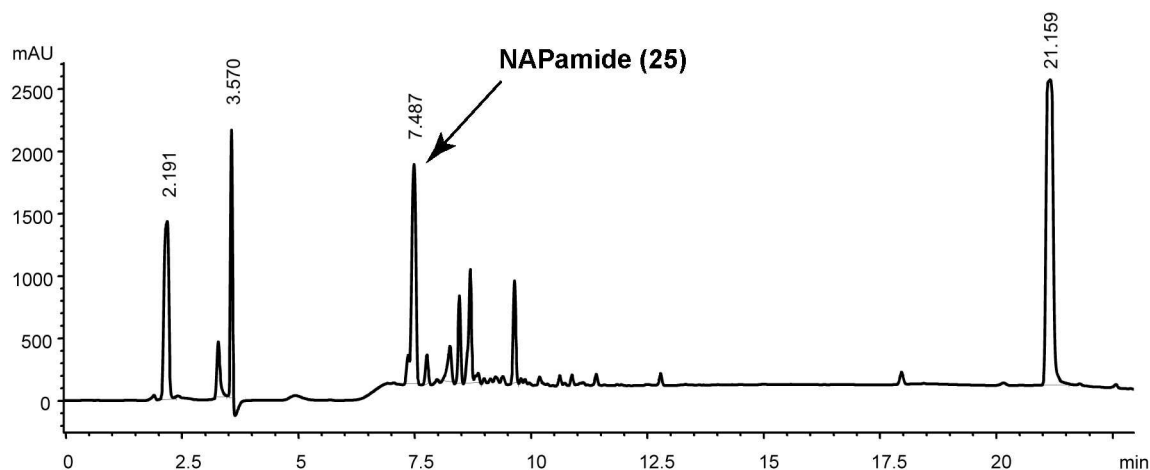

Figure 41: Chromatogram of crude NAPamide (**25**) recorded at 214 nm. A gradient of acetonitrile in water (both containing 0.1% HCOOH) from 5-95% for 20 min was run together with Phenomenex Gemini column (4.6 × 250 mm, 5 μM). Product peak of NAPamide is visible at t_R = 7.847 min.

The peak at 7.487 min corresponds to the NAPamide (**25**), which was verified by MS analysis. The huge peak at the end could not be identified, which might indicate that it is a low molecular weight compound and non peptidic. The rest of the impurities are formed by incomplete peptides, cleaved protecting groups, scavengers, and coupling reagents, which could not be completely removed by precipitation.

With another batch of 35 mg resin, the purification using the "phenanthroline method" was performed. Before peptide cleavage from the solid-phase, the phenanthroline-tag (**33**) had to be attached to the peptide (Scheme 11).
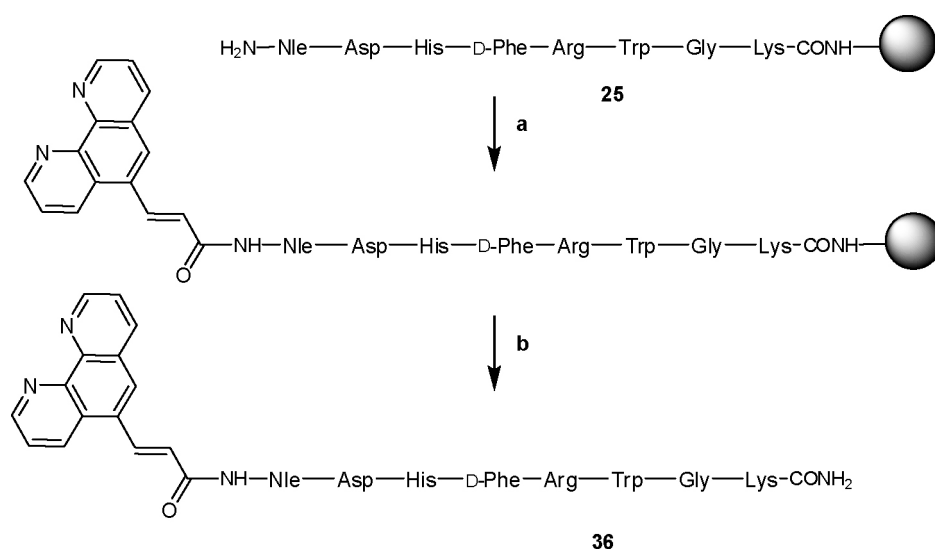
Scheme 11: Synthesis of phenanthroline-tagged NAPamide; a) HATU, DIPEA, DMF, rt, o/n; b) TFA, EDT, thioanisole, water, rt, 45 min.

The coupling was done by standard solid-phase peptide synthesis methods with the peptide still bound to the resin. Peptide molecules, which do not react with the tag, will be lost during purification on the Ni-NTA column leading to lower yields for the strategy. Therefore, the potent coupling agent HATU was used to enable the highest possible yield for this step. In addition, a huge excess of phenanthroline-tag **33** (8.4 eq) was used. The reaction was done over night. After extensive washing with DMF and isopropanol the resin beads showed a red staining resulting from the tagged peptide (**33**).

In the next step, the peptide-tag construct was cleaved from the solid-phase. To avoid the addition of the soft nucleophile ethane-1,2-dithiol used as scavenger to the unsaturated compound, the cleavage time was reduced to 45 min compared to a total cleavage time of 1.5 h for the NAPamide without tag. The decreased cleavage time did not elicit a significant effect on the yield as could be later shown (see quantification in section 5.3.4). After concentration *in vacuo*, the crude peptide still showed a strong red staining, compared to a transparent/white color for the crude NAPamide without tag.

5.3.3. Evaluation of Purification System with 1,10-Phenanthroline

Before the purification strategy could be applied to the tagged peptide, the optimal conditions were evaluated with the tag itself. The Ni-NTA system is widely used for the hexahistidine-tag, but not much information is known for purifications with

phenanthroline-tags, except the already mentioned patent application from Lonza [*169*].

First, the optimal buffer system was identified. For this purpose, small samples of 1,10-phenanthroline (4 mg) were dissolved in loading buffer and loaded onto the column. After washing, phenanthroline was eluted with elution buffer containing 500 mM imidazole. For higher sample recovery, the wash fractions were concentrated *in vacuo* and loaded again onto the column.

Imidazole with its maximal absorption around 230 nm interferes with the maximal absorption of 1,10-phenanthroline (λ_{max} = 230 nm), making a quantification impossible at this wavelength (Figure 42). At 260 nm, 1,10-phenanthroline has a second smaller maximum, which is clearly isolated from the imidazole signal and could be used for the quantification.
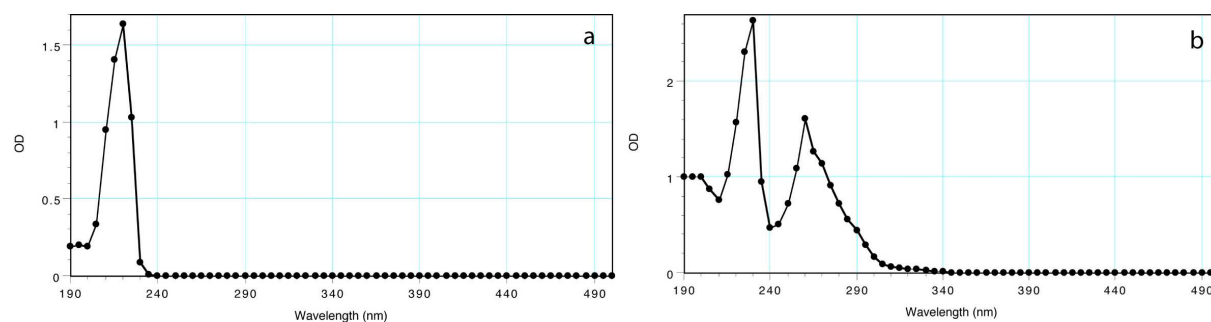

Figure 42: a: Spectrum of imidazole (0.36 mg/mL), λ_{max} = 230 nm; b: Spectrum of 1,10-phenanthroline (0.028 mg/mL), $\lambda_{max}1$ = 230 nm, $\lambda_{max}2$ = 260 nm.

Three different buffer systems were compared for the purification process (Table 33). As a first buffer, the eluent buffer from the Biacore experiments was used. HEPES-based buffer with a *pH* 7.4 was thought to be suitable for the purification of peptides or proteins, because its buffer capacity is around the physiological *pH*. The second buffer was a 1:1 mixture of eluent buffer and acetonitrile. In Biacore experiments with NTA chips, a small amount (50 μM) of EDTA is added to the running buffer to scavenge contaminating ions, which was also thought to be beneficial for the purification process. The third buffer system does not contain EDTA. An overview of the three buffer systems and the results from the test purifications with 1,10-phenanthroline is given in Table 33.

Table 33: Ni-NTA purifications of 1,10-phenanthroline with different buffer systems.

No.	Buffer system [a]	Amount with 1st elution [mg]	Amount with 2nd elution [mg]	Total recovery [b] [mg]		Total recovery [%]
				Exp.	Theor.	
I	0.01 M HEPES *pH* 7.4, 0.15 M NaCl, **50 μM EDTA** in **H₂O**	0	0	0	4.0	**0**
II	0.005 M HEPES *pH* 7.4, 0.0725 M NaCl, **25 μM EDTA** in **H₂O/CH₃CN (1:1)**	0.53	0	0.53	4.0	**13**
III	0.005 M HEPES *pH* 7.4, 0.0725 M NaCl in **H₂O/CH₃CN (1:1)**	2.4	1.4	3.8	4.0	**95**

[a] composition of the loading buffer, for elution the same buffer was used with additional 500 mM imidazole

[b] Exp.: Experimentally determined amount of total recovery; Theor.: Theoretical amount, total amount used in this experiment

Most evident is the fact that without acetonitrile in the loading buffer, the sample was completely lost, most likely due to insolubility of phen in water. As nothing of the sample was detected in any of the wash solutions, the problem is most likely a precipitation on the column or already in the syringe during loading. As soon as acetonitrile is added, at least 13% of the 1,10-phenanthroline can be recovered. Interestingly, only one elution step was necessary to recover the sample. Reloading of the wash fractions did not contribute to a higher recovery. For the third purification EDTA was completely omitted from the buffer solutions and this led to a sudden increase in sample recovery. From 4 mg of injected 1,10-phenanthroline, 3.8 mg (95%) could be regained. The first elution step gave the highest amount of 1,10-phenanthroline with 60%. The rest of 35% could be recovered with a second loading of the 1st wash fraction.

With a recovery of 95%, 1,10-phenanthroline was found to be applicable as a tag in purifications on Ni-NTA columns. Buffers only based on pure water as buffer I are not recommendable for purifications with 1,10-phenanthroline. The low solubility of 1,10-phenanthroline in water of 3 mg/mL derived from literature seems to confirm this assumption [*190*]. The effect of EDTA in the buffer is not clear. A possible explanation is that EDTA is able to withdraw nickel ions from the column matrix and therefore decreases the binding capacity of the column. This might explain the low recovery of the phenanthroline with buffer II in the purification process. Although, Nieba *et al.* could demonstrate at least for the Biacore setup that inclusion of EDTA in the running buffer has no impact on nickel loading of the NTA sensor chip up to a

concentration of 300 µM [*126*], the situation might look different in case of a Ni-NTA column.

5.3.4. Purification of NAPamide using 1,10-Phenanthrolinyl Tag

Buffer system I and II from section 5.3.4 (see Table 33) were compared in this purification of the phenanthroline-tagged NAPamide (see section 5.3.2). The red color of the phenanthroline-tagged NAPamide enabled a qualitative tracking of the purification process (Figure 43).
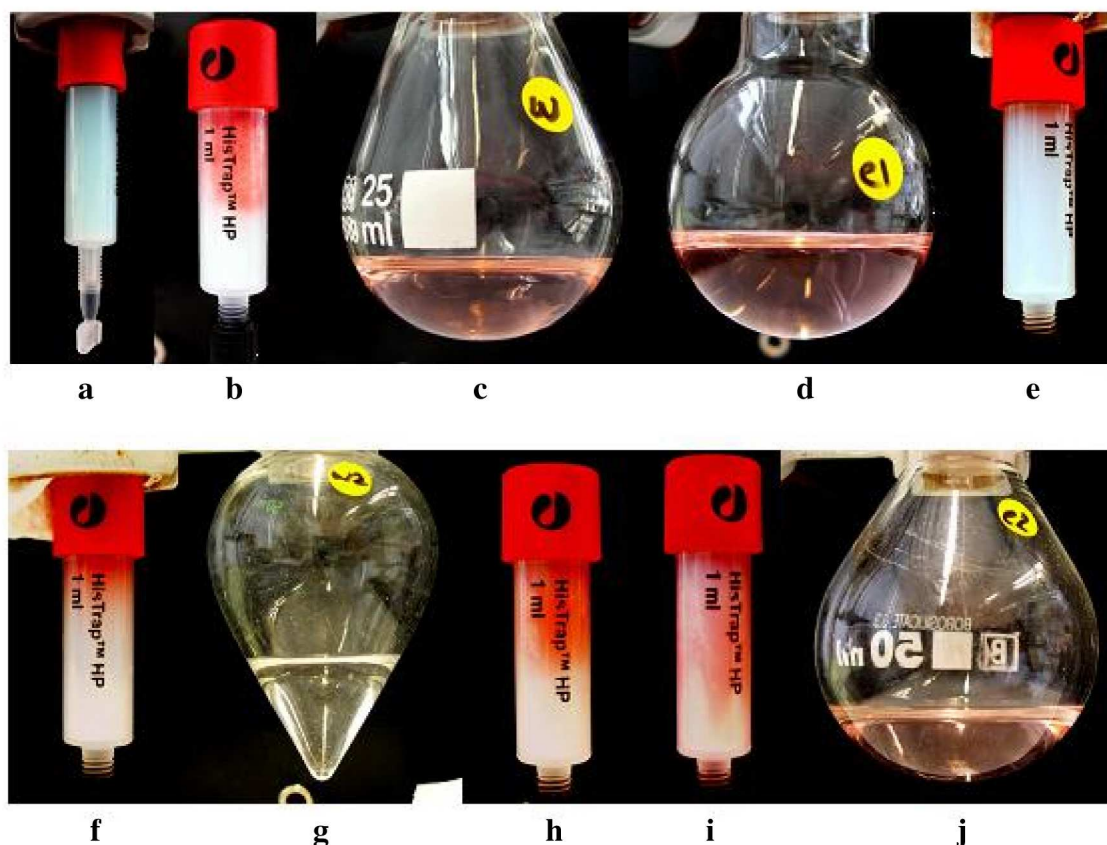

Figure 43: Purification of 1,10-phenanthroline-tagged NAPamide on HisTrap column: a: before sample loading; b: after sample loading; c: pooled fractions of first wash; d: pooled fractions of first elution; e: after first elution; f: reloading of first wash; g: second wash; h: during second elution I; i.: during second elution II; j: pooled fraction of second elution.

On picture **a** (Figure 43), the blue color of the nickel loaded NTA column is shown. Upon loading of the sample, the red color settles in the upper half of the column (**b**). The first wash showed a strong red coloring (**c**), indicating that the column might be overloaded, or that the half-life time of the complex of

phenanthroline and Ni-NTA is too short, leading to an immediate release of the sample. At least part of the phenanthroline-tagged peptide is clearly retained on the column, as demonstrated with the clear red solution achieved after elution with 500 mM imidazole (**d**). Only a small fraction of the product gets stuck on the column and is not eluted, as visible in picture **e** (small red band at the very top of the regenerated column). The remaining sample, present in the first wash (**c**) was then reloaded onto the column after concentration *in vacuo*. This is a common process, which is also frequently applied to histidine-tagged proteins. Again, the red staining is visible after loading the first wash onto the column due to its red staining (**f**). The second wash was colorless indicating that the whole product present in the first wash was retained on the column (**g**). Again, the last elution with 500 mM imidazole could clearly be followed as the red sample migrates towards the bottom of the column after injection of 2 mL (**h**) and 4 mL (**i**) elution buffer. The red color from the pooled elution fractions of the second round (**j**) demonstrated that the purification was successful.

A comparison of samples before and after the Ni-NTA purification by HPLC analysis clearly demonstrated the successful purification procedure (Figure 44).

The chromatograms showed that out of a heterogeneous mixture the desired target peptide could be purified. By MS analysis it could be shown that peaks at 11.119 min in **b** and 11.093 min in **c** correspond with the phenanthroline-tagged NAPamide (**36**). The huge absorption in these chromatograms around the injection peak are mainly caused from imidazole present in high amounts in the elution buffer. Chromatogram **a** showed a number of peaks around a retention time of 9 min, which could not be assigned to peptidic moieties (*e.g.* non-tagged NAPamide or incomplete NAPamide) as well as the impurity. The impurity in **c** was of non-peptidic nature as could be later demonstrated by dabsylation. The non-tagged NAPamide, which eluted at 7.5 min (see Figure 41), was only visible as a small peak compared to the product peak at 11.160 min in chromatogram **a**, eliciting a high yield of the final coupling of the phenanthroline-tag to the peptide.
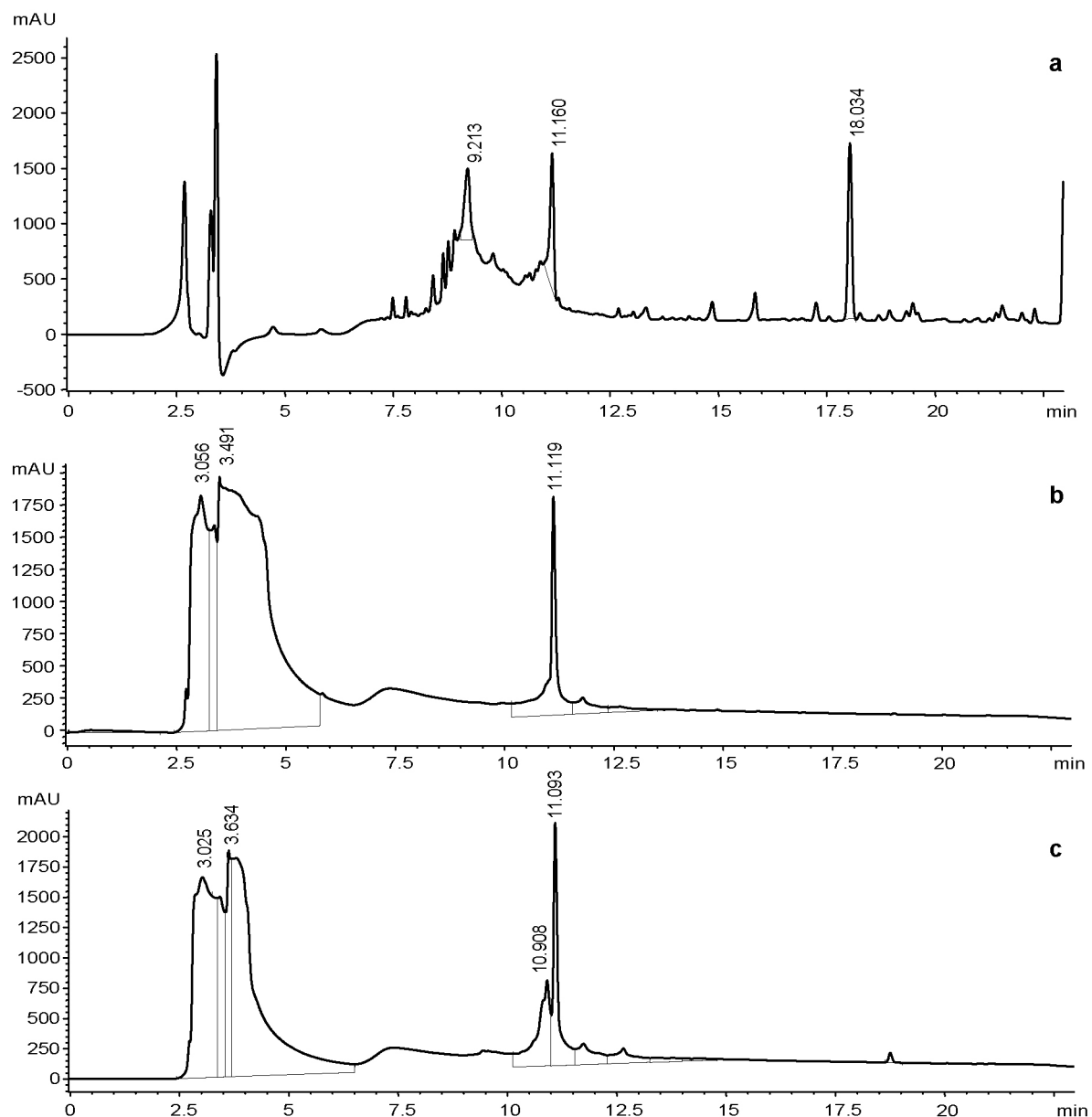
Figure 44: HPLC analysis at 214 nm on a Phenomenex Gemini column (4.6 × 250 mm, 5 μM) of phenanthroline-tagged NAPamide before Ni-NTA purification (a), after 1st elution (b), and after elution of reinjected 1st wash fraction (c). A gradient of acetonitrile in water (both containing 0.1% HCOOH) from 5-95% for 20 min was run.

The quantitative analysis was performed to compare the new phenanthroline method with the standard HPLC purification of NAPamide. The quantification was done by gas-phase hydrolysis and subsequent dabsylation of the free amino-groups of the amino acids as described in section 4.3.1. Due to the presence of imidazole in the elution buffer, the sample **36** had to be separated from imidazole by HPLC after elution from the Ni-NTA column. Since the large excess of imidazole in the samples might interfere with the dabsylation reaction, as imidazole can react with DABS-Cl as well, a correct quantification would not be possible. The data from the quantification via dabsyl derivatization is shown in Table 34.

Table 34: Ni-NTA purification of phenanthroline-tagged NAPamide (**36**) compared to standard purification of NAPamide (**25**) with HPLC.

Sample	Purification System [a]	Quantity of purified product [b] [mg]		Yield of Synthesis [%]
		Exp.	Theor.	
Phen-tagged NAPamide (**36**)	Ni-NTA, buffer system II	1.2	2.9	**41**
Phen-tagged NAPamide (**36**)	Ni-NTA, buffer system III	1.0	2.3	**43**
NAPamide (**25**)	HPLC	2.0	5.8	**34**

[a] composition of the loading buffer, for elution the same buffer was used with additional 500 mM imidazole

[b] Exp.: Amount of product determined by dabsylation; Theor.: Amount of product estimated from the amount of resin

The yields of the NAPamide synthesis were in the expected range for all purification strategies. A comparison between the HPLC and the Ni-NTA purification methods showed a satisfying result. Both purifications of the tagged peptide (with system II and system III) showed similar or even higher yields compared to the HPLC purified peptide. In contrary to the purification with phenanthroline alone, no differences in the purification yield between buffers with and without EDTA were found. The derivatized peptides showed in all three cases the correct ratios of the amino acids present in NAPamide. Therefore, only the full length peptide is present in the purified sample demonstrating the success of the capping strategy.

5.3.5. Influence of Spacer and Peptide on Binding Affinity and Kinetics

A fundamental question to be answered when an affinity tag is developed is the required affinity. The much higher binding affinity of His6 (**5**) compared to a His-tagged protein reported by Nieba *et al.* [*126*] was already discussed in section 5.1.5. With the phenanthroline system, the same effect is expected, as the phenanthroline-tagged peptide contains a plethora of additional rotational bonds. This will truly lead to an increased entropy penalty upon binding, probably due to electrostatic interactions between peptide and phen, or to steric hindrance. With a peptide directly coupled to the phenanthroline tag, the binding behavior of the tag alone and coupled to a peptide could be studied.

For this purpose, Biacore experiments were performed with 1,10-phenanthroline derivatized with the acrylate spacer (**34**) and phenanthroline-tagged NAPamide (**36**), which could then be compared with 1,10-phenanthroline (**42**). The sensorgrams of the three compounds are shown in Figure 45.
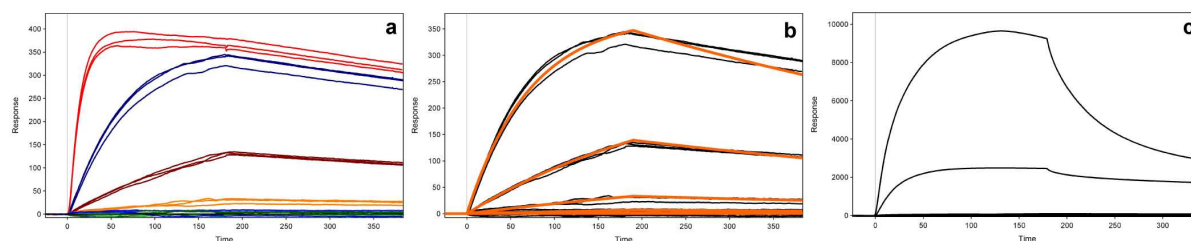

Figure 45: Biacore analysis of Heck coupling products. A: Sensorgram of 3-(1,10-phenanthrolin-5-yl)prop-2-enoic acid (**34**), 10 μM – 4 nM, 5-fold dilutions; b: kinetic fit of **34,** 2 μM – 4 nM, 5-fold dilutions; c: Sensorgram of phen-tagged NAPamide (**33**), 30 μM – 469 nM, 2-fold dilutions.

The acrylate spacer linked to the phenanthroline altered its binding behavior significantly. The free carboxylic acid seems to lead to rebinding at concentrations in the low micromolar range as was evident by the parallel dissociation phase of the two highest concentrations in the sensorgram of **34** (Figure 45a). With the additional Ni^{2+}-ligand formed by the carboxylic acids, a complete dissociation of **34** from the Ni-NTA surface was aggravated. When more than one binding motif is present in a single molecule, rebinding becomes apparent in the sensorgrams as already observed for the oligohistidines in section 5.1.1. Due to the rebinding, the highest concentration (red curve) was omitted for fitting to a 1:1 binding model (Figure 45b). Binding of phen-tagged NAPamide (**36**) did not show a sensorgram, which was fittable to a 1:1 binding model, neither kinetically nor by a steady state fit (Figure 45c). The expected saturation level R_{max} according to Equation 7, would have been at about 2000 RU. The experimental binding level observed with a concentration of 30 μM was up to 5-fold higher, suggesting an overlay of different binding events. At higher concentrations, a complete loss of binding signal or even negative binding signals were observed, indicating a possible influence of the dextran matrix. These effects might arise due to the charges on the Ni-NTA complex and on the peptide as well. The negatively charged NTA-dextran matrix might also explain the high binding signal reached for a concentration of 30 μM. As soon as the Ni-NTA complexes are saturated, electrostatic interactions between the negatively charged chip surface and the positively charged

peptide (due to the counterions from the HPLC purifications) leads to a coating of the surface and therefore to this huge binding signals. Nevertheless, a stable immobilization of product **36** was possible at a concentration of 15 μM, where the binding signal remains stable during dissociation phase indicating a specific interaction between phenanthroline and Ni-NTA. At higher concentrations, some product was lost at the beginning of the dissociation phase, which is comparable with the wash step of an overloaded Ni-NTA column.

Only the sensorgram of **33** allowed a kinetic fit to a simple 1:1 binding model. However, the highest concentration of 10 μM had to be excluded due to the strong rebinding, in order to achieve a satisfying fit with a res SD of 7.5. For the phen-tagged NAPamide (**36**) a rough estimate of the binding affinity was made: Binding was detected for concentrations above 7.5 μM, which corresponds to a binding affinity in the mid micromolar range as a very rough estimate. Fitting of the 30 μM and the 15 μM binding curve kinetically to a simple 1:1 binding model reveals a binding affinity of 10 μM and 80 μM, respectively.

Table 35: Evaluation of kinetics and binding affinity of phenanthroline series.

Compound	No.	k_{on} [$M^{-1}s^{-1}$]	k_{off} [s^{-1}]	$T_{1/2}$ [min]	K_D (kin [a]) [μM]
1,10-Phen	(**42**)	3546 ± 181	0.00229 ± 0.00021	5.0	0.650 ± 0.093
(*E*)-3-(1,10-Phenanthrolin-5-yl)acrylic acid	(**34**)	1240 ± 60	0.00131 ± 0.00008	8.8	1.06 ± 0.11
Phen-tagged NAPamide	(**36**)	-	-	-	10 – 100 [b]

[a] kinetic fit, $K_D = k_{off}/k_{on}$

[b] rough estimate

The binding affinity of phen (**42**) decreases upon attachment of the acrylate spacer (1.6-fold) due to the significantly lower k_{on}. Interestingly, the decreased k_{off} is leading to an increase in the half-life time of the complex from $T_{1/2}$ = 5 min to 8.8 min. The same effect was already observed within the phenanthroline series, where the increased solubility on the outer face of the molecule also led to a decreased k_{off}. The same must be true for **34**, because of the favorable solvation by the carboxylic acid, although the k_{off} might be slightly underestimated due to the rebinding.

The difference of the K_Ds of phen (**42**) alone and attached to the target peptide (**36**) was >15-fold and therefore in the same range as already observed for the

affinity of the His6 (**5**) and a His-tagged protein reported by Nieba *et al*. [*126*], although the attached protein in case of Nieba *et al.* and the peptide in our case significantly differ in size. This observation was already confirmed with the results of the His_xAla_y series (section 5.1.3). The difference in binding affinity between HH (**1**) and AHH (**19**) was much more pronounced than for AAAHH (**17**) and AAAAHH (**10**), where almost the same affinities were measured.

5.4. Refinement of the Purification Strategy: Introduction of Photolinker

With the successful purification of a peptide with the IMAC technique, the project was guided towards further refinements. Introduction of a linker between the tag and the product would allow a site specific cleavage to get finally the pure product without tag traces. The use of a photochemically cleavable linker for solid-phase peptide synthesis has received considerable attention during the last two decades. It is widely recognized that photolysis offers a mild method of cleavage [*199*]. Very recently, a successful application of a photolinker (**50**, Scheme 12) was reported, which allows selective cleavage by photoirradiation at 365 nm [*170*]. The photolytic cleavage is supposed to give high yields without side reactions.
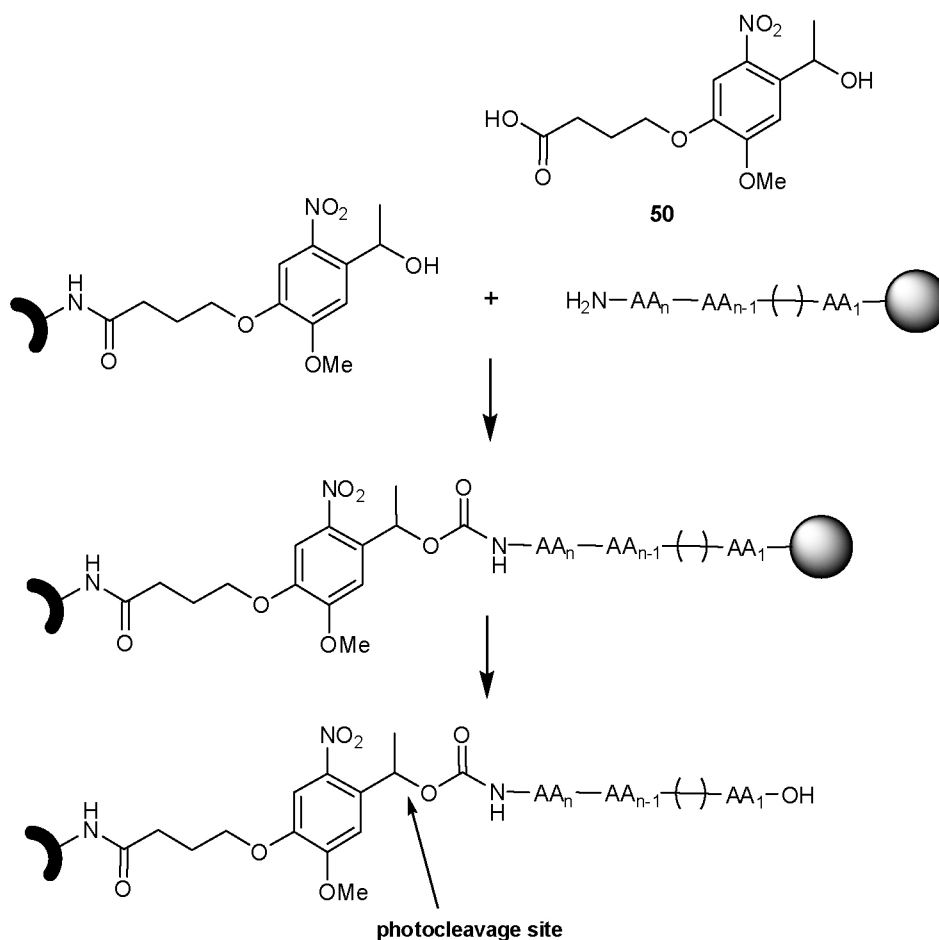

Scheme 12: Introduction of the tag-photolinker for purification of a solid-phase product. After the final coupling step of the peptide synthesis, the tag-linker construct is coupled via a carbamate to the peptide. Cleavage of the product form the solid-phase allows loading of the product onto a purification column. Upon irradiation, the tag can be cleaved from the peptide at the indicated site.

The application of the photolinker to our purification process is outlined in Scheme 12. 1,10-phenanthroline is coupled via a glycine spacer to the photolabile linker. After cleavage from the solid-phase, the product will be loaded onto the Ni-NTA support for purification as described in section 5.3. The carbamate linking photolinker and peptide as well as the amide bond between photolinker and phen are stable in 90% TFA during deprotection and cleavage of the product from the solid support [170]. After all non-tagged side-products have been eluted, the peptide-photolinker-tag construct still immobilized on the affinity column, is irradiated leading to the release of the product. Finally, the product is eluted at neutral pH. The tag-photolinker construct will remain attached to the Ni-NTA surface.

The synthesis of the tag-photolinker construct is discussed in the following sections.

5.4.1. Preparation of the Tag-Photolinker Construct

The coupling of the photolinker to the tag was achieved by the attachment of a glycine spacer to the 1,10-phenanthroline. The starting material was the commercially available 5-nitro derivative. Preparation of this 5-glycyl-phen is shown in Scheme 13.
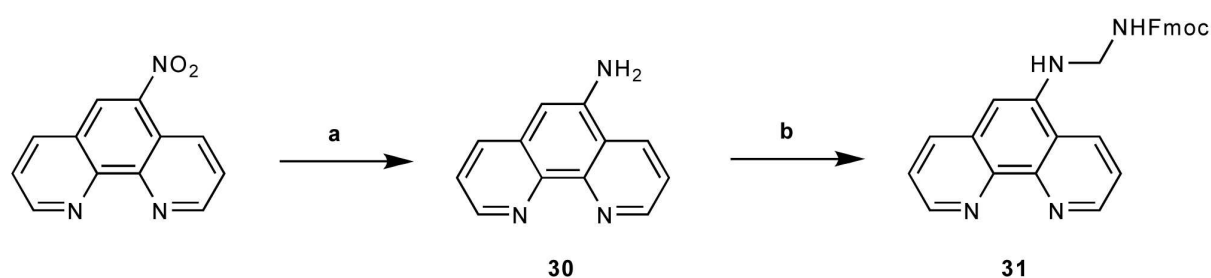

Scheme 13: Introduction of a glycine spacer to 1,10-phenanthroline: a) H_2, Pd/C, MeOH, atm. pressure, rt, 24h, (quant.); b) HATU, DIPEA, DMF, rt, o/n (71%).

5-nitro-1,10-phenanthroline was reduced to the 5-amino derivative (**30**). NMR analysis of the crude product did not show any byproducts, therefore no additional purification step was necessary. Fmoc-Gly-OH was attached as a spacer using standard conditions of peptide synthesis. When the reaction was performed with the more reactive HATU, full consumption of 5-amino-1,10-phenanthroline was observed, whereas with HOBt/TBTU some starting material was still present, even after

prolonged reaction times. With HATU as coupling reagent, the reaction afforded product **31** in 71% yield. However, a purity check showed some minor impurities even after LC-MS analysis.

The next step in the photolinker strategy was the coupling of phen to the photolabile linker (Scheme 14).
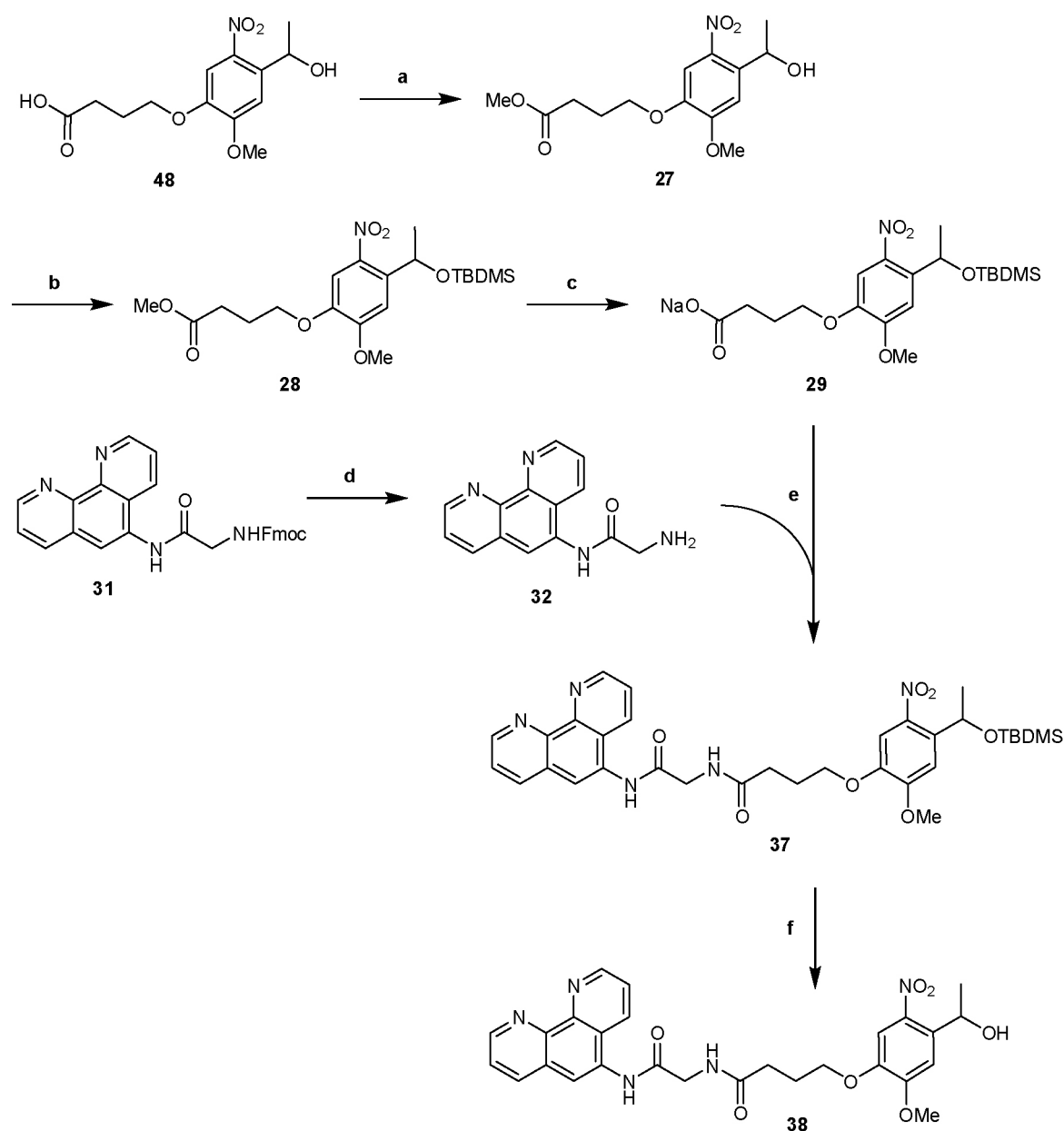

Scheme 14: Protection of photolinker and subsequent attachment to 5-glycyl-1,10-phenanthroline (**32**): a) SOCl$_2$, MeOH/DMF, rt, o/n (quant.); b) TBDMS-Cl, imidazole, DMF, rt, o/n (98%); c) NaOH, rt, o/n (quant.); d) 20% piperidine, DMF, rt, 2 h (quant.); e) EDC•HCl, HOBt, DIPEA, rt, o/n; f) TBAF, THF, rt, o/n (e+f: 11%).

For this purpose, the free hydroxyl group of the linker had to be protected as silylether to avoid formation of linker dimmers. The methyl ester was formed using

thionyl chloride in methanol to afford quantitatively **27** after acid-base extraction. Protection of the secondary hydroxyl group was performed by silylation with TBDMS-Cl yielding **28** in 98%. Finally, hydrolysis in sodium hydroxide gave the sodium salt of the photolinker **29**.

Before coupling to the photolinker, the glycine derivative **31** was deprotected with 20% pyridine. The reaction was quantitative, and the product **32** was further used without chromatographic purification. The *tert.* amine formed as a byproduct during Fmoc-cleavage (1-((9*H*-fluoren-9-yl)methyl)piperidine) was thought to be significantly less reactive than the primary amine of the glycine, and should therefore not compete with the coupling of the photolinker. Unfortunately, HPLC purification revealed that only traces of **38** had been formed.

In addition to the phen-photolinker construct **32**, the His$_6$-amide-photolinker **41** was synthesized (Scheme 15).
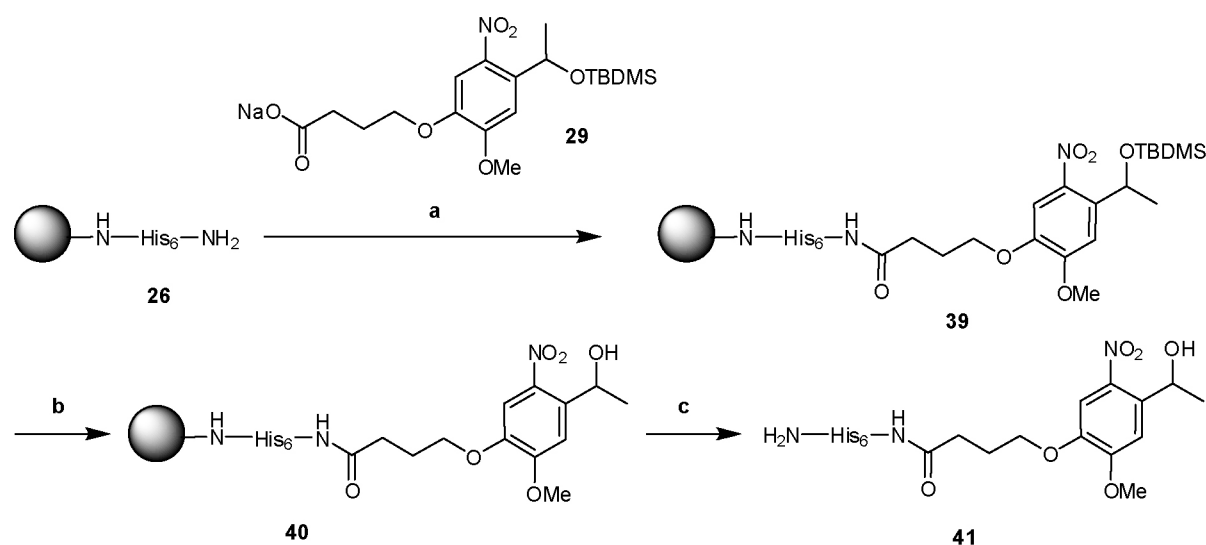
Scheme 15: Aattachment of His6-amide (**26**) to photolinker (**29**): a) EDC•HCl, HOBt, DIPEA, rt, o/n; b) TBAF, THF, rt, o/n c) TFA, H2O, triisopropyl silane, rt, 2 h (a+b+c: 65%).

After synthesis of His$_6$-amide (**26**) on solid-phase, the amide bond formation was performed with the EDC•HCl to yield product **i1**. After cleavage of the silyl ether with TBAF (**i2**), the construct PL-His$_6$-amide (**41**) was cleaved from the solid support. Regarding the low excess (only 1.2-fold) of **29** compared to His$_6$-amide, the yield of the amide formation was satisfying (65%). After purification by HPLC, the His$_6$-amide-PL (**41**) was characterized by MS. As the compound was later used for analysis

on Biacore (section 5.4.3), quantification with dabsylation was performed, to avoid concentration problems as a consequence of the salt load. The salt content of the PL-His$_6$-amide was 58% and in the same range as for the His6 (**5**) peptide.

5.4.2. Solubility of Phenanthroline Derivatives

All phenanthroline derivatives showed a critical behavior during HPLC purification. Separation of products and byproducts on normal-phase support was not successful, probably as a consequence of the high logP values. ALOGPS 2.1 from Virtual Computational Chemistry Laboratory [*200*] was used to predict the logP of different phenanthroline containing structures synthesized in this project. The results are given as the mean value including standard deviations over the various logP. A second logP calculation was performed with the so-called Moriguchi method [*201*], which is based on 13 descriptors adding either to an increase or a decrease in lipophilicity. The results of both logP predictions are summarized in Table 36.

Table 36: LogP prediction of phenanthroline derivatives by software ALOGPS 2.1 and Moriguchi.

Compound	No.	Avg. logP (ALOGPS 2.1)	MlogP (Moriguchi)
1,10-Phenanthroline	(**42**)	2.18 ± 0.26	1.90
(*E*)-*tert*-Butyl-3-(1,10-phenanthrolin-5-yl)acrylate	(**33**)	3.75 ± 0.49	3.18
(*E*)-3-(1,10-Phenanthrolin-5-yl)acrylic acid	(**34**)	2.00 ± 0.43	1.97
Fmoc-protected glycyl-phen	(**31**)	4.38 ± 0.56	3.64
TBDMS-protected PL-phen	(**37**)	5.32 ± 0.40	3.04
Phen-PL	(**38**)	2.11 ± 0.55	0.85
His$_6$-amide-PL	(**41**)	-3.90 ± 1.92	-6.51

Calculations with the ALOGPS software and with Moriguchi predicted a good solubility in water for PL-His$_6$-amide (**41**) (8000-fold better solubility in water than in octanol for ALOGPS). This correlates with the observations made during RP-HPLC purifications of **41**. All the phenanthroline containing compounds showed a much higher logP value.

5.4.3. Biacore Experiments with Photolinker Constructs and Precursors

The influence of the photolinker on the binding affinity of the tag was analyzed by SPR. For this purpose, phen-PL (**38**) and His$_6$-amide-PL (**41**) were analyzed (Figure 46).
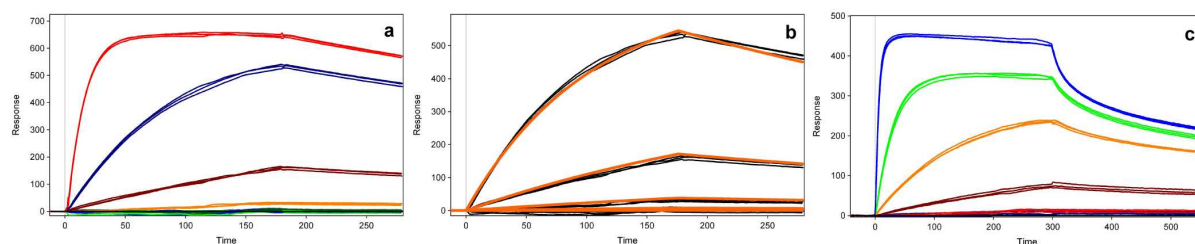

Figure 46: Biacore experiments with photolinker constructs: a: Sensorgram of phen-PL (**38**) from 200 μM – 13 n (5-fold dilutions); b: kinetic fit of phen-PL (**38**) from 40 μM – 13 n (5-fold dilutions); c: sensorgram of His$_6$-amide-PL (**41**) from 200 μM – 3 n (5-fold dilutions).

The sensorgram of **38** showed a concentration dependent slow dissociation as generally observed for rebinding (Figure 46a). At high concentrations (>200 μM, red curve), the compound elicited strong rebinding. Therefore, the 200 μM concentration was omitted for the kinetic fitting of **38** (Figure 46b), leading to a good fit with a res SD of 6.5. Rebinding is likely to occur due to the oxygen of the free hydroxyl group, which is able to complex Ni^{2+}.

Rebinding was even more pronounced for **41** (Figure 46c). Similar to some oligohis (Figure 19), binding curves at high concentrations seem to establish stable immobilization after an initial dissociation phase. Therefore, the photolabile linker does not strongly interfere with the rebinding ability of the His-tag.

The kinetic parameters and the binding affinity of the above mentioned compounds were compared with the free tags phen (**42**) and His6 (**5**), respectively (Table 37).

Table 37: Evaluation of kinetics and binding affinity of photolinker constructs.

Compound	No.	k_{on} [M^{-1}s^{-1}]	k_{off} [s^{-1}]	$T_{1/2}$ [min]	K_D [µM]
His6	(**5**)	-	-	-	0.014 ± 0.001 [a]
His$_6$-amide-PL	(**41**)	-	-	-	0.128 ± 0.002 [a]
1,10-Phen	(**42**)	3546 ± 181	0.00229 ± 0.00021	5.0	0.650 ± 0.093 [b]
Phen-PL	(**38**)	139 ± 8	0.00161 ± 0.00002	8.6	8.36 ± 0. 41 [b]

[a] steady state fit

[b] kinetic fit, $K_D = k_{off}/k_{on}$

The binding affinity of His$_6$-amide-PL (**41**) was 9.1-fold lower compared to His6 (**5**) as a consequence of the increased entropic costs upon binding of **41**. Phen-PL (**38**) showed a 12.9-fold lower affinity than phen. Attachment of the photolinker had therefore comparable effects on the affinity of the tag.

The bulky photolinker had a high effect on the on-rate. A 25-fold decrease of the k_{on} was observed for **38** compared with phen (**42**). The k_{off} slightly added to a better binding affinity and was 1.8-fold lower than for phen.

5.5. A New Series of Potential Tags

One goal of this thesis was to screen for new purification tags suitable for SPPS. Such tags must meet many requirements like high affinity to Ni-NTA, good solubility in aqueous solvents, and high stability towards chemical conditions. The search was restricted to commercially available substances or to substances, which can be synthesize with minor efforts. According to a search in the CSD, the main group of ligands binding to Ni^{2+} contains nitrogen. Carbonyls or sulfur could be found as well, although to some lesser extent. For bidentate ligands, a combination of two of the three elements is possible. Octahedral coordination is the preferred geometry for Ni^{2+}. In such a complex the angle formed by the ligand atom, the nickel ion, and the second ligand atom is 90°. Potential bidentate ligands are shown in Figure 47. The search for new ligands was supported by the computational model mentioned already for the phenanthroline series in section 5.2.1
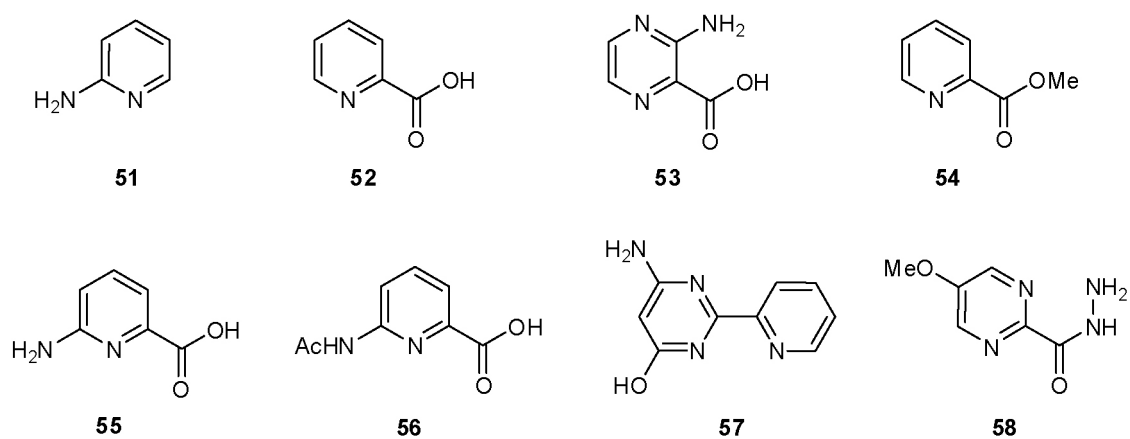

Figure 47: New series of potential tags for purification on Ni-NTA columns, the picolinic acid series.

Except for **57** in Figure 47, the main motif is an aromatic nitrogen and a carbonyl oxygen binding in a bidentate manner to the nickel ion.

5.5.1. Biacore Experiments with Picolinic Acid Derivatives

Generally, the picolinic acid series showed a higher solubility than the phenanthroline series. Therefore, except for **57**, no DMSO was used for the Biacore

experiments. A selection of some sensorgrams including a kinetic fit is shown in Figure 48.
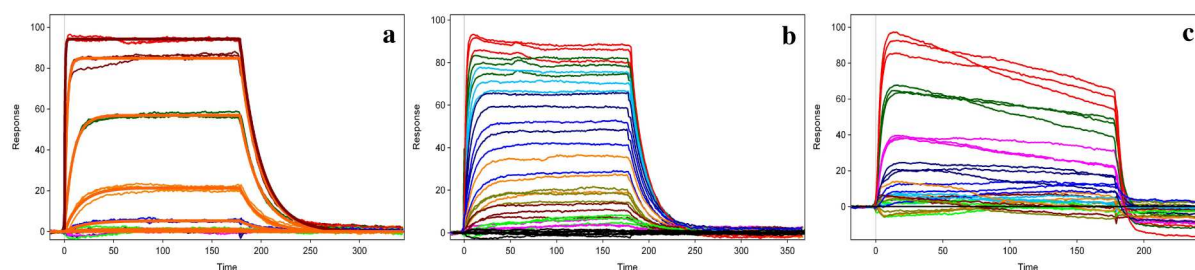

Figure 48: Selection of sensorgrams from picolinic acid series: a) Kinetic fit to simple 1:1 binding model of picolinic acid (**52**); b) sensorgram of methyl picolinate (**54**); c) sensorgram of 6-amino-2-(2-pyridyl)pyrimdin-4-ol (**57**).

The sensorgrams of **52**, **55,** and **56** was highly reproducible data. The data could be kinetically fitted to a simple 1:1 binding model as demonstrated for **52** (Figure 48a). The res SD was 2 or even lower for all compounds of this series. For methyl picolinate (**54**), reproducibility was much lower, therefore the values of k_{on}, k_{off}, and K_D showed much higher SD (see Table 38). Compound **57** showed again the common decrease in binding signal during steady state phase as was already demonstrated for bipy and phen (Figure 48c). Due to this decrease, kinetic parameters could not be determined, but an approximation of the binding affinity was obtained by a steady state fit to a simple 1:1 binding model. The results of the kinetic or steady state fits of the picolinic acid series are summarized in Table 38.

Table 38: Evaluation of kinetics and binding affinity of picolinic acid series (**51** – **58**).

Compound	No.	k_{on} [M^{-1}s^{-1}]	k_{off} [s^{-1}]	$T_{1/2}$ [s]	K_D [µM]
2-Aminopyridine	(**51**)	-	-	-	$>10^4$ [a]
Picolinic acid	(**52**)	3412 ± 389	0.0480 ± 0.0065	14.4	14.0 ± 0.5 [b]
3-Aminopyrazine-2-carboxylic acid	(**53**)	3544 ± 321	0.139 ± 0.006	5.0	39.4 ± 2.3 [b]
Methyl picolinate	(**54**)	1590 ± 690	0.0497 ± 0.0011	13.9	35.3 ± 3.2 [b]
6-Aminopicolinic acid	(**55**)	1663 ± 9	0.0181 ± 0.0003	38.3	10.9 ± 0.1 [b]
6-(Acetylamino)pyridine-2-carboxylic acid	(**56**)	1274 ± 68	0.168 ± 0.010	4.1	132 ± 4 [b]
6-Amino-2-(2-pyridyl)-pyrimidin-4-ol	(**57**)	-	-	-	83 ± 6 [a]
5-Methoxy-pyrimidine-2-carboxylic acid hydrazide	(**58**)	378 ± 9	0.213 ± 0.001	3.3	563 ± 11 [b]

[a] steady state fit

[b] kinetic fit, $K_D = k_{off}/k_{on}$

For 2-aminopyridine (**51**), binding was only detected at concentrations $\geq$ 10 mM. One reason could be the pK_a of 6.86 of the aromatic nitrogen [*202*], which is close to the *pH* of the eluent buffer (*pH* 7.4). Therefore, protonation of the binding nitrogen could explain the low binding affinity. Picolinic acid (**52**) showed an affinity in the low micromolar range. Compared to the affinity of phen (**42**) with a K_D of 650 nM, the affinity is about a factor 20 lower. The lower affinity is a consequence of the lower stability of the complex as seen in the half-life time $T_{1/2}$ of 14 s for **52** compared to 5 min for phen. Due to the carboxylic acid, the molecule is negatively charged, which might lead to a repulsion of the negatively charged Ni-NTA complex. For pyrazine derivative **53,** two possible binding modes, either the "picolinic acid" or the "2-aminopyridine mode" are possible. Whereas the k_{on} did not change compared to picolinic acid, the off-rate was slightly higher, leading to the increased K_D. Unsubstituted pyrazines have a smaller negative charge and therefore less nucleophilicity on the nitrogens compared to pyridine, which might explain the lower binding affinity. In compound **54**, the carboxylic acid is replaced by a methyl ester reducing the overall charge of the ligand. Unfortunately, the binding affinity was reduced by a factor 2.5 compared to **52**. This effect is due to the low on-rate resulting from the methyl ester orientation. Whereas picolinic acid is almost correctly prealigned (only a small rotation of the carboxylic acid into the phen plane occurs in a conformational search), ligand **54** populates two equally stable conformations in

solution with the carbonyl oxygen on the same or on opposite sides. Compound **55** was measured to test the effect of an amino group adjacent to the binding nitrogen, which could establish a hydrogen bond to one of the carboxylic acid of NTA. Indeed, the substituent had a positive effect on binding affinity, leading to the lowest binding affinity in the whole series (10.9 µM). Although the k_{on} was 2-fold lower than for picolinic acid, the k_{off} was significantly decreased resulting in a half-life time of the complex of 39 s. This might indicate a tighter binding as a consequence of the hydrogen bond. The lower k_{on} can be explained by the loss of binding symmetry, as the molecule can bind only in one orientation compared to two for picolinic acid. The acetylated compound **56** was more than a factor 10 weaker in affinity than **55**, although it was expected to decrease solvation on the 6-amino group, which would be beneficial for binding. Most probably the orientation of the acetyl group leads to an unfavorable interaction with the Ni-NTA complex. Derivative **57** was thought to increase the affinity of bipy because of a symmetric arrangement of the binding nitrogens in the second benzene ring. Additionally, the ligand could choose between a hydroxyl or an amino group to form an H-bond to the carboxylic acid of NTA. However, most likely due to a tautomery effect as shown in Scheme 15 the binding affinity was not improved.
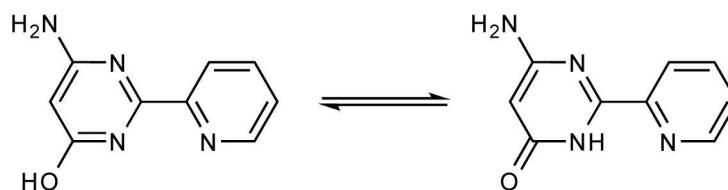
Scheme 15: Tautomery effect in 6-Amino-2-(2-pyridyl)pyrimidin-4-ol (**58**), leading to a protonation of the binding nitrogen.

The last compound of this series was a pyrimidine derivative (**58**). Pyrimidines are supposed to have higher negative charges on the ring nitrogens, which would increase the charge transfer to the nickel. In addition, the symmetric arrangement of two nitrogens in para position of the carboxylic acid should avoid the problem of pre-orientation encountered with the methyl picolinate **54**. Unfortunately with a K_D of 378 µM, the binding affinity was the weakest of the whole series.

6. CONCLUSION AND OUTLOOK

The main goal of this thesis was to improve the knowledge about small tags binding to Ni-NTA and to provide new purification tags for solid-phase peptide synthesis. In a first part, existing purification tags such as the His-tag were investigated. With the Biacore 3000 system, a tool to simulate the binding process of such ligands was available in house. The His-tag [*126, 129*], the very recently reported phenanthroline-tag [*169*] and derivatives thereof were analyzed with SPR to determine binding affinities and kinetic parameters of the tags and of derivatives thereof. In the second part, a purification strategy was accomplished by using a novel phenanthroline-containing construct for the purification of a test peptide. In parallel, a computational model for the prediction of binding affinities of various ligands to Ni-NTA was developed in collaboration with Dr. M. Smiesko. This computational model was then used to identify new purification tags suitable for SPPS, before they were analyzed by SPR.

The Histidine-Tag

Although the His-tag is the most widely used method for the purification of recombinant proteins, only little information is available on its binding properties. Therefore, the binding affinities and kinetics of different His-containing peptides were determined using SPR analysis. The hexahistidine (**5**) turned out to be the peptide with the highest affinity to Ni-NTA (K_D = 14 nM). The six histidines represent the optimal balance between enthalpic and entropic contributions to the binding process. Furthermore, divalent ligands formed by two histidines either in the positions i and i+2 or i and i+5 of the hexapeptide are contributing more to the overall binding than the other possible divalent ligands (i+1, i+3, and i+4). In addition, when the His-tag is further elongated, *i.e.* from heptahistidine (**6**) to decahistidine (**9**), a slight reduction of the affinity is observed, probably due to increased entropy costs upon binding. Finally, rebinding becomes more pronounced with increasing peptide length. This enables stable immobilization even with moderate dissociation constants, as shown for the decahistidine (**9**). Tags with strong rebinding would be appropriate for the immobilization of fusion proteins to solid supports for binding studies. Rebinding and

therefore multiple binding events mainly contribute to the high affinity of the His-tag to Ni-NTA. Single molecular interaction events as demonstrated with the His$_2$Ala$_4$ (**10** - **14**) and the HXH (**20** – **24**) series did not lead to high binding affinities (K$_D$ in the micromolar range).

The proper orientation is crucial for the high binding affinity in tags consisting of two histidine residues. The k$_{on}$ can be positively influenced enabling a faster association of the tag, if rotational restriction and fixation of the histidines is applied leading to higher binding affinities to Ni-NTA.

The Phenanthroline-Tag

1,10-phenanthroline (phen) is a promising scaffold for a purification tag. It showed a binding affinity of 650 nM. The low K$_D$ results mainly from a slow dissociation rate leading to a long half-life time of the complex (T$_{1/2}$ = 5.0 min). Manifold positive and negative influences on the binding affinity of phen were observed with the SPR analysis and the computational approach. Solubility played a key role in this complex system. Ligands that can establish on the side facing the solvent a well-organized solvation shell, showed improved binding properties for the Ni^{2+}-surface. Therefore, the affinity 5-amino-1,10-phenanthroline (**47**) was improved by a factor of 1.6 compared to phen (**42**). However, on the ligand side involved in binding weaker salvation is desired, because the exchange of well organized solvent molecules prior to binding is decreasing the gain in binding enthalpy. On the other hand, modifications on the two pyridine rings in para or ortho position increasing the nucleophilicity of the nitrogens. Therefore, a balance has to be found between moderate solvation on the side involved in binding and a high nucleophilicity of the nitrogens.

In addition, the complex [Ni(II)(nta)(phen)]$^-$ was crystallized for the development of a computational model for the prediction of binding affinities of various ligands to Ni-NTA. Analysis of the crystal structure revealed some unexpected facts: Phen was shifted out of the plane formed by nickel, the amino nitrogen of NTA, and a carboxylic acid arm of the NTA leading to an asymmetric complex. This was due to a steric clash between the hydrogen in position 2 of the phen and a CH$_2$ hydrogen of one of the carboxylic acid arms in NTA. Therefore, the number of possible alignments of phen in

a complex with Ni-NTA is cut from two to one, if substituents are present at position 2 or 9 in the phen scaffold. This effect was clearly demonstrated with the more than 2-fold decrease of k_{on} for 2-amino-phenanthroline (**46**) compared to phen (**42**). Furthermore, the amino group at position 2 was thought to interact with the carboxylic acid of NTA via an H-bond. However, no effect on k_{off} and K_D was observed, probably due to a suboptimal directionality of the H-bond.

Purification of SPPS Products

A new method was presented to link the phenanthroline-tag to a peptide synthesized via SPPS: For this purpose, an acrylate spacer was introduced to phen. *Tert*-butyl acrylate was coupled via a Heck reaction to 5-chloro-1,10-phenanthroline with a yield of 69%. After coupling of the tag to the test peptide NAPamide using standard SPPS chemistry, the construct was cleaved from the solid-phase. Attachment of the tag to the peptide could be qualitatively followed by the characteristic red color of the tag-spacer construct. The final purification was performed using a commercially available Ni-NTA column leading to a pure peptide with a yield of 43 % for the total synthesis. The purification strategy was even superior compared to the standard HPLC purification, where only a yield of 34% was achieved. Therefore, the newly designed acrylate spacer attached to phenanthroline is a suitable purification tag, to be used in solid-phase peptide synthesis.

The Biacore assay revealed only a small effect of the spacer on the binding affinity of the phen-tag. The K_D was slightly increased by a factor of 1.6 to about 1 μM. This is still sufficient to achieve a stable immobilization of the phen-tagged NAPamide on the Ni-NTA surface at a concentration of 10 μM. At higher concentrations, fast dissociation rates at the onset of dissociation were observed.

Photolabile linker

Introduction of a photolabile linker (PL) between the peptide and the phen-tag would enable to release the peptide from the tag, while the tag is still bound to the Ni-NTA support. This would allow the production of native peptides or proteins. The photolinker was coupled via an amide bond to phen. For this purpose, 5-nitro-1,10-phenanthroline was reduced to the 5-amino derivative. The nucleophilicity of the

aniline nitrogen was supposed to be too low for the amide formation. Therefore, Fmoc-Gly-OH was coupled to 5-amino-1,10-phenanthroline to obtain a primary amine after Fmoc deprotection. Unfortunately, solubility problems appeared with the introduction of the Fmoc-Gly-OH and became even worse upon attachment of the photolinker leading to precipitation of the PL-phen construct (**38**) during HPLC purification.

Picolinic acid

Picolinic acid (**52**) was demonstrated to bind via one oxygen of the carboxylic acid and the aromatic nitrogen to Ni-NTA with a K_D of 14 µM. This value further improved with 6-aminopicolinic acid (**55**) (K_D = 11 µM). The anilinic amino group at position 6 (**55**) is able to interact with one oxygen of the carboxylate of NTA leading to a 2.7-fold lower k_{off} compared to **52**. Therefore, the half-life time of the complex was increased from $T_{1/2}$ = 14 s for **52** to $T_{1/2}$ = 38 s for **55**. However, **55** is able to bind to Ni-NTA in only one orientation instead of two. This led to a 2-fold decrease of the k_{off} compared to **52**, and finally only to a small increase in binding affinity.

Outlook

This investigation illustrates the suitability of SPR experiments for the development of new tags for solid-phase peptide synthesis allowing both qualitative and quantitative investigations of the binding events. Nevertheless, a more detailed view could be gained with NMR experiments. Saturation Transfer Difference (STD) experiments could monitor, which atoms of a tag are involved in binding. This is especially beneficial for tags with more than one binding motif and could support the development of multivalent ligands. *E.g.* cyclic structures containing a symmetric arrangement of two binding motifs would help on one hand to increase the rebinding effect but would also add to a higher affinity.

The cleavage of the tag from the target molecule is essential for the production of native peptides or proteins. Chemically cleavable linkers such as the Fmoc-linker [*203*] could be an alternative to photolabile linkers. Such a lipophilic linker would require the change from phen-tags to more hydrophilic tags to increase

solubility in aqueous solvents. The introduction of PEG or PEGA spacers between the tag and the cleavable linker could further increase the solubility.

Finally, different combinations of metal ions and chelating groups could influence the binding affinity either positively or negatively. With the commercially available NTA chip, other transition metals such as Fe^{2+}, Co^{2+}, and Zn^{2+} could be immobilized to study the effect on binding affinity and kinetics to various tags.

7. LITERATURE

1. URL, http://www.ornl.gov/TechResources/Human_Genome/home.html.

2. Rudolph, R., and Lilie, H. (1996) In vitro folding of inclusion body proteins, *Faseb J 10*, 49-56.

3. Kent, S. B. H. (1988) Chemical Synthesis of Peptides and Proteins, *Annu Rev Biochem 57*, 957-989.

4. Gutte, B., and Merrifield, R. B. (1971) The synthesis of ribonuclease A, *J Biol Chem 246*, 1922-1941.

5. Fischer, E. (1906) Untersuchungen über Aminosäuren, Polypeptide und Proteïne, *Ber. Dtsch. Chem. Ges. 39*, 530.

6. Nishiuchi, Y., Inui, T., Nishio, H., Bodi, J., Kimura, T., Tsuji, F. I., and Sakakibara, S. (1998) Chemical synthesis of the precursor molecule of the Aequorea green fluorescent protein, subsequent folding, and development of fluorescence, *Proc Natl Acad Sci U S A 95*, 13549-13554.

7. Curtius, T. (1882) Ueber einige neue Hippursäureanalog constituierte synthetisch dargestellte Aminosäuren., *J. Prakt. Chemie 26*, 145-208.

8. Curtius, T. (1904) Verkettung von Aminosäuren., *J. Prakt. Chemie 70*, 51-108.

9. Fischer, E. (1905) Synthese von Polypeptiden, IX. Chloride der Aminosäuren und ihrer Acylderivate., *Ber. Dtsch. Chem. Ges. 38*, 605-620.

10. Merrifield, B. (1986) Solid phase synthesis, *Science 232*, 341-347.

11. Tam, J. P., Heath, W. F., and Merrifield, R. B. (1983) Sn2 Deprotection of Synthetic Peptides with a Low Concentration of Hf in Dimethyl Sulfide - Evidence and Application in Peptide-Synthesis, *J Am Chem Soc 105*, 6442-6455.

12. Carpino, L. A., and Han, G. Y. (1970) 9-Fluorenylmethoxycarbonyl Function, a New Base-Sensitive Amino-Protecting Group, *J Am Chem Soc 92*, 5748-&.

13. Miranda, L. P., and Alewood, P. F. (2000) Challenges for protein chemical synthesis in the 21st century: bridging genomics and proteomics, *Biopolymers 55*, 217-226.

14. Adams, J. H., Cook, R. M., Hudson, D., Jammalamadaka, V., Lyttle, M. H., and Songster, M. F. (1998) A reinvestigation of the preparation, properties, and

applications of aminomethyl and 4-methylbenzhydrylamine polystyrene resins, *J Org Chem 63*, 3706-3716.

15. Rapp, W., Zhang, L., Habish, R., and Bayer, E. (1989) Proceedings of the Twentieth European Peptide Symposium, in *Peptides 1988* (Jung, G., and Bayer, E., Eds.), de Gruyter, Berlin.

16. Larhed, M., Lindeberg, G., and Hallberg, A. (1996) Rapid microwave-assisted Suzuki coupling on solid-phase, *Tetrahedron Lett 37*, 8219-8222.

17. Meldal, M. (1992) Pega - a Flow Stable Polyethylene-Glycol Dimethyl Acrylamide Copolymer for Solid-Phase Synthesis, *Tetrahedron Lett 33*, 3077-3080.

18. Ulijn, R. V., Moore, B. D., Janssen, A. E. M., and Halling, P. J. (2002) A single aqueous reference equilibrium constant for amide synthesis-hydrolysis, *J Chem Soc Perk T 2*, 1024-1028.

19. Jursic, B. S., and Zdravkovski, Z. (1993) A Simple Preparation of Amides from Acids and Amines by Heating of Their Mixture, *Synthetic Commun 23*, 2761-2770.

20. Han, Y. X., Albericio, F., and Barany, G. (1997) Occurrence and minimization of cysteine racemization during stepwise solid-phase peptide synthesis, *J Org Chem 62*, 4307-4312.

21. Robertson, N., Jiang, L., and Ramage, R. (1999) Racemisation studies of a novel coupling reagent for solid phase peptide synthesis, *Tetrahedron 55*, 2713-2720.

22. Sheehan, J. C., and Hess, G. P. (1955) A New Method of Forming Peptide Bonds, *J Am Chem Soc 77*, 1067-1068.

23. Rich, D. H., and Singh, J. (1975-1987) The Carbodiimide Method, in *The Peptides: Analysis, Synthesis, Biology* (E., G., and J., M., Eds.), Academic Press, New York.

24. Sarantakis, D., Teichman, J., Lien, E. L., and Fenichel, R. L. (1976) Novel Cyclic Undecapeptide, Wy-40,770, with Prolonged Growth-Hormone Release Inhibiting Activity, *Biochem Bioph Res Co 73*, 336-342.

25.   Izdebski, J., Bondaruk, J., Gumulka, S. W., and Krzascik, P. (1989) Synthesis and Biological Evaluation of Human Preproenkephalin (100-111) and Its Analogs, *Int J Pept Prot Res 33*, 77-81.

26.   Chen, F. M., Kuroda, K., and Benoiton, N. L. (1978) A Simple Preparation of Symmetrical Anhydrides of N-Alkyloxycarbonylamino Acids, *Synthesis*, 928.

27.   Heimer, E. P., Chang, C. D., Lambros, T., and Meienhofer, J. (1981) Stable Isolated Symmetrical Anhydrides of N-Alpha-9-Fluorenyl-methyloxycarbonylamino Acids in Solid-Phase Peptide-Synthesis - Methionine-Enkephalin Synthesis as an Example, *Int J Pept Prot Res 18*, 237-241.

28.   Carlquist, M. (1987) Solid-Phase Synthesis of a 31-Residue Fragment of Human Glucose-Dependent Insulinotropic Polypeptide (Gip) by the Continuous-Flow Polyamide Method, *Acta Chem Scand B 41*, 494-498.

29.   Fields, G. B., and Noble, R. L. (1990) Solid-Phase Peptide-Synthesis Utilizing 9-Fluorenylmethoxycarbonyl Amino-Acids, *Int J Pept Prot Res 35*, 161-214.

30.   LeNguyen, D., and Castro, B. (1988) in *Peptide Chemistry 1987* (Shiba, T., and Sakakibara, S., Eds.), p 231, Protein Research Foundation, Osaka.

31.   Steinauer, R., Chen, F. M. F., and Benoiton, N. L. (1989) Studies on Racemization Associated with the Use of Benzotriazol-1-Yl-Tris (Dimethylamino)Phosphonium Hexafluorophosphate (Bop), *Int J Pept Prot Res 34*, 295-298.

32.   Coste, J., Lenguyen, D., and Castro, B. (1990) Pybop - a New Peptide Coupling Reagent Devoid of Toxic by-Product, *Tetrahedron Lett 31*, 205-208.

33.   Chen, S. Q., and Xu, J. C. (1992) A New Coupling Reagent for Peptide-Synthesis - Benzotriazolyloxy-Bis(Pyrrolidino)-Carbonium Hexafluoro-phosphate (Bbc), *Tetrahedron Lett 33*, 647-650.

34.   Carpino, L. A. (1993) 1-Hydroxy-7-azabenzotriazole. An Efficient Peptide Coupling Additive, *J Am Chem Soc 115*, 4397-4398.

35.   Marder, O., Shvo, Y., and Albericio, F. (2002) HCTU and TCTU: new couplin reagents: development and industrial aspects, *Chim. Oggi. 20*, 37-41.

36. Kisfaludy, L., and Schon, I. (1983) Preparation and Applications of Pentafluorophenyl Esters of 9-Fluorenylmethyloxycarbonyl Amino-Acids for Peptide-Synthesis, *Synthesis-Stuttgart*, 325-327.

37. Anderson, G. W., Zimmerman, J. E., and Callahan, F. M. (1963) N-Hydroxysuccinimide Esters in Peptide Synthesis, *J Am Chem Soc 85*, 3039-&.

38. Irie, H., Fujii, N., Ogawa, H., Yajima, H., Fujino, M., and Shinagawa, S. (1976) Role of Methionine in Facilitated Cleavage of Aromatic Ethers by Methanesulphonic Acid, *Journal of the Chemical Society-Chemical Communications*, 922-923.

39. Kiso, Y., Nakamura, S., Ito, K., Ukawa, K., Kitagawa, K., Akita, T., and Moritoki, H. (1979) Deprotection of O-Methyltyrosine by a Push-Pull Mechanism Using the Thioanisole-Trifluoromethanesulphonic Acid System - Application to the Convenient Synthesis of a Potent N-Methylenkephalin Derivative, *Journal of the Chemical Society-Chemical Communications*, 971-972.

40. Pearson, D. A., Blanchette, M., Baker, M. L., and Guindon, C. A. (1989) Trialkylsilanes as Scavengers for the Trifluoroacetic-Acid Deblocking of Protecting Groups in Peptide-Synthesis, *Tetrahedron Lett 30*, 2739-2742.

41. Schnolzer, M., Alewood, P., Jones, A., Alewood, D., and Kent, S. B. (1992) In situ neutralization in Boc-chemistry solid phase peptide synthesis. Rapid, high yield assembly of difficult sequences, *Int J Pept Protein Res 40*, 180-193.

42. Seebach, D., Thale, A., and Beck, K. (1989) Solubilization of Peptides in Non-polar Organic Solvents by the Addition of Inorganic Salts: Facts and Implications, *Helv Chim Acta 72*, 857-867.

43. Englebretsen, D. R., and Alewood, P. F. (1996) Boc SPPS of two hydrophobic peptides using a "solubilising tail" strategy: Dodecaalanine and chemotactic protein 10(42-55), *Tetrahedron Lett 37*, 8431-8434.

44. Miranda, L. P., and Alewood, P. F. (1999) Accelerated chemical synthesis of peptides and small proteins, *Proceedings of the National Academy of Sciences of the United States of America 96*, 1181-1186.

45. Haack, T., and Mutter, M. (1992) Serine Derived Oxazolidines as Secondary Structure Disrupting, Solubilizing Building-Blocks in Peptide-Synthesis, *Tetrahedron Lett 33*, 1589-1592.

46. Johnson, T., Quibell, M., and Sheppard, R. C. (1995) N,O-bisFmoc derivatives of N-(2-hydroxy-4-methoxybenzyl)-amino acids: useful intermediates in peptide synthesis, *J Pept Sci 1*, 11-25.

47. Tam, J. P., Yu, Q. T., and Miao, Z. W. (1999) Orthogonal ligation strategies for peptide and protein, *Biopolymers 51*, 311-332.

48. Wieland, T., Bokelmann, E., Bauer, L., Lang, H. U., and Lau, H. (1953) Ueber Peptidsynthesen .8. Bildung Von S-Haltigen Peptiden Durch Intramolekulare Wanderung Von Aminoacylresten, *Annalen Der Chemie-Justus Liebig 583*, 129-149.

49. Canne, L. E., Botti, P., Simon, R. J., Chen, Y. J., Dennis, E. A., and Kent, S. B. H. (1999) Chemical protein synthesis by solid phase ligation of unprotected peptide segments, *J Am Chem Soc 121*, 8720-8727.

50. Regnier, F. E. (1987) The Role of Protein-Structure in Chromatographic Behavior, *Science 238*, 319-323.

51. URL, (2008) http://www.sigmaaldrich.com/Brands/Sigma_Genosys/ Custom_Peptides/Key_Resources/Peptide_Solubility.html.

52. Axen, R., Porath, J., and Ernback, S. (1967) Chemical Coupling of Peptides and Proteins to Polysaccharides by Means of Cyanogen Halides, *Nature 214*, 1302.

53. Cuatreca, P., Wilchek, M., and Anfinsen, C. B. (1968) Selective Enzyme Purification by Affinity Chromatography, *Proceedings of the National Academy of Sciences of the United States of America 61*, 636-&.

54. Terpe, K. (2003) Overview of tag protein fusions: from molecular and biochemical fundamentals to commercial systems, *Appl Microbiol Biotechnol 60*, 523-533.

55. Sassenfeld, H. M., and Brewer, S. J. (1984) A Polypeptide Fusion Designed for the Purification of Recombinant Proteins, *Bio-Technology 2*, 76-81.

56. Hopp, T. P., Prickett, K. S., Price, V. L., Libby, R. T., March, C. J., Cerretti, D. P., Urdal, D. L., and Conlon, P. J. (1988) A Short Polypeptide Marker

Sequence Useful for Recombinant Protein Identification and Purification, *Bio-Technology 6*, 1204-1210.

57. Evan, G. I., Lewis, G. K., Ramsay, G., and Bishop, J. M. (1985) Isolation of Monoclonal-Antibodies Specific for Human C-Myc Proto-Oncogene Product, *Molecular and Cellular Biology 5*, 3610-3616.

58. Schmidt, T. G., and Skerra, A. (1993) The random peptide library-assisted engineering of a C-terminal affinity peptide, useful for the detection and purification of a functional Ig Fv fragment, *Protein Eng 6*, 109-122.

59. Hochuli, E., Dobeli, H., and Schacher, A. (1987) New metal chelate adsorbent selective for proteins and peptides containing neighbouring histidine residues, *J Chromatogr 411*, 177-184.

60. Bucher, M. H., Evdokimov, A. G., and Waugh, D. S. (2002) Differential effects of short affinity tags on the crystallization of Pyrococcus furiosus maltodextrin-binding protein, *Acta Crystallographica Section D-Biological Crystallography 58*, 392-397.

61. Stofkohahn, R. E., Carr, D. W., and Scott, J. D. (1992) A Single Step Purification for Recombinant Proteins - Characterization of a Microtubule Associated Protein (Map-2) Fragment Which Associates with the Type-Ii Camp-Dependent Protein-Kinase, *Febs Letters 302*, 274-278.

62. Keefe, A. D., Wilson, D. S., Seelig, B., and Szostak, J. W. (2001) One-step purification of recombinant proteins using a nanomolar-affinity streptavidin-binding peptide, the SBP-tag, *Protein Expression and Purification 23*, 440-446.

63. Watanabe, T., Ito, Y., Yamada, T., Hashimoto, M., Sekine, S., and Tanaka, H. (1994) The Roles of the C-Terminal Domain and Type-Iii Domains of Chitinase A1 from Bacillus-Circulans Wl-12 in Chitin Degradation, *Journal of Bacteriology 176*, 4465-4472.

64. Smith, D. B., and Johnson, K. S. (1988) Single-Step Purification of Polypeptides Expressed in Escherichia-Coli as Fusions with Glutathione S-Transferase, *Gene 67*, 31-40.

65. Diguan, C., Li, P., Riggs, P. D., and Inouye, H. (1988) Vectors That Facilitate the Expression and Purification of Foreign Peptides in Escherichia-Coli by Fusion to Maltose-Binding Protein, *Gene 67*, 21-30.

66. Nock, S., Spudich, J. A., and Wagner, P. (1997) Reversible, site-specific immobilization of polyarginine-tagged fusion proteins on mica surfaces, *Febs Letters 414*, 233-238.

67. Hopp, T. P., Gallis, B., and Prickett, K. S. (1996) Metal-binding properties of a calcium-dependent monoclonal antibody, *Molecular Immunology 33*, 601-608.

68. Schuster, M., Wasserbauer, E., Einhauer, A., Ortner, C., Jungbauer, A., Hammerschmid, F., and Werner, G. (2000) Protein expression strategies for identification of novel target proteins, *Journal of Biomolecular Screening 5*, 89-97.

69. Voss, S., and Skerra, A. (1997) Mutagenesis of a flexible loop in streptavidin leads to higher affinity for the Strep-tag II peptide and improved performance in recombinant protein purification, *Protein Engineering 10*, 975-982.

70. Hans, M., and Buckel, W. (2000) Purification of recombinant component A of 2-hydroxylglutaryl-CoA dhydratase from Acidaminococcus fermentans using Strep-Tactin affinity-chromatography, *Biotechnol Intl September*, 12.

71. Gross, R., Pisa, R., Simon, J., and Kröger, A. (2002) Isolierung der trimeren Hydrogenase aus Wolinella succinogenes durch StrepTactin-Affinitätschromatographie, *Biospektrum 1*, 101.

72. Ostermeier, C., Harrenga, A., Ermler, U., and Michel, H. (1997) Structure at 2.7 angstrom resolution of the Paracoccus denitrificans two-subunit cytochrome c oxidase complexed with an antibody F-V fragment, *Proceedings of the National Academy of Sciences of the United States of America 94*, 10547-10553.

73. Manstein, D. J., Schuster, H. P., Morandini, P., and Hunt, D. M. (1995) Cloning Vectors for the Production of Proteins in Dictyostelium-Discoideum, *Gene 162*, 129-134.

74. Connelly, P. R., Varadarajan, R., Sturtevant, J. M., and Richards, F. M. (1990) Thermodynamics of Protein Peptide Interactions in the Ribonuclease-S System Studied by Titration Calorimetry, *Biochemistry 29*, 6108-6114.

75. Kelemen, B. R., Klink, T. A., Behlke, M. A., Eubanks, S. R., Leland, P. A., and Raines, R. T. (1999) Hypersensitive substrate for ribonucleases, *Nucleic Acids Research 27*, 3696-3701.

76. Blumenthal, D. K., Takio, K., Edelman, A. M., Charbonneau, H., Walsh, K., Titani, K., and Krebs, E. G. (1985) Identification of the Calmodulin-Binding Domain of Skeletal-Muscle Myosin Light Chain Kinase, *Biophysical Journal 47*, A76-A76.

77. Head, J. F. (1992) A better grip on calmodulin, *Curr Biol 2*, 609-611.

78. Tomme, P., Boraston, A., McLean, B., Kormos, J., Creagh, A. L., Sturch, K., Gilkes, N. R., Haynes, C. A., Warren, R. A. J., and Kilburn, D. G. (1998) Characterization and affinity applications of cellulose-binding domains, *Journal of Chromatography B 715*, 283-296.

79. Tomme, P., Warren, R. A. J., and Gilkes, N. R. (1995) Cellulose hydrolysis by bacteria and fungi, *Adv Microb Physiol 37*, 1-81.

80. McCormick, M., and Berg, J. (1997) Purification and S.box-solid.Tag detection of CBD fusion proteins, *inNovations 7*, 12-15.

81. Zhang, J. B., Zhang, X. E., Zhou, Y. F., Bi, L. J., Zhang, Z. P., Wang, S. H., Chen, Y. Y., Guo, Y. C., Wen, J. K., and Yu, Z. N. (2007) Construction and characterization of an anti-prion scFv fusion protein pair for detection of prion protein on antibody chip, *Analytical Letters 40*, 855-873.

82. Taylor, M. G., Bushara, H., Capron, A., Xu, S., and Butterworth, A. (1994) Laboratory and field evalutaion of defined antigen vaccines against Schistosoma bovis and S. japonicum in animals and of defined antigens for the immunodiagnosis of human S. japonicum infection, in *Science and technology for development-health-second programme (1978-1991). Summaries of the final reports of the research contracts.* (Jepsen, S., Hagan, P., Klein, R., and Taylor, D., Eds.), pp 189-200, Parasitology European Commission DGXII.

83. Sachdev, D., and Chirgwin, J. M. (2000) Fusions to maltose-binding protein: Control of folding and solubility in protein purification, *Applications of Chimeric Genes and Hybrid Proteins, Pt A 326*, 312-321.

84. Davis, G. D., Elisee, C., Newham, D. M., and Harrison, R. G. (1999) New fusion protein systems designed to give soluble expression in Escherichia coli, *Biotechnology and Bioengineering 65*, 382-388.

85. LaVallie, E. R., DiBlasio, E. A., Kovacic, S., Grant, K. L., Schendel, P. F., and McCoy, J. M. (1993) A thioredoxin gene fusion expression system that

circumvents inclusion body formation in the E. coli cytoplasm, *Biotechnology (N Y) 11*, 187-193.

86.   Zhang, Y. B., Howitt, J., McCorkle, S., Lawrence, P., Springer, K., and Freimuth, P. (2004) Protein aggregation during overexpression limited by peptide extensions with large net negative charge, *Protein Expression and Purification 36*, 207-216.

87.   Kapust, R. B., Tozser, J., Fox, J. D., Anderson, D. E., Cherry, S., Copeland, T. D., and Waugh, D. S. (2001) Tobacco etch virus protease: mechanism of autolysis and rational design of stable mutants with wild-type catalytic proficiency, *Protein Eng 14*, 993-1000.

88.   Walker, P. A., Leong, L. E. C., Ng, P. W. P., Tan, S. H., Waller, S., Murphy, D., and Porter, A. G. (1994) Efficient and Rapid Affinity Purification of Proteins Using Recombinant Fusion Proteases, *Bio-Technology 12*, 601-605.

89.   Hirabayashi, J., and Kasai, K. (1992) Arginine-Tail Method, an Affinity Tag Procedure Utilizing Anhydrotrypsin Agarose, *Journal of Chromatography 597*, 181-187.

90.   Hochuli, E., Bannwarth, W., Döbeli, H., Gentz, R., and Stüber, D. (1988) Genetic Approach to Facilitate Purification of Recombinant Proteins with a Novel Metal Chelate Adsorbent, *Bio/Technology 6*, 1321-1325.

91.   Chong, S. R., Mersha, F. B., Comb, D. G., Scott, M. E., Landry, D., Vence, L. M., Perler, F. B., Benner, J., Kucera, R. B., Hirvonen, C. A., Pelletier, J. J., Paulus, H., and Xu, M. Q. (1997) Single-column purification of free recombinant proteins using a self-cleavable affinity tag derived from a protein splicing element, *Gene 192*, 271-281.

92.   Tropea, J. E., Cherry, S., Nallamsetty, S., Bignon, C., and Waugh, D. S. (2007) A generic method for the production of recombinant proteins in Escherichia coli using a dual hexahistidine-maltose-binding protein affinity tag, *Methods Mol Biol 363*, 1-19.

93.   Porath, J., Carlsson, J., Olsson, I., and Belfrage, G. (1975) Metal chelate affinity chromatography, a new approach to protein fractionation, *Nature 258*, 598-599.

94.   Helferich, F. (1961) 'Ligand Exchange': a Novel Separation Technique, *Nature 189*, 1001.

95.   Pearson, R. G. (1968) Hard and Soft Acids and Bases Hsab .1. Fundamental Principles, *Journal of Chemical Education 45*, 581-&.

96.   Porath, J. (1988) Imac - Immobilized Metal-Ion Affinity Based Chromatography, *Trac-Trends in Analytical Chemistry 7*, 254-259.

97.   Ueda, E. K., Gout, P. W., and Morganti, L. (2003) Current and prospective applications of metal ion-protein binding, *J Chromatogr A 988*, 1-23.

98.   Arnold, F. H. (1991) Metal-affinity separations: a new dimension in protein processing, *Biotechnology (N Y) 9*, 151-156.

99.   Hemdan, E. S., Zhao, Y. J., Sulkowski, E., and Porath, J. (1989) Surface-Topography of Histidine-Residues - a Facile Probe by Immobilized Metal-Ion Affinity-Chromatography, *Proceedings of the National Academy of Sciences of the United States of America 86*, 1811-1815.

100.   Sawadogo, M., and Van Dyke, M. W. (1995) Indirect use of immobilized metal affinity chromatography for isolation and characterization of protein partners, *Genet Eng (N Y) 17*, 53-65.

101.   Wong, J. W., Albright, R. L., and Wang, N. H. L. (1991) Immobilized Metal-Ion Affinity-Chromatography (Imac) Chemistry and Bioseparation Applications, *Separation and Purification Methods 20*, 49-106.

102.   Hansen, P., and Lindeberg, G. (1995) Importance of the alpha-amino group in the selective purification of synthetic histidine peptides by immobilised metal ion affinity chromatography, *J Chromatogr A 690*, 155-159.

103.   Kagedal, L. (1998) in *Protein Purification: Principles, High-Resolution Methods, and Applications* (Janson, J.-C., and Ryden, L., Eds.), p 311, Wiley-VCH, New York.

104.   Porath, J. (1992) Immobilized metal ion affinity chromatography, *Protein Expr Purif 3*, 263-281.

105.   Zaveckas, M., Baskeviciute, B., Luksa, V., Zvirblis, G., Chmieliauskaite, V., Bumelis, V., and Pesliakas, H. (2000) Comparative studies of recombinant human granulocyte-colony stimulating factor, its Ser-17 and (His)6-tagged forms interaction with metal ions by means of immobilized metal ion affinity

partitioning. Effect of chelated nickel and mercuric ions on extraction and refolding of proteins from inclusion bodies, *J Chromatogr A 904*, 145-169.

106. Grinstead, R. R., and Nasutavicus, W. A. (1978) Water-insoluble chelate exchange resins from aminopyridines and process for the selective extraction of valuable metals using the same, The Dow Chemical Company, US Patent.

107. Zachariou, M., and Hearn, M. T. (2000) Adsorption and selectivity characteristics of several human serum proteins with immobilised hard Lewis metal ion-chelate adsorbents, *J Chromatogr A 890*, 95-116.

108. Lehr, R. V., Elefante, L. C., Kikly, K. K., O'Brien, S. P., and Kirkpatrick, R. B. (2000) A modified metal-ion affinity chromatography procedure for the purification of histidine-tagged recombinant proteins expressed in Drosophila S2 cells, *Protein Expr Purif 19*, 362-368.

109. Belew, M., and Porath, J. (1990) Immobilized metal ion affinity chromatography. Effect of solute structure, ligand density and salt concentration on the retention of peptides, *J Chromatogr 516*, 333-354.

110. Arvidsson, P., Ivanov, A. E., Galaev, I., and Mattiasson, B. (2001) Polymer versus monomer as displacer in immobilized metal affinity chromatography, *J Chromatogr B Biomed Sci Appl 753*, 279-285.

111. Chung, B. H., Bailey, D., and Arnold, F. H. (1994) Metal Affinity Partitioning, *Aqueous Two-Phase Systems 228*, 167-179.

112. Holmes, L. D., Serag, A. A., Plunkett, S. D., Todd, R. J., and Arnold, F. H. (1992) Metal-affinity electrophoresis of histidine-containing proteins, *Methods 4*, 103-108.

113. Nanak, E., Abdul-Nour, J., and Vijayalakshmi, M. A. (1992) Metal affinity electrophoresis: an analytical tool, *Methods 4*, 97-102.

114. Haupt, K., Roy, F., and Vijayalakshmi, M. A. (1996) Immobilized metal ion affinity capillary electrophoresis of proteins - A model for affinity capillary electrophoresis using soluble polymer-supported ligands, *Analytical Biochemistry 234*, 149-154.

115. Crowe, J., Dobeli, H., Gentz, R., Hochuli, E., Stuber, D., and Henco, K. (1994) 6xHis-Ni-NTA chromatography as a superior technique in recombinant protein expression/purification, *Methods Mol Biol 31*, 371-387.

116. Nelson, P. S., Yang, T.-T., and Kain, S. R. (1999) Method for purification of recombinant proteins, Clontech Laboratories, Inc., US Patent.

117. Chang, M. S., Bolton, J. L., and Blond, S. Y. (1999) Expression and purification of hexahistidine-tagged human glutathione S-transferase P1-1 in Escherichia coli, *Protein Expression and Purification 17*, 443-448.

118. Begum, R. R., Newbold, R. J., and Whitford, D. (2000) Purification of the membrane binding domain of cytochrome b(5) by immobilised nickel chelate chromatography, *Journal of Chromatography B-Analytical Technologies in the Biomedical and Life Sciences 737*, 119-130.

119. Cha, H. J., Dalal, N. G., Vakharia, V. N., and Bentley, W. E. (1999) Expression and purification of human interleukin-2 simplified as a fusion with green fluorescent protein in suspended Sf-9 insect cells, *Journal of Biotechnology 69*, 9-17.

120. Chaga, G., Hopp, J., and Nelson, P. (1999) Immobilized metal ion affinity chromatography on Co2+-carboxymethylaspartate-agarose Superflow, as demonstrated by one-step purification of lactate dehydrogenase from chicken breast muscle, *Biotechnology and Applied Biochemistry 29*, 19-24.

121. Fiore, C., Trezeguet, V., Roux, P., Le Saux, A., Noel, F., Schwimmer, C., Arlot, D., Dianoux, A. C., Lauquin, G. J. M., and Brandolin, G. (2000) Purification of histidine-tagged mitochondrial ADP/ATP carrier: Influence of the conformational states of the C-terminal region, *Protein Expression and Purification 19*, 57-65.

122. Tallet, B., Astier-Gin, T., Castroviejo, M., and Santarelli, X. (2001) One-step chromatographic purification procedure of a His-tag recombinant carboxyl half part of the HTLV-I surface envelope glycoprotein overexpressed in Escherichia coli as a secreted form, *Journal of Chromatography B-Analytical Technologies in the Biomedical and Life Sciences 753*, 17-22.

123. Georgiou, G., and Valax, P. (1996) Expression of correctly folded proteins in Escherichia coli, *Current Opinion in Biotechnology 7*, 190-197.

124. Sinha, D., Bakhshi, M., and Vora, R. (1994) Ligand-Binding Assays with Recombinant Proteins Refolded on an Affinity Matrix, *Biotechniques 17*, 509.

125.   Ordaz, E., Garrido-Pertierra, A., Gallego, M., and Puyet, A. (2000) Covalent and metal-chelate immobilization of a modified 2-haloacid dehalogenase for the enzymatic resolution of optically active chloropropionic acid, *Biotechnology Progress 16*, 287-291.

126.   Nieba, L., Nieba-Axmann, S. E., Persson, A., Hamalainen, M., Edebratt, F., Hansson, A., Lidholm, J., Magnusson, K., Karlsson, A. F., and Pluckthun, A. (1997) BIACORE analysis of histidine-tagged proteins using a chelating NTA sensor chip, *Anal Biochem 252*, 217-228.

127.   Zhu, H., Bilgin, M., Bangham, R., Hall, D., Casamayor, A., Bertone, P., Lan, N., Jansen, R., Bidlingmaier, S., Houfek, T., Mitchell, T., Miller, P., Dean, R. A., Gerstein, M., and Snyder, M. (2001) Global analysis of protein activities using proteome chips, *Science 293*, 2101-2105.

128.   Schmitt, L., Ludwig, M., Gaub, H. E., and Tampe, R. (2000) A metal-chelating microscopy tip as a new toolbox for single-molecule experiments by atomic force microscopy, *Biophys J 78*, 3275-3285.

129.   Gershon, P. D., and Khilko, S. (1995) Stable chelating linkage for reversible immobilization of oligohistidine tagged proteins in the BIAcore surface plasmon resonance detector, *J Immunol Methods 183*, 65-76.

130.   Conti, M., Falini, G., and Samori, B. (2000) How Strong Is the Coordination Bond between a Histidine Tag and Ni - Nitrilotriacetate? An Experiment of Mechanochemistry on Single Molecules, *Angew Chem Int Ed Engl 39*, 215-218.

131.   Liu, H. L., Ho, Y., and Hsu, C. M. (2003) Molecular simulations to determine the chelating mechanisms of various metal ions to the His-tag motif: a preliminary study, *J Biomol Struct Dyn 21*, 31-41.

132.   Bernaudat, F., and Bullow, L. (2005) Rapid evaluation of nickel binding properties of His-tagged lactate dehydrogenases using surface plasmon resonance, *J Chromatogr A 1066*, 219-224.

133.   Kozlov, I. A., Kermani, B. G., Melnyk, P. C., Barker, D. L., Zhao, C., Hachmann, J. P., and Lebl, M. (2007) Retention of histidine-containing peptides on a nickel affinity column, *J Chromatogr Sci 45*, 207-211.

134. Carson, M., Johnson, D. H., McDonald, H., Brouillette, C., and Delucas, L. J. (2007) His-tag impact on structure, *Acta Crystallogr D Biol Crystallogr 63*, 295-301.

135. Miras, R., Cuillel, M., Catty, P., Guillain, F., and Mintz, E. (2001) Purification of heterologous sarcoplasmic reticulum Ca2+-ATPase Serca1a allowing phosphoenzyme and Ca2+-affinity measurements, *Protein Expr Purif 22*, 299-306.

136. Fonda, I., Kenig, M., Gaberc-Porekar, V., Pristovaek, P., and Menart, V. (2002) Attachment of histidine tags to recombinant tumor necrosis factor-alpha drastically changes its properties, *ScientificWorldJournal 2*, 1312-1325.

137. Suh, J. K., Poulsen, L. L., Ziegler, D. M., and Robertus, J. D. (1996) Molecular cloning and kinetic characterization of a flavin-containing monooxygenase from Saccharomyces cerevisiae, *Arch Biochem Biophys 336*, 268-274.

138. Woestenenk, E. A., Hammarstrom, M., van den Berg, S., Hard, T., and Berglund, H. (2004) His tag effect on solubility of human proteins produced in Escherichia coli: a comparison between four expression vectors, *J Struct Funct Genomics 5*, 217-229.

139. Chant, A., Kraemer-Pecore, C. M., Watkin, R., and Kneale, G. G. (2005) Attachment of a histidine tag to the minimal zinc finger protein of the Aspergillus nidulans gene regulatory protein AreA causes a conformational change at the DNA-binding site, *Protein Expr Purif 39*, 152-159.

140. Wu, J., and Filutowicz, M. (1999) Hexahistidine (His6)-tag dependent protein dimerization: a cautionary tale, *Acta Biochim Pol 46*, 591-599.

141. Tang, H., and Chitnis, P. R. (2000) Addition of C-terminal histidyl tags to PsaL and PsaK1 proteins of cyanobacterial photosystem I, *Indian J Biochem Biophys 37*, 433-440.

142. Rosales, J. L., and Lee, K. Y. (2000) Purification of dual-tagged intact recombinant proteins, *Biochem Biophys Res Commun 273*, 1058-1062.

143. Ledent, P., Duez, C., Vanhove, M., Lejeune, A., Fonze, E., Charlier, P., Rhazi-Filali, F., Thamm, I., Guillaume, G., Samyn, B., Devreese, B., Van Beeumen, J., Lamotte-Brasseur, J., and Frere, J. M. (1997) Unexpected influence of a C-

terminal-fused His-tag on the processing of an enzyme and on the kinetic and folding parameters, *FEBS Lett 413*, 194-196.

144. Smith, M. C., Furman, T. C., Ingolia, T. D., and Pidgeon, C. (1988) Chelating Peptide-Immobilized Metal-Ion Affinity-Chromatography - a New Concept in Affinity-Chromatography for Recombinant Proteins, *Journal of Biological Chemistry 263*, 7211-7215.

145. Smith, M. C., Furman, T. C., and Pidgeon, C. (1987) Immobilized Iminodiacetic Acid Metal Peptide Complexes - Identification of Chelating Peptide Purification Handles for Recombinant Proteins, *Inorganic Chemistry 26*, 1965-1969.

146. Sulkowski, E., Vastola, K., Oleszek, D., and Von Muenchhausen, W. (1982) Surface Topography of Interferons: A Probe by Metal Chelate Chromatography, *Anal Chem Symp Ser 9*, 313.

147. Beitle, R. R., and Ataai, M. M. (1993) One-Step Purification of a Model Periplasmic Protein from Inclusion-Bodies by Its Fusion to an Effective Metal-Binding Peptide, *Biotechnology Progress 9*, 64-69.

148. Ljungquist, C., Breitholtz, A., Brink-Nilsson, H., Moks, T., Uhlen, M., and Nilsson, B. (1989) Immobilization and affinity purification of recombinant proteins using histidine peptide fusions, *Eur J Biochem 186*, 563-569.

149. Turbadar, T. (1959) Complete Absorption of Light by Thin Metal Films, *Proceedings of the Physical Society of London 73*, 40-44.

150. Kaambhampati, D. (2003) *Protein Microarray Technology*, Wiley-VCH Verlag.

151. Kretschm, E., and Raether, H. (1968) Radiative Decay of Non Radiative Surface Plasmons Excited by Light, *Zeitschrift Fur Naturforschung Part a-Astrophysik Physik Und Physikalische Chemie A 23*, 2135-&.

152. Biacore AB, (2001) Surface Plasmon Resonance (Technology Note 1), pp 1-4.

153. Jonsson, U., Fagerstam, L., Ivarsson, B., Johnsson, B., Karlsson, R., Lundh, K., Lofas, S., Persson, B., Roos, H., Ronnberg, I., and et al. (1991) Real-time biospecific interaction analysis using surface plasmon resonance and a sensor chip technology, *Biotechniques 11*, 620-627.

154. Nagata, K. H., H. (2000) *Real-Time Analysis of Biomolecular Interactions: Applications of BIACORE*, Springer, Japan.

155. Stenberg, E., Persson, B., Roos, H., and Urbaniczky, C. (1991) Quantitative determination of surface concentration of protein with surface plasmon resonance using radiolabeled proteins, *J Colloid Interface Sci 143*, 513-526.

156. Mannen, T., Yamaguchi, S., Honda, J., Sugimoto, S., Kitayama, A., and Nagamune, T. (2001) Observation of charge state and conformational change in immobilized protein using surface plasmon resonance sensor, *Anal Biochem 293*, 185-193.

157. Lofas, S., and Johnson, B. (1990) A novel hydrogel matrix on gold surfaces in surface plasmon resonance sensors for fast and efficient covalent immobilization of ligands, *J Chem Soc Chem Commun*, 1526-1528.

158. Biacore. (2002) Application Note 12: Capture of histidine-tagged proteins using NTA or anti-histidine antibodies, pp 1-4.

159. Rich, R. L., and Myszka, D. G. (2006) Survey of the year 2005 commercial optical biosensor literature, *Journal of Molecular Recognition 19*, 478-534.

160. Myszka, D. G. (1997) Kinetic analysis of macromolecular interactions using surface plasmon resonance biosensors, *Curr Opin Biotechnol 8*, 50-57.

161. Myszka, D. G. (1999) Improving biosensor analysis, *J Mol Recognit 12*, 279-284.

162. O'Shannessy, D. J., Brigham-Burke, M., Soneson, K. K., Hensley, P., and Brooks, I. (1993) Determination of rate and equilibrium binding constants for macromolecular interactions using surface plasmon resonance: use of nonlinear least squares analysis methods, *Anal Biochem 212*, 457-468.

163. Karlsson, R., Michaelsson, A., and Mattsson, L. (1991) Kinetic analysis of monoclonal antibody-antigen interactions with a new biosensor based analytical system, *J Immunol Methods 145*, 229-240.

164. Roden, L. D., and Myszka, D. G. (1996) Global analysis of a macromolecular interaction measured on BIAcore, *Biochem Biophys Res Commun 225*, 1073-1077.

165. Schnolzer, M., and Kent, S. B. (1992) Constructing proteins by dovetailing unprotected synthetic peptides: backbone-engineered HIV protease, *Science 256*, 221-225.

166. Bang, D., and Kent, S. B. (2004) A one-pot total synthesis of crambin, *Angew Chem Int Ed Engl 43*, 2534-2538.

167. Bang, D., and Kent, S. B. (2005) His6 tag-assisted chemical protein synthesis, *Proc Natl Acad Sci U S A 102*, 5014-5019.

168. Comely, A. C., Gibson, S. E., Hales, N. J., and Peplow, M. A. (2001) Transition metal complexes as linkers for solid phase synthesis: chromium carbonyl complexes as linkers for arenes, *J. Chem. Soc., Perkin Trans. 1*, 2526.

169. Frank, H.-G., Casaretto, M., and Knorr, K. (2006) Method for solid-phase peptide synthesis and purification, Lonza AG, International Patent.

170. Fumoto, M., Hinou, H., Matsushita, T., Kurogochi, M., Ohta, T., Ito, T., Yamada, K., Takimoto, A., Kondo, H., Inazu, T., and Nishimura, S. (2005) Molecular transporter between polymer platforms: highly efficient chemoenzymatic glycopeptide synthesis by the combined use of solid-phase and water-soluble polymer supports, *Angew Chem Int Ed Engl 44*, 2534-2537.

171. Smiesko, M., Knecht, S., Schmidt, T., and Ernst, B. Structural and electronic properties of phenanthroline-based ligands for immobilized metal ion chromatography, *in preparation*.

172. Wilkins, M. R., Lindskog, I., Gasteiger, E., Bairoch, A., Sanchez, J. C., Hochstrasser, D. F., and Appel, R. D. (1997) Detailed peptide characterization using PEPTIDEMASS--a World-Wide-Web-accessible tool, *Electrophoresis 18*, 403-408.

173. Chang, J. Y., Knecht, R., and Braun, D. G. (1983) Amino acid analysis in the picomole range by precolumn derivatization and high-performance liquid chromatography, *Methods Enzymol 91*, 41-48.

174. Knecht, R., and Chang, J. Y. (1986) Liquid chromatographic determination of amino acids after gas-phase hydrolysis and derivatization with (dimethylamino)azobenzenesulfonyl chloride, *Anal Chem 58*, 2375-2379.

175. Rich, R. L., and Myszka, D. G. (2000) Advances in surface plasmon resonance biosensor analysis, *Curr Opin Biotechnol 11*, 54-61.
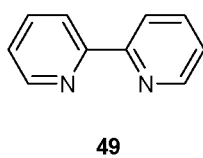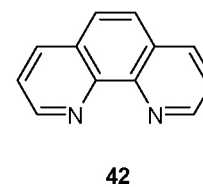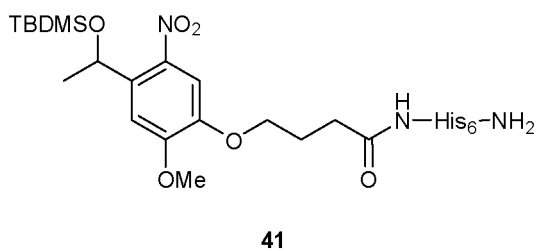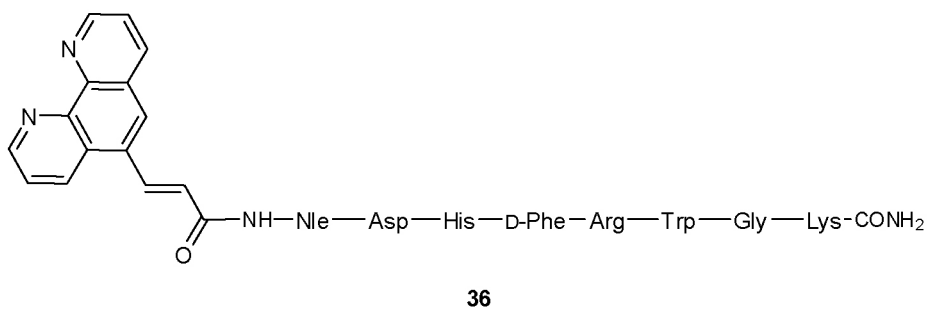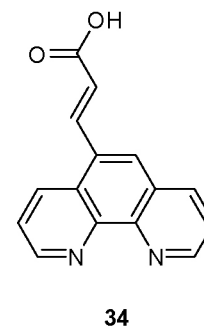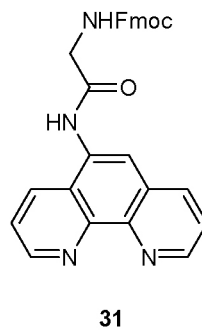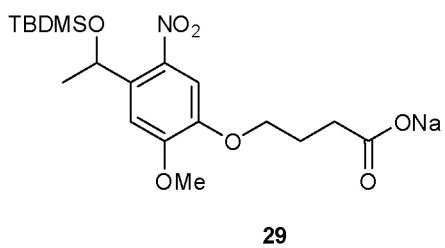
176. Frostell-Karlsson, A., Remaeus, A., Roos, H., Andersson, K., Borg, P., Hamalainen, M., and Karlsson, R. (2000) Biosensor analysis of the interaction between immobilized human serum albumin and drug compounds for prediction of human serum albumin binding levels, *J Med Chem 43*, 1986-1992.

177. Fletcher, A. R., Jones, J. H., Ramage, W. I., and Stachulski, A. V. (1979) The Use of the N(Pi)-Phenacyl Group for the Protection of the Histidine Side Chain in Peptide Synthesis, *J. Chem. Soc., Perkin Trans. 1*, 2261.

178. Jones, J. H., and Ramage, W. I. (1978) Approach to Prevention of Racemization in Synthesis of Histidine-Containing Peptides, *Journal of the Chemical Society-Chemical Communications*, 472-473.

179. Johnson, R. D., and Arnold, F. H. (1995) The Temkin isotherm describes heterogeneous protein adsorption, *Biochim Biophys Acta 1247*, 293-297.

180. Johnson, R. D., Todd, R. J., and Arnold, F. H. (1996) Multipoint binding in metal-affinity chromatography II. Effect of pH and imidazole on chromatographic retention of engineered histidine-containing cytochromes c, *J Chromatogr A 725*, 225-235.

181. Todd, R. J., Johnson, R. D., and Arnold, F. H. (1994) Multiple-site binding interactions in metal-affinity chromatography. I. Equilibrium binding of engineered histidine-containing cytochromes c, *J Chromatogr A 662*, 13-26.

182. Andersson, L., Sulkowski, E., and Porath, J. (1987) Purification of commercial human albumin on immobilized IDA-Ni2+, *J Chromatogr 421*, 141-146.

183. Furia, T. E. (1972) *CRC handbook for food additives*, 2nd ed., The Chemical Rubber Co., Cleveland.

184. Albericio, F., Bofill, J. M., El-Faham, A., and Kates, S. (1998) Use of Onium Salt-Based Coupling Reagents in Peptide Synthesis, *J Org Chem 63*, 9678-9683.

185. Enzelberger, M. M., Minning, S., and Schmid, R. D. (2000) Designing new metal affinity peptides by random mutagenesis of a natural metal-binding site, *J Chromatogr A 898*, 83-94.

186. Blau, F. (1898) Ueber neue organische Metallverbindungen, *Monatsh. Chem. 19*, 647.

187. Margerum, D. W., Bystroff, R. I., and Banks, C. V. (1956) Kinetics of 1,10-Phenanthroline Chelation. I. Mono-(1,10-phenanthroline)-nickel(II), *J Am Chem Soc 78*, 4211-4217.

188. Vosburgh, W. C., and Cooper, G. R. (1941) Complex Ions. I. The Identification of Complex Ions in Solution by Spectrophotometric Measurements, *J Am Chem Soc 63*, 437.

189. Salam, M., and Aoki, K. (2000) Interligand interactions affecting specific metal bonding to nucleic acid bases: the tripodal nitrilotriacetato (nta) ligand-system., *Inorg. Chim. Acta. 311*, 15-24.

190. Sengupta, D., Pal, A., and Lahiri, S. C. (1983) Studies on the Solubility of 2,2'-Bipyridyl, 1,10-Phenanthroline, and Their Tris Iron(Ii) Perchlorates in Methanol Water Mixtures, and the Determination of the Medium Effect of Ions, *J Chem Soc Dalton*, 2685-2688.

191. Page, M. I., and Jencks, W. P. (1971) Entropic contributions to rate accelerations in enzymic and intramolecular reactions and the chelate effect, *Proc Natl Acad Sci U S A 68*, 1678-1683.

192. Lundback, T., and Hard, T. (1996) Sequence-specific DNA-binding dominated by dehydration, *Proceedings of the National Academy of Sciences of the United States of America 93*, 4754-4759.

193. Kotrl, S., and Sucha, L. (1985) Handbook of Chemical Equilibrium in Analytical Chemistry, in *Ellis Horwood Series in Analytical Chemistry* (Horwood, E., Ed.), Chichester, UK.

194. Yamada, M., Kimura, M., Nishizawa, M., Kuroda, S., and Shimao, I. (1991) Electronic-Spectra of Phenanthrolinediones, Phenanthrolinones, Bipyridinediones, and Amino-Substituted Phenanthrolines, *B Chem Soc Jpn 64*, 1821-1827.

195. Chemler, S. R., Trauner, D., and Danishefsky, S. J. (2001) The B-Alkyl Suzuki-Miyaura Cross-Coupling Reaction: Development, Mechanistic Study, and Applications in Natural Product Synthesis A list of abbreviations can be found at the end of the article, *Angew Chem Int Ed Engl 40*, 4544-4568.

196.   Shaughnessy, K. H., Kim, P., and Hartwig, J. F. (1999) A fluorescence-based assay for high-throughput screening of coupling reactions. Application to Heck chemistry, *J Am Chem Soc 121*, 2123-2132.

197.   Huang, X., Anderson, K. W., Zim, D., Jiang, L., Klapars, A., and Buchwald, S. L. (2003) Expanding Pd-catalyzed C-N bond-forming processes: the first amidation of aryl sulfonates, aqueous amination, and complementarity with Cu-catalyzed reactions, *J Am Chem Soc 125*, 6653-6655.

198.   Sinnokrot, M. O., and Sherrill, C. D. (2003) Unexpected substituent effects in face-to-face pi-stacking interactions, *J Phys Chem A 107*, 8377-8379.

199.   Lloyd-Williams, P., Albericio, F., and Giralt, E. (1991) Convergent solid-phase peptide synthesis. VIII. Synthesis, using a photolabile resin, and purification of a methionine-containing protected peptide., *Int J Pept Protein Res 37*, 58-60.

200.   Tetko, I. V., Gasteiger, J., Todeschini, R., Mauri, A., Livingstone, D., Ertl, P., Palyulin, V. A., Radchenko, E. V., Zefirov, N. S., Makarenko, A. S., Tanchuk, V. Y., and Prokopenko, V. V. (2005) Virtual computational chemistry laboratory--design and description, *J Comput Aided Mol Des 19*, 453-463.

201.   Moriguchi, I., Hirono, S., Liu, Q., Nakagome, I., and Matsushita, Y. (1992) Simple Method of Calculating Octanol Water Partition-Coefficient, *Chem Pharm Bull 40*, 127-130.

202.   Jones, R. A., and Katritzky, A. R. (1959) Potentially Tautomeric Pyridines .2. 2-Acetamido-Pyridine,3-Acetamido-Pyridine, and 4-Acetamido-Pyridine and 2-Benzamido-Pyridine, 3-Benzamido-Pyradine, 4-Benzamido-Pyridine, *J Chem Soc*, 1317-1323.

203.   Rabanal, F., Albericio, F., Cotton, R., and Giralt, E. (1992) in *Peptides 1992* (Schneider, C. H., and Eberle, A. N., Eds.), p 288, ESCOM Sciences Publisher, Leiden, NL.

8. APPENDIX

(**1**)   H-His-His-OH

(**2**)   H-His-His-His-OH

(**3**)   H-His-His-His-His-OH

(**4**)   H-His-His-His-His-His-OH

(**5**)   H-His-His-His-His-His-His-OH

(**6**)   H-His-His-His-His-His-His-His-OH

(**7**)   H-His-His-His-His-His-His-His-His-OH

(**8**)   H-His-His-His-His-His-His-His-His-His-OH

(**9**)   H-His-His-His-His-His-His-His-His-His-His-OH

(**10**)   H-Ala-Ala-Ala-Ala-His-His-OH

(**11**)   H-Ala-Ala-Ala-His-Ala-His-OH

(**12**)   H-Ala-Ala-His-Ala-Ala-His-OH

(**13**)   H-Ala-His-Ala-Ala-Ala-His-OH

(**14**)   H-His-Ala-Ala-Ala-Ala-His-OH

(**15**)   H-His-Ala-His-Ala-Ala-His-OH

(**16**)   H-His-Ala-Ala-His-Ala-His-OH

(**17**)   H-Ala-Ala-Ala-His-His-OH

(**18**)   H-Ala-Ala-His-His-OH

(**19**)   H-Ala-His-His-OH

(**20**)   H-His-Gly-His-OH

(**21**)   H-His-Ala-His-OH

(**22**)   H-His-Sar-His-OH

(**23**)   H-His-Aib-His-OH

(**24**)   H-His-Pro-His-OH

(**25**)   H-Nle-Asp-His-D-Phe-Arg-Trp-Gly-Lys-NH$_2$

(**26**)   H-His-His-His-His-His-His-NH$_2$

29

31

34

36

38

41

42

49

52

9.   ACKNOWLEDGMENT

10. CURRICULUM VITAE

Name, Address:	Steven Knecht Landskronstr. 71 CH - 4056 Basel Phone: +41 (0)61 321 19 01 Mobile: +41 (0)76 565 77 21 steven.knecht@unibas.ch
Date of birth:	August 21, 1978
Native place:	Eschlikon, Switzerland
Nationality:	Swiss
Martial status:	Single

EDUCATION

09/2004-06/2008	Dissertation, Institute for Molecular Pharmacy, Basel *Research into a Purification System Suitable for Solid-phase Peptide Synthesis*
10/2003	Diploma in Biology II equivalent to M Sc Mol Biol
09/2002-06/2003	Diploma thesis in Endocrinology, Department of Research, University Hospital Basel *Synthesis of Rhenium-cyclized α-MSH Analogs for Targeting of B16F1 Mouse Melanoma Cells*
10/2001-10/2003	Second part of studies in Biology II (Molecular Biology, Structural Biology / Biophysics, Biochemistry, Cell Biology), University of Basel
10/1998-10/2000	First part of studies in Biology II (Basics in Biology, Mathematics, Physics, Chemistry) including first and second pre-degree, University of Basel
08/1994-12/1997	Grammar school, Matura Typus C (Mathematics), Liestal

PROFESSIONAL EXPERIENCE

10/2000-06/2001	Full-time employee at Bank Coop, Process and Facilities, Architecture, Basel
07/1998-04/1999	Employee at Statistics Agency, Financial Statistics, Liestal

LANGUAGES

German	native language
English	fluent
French	fluent
Spanish	basic knowledge

01/2004-06/2004	Language stay in South America

ADDITIONAL SKILLS

Computer	Advanced skills in Microsoft Excel and programming (Visual Basic for Applications, Pascal)

SCIENTIFIC QUALIFICATIONS

Papers	Steven Knecht, Daniel Ricklin, Alex N. Eberle, Beat Ernst, *The Oligohis-Tag: Mechanism of Binding to Ni-NTA surfaces*; submitted to J Mol Recognit
	Steven Knecht, Nadine Hafner, Alex N. Eberle, Beat Ernst, *Development of a New Tag for Solid-phase Peptide Synthesis*, in preparation
	Martin Smiesko, Steven Knecht, Tobias Schmidt, Beat Ernst, *Structural and electronic properties of phenanthroline-based ligands for immobilized metal ion chromatography*, in preparation
Posters	Steven Knecht, Daniel Ricklin, Alex N. Eberle, Beat Ernst, *Has the 6His-Tag the Optimal Length?*; Fall Meeting of the Swiss Chemical society 2005

Teaching	Supervisor of several practical courses in Pharmaceutical Chemistry
	Supervision of a diploma thesis with the title "*Development of new tags for purification of synthetically developed peptides*"
Courses	Biacore User Days 2006, Heidelberg, Germany
	Numerous lectures and seminars (drug discovery, analytics)